

AD 670469

Research Publication GMR-767

INVESTIGATIONS ON THE DIRECT CONVERSION OF NUCLEAR
FISSION ENERGY TO ELECTRICAL ENERGY IN A PLASMA DIODE

FINAL REPORT

for

Nonr-3109(00)

VOLUME I

October 31, 1967

RESEARCH LABORATORIES
GENERAL MOTORS CORPORATION
Warren, Michigan

DDC
RECEIVED
JUN 18 1968
B

This document has been approved
for reproduction by the
CLEARINGHOUSE
for Federal Scientific & Technical
Information Springfield Va. 22151

204

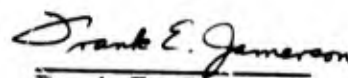
OFFICE OF NAVAL RESEARCH
Contract Nonr-3109(00)

Investigations on the Direct Conversion of Nuclear
Fission Energy to Electrical Energy in a Plasma Diode
Final Report No. 8

VOLUME I

Authors

Charles B. Leffert
David B. Rees


Frank E. Jamerson
Project Supervisor

Report for Period November 1, 1966 to October 31, 1967
Report Published February 29, 1968

Research Laboratories, General Motors Corporation
Warren, Michigan

Reproduction in whole or in part is permitted for any
purpose of the United States Government

This report has been prepared under Contract
Nonr-3109(00) for the Office of Naval Research and
technically supervised by Commander William F. Diehl
and Dr. Ralph Roberts.

ABSTRACT

This is the unclassified section (Vol. I) of the Final Report under Contract Nonr-3109(00), Office of Naval Research, dealing with fission-fragment-generated plasmas for thermionic energy conversion. Results of the past year's work are presented under three major headings, viz., "(A) - Reaction Kinetic Studies of Ar-Cs Plasmas", where the possible influence of a heteronuclear ArCs^+ ion is considered and rejected; "(B) - Calculation of Electron Temperatures in Plasmas Produced by Fission Fragments", where we discover that a non-equilibrium electron temperature exists at the higher values of neutron flux; and "(C) - Electron Densities in Fission-Fragment-Induced Plasmas in Microwave Cavities", where much of our previous theories are collected, enlarged and incorporated into a comprehensive set of computer codes which predict accurately electron densities in the Ne-Ar system. Preceding the detailed discussion of these 3 topics is a summary (in Section I) of the main results of studies (A), (B), and (C). Also in Section I we survey our past work and offer some general comments and conclusions on the present status and utility of the fission-fragment ionization scheme for use in thermionic diodes.

TABLE OF CONTENTS

	<u>Page</u>
ABSTRACT	i
<u>SECTION I - INTRODUCTION, SUMMARIES AND CONCLUSIONS</u> , D.B.Rees.	1
1. INTRODUCTION AND PREVIOUS WORK	1
2. OBJECTIVES FOR CURRENT REPORTING PERIOD	6
3. SUMMARY AND CONCLUSIONS OF THE THREE DETAILED SECTIONS OF THIS VOLUME	6
A. Reaction Kinetic Studies of Argon-Cesium Plasmas	6
B. Calculation of Electron Temperatures in Plasmas Produced by Fission Fragments	7
C. Electron Densities in Fission-Fragment- Induced Plasmas in Microwave Cavities	8
4. CONCLUDING REMARKS	9
ACKNOWLEDGMENTS	12
REFERENCES	13
<u>INVESTIGATIONS:</u>	
SECTION A - REACTION KINETICS STUDIES OF ARGON-CESIUM PLASMAS, C. B. Leffert	33 pages
SECTION B - CALCULATION OF ELECTRON TEMPERATURES IN PLASMAS PRODUCED BY FISSION FRAGMENTS, D. B. Rees	30 pages
SECTION C - ELECTRON DENSITIES IN FISSION-FRAGMENT-INDUCED PLASMAS IN MICROWAVE CAVITIES, C. B. Leffert	122 pages
DISTRIBUTION	5 pages

SECTION I

INTRODUCTION, SUMMARIES AND CONCLUSIONS

1. INTRODUCTION AND PREVIOUS WORK

From early in our program, our research work on inpile thermionic energy conversion has been directed toward answering the question of whether a relatively low-temperature thermionic emitter coupled to a fission-fragment-generated plasma can lead to a useful energy conversion scheme. Because of the novelty of this approach, most of our work has been of a basic rather than device-oriented nature, and has progressed along the following lines.

The development program for an unclad nuclear-heated emitter material that could be operated over a temperature range of 1100-1300°C with a current density capability of about 10 A cm^{-2} was successfully completed in 1964. This work is fully described in Part I (unclassified) and Part II (classified) of the Final Report, Contract Nonr-3870(00), Office of Naval Research, July 1, 1964. The thermionic-electron and fission-fragment emitter that was developed is an unclad BaO-UO₂-W cermet in which the UO₂ acts as the source of heat, and the BaO as the source of barium which subsequently diffuses to the surface of the emitter. A coating of barium is thus formed on the tungsten phase of the emitter and this provides a relatively low work function for thermionic electron emission. In addition, the uranium residing on the surface of the emitter serves as the source of fission fragments which penetrate the gas generating a plasma. Although we have encountered many difficulties of technique in going from the successful small (0.3 cm diam) emitters of 1964 to the larger (1.9 cm diam) emitters of our recent electron transport tubes (discussed in the classified Volume II of the present Final Report), we have persisted to regard the emitter concept and structure as satisfactory particularly from an electron emission standpoint. As a result, in the past few years we have concentrated our efforts on trying to understand more fully the nature of plasmas induced by fission-fragment excitation and ionization of a noble gas.

Our reasons for using noble gases for the plasma medium have been, firstly, that they are chemically inert, and secondly, that their electron-neutral atom scattering cross section is 100 to 1,000 times smaller than the comparable

cross section for cesium. This smaller noble gas cross section could well lead to smaller internal power losses in a converter, or permit greater electrode spacings than present-day cesium devices. The prospect of a thermionic converter with a low temperature emitter, chemically-inert filling, and relatively wide electrode spacing is extremely attractive from a fabrication standpoint and potential for long-lived operation.

The first basic inpile study of the plasma was the ion generation rate study.¹ A series of experiments were conducted on the plasma alone using small ceramic-metal diodes containing a thin uranium-235 foil and filled with noble gases at a variety of pressures between 30 and 400 torr. The uranium foil provided a copious flux of fission fragments but remained cool with consequently no thermionic emission. The value of the ion generation rate due to fission fragments could be obtained directly from the current-voltage (I-V) data of these diodes. Our final procedure^{2,3} was to compute the ion generation rate and the corresponding I-V relationship from first principles for the gases studied, viz., Ne, Ar, Xe, and Ne-Ar with $[Ar]/[Ne]=10^{-3}$, and these computed characteristics all agreed with the experimental data within $\pm 10\%$. We thus confirmed that we knew well the primary rate of ion production in such plasmas.

With this knowledge of ion generation rate, we were able to calculate the electron density in all the single gases³ where the predominant charge loss process was dissociative recombination. We concluded that the electron density n_e in the single noble gases, extrapolated to a power reactor, were too low ($n_e \approx 10^{12} \text{ cm}^{-3}$) by factors of between 10 to 100 to be of interest for thermionic energy conversion. The situation, however, was not as simple for neon mixed with traces of argon. It was clear from both experiment and computation that the ion generation rate for Ne-Ar at pressures ~ 100 torr was about 50% higher than that for pure neon. This was due to the Penning Effect, i.e., the ionization of argon in collisions of the second kind with neon metastable states generated by fission fragments. However, the value of the electron density in Ne-Ar was much less clear since the total volume charge loss in this mixed system could not be represented by a single volume loss coefficient as in the single gases. Importantly, there arose the possibility of making the lifetime of the Ar^+ ion much longer than the lifetime of Ne^+ and Ne_2^+ ions, thus

greatly enhancing the electron density and conductivity of the plasma. This led to the next phase of the plasma program, viz., experimental and theoretical studies of electron density in binary Penning-type gas mixtures ionized by fission fragments.

In the theoretical studies of the Penning-type gas mixture,² in the first instance Ne-Ar, we proceeded to write down five simultaneous equations describing what we judged to be the important production and loss processes for Ne^+ , Ne_2^+ , Ne^m , Ar^+ and Ar_2^+ . The electron density was the sum of the density of the four ion species each of which was determined by solving this set of simultaneous equations with a digital computer. About 30 reaction rates needed to be known representing processes such as diffusion, recombination, molecular-ion formation, and volume destruction of metastable states, in addition to accurate values of the generation rate of ions and metastable states obtained from our earlier studies. These reaction rates for Ne-Ar were mostly known, or could be readily extracted from the literature or were estimated with sufficient accuracy.² Thus we obtained computed contour maps of electron density as a function of total gas pressure p and $[\text{Ar}]/[\text{Ne}]$ seeding. The important result was that for the temperatures expected in a thermionic converter, there existed a maximum in the value of n_e at $[\text{Ar}]/[\text{Ne}] \approx 10^{-4}$ and $p \approx 100$ torr. This maximum value of n_e arose from a maximum in the lifetime of the dominant Ar^+ ion under these conditions. Also the predicted value of n_e of greater than 10^{12} cm^{-3} in an experimental reactor indicated a significant electron-density gain of about a factor of 10 over the single gas.

We then used the above reaction kinetics equations to study the electron density in argon seeded with cesium.^{4,5} This is, we think, the most promising mixture for the fission-fragment plasma scheme. The presence of a trace of cesium does not, however, mean a plasma behavior akin to the conventional cesium converter. The cesium is present in such minor concentration ($\lesssim 10^{-2}$ torr) that the undesirable elastic scattering from electron-neutral cesium impacts is still negligibly small. The advantages of this mixture are that argon has a higher stopping power than neon for fission fragments, argon has an exceedingly low Ramsauer minimum (i.e. low resistance to electron flow) at the right energy point (~ 0.2 eV) for a converter, argon metastables have a very large cross section ($\approx 10^{-14} \text{ cm}^2$) for ionizing neutral cesium, and a cesium covering can be used on the collector to yield a low work function surface. The

results of our computations of electron density in Ar-Cs^{4,5} indicated a behavior rather similar to that in Ne-Ar, viz., that a single maximum value of n_e existed and occurred around $[Cs]/[Ar] \approx 10^{-4}$ and $p \approx 100$ torr. The value of n_e in Ar-Cs however, was twice as high as in Ne-Ar, although greater uncertainty existed in several of the reaction rate coefficients for Ar-Cs.

The predictions of the reaction kinetics theory for Ne-Ar and Ar-Cs were checked as follows. We measured the inpile electron density in each plasma using small metal microwave cavities at the end of a long evacuated K-band waveguide.⁴ Each cavity was a right-circular cylinder, containing again a thin uranium-235 foil, and the average electron density of the plasma was determined from the change in resonant frequency of the cavity due to the presence of the electrons. Considerable care was necessary in the experimental setup to ensure a good reflected signal from the distant inpile cavity. Electron density measurements from the neon-argon cavities with $[Ar]/[Ne] = 10^{-4}$ and $p = 90$ torr yielded values of n_e as a function of neutron flux ϕ which agreed quite well with the predicted values of n_e .^{5,6} With the 90 torr argon-cesium cavity we were also able to vary the cesium pressure by varying the temperature of the cesium reservoir and so obtain values of n_e as a function of $[Cs]/[Ar]$.^{6,7} In this case the reaction kinetics theory predicted well the general magnitude and trend of the electron density but the experimental values of n_e were higher than expected particularly for values of $[Cs]/[Ar] < 10^{-4}$.

Very importantly, the experimental values of n_e showed a dependence on ambient temperature which could not be accounted for by theory.⁶ The fissioning of the uranium foil heated the microwave cavities slightly and by means of a cooling jet of nitrogen gas we were able to vary the average cavity temperature in the range 300-600°K. We found that for Ar-Cs, an increase of ambient temperature of 100°K in this range increased the value of n_e by a factor of about 3. In sharp contrast the effect of temperature on n_e in Ne-Ar was smaller than expected at that time. Then in the reaction kinetics theory, we assumed that the electron temperature T_e was at the ion/gas temperature $T_{i,a}$. The most temperature-sensitive reaction rate in the theory was collisional-radiative recombination of the trace gas atomic ion ($\propto T_e^{-5}$). If we assume this important loss process to be completely dominant, then $S = \alpha_0 T_e^{-5} n_e^3$ so that $n_e = (S/\alpha_0)^{1/3} T_e^{5/3}$; for the temperature range 500-600°K we then obtain a variation of n_e of 1.3 which is much smaller than the factor of 3 increase in the experimental value of n_e in Ar-Cs. Also because of the nature of the high vacuum ceramic-metal seal of

the cavity window for admitting microwaves, we could not independently heat the microwave cavity up to temperatures of 1300°K or so of interest for a converter.

Thus the position was that we could not predict the electron density in Ne-Ar or particularly Ar-Cs at 1300°K because of an observed temperature behavior over 300-600°K that was not in accord with the temperature predictions of our reaction kinetics theory. That is, extrapolation of our microwave cavity results to the all-important conditions of a converter in a power reactor necessitated a much better understanding of the dependence of n_e upon $T_{i,a}$. This aspect of the plasma has motivated much of our recent investigations. Several possible temperature-sensitive surface and volume reactions in Ar-Cs were considered in last year's report⁶ but none appeared capable of yielding the observed behavior. This brings our basic plasma studies up to their position at the beginning of the current reporting period.

The other parallel investigations that we have conducted over the past three years have been on inpile thermionic electron transport. This has involved experimental and theoretical studies on the current-carrying capability of the Ar-Cs plasma when coupled to the BaO-UO₂-W emitter. The inpile experimental results from several thermionic diodes, each with important modifications, are classified and reported in Volume II of this present Final Report. The theoretical studies have been concerned with incorporating the physics of the reaction kinetics theory in a thermionic electron transport theory for predicting current-voltage characteristics. Note that it is here we need the reaction kinetics theory extrapolated to elevated temperature. Up to the present reporting period a full transport theory including important non-linear volume effects from the reaction kinetics theory has not been completed. Rather, a restricted transport model for thermionic electrons through a fission fragment plasma has been developed for the case when the electron density was controlled by ambipolar diffusion loss of the long-lived atomic ions of the trace species.^{4,6} In Volume II we discuss the comparison between the predictions of this diffusion-type theory and the experimental transport data, and also their implications for a practical device.

2. OBJECTIVES FOR CURRENT REPORTING PERIOD

As may be discerned from the preceding summary of our past work, the two main objectives for the current reporting period were:

- 1) To study, from a basic kinetics standpoint, the nature of the observed critical dependence of electron density upon ambient gas and wall temperatures in mixed gas plasmas generated by fission fragments, particularly in argon seeded with cesium, so that the electron density of such a plasma in a thermionic electron transport tube could be much better predicted.
- 2) To operate several inpile thermionic electron transport diodes with appropriate Ar-Cs fillings, and extend the theoretical transport studies to include reaction kinetic results, with the purpose of understanding electron transport sufficiently well to enable us to extrapolate the results to a power reactor and thus assess the utility of the fission-fragment scheme.

The manner in which we have attacked the first objective and our conclusions are contained in the present report (Vol.I) and summarized below. Investigations pertinent to the second objective are to be found in Volume II (classified). Suffice it to say here regarding Volume II that experiment and theoretical limits are not in accord, yet the differences are, in many ways, unexpectedly encouraging. Nevertheless the differences prohibit extrapolation of our results to a power reactor.

3. SUMMARY AND CONCLUSIONS OF THE THREE DETAILED SECTIONS OF THIS VOLUME

Section A. Reaction Kinetic Studies of Argon-Cesium Plasmas. An attempt was made in argon-cesium to account for the sensitive dependence of electron density n_e upon the ion/atom or gas temperature $T_{i,a}$ by, first, postulating the significant production, at pressures of 100 torr, of the heteronuclear ArCs^+ ion both from metastable argon-cesium collisions and associative reactions involving the Cs^+ ion; and secondly, by postulating a highly temperature-dependent dissociative reaction, viz., $\text{ArCs}^+ + \text{Ar} \longrightarrow \text{Cs}^+ + 2\text{Ar}$. By incorporating this additional reaction scheme into the existing reaction kinetics

model, it was found possible to fit well the theory (essentially a 3-parameter fit) to the experimental values of electron density over the entire range of gas temperature, Cs/Ar ratio and neutron flux. However to obtain this agreement, a physically unrealistic dissociative rate was persistently required. As a result we concluded that the marked dependence of n_e upon $T_{i,a}$ was not attributable to the ArCs^+ ion.

During the course of this study, we observed that to bring theory into agreement with experiment at low values of Cs/Ar it was necessary to reduce the collisional-radiative recombination rate of Cs^+ ions by a factor of about 10. This implied an electron temperature in the plasma notably higher than the gas temperature, and we pursued this further as outlined in the next section.

Section B. Calculation of Electron Temperatures in Plasmas Produced by Fission Fragments. We had previously considered the electrons to be at or very close to thermal equilibrium with the ambient ions and atoms, i.e. $T_e \approx T_{i,a}$. Such a notion arose principally from our estimates that the high-energy electrons produced by the fission fragments were rapidly thermalized to ambient temperatures. However, in this section of the report, we present a more careful energy-balance analysis of the energy-relaxation of the fast electrons where we found that $T_e > T_{i,a}$ generally by an important amount.

Knowledge of the production rate, initial energy and energy-degradation rate of the fast electrons created directly by the fragments was used to determine the energy input rate by electron-electron collisions to the Maxwellian electron swarm which, in turn, lost energy via elastic collisions to the ambient ions and atoms. For the Penning-type gas mixture, the additional source of electron energy from the metastable-ionization process was also taken into account. Results of the calculation for Ne-Ar at 90 torr with $[\text{Ar}]/[\text{Ne}] = 10^{-4}$ showed that at low values of neutron flux ($\sim 10^{10} \text{ cm}^{-2} \text{ sec}^{-1}$) and electron densities ($\sim 10^{10} \text{ cm}^{-3}$), the electron temperature was at or near the gas temperature, but at high neutron flux ($\sim 10^{13} \text{ cm}^{-2} \text{ sec}^{-1}$) and electron densities ($\sim 10^{12} \text{ cm}^{-3}$), the electron temperature was higher than the gas temperature by a significant amount ($\sim 500^\circ \text{K}$). For Ar-Cs, the calculation is less complete because we have not yet included the electron energy lost to excited cesium states. However, when this loss was neglected (approximately

justified for low $[Cs]/[Ar]$ concentrations) we found that T_e was $\sim 2000^\circ K$ for $T_{i,a} \sim 500^\circ K$.

These findings made it expedient to modify our reaction kinetics analysis to include the marked effect of the non-equilibrium electron temperature on various of the reaction rates; this is discussed in the next section.

Section C. Electron Densities in Fission-Fragment-Induced Plasmas in Microwave Cavities. We have brought together here all the theories which we consider necessary for predicting from first principles the electron density in our resonant microwave cavities. Also the many digital computer codes embodying the theories, and the methods for executing these codes, are described in considerable detail.

The ion generation rate in the plasma from fission fragments was computed from known constants of the fission fragments and gases. The reaction kinetics theory for a binary Penning-type gas plasma, and the non-equilibrium electron temperature theory, were incorporated together into a digital computer scheme which, with the aid of the ion generation rate code, computed a self-consistent electron temperature-electron density (n_e, T_e) pair for a point in the plasma. Since the ion generation rate varied radially across the cavity, several (n_e, T_e) pairs were next computed for selected radii until the radial dependence of n_e was clearly established. Finally, with this radial dependence of n_e , and the known radial dependence of the microwave electric field probing the cavity, an integrating computer code was used to obtain a value of electron density averaged over the square of the electric field $\langle n_e \rangle_{av}$ for direct comparison with the inpile measured values from the Ne-Ar and Ar-Cs microwave cavities.

Our values of $\langle n_e \rangle_{av}$ for the Ne-Ar cavity ($[Ar]/[Ne] = 10^{-4}$), computed with no adjustable parameters, were in excellent agreement (within $\pm 20\%$) with the inpile microwave measurements over the complete range of neutron flux ($10^{10} \lesssim \phi \lesssim 10^{13} \text{ cm}^{-2} \text{ sec}^{-1}$). This strongly substantiates the many ideas, assumptions and methods of computation used to arrive at predicted values of $\langle n_e \rangle_{av}$. We confirmed that the electron swarm temperature was as much as a factor of two higher than the gas temperature at high values of neutron flux, and furthermore, this non-equilibrium condition accounted in large part for the small observed variation of n_e with $T_{i,a}$. Note also that the computation yielded values for

the density of neon metastables and of the atomic and molecular ions of the major and minor gas; therefrom we also knew, of course, the total rates at which these species interacted in the plasma.

As indicated earlier, the proper calculation of $\langle n_e \rangle_{av}$ for Ar-Cs, which should include the influence on electron temperature of inelastic losses to cesium, was not completed in time for this report. Nevertheless, we applied the existing computational scheme to Ar-Cs for a value of $[Cs]/[Ar]=10^{-6}$ where errors due to the neglect of inelastic cross sections are likely to be small. Interestingly, the computed value of $\langle n_e \rangle_{av}$ agreed very well with the inpile microwave results at $[Cs]/[Ar]=10^{-6}$ where computed values of T_e were $\sim 2000^\circ K$. The necessary modifications to the code to take into account the quenching effect on T_e of inelastic cesium cross sections (with possible significant production of Cs^+) are outlined.

4. CONCLUDING REMARKS

Our theoretical work and unclassified experimental inpile studies have thus brought us to the following general position in this field of fission-fragment-generated plasmas for thermionic energy conversion.

- (i). A physical model has been developed to predict the electrical behavior of experimental non-thermionic devices filled with either a single noble gas or a Penning type binary-gas mixture and ionized by fission fragments. The model includes detailed computations of (a) the direct ionization source by fission fragments, (b) the interaction of the ion species and metastable states among themselves, with neutral atoms and with electrons, (c) the equilibrium electron temperature in such systems, and (d) the enhancement of ion density that can accrue through suitable manipulation of major and minor gas species densities.
- (ii). The theory has been used to compute electron densities for a gas mixture consisting of neon with a small admixture of argon. This required detailed knowledge of about 30 atomic cross sections or reaction rate coefficients and no adjustable parameters were allowed. Experimental measurement by microwave techniques of the electron density in tubes specially prepared for the purpose and filled with

neon-argon gave results in excellent agreement ($\pm 20\%$) with theory over the full range of 3 orders of magnitude in neutron flux. Thus the general principles of our theory appear valid.

- (iii). Similar experimental and theoretical calculations for tubes containing argon with a trace of cesium (in which the predominant ions are Cs^+) gave less satisfactory agreement. This circumstance is certainly attributable in part to our less exact knowledge of all the applicable basic cross sections and to the fact that the computation of electron temperature, which is dependent on inelastic cesium cross sections, is presently incomplete. Nevertheless, with argon-cesium there remains this important observation: the measured electron density is a very strong and increasing function of gas temperature in the microwave tubes. As yet we find no good theoretical basis for such a strong dependence and we shall be surprised if our more complete electron temperature computations, presently under way, offer a full explanation. We also note here that in an argon-cesium electron-transport device at high temperature, theory and experiment did not agree either.
- (iv). A better understanding of the behavior of the argon-cesium plasma requires research work in the following areas of greatest uncertainty to determine: (a) the cross section for the ionization of cesium atoms by argon metastable states; (b) the production rate of argon metastable states from dissociative recombination of molecular argon ions with electrons; (c) the ion species present in argon-cesium at pressures of around 100 torr; and (d) the interaction of argon ions, metastable states and photons with cesium atoms residing on moderately hot surfaces. There is a need to know the rates of these interactions as functions of electron and neutral gas temperatures to assist in determining the origin of the strong dependence of electron density upon ambient temperatures.
- (v). We emphasize that the fission-fragment flux (and hence gas ionization rate) from the $\text{BaO-UO}_2\text{-W}$ thermionic emitter is appreciably lower (e.g., by factors of 4 to 8) than that from the uranium-235 foils used in the above plasma studies. This arises not only from the presence in the thermionic emitter of non-fissionable materials necessary for

good thermionic-electron emission; equally as important is the fact that the $\text{BaO-UO}_2\text{-W}$ emitter has to be relatively thick to yield the high temperature for thermionic emission, and this very thickness leads to significant neutron attenuation which depresses the neutron flux at the emitter surface and thus reduces the fission-fragment flow from the emitter into the gas. In contrast the cool thin uranium-235 foils in our ion tubes and microwave cavities were largely opaque to neutrons and so did not significantly depress the neutron flux at the fission-fragment-emitting surface. This reduction of fission fragments for a converter could be largely overcome by placing thin uranium-235 foil on the collector; additionally, this leads to the possibility of operating a pure thermionic-electron emitter which need not necessarily supply any fission fragments. In fact, our final electron transport tube (ETT-5) was such a device and its design and construction is described in the accompanying Vol. II (classified). However, we do not know whether a layer of cesium (from the argon-cesium gas mixture) on a fissioning uranium-235 surface at the expected collector temperatures of about 900°K would yield a collector work function sufficiently low to make such a scheme plausible.

- vi. We conclude that the utility of fission-fragment generated plasmas for thermionic energy conversion is difficult to assess completely in this report independent of the classified inpile data. Conclusions can only be based here on our electron density studies, and our electron transport theory which shows the electron density distribution expected in a thermionic diode operating in a diffusion-controlled mode. This transport theory points to the need of high ($\gtrsim 10^{13} \text{ cm}^{-3}$) electron densities at the collector sheath-plasma boundary in order to obtain output current densities ($\gtrsim 7.5 \text{ A cm}^{-2}$) of practical interest.

We conclude, on the above basis, that a single noble gas and the binary mixture neon-argon are not promising for thermionic conversion for the following reasons:

- | | |
|-------------------|---|
| Single noble gas: | maximum electron density in a power reactor
$\sim 10^{12} \text{ cm}^{-3}$; density at sheath $\ll 10^{13} \text{ cm}^{-3}$. |
| Neon-argon: | maximum electron density in a power reactor
$\sim 10^{13} \text{ cm}^{-3}$; density at sheath $\ll 10^{13} \text{ cm}^{-3}$. |

For argon-cesium tubes, the prediction is more ambiguous. Our theories imply that argon-cesium would yield electron densities and transport currents only about twice as high as those in neon-argon. However, we find that our theoretical predictions are often much lower than the experimental results, and because we do not understand the marked increase of electron density with gas temperature observed in our argon-cesium devices we do not know how to extrapolate our experimental argon-cesium data to a practical device in a power reactor. Thus we can offer no real recommendation of the utility of the argon-cesium plasma without further basic work.

Finally we suggest that the generation by fission fragments of uniform, quiescent, well-behaved inpile plasmas of electron densities $\sim 10^{13} \text{ cm}^{-3}$ in a power reactor may find several practical applications. For example, the electron densities and temperatures in argon-cesium may prove useful for inpile magnetohydrodynamic schemes. Also it is conceivable that fission fragments may be used to generate inpile chemical plasmas for the catalytic rearrangement of radicals and hence production of chemical compounds.

ACKNOWLEDGMENTS

This work was performed under the direct supervision of Dr. Frank E. Jamerson: his encouragement, interest and guidance throughout these studies are gratefully acknowledged. The authors also wish to thank Professor David J. Rose of the Massachusetts Institute of Technology for many stimulating and enlightening discussions on plasmas. Invaluable technical assistance in the design and fabrication of the tubes and inpile test systems was given by Messrs. F.E.Gifford, R.J.Dusman, R.M.Aikin, D.M.Lee, and their contributions throughout the program are gratefully recognized. Thanks are also expressed to the University of Michigan reactor staff for their ready cooperation and help during the inpile experiments.

REFERENCES

1. C. B. Leffert, F. E. Jamerson and D. B. Rees, ONR Annual Report No. 4, Contract Nonr-3109(00), AD 425 231 (Oct. 1963).
2. C. B. Leffert, D. B. Rees and F. E. Jamerson, ONR Annual Report No. 5, Contract Nonr-3109(00), AD 609 177, (Oct. 1964).
3. C. B. Leffert, D. B. Rees and F. E. Jamerson, J. Appl. Phys., 37, 133, (1966).
4. C. B. Leffert, D. B. Rees and F. E. Gifford, ONR Annual Report No. 6, Contract Nonr-3109(00), AD 475 633, (Oct. 1965).
5. D. B. Rees, C. E. Leffert and F. E. Jamerson, Proc. IEEE Thermionic Specialists Conference (San Diego), p. 166 (1965).
6. C. B. Leffert and D. B. Rees, ONR Annual Report No. 7, Contract Nonr-3109(00), AD 806 963, (1966).
7. C. B. Leffert, D. B. Rees and F. E. Jamerson, Phys. Letters, 22, 423, (1966).

SECTION A

SECTION A

REACTION KINETICS STUDIES OF ARGON-CESIUM PLASMAS

ABSTRACT

A reaction kinetics model of argon-cesium plasma postulated a heteronuclear ion, ArCs^+ , which participates in a highly temperature-dependent reaction ($\text{ArCs}^+ + \text{Ar} \longrightarrow \text{Cs}^+ + 2\text{Ar}$). This model gives agreement with experimental measurements of electron density only if (a) unrealistically large reaction cross sections are assumed for the heteronuclear ion, ArCs^+ and (b) greatly reduced collisional radiative recombination rates (about one-tenth the values reported for the gas temperature) are assumed for the atomic ion Cs^+ . Therefore it is concluded that (a) the large experimentally observed temperature dependence of the electron density in the argon-cesium system cannot be attributed to the heteronuclear ion ArCs^+ and (b) the electron swarm temperature is appreciably higher than the gas temperature to account for the reduced collisional radiative recombination rates.

CONTENTS

ABSTRACT	
OBJECT	1
CONCLUSIONS	1
INTRODUCTION	1
MODIFIED REACTION KINETICS (II)	3
Reactions for Heteronuclear Ion $(NA)_+ = ArCs^+$	5
Reaction Rate Coefficients	5
$C_4, C_{20}, C_{14}, C_{22}$ (and C_3)	7
$C_{25}, C_{27}, C_{28}, C_{30}, C_{31}, C_{33}$	8
Coefficients Not Used	8
Diffusion Coefficients	8
Computer Code	9
RESULTS	9
Reduced Collisional Radiative Recombination Rate	10
Variation of $ArCs^+$ Reaction Rates	10
Fit of Kinetics II Model to Experimental Data	11
Effect of $\langle T_{gas} \rangle_{av}$ on Electron Density	12
Effect of Cs/Ar on Electron Density	13
Effect of Neutron Flux on Electron Density	13
REFERENCES	14
ILLUSTRATIONS	15
APPENDIX A - REACTION KINETICS CODE II	21
Table A-I. Listing of Main Program and Subroutines: NONLIN, CROUT, PUNT, ITER and FINAL	21
Table A-II. Listing of Subroutine EVAL	26
Table A-III. Example of Input Cards to Computer Cards	28
Table A-IV. Example of Output from Computer Code	29

OBJECT

The objective of these studies was to fit the inpile microwave measurements of the electron density in argon-cesium plasmas with our reaction kinetics theory modified to include the heteronuclear ion ArCs^+ .

CONCLUSIONS

1. From parametric computer studies on the argon-cesium system with the older reaction kinetics model, it was concluded that no reasonable adjustment of any combination of the 22 reaction rate coefficients could bring about a theoretical fit to the experimental microwave result. Only by introducing to the model additional volume or surface reactions with very large thermal activation energies could a fit be possible. A likely candidate appeared to be an association-dissociation volume reaction involving a postulated heteronuclear ion, ArCs^+ , which participates in a highly temperature dependent dissociation reaction ($\text{ArCs}^+ + \text{Ar} \rightarrow \text{Cs}^+ + 2\text{Ar}$).
2. By assuming a temperature dependence for the dissociation reaction of the form $C_0 \exp(-\epsilon/kT_e)$ and by adjustment of two other reaction rates it was possible to obtain a fit of the computed and experimental values for the electron density over the entire range investigated of the three independent variables of gas temperature ($\langle T_{\text{gas}} \rangle_{\text{av}}$), cesium to argon ratio (Cs/Ar) and neutron flux (ϕ).
3. The fit was obtained with a reasonable activation energy of $\epsilon = 0.74$ volts but the magnitude of the coefficient ($C_0 = 2.4 \times 10^{-5} \text{ cm}^3 \text{ sec}^{-1}$) was many orders of magnitude higher than could be expected on physical grounds and we cannot, therefore, attribute the extreme temperature dependence of the electron density in our argon-cesium plasmas to the presence of ArCs^+ alone.
4. In order to fit the experimental data, particularly for low Cs/Ar , it was necessary to reduce the collisional radiative recombination rate by a factor of 10. This implies an electron temperature in the plasma appreciably higher than the gas temperature ($T_e \sim 1.5 \langle T_{\text{gas}} \rangle_{\text{av}}$).

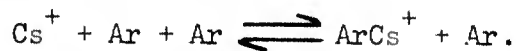
INTRODUCTION

Inpile microwave measurements of the electron density in mixed gas plasmas have been reported previously.¹ The measured electron densities in the neon-argon plasma agreed fairly well with predicted values from our reaction kinetics theory (I).² The measured electron densities in various argon-cesium plasmas also agreed fairly well in magnitude and gross trends with this theory but showed appreciable differences in the fine structure of the data.¹ As the cesium concentration in the argon was varied by changing the cesium bath temperature (at constant neutron flux) the electron density passed through a maximum value as expected but at a cesium concentration much lower than that predicted.³ Also an unexpected phenomenon was

that the electron density was very sensitive to the temperature of the cavity walls. Several processes, additional to those included in the reaction kinetics equations, were considered in an attempt to explain this anomalous temperature variation of the electron density but no convincing explanation was found.¹ One of the processes that had not been included in the original reaction kinetics equations but which we thought might explain some of the anomalous behavior was the process involving the production and destruction of the heteronuclear ion, ArCs^+ . It had been concluded, however, that the neglect of this particular ion would not in itself account for all of the differences between theory and experiment.¹

This ion (ArCs^+) has been observed in mass spectrograph analyses by Herman and Chermak⁴ and Channin⁵ but little is known about the reaction rates leading to its formation or destruction. We had decided from the reaction kinetics studies already carried out on the Ar-Cs system that evidently one (or a combination) of the missing reactions had an extremely high temperature dependence — even much higher than the very important collisional radiative recombination rate which varies as T^{-5} .⁶ Therefore if the anomalous behavior was to be connected to ArCs^+ there must surely have been some production and/or destruction reaction of ArCs^+ that was extremely temperature sensitive.

Some association-dissociation reactions are known to exhibit very sensitive temperature dependences. For example with electron attachment and detachment to molecular oxygen, O_2 , the two-body collisional detachment coefficient for O_2^- increases from $9 \times 10^{-17} \text{ cm}^3/\text{sec}$ at 375°K to $1.4 \times 10^{-14} \text{ cm}^3/\text{sec}$ at 575°K where the electron affinity is 0.43 eV .⁷ We have already observed that for our microwave measurements of electron density versus (inverse) temperature that the data could be fitted with the exponential function $n = n_0 \exp [-\xi / (kT/e)]$ with an "activation energy" $\xi = 0.22 \text{ eV}$. It seemed hopeful, therefore, that we might be able to explain our results with an association-dissociation reaction like



This report presents the results of a computer study to fit a revised model (II) of the reaction kinetics (including ArCs^+) to the inpile Ar-Cs microwave data.

MODIFIED REACTION KINETICS (II)

Our previous reaction kinetics theory for a plasma generated by fission fragment ionization of a Penning-type gas mixture has been described in several previous reports.^{8,2,9} The equations for this first model (I) are the continuity equations (2) through (7) in Table I (but including only the terms through C_{22}) and the charge neutrality equation

$$n_e - N_+ - N_{2+} - A_+ - A_{2+} - (NA)_+ = 0 \quad (1)$$

where

$$\begin{aligned} n_e &= \text{electron density} \\ N_o, N_m, N_x &= \text{neutral, metastable excited and} \\ &\quad \text{non-metastable excited state} \\ &\quad \text{densities of the major gas} \\ N_+, N_{2+} &= \text{atomic ion and molecular ion} \\ &\quad \text{densities of the major gas} \\ A_o, A_+, A_{2+} &= \text{neutral, atomic ion and molecular} \\ &\quad \text{ion densities of the minor gas} \\ \text{and } (NA)_+ &= \text{heteronuclear ion density (not} \\ &\quad \text{included in kinetics I model).} \end{aligned}$$

For a more detailed discussion of the various terms in the equations for the first model (I) the reader is referred to our previous report.^{8,2}

The modifications to the reaction kinetics (for Model II) include a generalized heteronuclear ion $(NA)_+$ in Eq. 1 with its rate Eq. 8 (Table I) and rate coefficients C_{23} to C_{34} in Table I. These will be discussed next for the specific heteronuclear ion $ArCs^+$ in the binary gas system argon-cesium.

TABLE I. Particle density equations for binary gas plasma.

Time Deriv- ative Flux	Diffusion	2- and 3-Body Recombination	3-Body Molecular Ion Formation	2-Body Ion Charge Exchange	Metastable- Metastable Collisions	Radia- tion	Molecular Ion Forma- tion Via N_x	Metastable Destruction Via N_o	Penning Ioniza- tion	2-and 3-Body Dissociation
(2) $\frac{dN_1}{dt} = \frac{S_1 N_o}{\Lambda^2}$	$\frac{-K_1 N_1}{N_o \Lambda^2}$	$-C_1 + C_2 N_o + C_3 n_e \left[\frac{N_1}{N_o} \right] N_1 n_e$	$\frac{C_1 N_1 N_2}{N_o \Lambda^2} - C_3 N_1 A_o N_o - C_2 N_1 A_o N_o - C_2 N_1 A_o N_o^2$	$-C_6 N_1 A_o$	$+C_7 N_1^2$					
(3) $\frac{dN_2}{dt} = \frac{K_2 N_2}{N_o \Lambda^2}$	$\frac{K_2 N_2}{N_o \Lambda^2}$	$-C_{16} N_2 n_e$	$\frac{C_4 N_2 N_2}{N_o \Lambda^2} + C_5 N_2 A_o N_o$	$-C_{17} N_2 A_o - C_{26} N_2 A_o$			$+C_9 N_2 N_o$			
(4) $\frac{dN_x}{dt} = \frac{S_x N_o}{\Lambda^2}$		$+C_8 \left[C_1 + C_2 N_o + C_3 n_e \right] N_x n_e$				$-\frac{N_x}{\tau x}$	$-C_9 N_x N_o$			
(5) $\frac{dN_m}{dt} = \frac{S_m N_o}{\Lambda^2}$	$\frac{K_m N_m}{N_o \Lambda^2}$	$+C_{11} \left[C_1 + C_2 N_o + C_3 n_e \right] N_m n_e + \frac{C_{11} C_{11} N_m^2 n_e}{N_o \Lambda^2}$			$-C_{12} N_m^2$		$-C_{13} N_m N_o - C_{14} N_m^2 N_o$	$-C_{13} N_m N_o - C_{14} N_m^2 N_o$	$-C_{15} N_m A_o - C_{25} N_m A_o$	
(6) $\frac{dA_+}{dt} = \frac{K_+ A_+}{N_o \Lambda^2}$	$\frac{-K_+ A_+}{N_o \Lambda^2}$	$- \left[C_{18} + C_{19} N_o + C_{22} n_e \right] A_+ n_e$	$\frac{C_{20} A_+ A_o N_o}{N_o \Lambda^2} - C_{27} A_+ N_o - C_{28} A_+ A_o N_o$	$+C_9 N_1 A_o + C_{17} N_2 A_o$			$+C_{15} N_1 A_o$		$+C_{31} (NA)_+ N_o + C_{32} (NA)_+ N_o^2$	
(7) $\frac{dA_{2+}}{dt} = \frac{K_{2+} A_{2+}}{N_o \Lambda^2}$	$\frac{K_{2+} A_{2+}}{N_o \Lambda^2}$	$-C_{21} A_{2+} n_e$	$\frac{C_{20} A_{2+} A_o N_o}{N_o \Lambda^2}$	$-C_{29} A_{2+} N_o$					$+C_{33} (NA)_+ A_o + C_{34} (NA)_+ A_o N_o$	
(8) $\frac{d(NA)_+}{dt} = \frac{-K_{-} (NA)_+}{N_o \Lambda^2}$	$\frac{-K_{-} (NA)_+}{N_o \Lambda^2}$	$-C_{30} (NA)_+ n_e$	$+C_{23} N_1 A_o N_o + C_{24} N_1 A_o N_o^2 + C_{27} A_{2+} N_o^2 + C_{28} A_{2+} A_o N_o$	$+C_{26} N_2 A_o + C_{29} A_{2+} N_o$				$+C_{25} N_1 A_o - C_{31} (NA)_+ N_o - C_{32} (NA)_+ N_o^2$	$-C_{33} (NA)_+ A_o - C_{34} (NA)_+ A_o N_o$	

Reactions for Heteronuclear Ion $(NA)_+ = ArCs^+$

Very little is known about the heteronuclear ion $ArCs^+$. The following Table II is a list of those 2- and 3-body reactions which were considered as possibly important to the production or destruction of $ArCs^+$.

TABLE II. Possible reactions involving $ArCs^+$.

Reaction Rate Coefficient	Reaction		Used
C_{23}	$Ar^+ + Cs + Ar$	$\longrightarrow ArCs^+ + Ar$	
C_{24}	$Ar^+ + Cs + Cs$	$\longrightarrow ArCs^+ + Cs$	
C_{25}	$Ar^m + Cs$	$\longrightarrow ArCs^+ + e^-$	Yes
C_{26}	$Ar_2^+ + Cs$	$\longrightarrow ArCs^+ + Ar$	
C_{27}	$Cs^+ + Ar + Ar$	$\longrightarrow ArCs^+ + Ar$	Yes
C_{28}	$Cs^+ + Cs + Ar$	$\longrightarrow ArCs^+ + Cs$	Yes
C_{29}	$Cs_2^+ + Ar$	$\longrightarrow ArCs^+ + Cs$	
C_{30}	$ArCs^+ + e^-$	$\longrightarrow Cs + Ar$	Yes
C_{31}	$ArCs^+ + Ar$	$\longrightarrow Cs^+ + Ar + Ar$	Yes
C_{32}	$ArCs^+ + Ar + Ar$	$\longrightarrow Cs^+ + Ar + Ar + Ar$	
C_{33}	$ArCs^+ + Cs$	$\longrightarrow Cs_2^+ + Ar$	Yes
C_{34}	$ArCs^+ + Cs + Ar$	$\longrightarrow Cs_2^+ + 2Ar$	

The reaction kinetics computer code (for the solution of simultaneous non-linear equations) was modified to include these 12 additional terms as shown in Table II but only 6 of these coefficients were actually used in the parameter studies (the remaining 6 coefficients were set to zero as discussed below). A flow diagram of this kinetics model (II) is shown in Fig. 1 neglecting the non-metastable excited states of argon (Ar^*).

Reaction Rate Coefficients

The values of the various argon-cesium reaction rate coefficients for Reaction Kinetics I have been presented before.² Four of these values have been updated* as follows:

*Changes of this magnitude (and larger) in the Reaction Kinetics I coefficients ($C_1 \longrightarrow C_{22}$) have shown no appreciable effect on the temperature dependence $\partial n_e / \partial T_{gas}$ and it was precisely this absence of effect that led to the search for another temperature dependent ion.

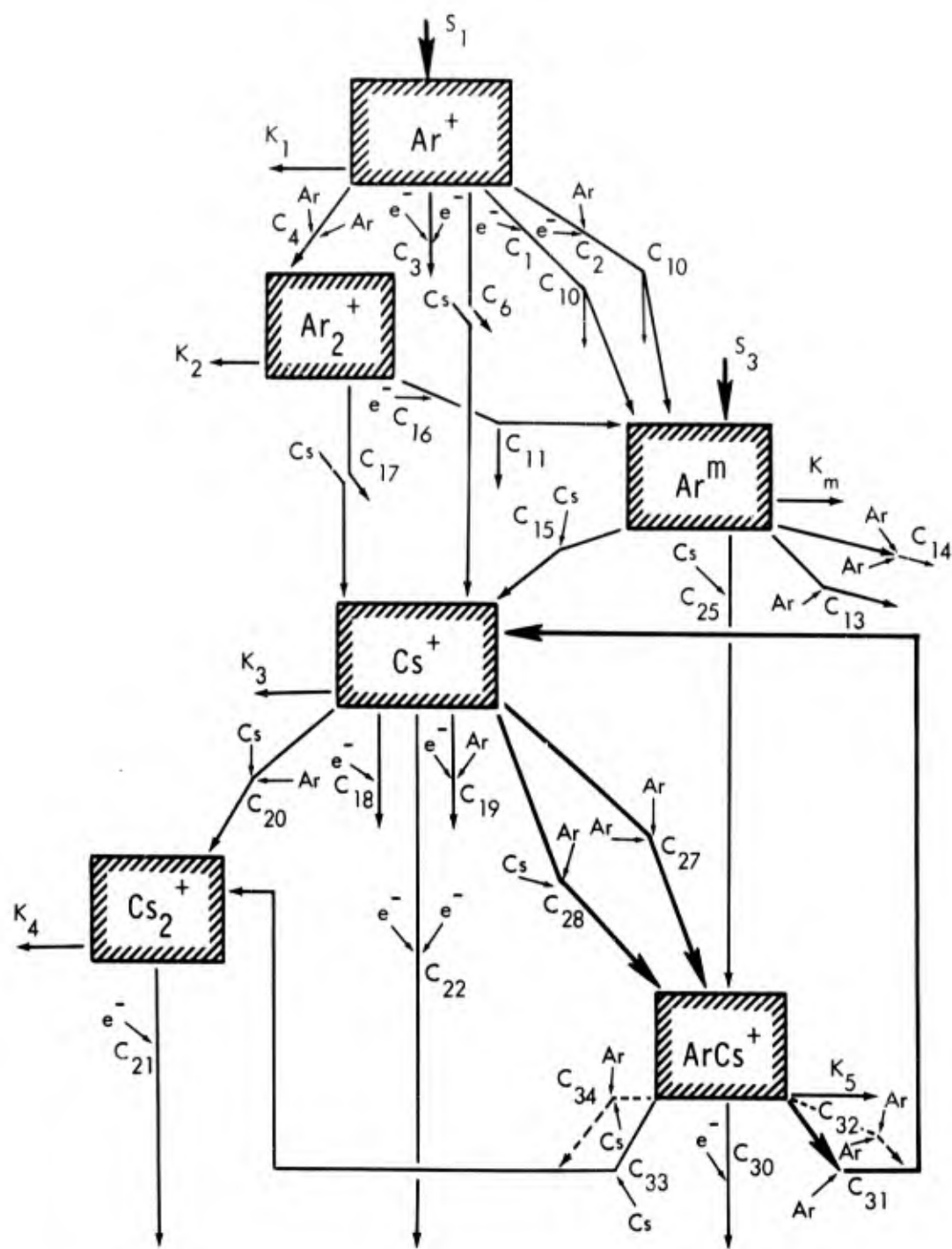


Fig. 1. Flow diagram for Reaction Kinetics II Model. The non-metastable excited states of argon Ar^* are neglected here.

C₄, Three-Body Molecular Ion Formation (Ar⁺ to Ar₂⁺): A more recent value for the conversion frequency of this reaction is $\nu = 71 \text{ p}^2 \text{ sec}^{-1(10)}$ which yields a value of $C_4 = 6.8 \times 10^{-32} \text{ cm}^6 \text{ sec}^{-1}$ or a value of about 1/8 the previous value.

C₂₀, Three-Body Molecular Ion Formation (Cs⁺ to Cs₂⁺): The previous calculation of this reaction rate from classical collision probability theory⁽²⁾ was corrected. The new value is one-third that used previously or $C_{20} = 1.6 \times 10^{-31} \text{ cm}^6 \text{ sec}^{-1}$.

C₁₄, Three-Body Volume Destruction of Metastable States: The previous value for the 3-body destruction of argon metastable states by argon atoms was determined by Phelps and Molnar¹¹ $\nu(300^\circ\text{K}) = 9 \text{ p}^2$. Somewhat later Futch and Grant¹² obtained $\nu(300^\circ\text{K}) = 13.5 \text{ p}^2$ and $\nu(77^\circ\text{K}) = 440 \text{ p}^2$. These two points were fitted by a straight line on log-log paper to give $C_{14} = 2.22 \times 10^{-26} T^{-5/2} \text{ cm}^6 \text{ sec}^{-1}$.

C₂₂ (and C₃), Collisional Radiative Recombination for Cs⁺ (and Ar⁺): A detailed discussion of this recombination process is presented in Reference 2. For the collisional dominated range of interest here ($T_e \leq 1300^\circ\text{K}, n_e \leq 10^{12} \text{ cm}^{-3}$) the following expression was obtained

$$C_{22}, C_3 = 2.7 \times 10^{-19} (250/T_e)^5 \text{ cm}^6 \text{ sec}^{-1}$$

where T_e is the electron temperature. In the past we have argued that the hot electrons from the primary fission ionization process (and from the Penning ionization process) are thermalized in times very short compared with the time for recombination and have assumed that the effective electron temperature is approximately equal to the average gas temperature, i.e. $T_e = \langle T_{\text{gas}} \rangle_{\text{av}}$. It will be pointed out later in this report that a fit to the experimental data could be obtained only if this important reaction rate was reduced by a factor of 10. This implies that the electrons are indeed hotter than the gas but this point will be discussed later.

For the Reaction Kinetics II Model with ArCs⁺ it was decided to try to fit the data using only the following additional six coefficients.*

*For the analysis of the argon-cesium inpile microwave data with the Reaction Kinetics theory, we used an ion source rate (S_1) averaged over the volume of the microwave cavity. S_1 was obtained from a pure argon run on the Q00 Ion Generation Rate Code as $S_1 = \langle S_+(\vec{r}) \rangle_{\text{av}} / N_0 = 2.40 \times 10^{-3} \text{ sec}^{-1}$ for a neutron flux of $\phi = 1.0 \times 10^{13} \text{ cm}^{-2} \text{ sec}^{-1}$. A calibration of the neutron flux gave $\phi = 1.44 \times 10^{13} \text{ cm}^{-2} \text{ sec}^{-1}$ at a reactor power of $P = 2.0 \text{ MW}$ so we have $S_1 = \langle S_+(\vec{r}) \rangle_{\text{av}} / N_0 P = 1.73 \times 10^{-3} \text{ sec}^{-1} \text{ MW}^{-1}$.

C₂₅, Penning-type Production of ArCs⁺ via Ar^m: This reaction rate coefficient was set equal to the Penning reaction rate coefficient C₁₅ (i.e., Ar^m+Cs → Ar+Cs⁺+e⁻) so C₂₅=C₁₅=4.6x10⁻¹⁰ cm³sec⁻¹. Some code runs were made where this coefficient was varied but this variation had little effect on the overall result.

C₂₇, C₂₈ Production of ArCs⁺ by 3-Body Attachment: These coefficients were arbitrarily varied as described later.

C₃₀, Dissociative Recombination Coefficient for ArCs⁺: This reaction rate coefficient was expected to be large and was set equal to the dissociative recombination coefficient for Cs₂⁺⁽²⁾ i.e. C₃₀=C₂₁=2.0x10⁻⁶ cm³sec⁻¹.

C₃₁, C₃₃, Dissociation of ArCs⁺ by 2-Body Collisions with Neutral Atoms: C₃₁ is the reaction rate coefficient (ArCs⁺+Ar → Cs⁺+2Ar) upon which most of the burden of the extreme temperature dependence is to be placed. C₃₃ is set equal to C₃₁ and both are varied as described later.

Coefficients Not Used: The reactions corresponding to the reaction rate coefficients C₂₃, C₂₄, C₂₆ and C₂₉ in Table II were not used because it was known from previous reaction kinetics studies that over the range of conditions of interest the concentrations of other ions (Ar⁺, Ar₂⁺, Cs₂⁺) were small compared to the concentration of the atomic cesium ion Cs⁺. The 3-body reaction corresponding to the rate coefficient C₃₂ was not used since its rate should be small compared to the 2-body dissociation reaction corresponding to the rate coefficient C₃₁ where momentum can be conserved by the third particle produced in the reaction. The reaction corresponding to the rate coefficient C₃₄ in Table II was not used since both molecular ions are assumed to recombine dissociatively at the same rate (C₃₀=C₂₁).

Diffusion Coefficients

The ambipolar diffusion coefficients D_a for the positive ions at a temperature T, °K are determined from measurements of the ion mobility μ_o⁺ (at standard conditions of 273°K and 760 torr) by the expression D_a=(2kT/e)μ_o⁺. The ambipolar diffusion coefficient K_a at unit neutral atom density (i.e. D_a/2.69x10¹⁹) and 300°K is K_a=1.4x10¹⁸ μ_o⁺ cm⁻¹sec⁻¹ where μ_o⁺ is in units of cm²(volt·sec)⁻¹. Values (K₁ to K₄) of K_a for the ions Ar⁺, Ar₂⁺, Cs⁺ and Cs₂⁺

were derived in Reference 2. The value of K_5 for the heteronuclear ion ArCs^+ was taken equal to K_4 for Cs_2^+ . For these studies the electron temperature was assumed equal to the gas temperature so the variation of the diffusion coefficients with the average gas temperature was

$$K_i(\langle T_{\text{gas}} \rangle_{\text{av}}) = K_{i,a}(300^\circ\text{K}) \times \left(\frac{\langle T_{\text{gas}} \rangle_{\text{av}}}{300} \right)$$

where the temperature is measured in $^\circ\text{K}$.

Computer Code

The Reaction Kinetics I code was modified to include the additional diffusion term K_5 and the additional volume processes C_{23} to C_{34} as shown in Table I for the ArCs^+ reactions listed in Table II. A listing of the Reaction Kinetics I code had not been published previously so a listing of the entire Reaction Kinetics II code is presented in Appendix A. The main control program is presented in Table A-I. The subroutines NONLIN, CROUT, PUNT, ITER and FINAL for the solution of N simultaneous non-linear algebraic equations in N unknowns had been coded by E. Stoneking for the IBM 7094 computer using the double precision Fortran IV language.¹³ The method of functional iteration is used and is equivalent to an N-dimensional Newton's method.¹⁴

The subroutine EVAL is given in Table A-II for the N=8 equations and the various partial derivatives. An example of the input to the code is given in Table A-III and an example of the output in Table A-IV.

RESULTS

The experimental microwave measurements of the electron density in argon-cesium plasmas were presented in the preceding ONR annual report for 1966¹ together with the computed curves from the reaction kinetics theory I. These data are again presented in Figs. 2 to 6 where the experimental data are shown as points and the previous predictions from the reaction kinetics I model are shown by the dashed curves. The new curves from the reaction kinetics II model are the solid curves. The steps required to fit the new model to the experimental data will now be discussed.

Reduced Collisional Radiative Recombination Rate

Introducing the heteronuclear ion ArCs^+ to the reaction kinetics model will tend to decrease the computed electron density. This comes about since most of the production reactions of ArCs^+ (Table II) involve the destruction of another ion. Only the production reaction from the metastable argon (C_{25}) can produce a new ion but this reaction competes with the production of the atomic ion Cs^+ (C_{15}). On the other hand the dissociative recombination reaction (C_{30}) can be expected to proceed very rapidly which would lower the electron density.

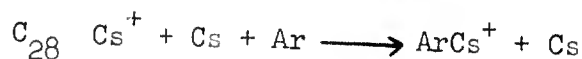
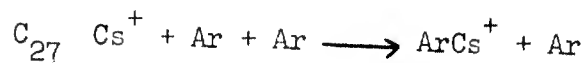
A comparison of the experimental data with the predicted values from the kinetics I model for low values of Cs/Ar (see Figs. 2 and 6) show that the computed values are as much as a factor of two too low. From previous reaction kinetics studies the only reasonable way to affect such an increase in the computed electron density would be to decrease the collisional radiative recombination rate — which implies an elevated electron temperature* in contrast to our previous assumption that $T_e \approx \langle T_{\text{gas}} \rangle_{\text{av}}$. To obtain a fair fit with the experimental data, the collisional radiative recombination rate was decreased by a factor of 10 so that the expression (for the collisional dominated range) became

$$C_{22}, C_3 = 2.7 \times 10^{-20} (250 / \langle T_{\text{gas}} \rangle_{\text{av}})^5 \text{ cm}^6 \text{ sec}^{-1}.$$

If this reaction rate is written as $2.7 \times 10^{-19} (\langle T_{\text{gas}} \rangle_{\text{av}} / T_e)^5 \times (250 / \langle T_{\text{gas}} \rangle_{\text{av}})^5$ such that $(\langle T_{\text{gas}} \rangle_{\text{av}} / T_e)^5 = 10^{-1}$, then $T_e \approx 950^\circ\text{K}$ for $\langle T_{\text{gas}} \rangle_{\text{av}} = 600^\circ\text{K}$ and the effective electron temperature is about 350°C better than the gas atoms.

Variation of ArCs^+ Reaction Rates

The primary reactions involved in the association-dissociation of ArCs^+ are the two production reactions



and the dissociation reaction



*Subsequent to the studies described here, a computation of the electron temperature from detailed energy balance considerations by D. B. Rees showed the electron temperature to be considerably higher than the gas temperature for most of our experimental conditions.¹⁵

The dependence of the concentration of ArCs^+ on the gas composition (Cs/Ar) is built into the first two production reactions and the dependence of the concentration of ArCs^+ on gas temperature was built into the last dissociation reaction. After some variation of these reaction rate coefficients a fair fit to the data was obtained with the following values:

$$C_{27} = 1.0 \times 10^{-34} \text{ cm}^6 \text{ sec}^{-1}$$

$$C_{28} = 1.0 \times 10^{-28} \text{ cm}^6 \text{ sec}^{-1}$$

$$C_{31} = 2.4 \times 10^{-5} \exp[-0.74/(kT/e)] \text{ cm}^3 \text{ sec}^{-1}$$

Only the magnitude of the first reaction rate (C_{27}) is physically realistic. The second reaction is at least one order of magnitude too high since the 3-body gas-kinetic collisional rate of the two neutral atoms and the ion, apart from the probability of a particular interaction is only about $1.5 \times 10^{-29} \text{ cm}^6 \text{ sec}^{-1}$. The leading factor of the last reaction is many orders of magnitude too large since the 2-body gas-kinetic collisional rate between the ion and neutral atom is only about $7 \times 10^{-9} \text{ cm}^3 \text{ sec}^{-1}$. It was concluded from these studies that the anomalous behavior of our argon-cesium plasmas could not be attributed to the presence of the heteronuclear ion ArCs^+ . Nevertheless the fit of the Kinetics II model (consider now as Kinetics I model with three additional adjustable coefficients) to the experimental data was sufficiently good that the fit to the data will be described next in some detail.

Fit of Kinetics II Model to Experimental Data

In view of the fact that the magnitude of the ArCs^+ reaction rate coefficients needed to fit the experimental data were physically unrealistic these additional coefficients should henceforth be viewed only as adjustable parameters to aid in curve fitting. As will be seen in the discussion to follow, the fit to the data is good compared to the predicted values from the reaction Kinetics I model. It is beneficial to have a mathematical model that fits the experimental data well for purposes of analysis and interpolation, however without a solid physical basis such a model has little extrapolation value for predicting results outside the range of proven agreement. In these studies it was assumed as before¹ that the electron density was uniform over the volume of the microwave cavity and the computed

values are those at the center of the cavity. Later studies¹⁵ have shown that the electron density does decrease with increasing distance from the center along the radius. This correction would decrease the computed values by about 20% and would require some further adjustment of the rate coefficients to reestablish the present fit. The main effect of this correction would be to decrease further the collisional radiative recombination rate (C_{22}) (increased electron temperature). However, the major conclusions would be unchanged since the magnitude of the ArCs^+ rate coefficients were determined more from fitting the temperature dependence of the electron density (dn_e/dt) rather than the magnitude of n_e .

Effect of $\langle T_{\text{gas}} \rangle_{\text{av}}$ on Electron Density: Three experimental runs at different constant values of Cs/Ar had been made to establish the dependence of the electron density on the average gas temperature (i.e. the average cavity wall temperature). The cavity wall temperature variation was obtained by varying the cooling gas flow rate to the uranium wall of the microwave cavity and at the same time adjusting the cooling flow to the cesium bath to maintain a constant Cs/Ar . These runs were made at different values of neutron flux to obtain the maximum temperature variation.

The experimental data and computed curves for these three runs are shown in Fig. 2 for a low $\text{Cs}/\text{Ar}=1.0 \times 10^{-6}$, in Fig. 3 for a medium $\text{Cs}/\text{Ar}=5.6 \times 10^{-5}$ and in Fig. 4 for a high $\text{Cs}/\text{Ar}=1.0 \times 10^{-3}$. For a low Cs/Ar (Fig. 2) the modified reaction Kinetics II curve exhibits a very strong temperature dependence in agreement with the experimental data (and in contrast to the Kinetics I curve) but the magnitude of the predicted values are still somewhat low. This indicates that, at least at low Cs/Ar , the collisional radiative recombination rate (C_{22}) could be reduced even further (indicating an ever higher electron temperature).

At a medium value of Cs/Ar (Fig. 3), the Kinetics II curve for electron density agrees well with the experimental data in both magnitude and temperature dependence. The Kinetics I model predicted approximately the correct magnitude of the electron density but the temperature dependence was too weak.

At a high value of Cs/Ar (Fig. 4) the Kinetics II model again fits the experimental data well in both magnitude and temperature dependence. In this

range of Cs/Ar the Kinetics I model had predicted values too high. Nevertheless even with the reduced collisional radiative recombination rate in the Kinetics II model, the higher concentration of cesium produced more ArCs^+ (via C_{28}) and therefore a greater loss of ions (via C_{30}) and a smaller electron density.

Effect of Cs/Ar on Electron Density: Two experimental runs were made in which the Cs/Ar was varied while holding the average gas temperature $\langle T_{\text{gas}} \rangle_{\text{av}}$ constant. The first run at the lower $\langle T_{\text{gas}} \rangle_{\text{av}} = 576^\circ\text{K}$ is shown in Fig. 5 and the neutron flux was $0.72 \times 10^{13} \text{ cm}^{-2} \text{ sec}^{-1}$. The second run at a higher $\langle T_{\text{gas}} \rangle_{\text{av}} = 644^\circ\text{K}$ is shown in Fig. 6 and the neutron flux was also higher at $1.44 \times 10^{13} \text{ cm}^{-2} \text{ sec}^{-1}$. In both of these runs the curve from the Kinetics II model fits the data much better than that from the Kinetics I model. In particular the maximum in the curve of n_e vs Cs/Ar is shifted to a much lower value of Cs/Ar more in agreement with the maximum in the experimental data.

Effect of Neutron Flux on Electron Density: One experimental run was made in which the neutron flux was varied while holding constant the Cs/Ar at 4.19×10^{-5} and the average gas temperature $\langle T_{\text{gas}} \rangle_{\text{av}}$ at 644°K . These data are shown in Fig. 7 together with the predicted curve from the Kinetics II model. The part of the curve for the Kinetics I model was drawn through a point taken from Fig. 6. The fit of the Kinetics II curve in Fig. 7 to the experimental data is good and considerably better than that predicted from the Kinetics I model.

REFERENCES

1. C. B. Leffert and D. B. Rees, ONR Annual Report No. 7, Contract Nonr-3109(00), (Oct. 1966).
2. C. B. Leffert, D. B. Rees and F. E. Gifford, ONR Annual Report No. 6, Contract Nonr-3109(00), (Oct. 1965)
3. C. B. Leffert, D. B. Rees and F. E. Jamerson, Phys. Letters, 22, 423 (1966).
4. Z. Herman and V. Cermak, Nature, 199, 588 (1963).
5. L. M. Chanin, Proc. IEEE Thermionic Specialist Conference (Palo Alto) (Oct. 1967).
6. D. R. Bates, A. E. Kingston, and R. W. P. McWhirter, Proc. Roy. Soc., A267, 297 (1962) and A270, 155 (1962); also D. R. Bates and A. E. Kingston, Proc. Phys. Soc., 83, 43 (1964).
7. J. L. Pack and A. V. Phelps, J. Chem. Phys. 44, 1870 (1966).
8. C. B. Leffert, D. B. Rees and F. E. Jamerson, ONR Annual Report No. 5, Contract Nonr-3109(00), (Oct. 1964).
9. D. B. Rees, C. B. Leffert, and F. E. Jamerson, Proc. IEEE Thermionic Specialist Conference (San Diego) (Oct. 1965).
10. F. E. Niles and W. W. Robertson, J. Chem. Phys. 43, 1076 (1965).
11. A. V. Phelps and J. P. Molnar, Phys. Rev. 89, 1202 (1953).
12. A. H. Futch and F. A. Grant, Phys. Rev. 104, 356 (1956).
13. F. Stoneking, DAC-1 Library Subroutines Manual, FS NON p 8-4-1, Computer Tech. Dept. (4-30-65) (Note: This version was coded in the NOMAD language.)
14. A. Householder, Principles of Numerical Analysis, p.175, McGraw-Hill (1953).
15. C. B. Leffert and D. B. Rees, ONR Annual Report No. 8, Section B, Contract Nonr-3109(00), (Oct. 1967).

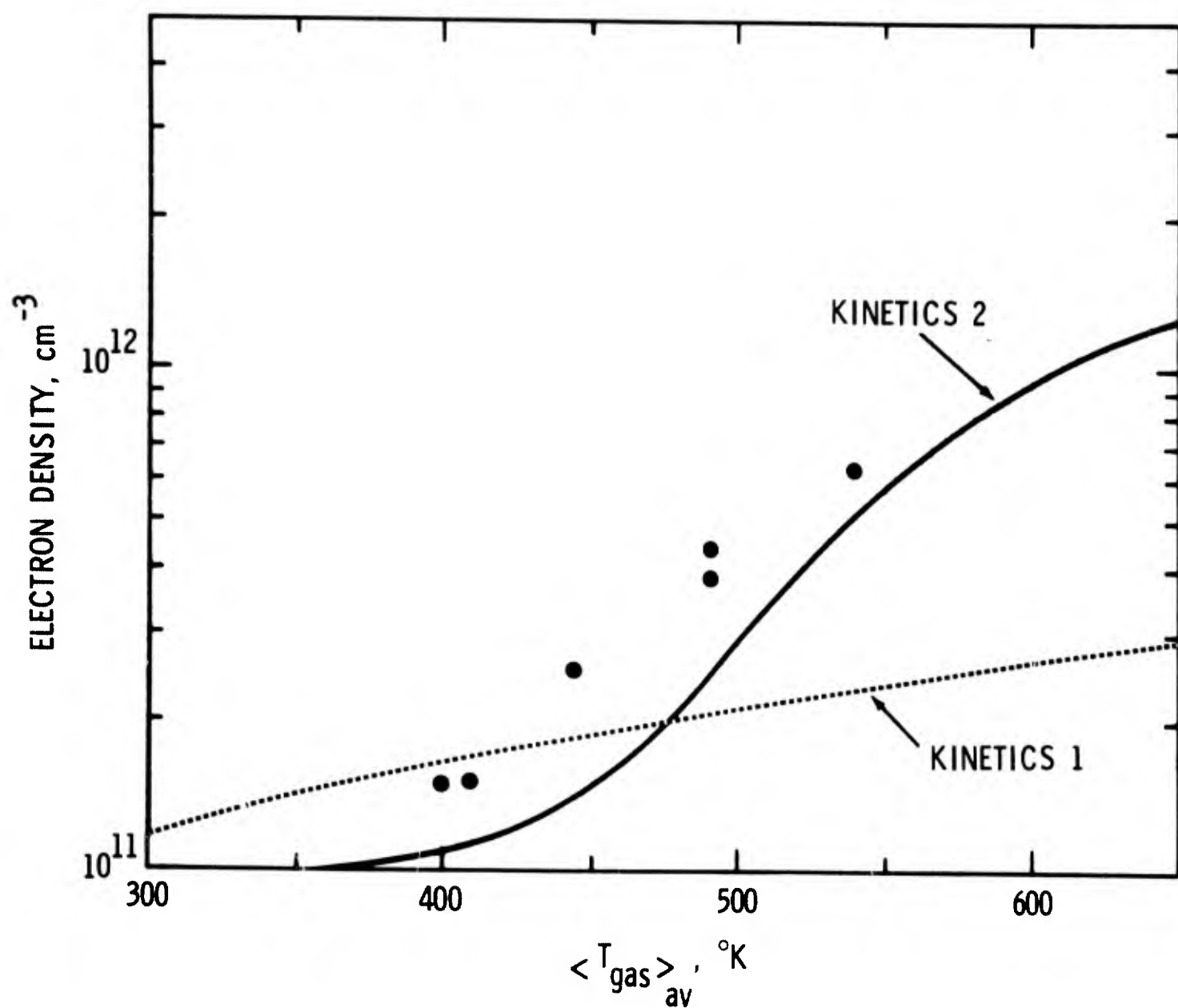


Fig. 2. Electron density versus $\langle T_{\text{gas}} \rangle_{\text{av}}$ for low $\text{Cs}/\text{Ar} = 1.0 \times 10^{-6}$. Neutron flux was $7.3 \times 10^{12} \text{ cm}^{-2} \text{ sec}^{-1}$.

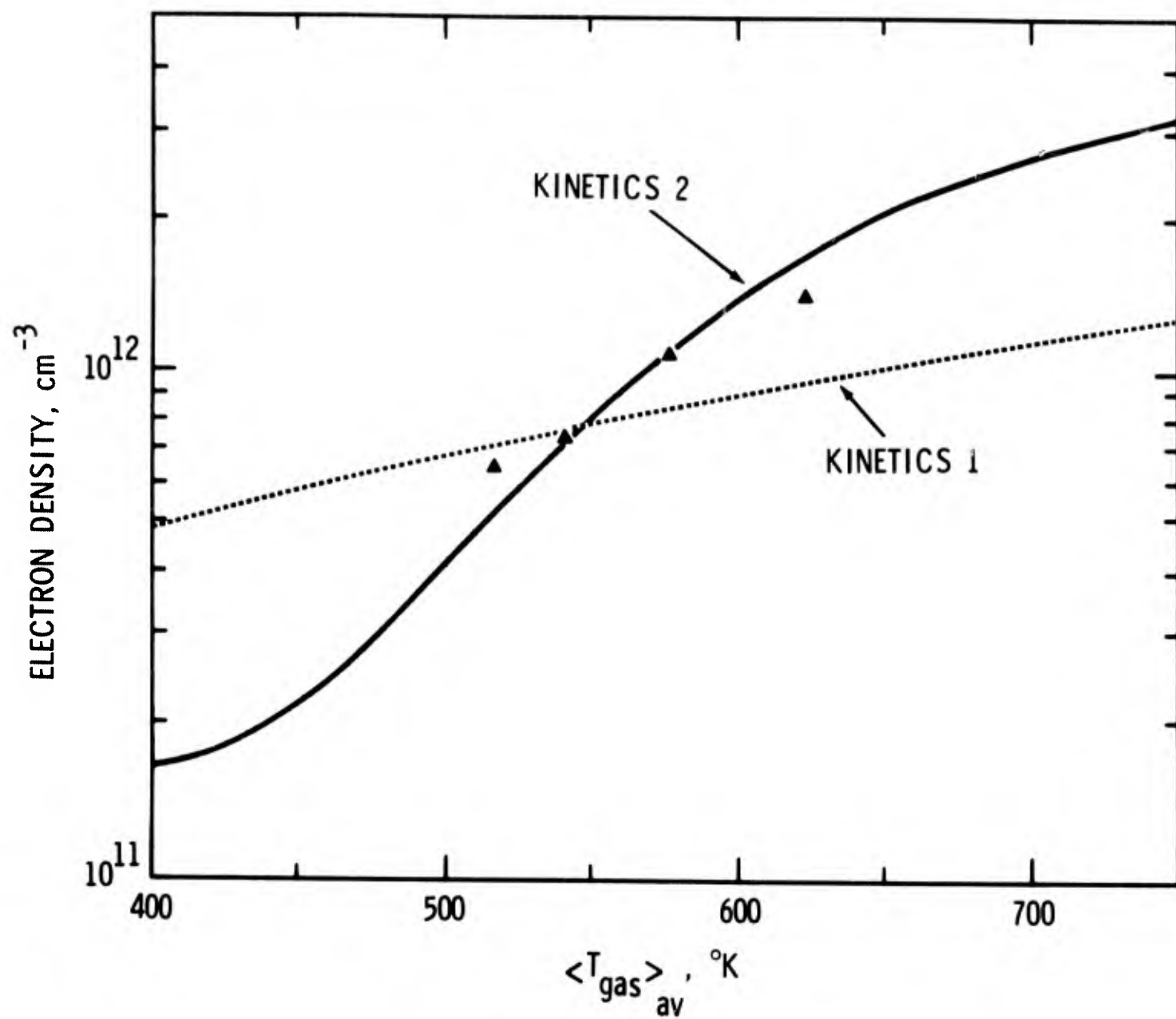


Fig. 3. Electron density versus $\langle T_{\text{gas}} \rangle_{\text{av}}$ for medium Cs/Ar- 5.6×10^{-5} .
Neutron flux was $1.0 \times 10^{-13} \text{ cm}^{-2} \text{ sec}^{-1}$.

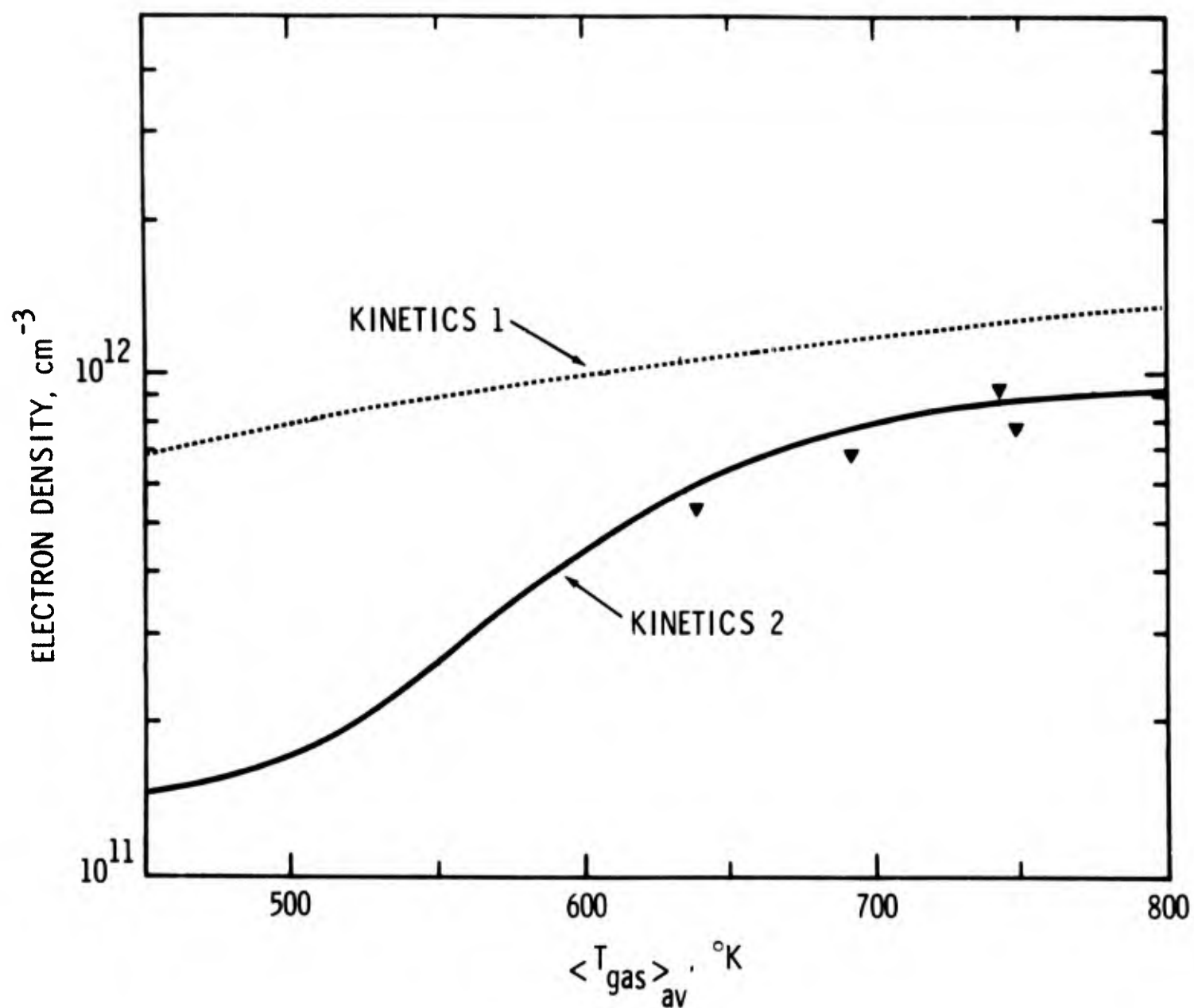


Fig. 4. Electron density versus $\langle T_{\text{gas}} \rangle_{\text{av}}$ for high $\text{Cs}/\text{Ar} = 1.0 \times 10^{-3}$.
Neutron flux was $1.22 \times 10^{15} \text{ cm}^{-2} \text{ sec}^{-1}$.

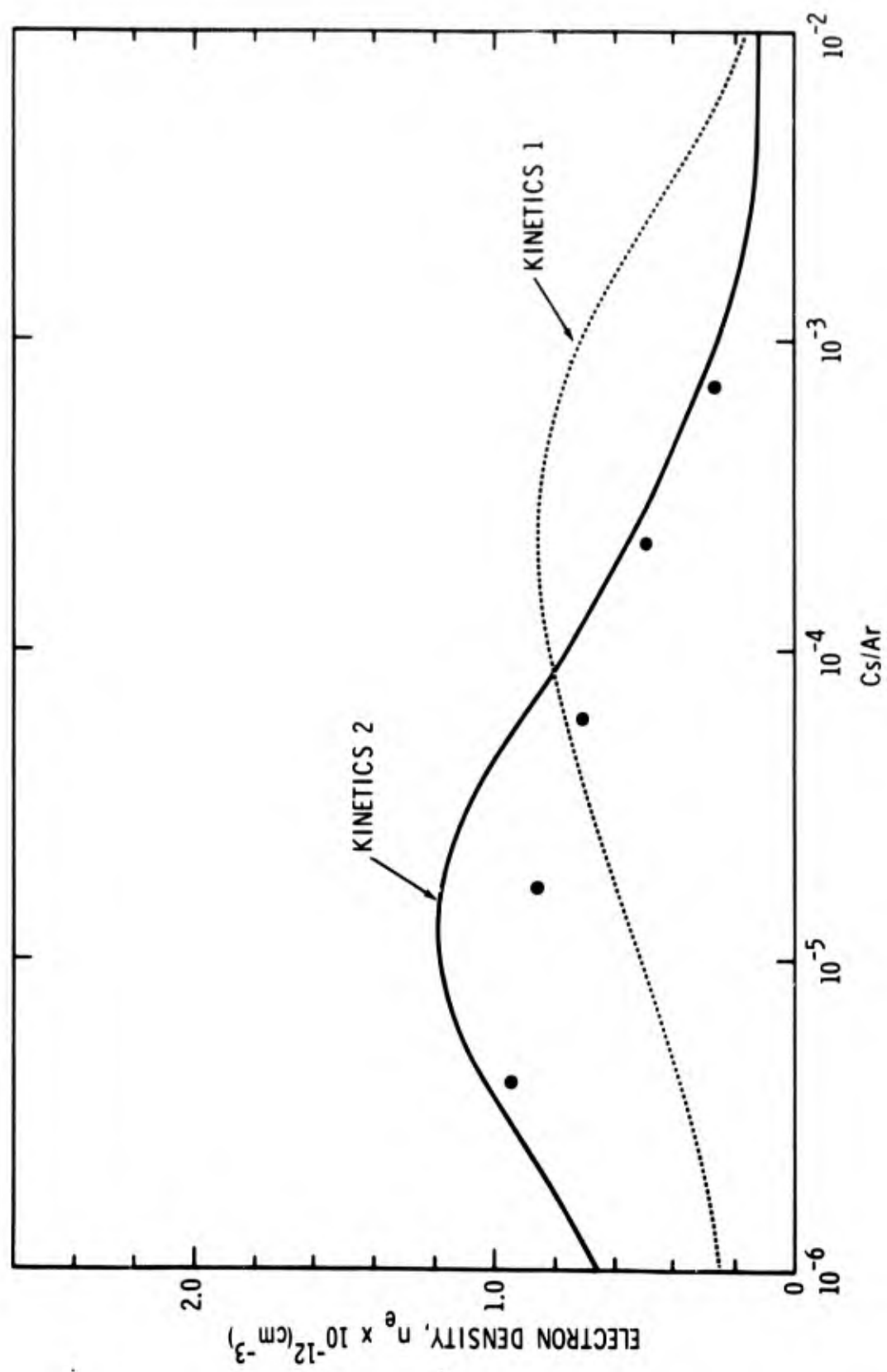


Fig. 5. Electron density versus Cs/Ar for $\langle T_{\text{gas}} \rangle_{\text{av}} = 576^\circ\text{K}$. The neutron flux was $0.72 \times 10^{13} \text{ cm}^{-2} \text{ sec}^{-1}$.

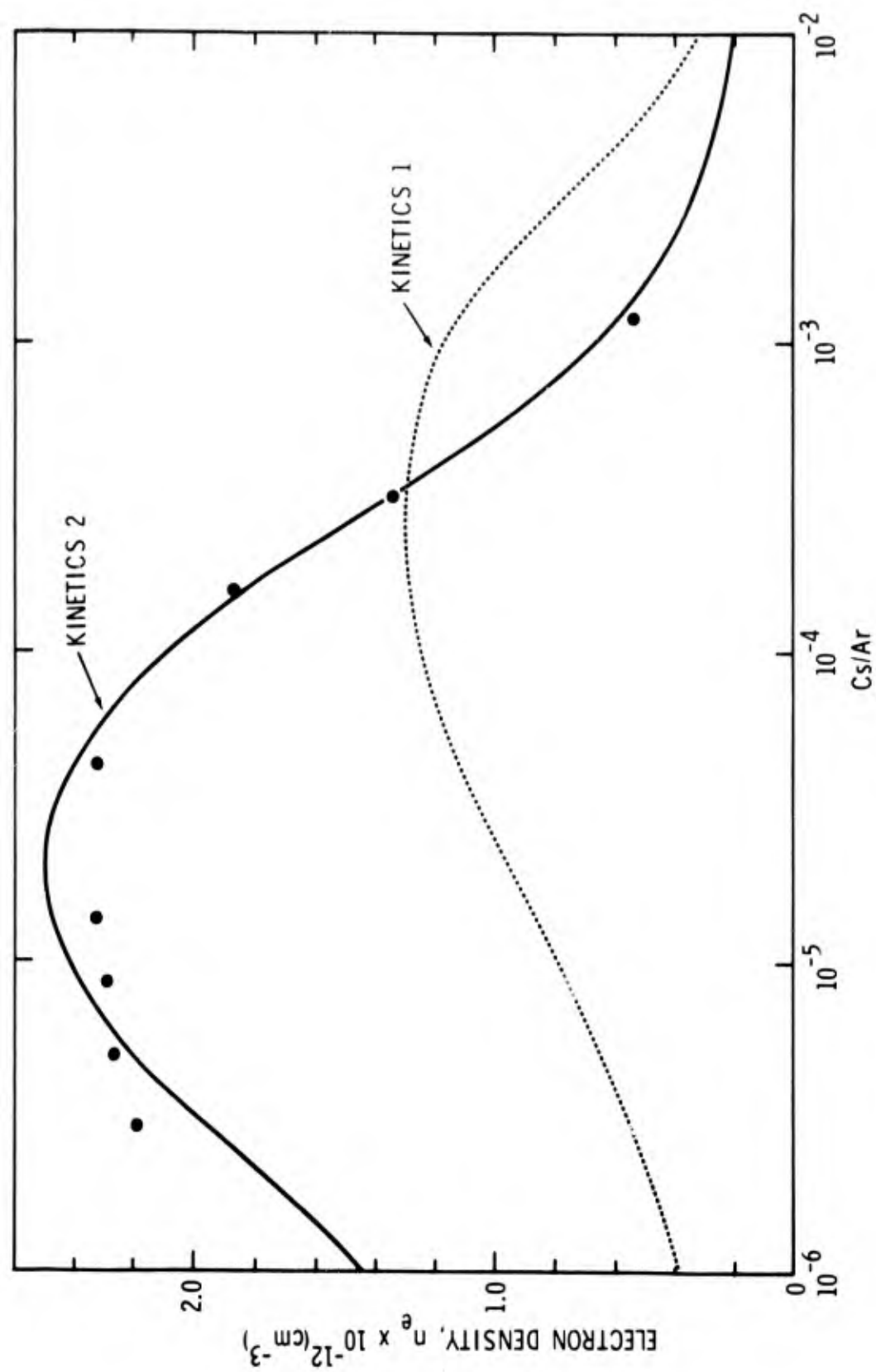


Fig. 6. Electron density versus Cs/Ar for $\langle T_{\text{gas}} \rangle_{\text{av}} = 644^\circ\text{K}$. The neutron flux was $1.44 \times 10^{13} \text{ cm}^{-2} \text{ sec}^{-1}$.

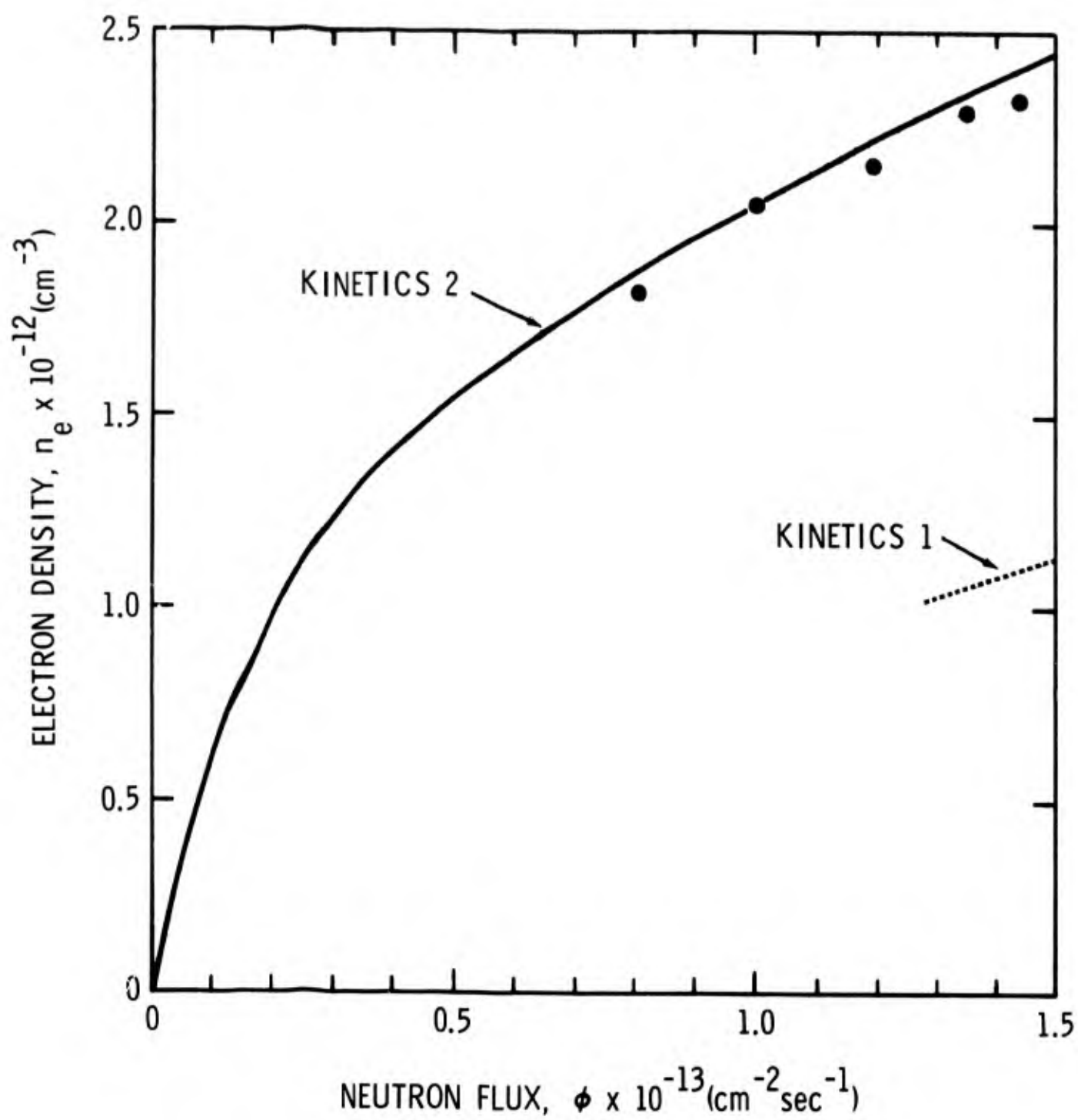


Fig. 7. Electron density versus neutron flux for $\langle T_{\text{gas}} \rangle_{\text{av}} = 644^\circ\text{K}$ and $\text{Cs}/\text{Ar} = 4.19 \times 10^{-5}$.

APPENDIX A
REACTION KINETICS CODE II

TABLE A-I. Listing of main program and subroutines: NONLIN, CROUT, PUNT, ITER and FINAL.

```

$IBFTC LFM2    FULIST,REF,DECK,M94,XR7,DD
C
C**** REACTION KINETICS CODE(III),JOB F36
C**** THIS IS THE MAIN CONTROL PROGRAM
      DIMENSION X(40)
      DIMENSION TITLE(24)
      LOGICAL MSW
      INTEGER PRINT,RTN
      DOUBLE PRECISION X,EPS
      COMMON X,MORE,MSW
      NAMELIST/GUESS/X,EPS,PRINT
      MSW=.FALSE.
10  READ(5,11)TITLE
11  FORMAT(12A6)
      WRITE(6,21)TITLE
21  FORMAT(1H1,20X,12A6/21X,12A6)
      READ(5,GUESS)
      WRITE(6,GUESS)
      MCKE=1
20  CALL NONLIN(8,X,EPS,PRINT,RTN)
      MSW=.TRUE.
      GO TO(20,10),MORE
      END

$IBFTC NONLIN  FULIST,REF,DECK,M94,XR7,DD
C
C**** THIS IS THE MAIN SUBROUTINE NONLIN
      SUBROUTINE NONLIN(N,X,EPS,ISW,L)
C**** N IS NUMBER OF INDEPENDENT VARIABLES AND EQUATIONS
C**** X IS INITIAL ESTIMATE OF ROOT AND MUST HAVE DIMENSION 40 IN
C**** CALLING PROGRAM.
C**** EPS IS ALLOWED ABSOLUTE ERROR
C**** ISW IS INTERMEDIATE OUTPUT SELECTOR
C**** 1 FOR NO INTERMEDIATE OUTPUT
C**** 2 FOR INTERMEDIATE OUTPUT
      DIMENSION F(40,41),G(40),DELT(40),X(40),REX(40),T(40),S(40),BEST(40)
10  DIMENSION CYCLE(40,10)
      COMMON X
      DOUBLE PRECISION F      , G      , DELT      , X      , REX
      DOUBLE PRECISION T      , S      , BEST      , REPS    , EPS
      DOUBLE PRECISION SSAFX  , SSAET   , DABS      , CYCLE   , SSRFX
      DOUBLE PRECISION DETERM
      REPS=.0100*EPS
      DO 1 I=1,20
      S(I)=0.000
      REX(I)=0.000
      DELT(I)=0.000
      BEST(I)=0.000
      G(I)=0.000
      DO 1 J=1,20
1  F(I,J)=0.000
      SSAEX=1.038
      SSAET=0.000
      IC=0
2  ISC=1
      K=0
3  CALL FVAL(F,G)

```

NONL0001
NONL0002
NONL0003
NONL0004
NONL0005
NONL0006
NONL0007
NONL0008
NONL0009
NONL0010
NONL0011
NONL0012
NONL0013
NONL0014
NONL0015
NONL0016
NONL0017
NONL0018
NONL0019
NONL0020
NONL0021
NONL0022
NONL0023
NONL0024
NONL0025
NONL0026
NONL0027
NONL0028
NONL0029
NONL0370
NONL0031
NONL0032
NONL0033
NONL0034
NONL0035

```

C**** X IS IN COMMON
      DO 17 I=1,N
17    G(I)=-G(I)
      DO 100 I=1,N
100   F(I,N+1)=G(I)
      DO 30 I=1,N
      T(I)=F(1,I)
      30 S(I)=G(I)
      CALL CROUT (F,N,1,DETERM,L)
      IF(L.NE.1) GO TO 102
      CALL PUNT(L,BEST,IC,ICB,N,ITRPT,ISW)
      RETURN
102   DO 101 I=1,N
101   DELT(I)=F(I,1)
      DO 21 I=1,N
      21 RFX(I)=DABS(DELT(I)/X(I))
      SSAET=0.000
      DO 23 I=1,N
      23 SSAET=SSAET+S(I)**2
      IF(SSAET-SSAEX)24,24,26
      24 DO 27 I=1,N
      27 BEST(I)=X(I)
      SSAEX=SSAET
      ICB=IC+1
      26 DO 11 I=1,N
      IF(RFX(I)-RFXS) 11,11,12
      11 CONTINUE
      DO 25 I=1,N
      IF( S(I)-FPS) 25,25,12
      25 CONTINUE
      GO TO 15
      12 IC=IC+1
      IF(ISW-2)13,14,13
      13 IF(IC-100) 18,18,19
      14 CALL ITER(N,IC,RFX,S)
      IF(IC-100) 18,18,19
      18 DO 20 I=1,N
      20 X(I)=X(I)+DELT(I)
      JC=MOD((IC-1),5)+1
      DO 40 I=1,N
      40 CYCLE(I,JC)=X(I)
      IF(IC-5) 42,41,41
      42 K=IC
      GO TO 43
      41 K=5
      43 DO 50 J=1,K
      IF(J-JC)44,50,44
      44 DO 46 I=1,N
      IF(CYCLE(I,JC)-CYCLE(I,J))50,46,50
      46 CONTINUE
      ITRPT=IC-MOD((5+JC-J),5)
      L=3
      CALL PUNT(L,BEST,IC,ICB,N,ITRPT,ISW)
      RETURN
      50 CONTINUE
      GO TO 2
      15 SSREX =0.000
      DO 16 I=1,N
      X(I)=X(I)+DELT(I)

```

NONL0036
NONL0037
NONL0038
NONL0039
NONL0040
NONL0041
NONL0042
NONL0043
NONL0044
NONL0045
NONL0046
NONL0047
NONL0048
NONL0049
NONL0050
NONL0051
NONL0052
NONL0053
NONL0054
NONL0055
NONL0056
NONL0057
NONL0058
NONL0059
NONL0060
NONL0061
NONL0062
NONL0063
NONL0064
NONL0065
NONL0066
NONL0067
NONL0068
NONL0069
NONL0070
NONL0071
NONL0072
NONL0073
NONL0074
NONL0075
NONL0076
NONL0077
NONL0078
NONL0079
NONL0080
NONL0081
NONL0082
NONL0083
NONL0084
NONL0085
NONL0086
NONL0087
NONL0088
NONL0089
NONL0090
NONL0091
NONL0092
NONL0093
NONL0094

```

16 SSREX=SSREX+REX(I)**2
   IF (ISW.EQ.3) GO TO 103
   CALL FINAL(N,SSREX,SSAEX)
103 L=4
   RETURN
19 L=2
   CALL PUNT(L,REST,IC,ICB,N,ITRPT,ISW)
   RETURN
   END

```

NONLOC95
NONLOC96
NONLOC97
NONLOC98
NONLOC99
NONL0100
NONL0101
NONL0102
NONL0103

C

```

SUBROUTINE CROUT (A,N,M,DETERM,IJL)
  DIMENSION A(40,41)
  DIMENSION INDEX(40)
  DOUBLE PRECISION A      , DET      , SUM      , HIGH      , DABS
  DOUBLE PRECISION SUM1    , DETERM
  VN=N+1
  DET=1.000
  JZ=N-1
  JA=N+1
  DO 30 I=1,N
30  INDEX(I)=I
  DO 700 J=1,NV
  DO 800 II=1,N
    SUM=0.000
    I=INDEX(II)
    IF (II-J) 23,24,24
33  IF (II-J) 9000,9200,9000
9000  LLLL=II-1
    DO 9100 K=1,LLLL
      IPPP=INDEX(K)
9100  SUM=SUM+A(I,K)*A(PPPP,J)
9200  A(I,J)=(A(I,J)-SUM)/A(I,II)
      GO TO 800
34  IF (J-1) 8000,8200,8000
8000  LLLL=J-1
    DO 9100 K=1,LLLL
      IPPP=INDEX(K)
9100  SUM=SUM+A(I,K)*A(PPPP,J)
8200  A(I,J)=A(I,J)-SUM
800  CONTINUE
    IF (J-N) 41,700,700
41  L=INDEX(J)
    KA=L
    HIGH=A(L,J)
    KZ=0
    DO 35 I=J,JZ
      JC=I+1
      L=INDEX(JC)
      IF (DABS(HIGH)-DABS(A(L,J))) 36,35,35
36  HIGH=A(L,J)
      KA=L
      KZ=1
35  CONTINUE
    IF (KZ-0) 9400,9310,9400
9400  DET=-DET
9310  IF (DABS(HIGH)-1.0-05) 31,31,3200
31  CONTINUE

```

NONL0105
NONL0106
NONL0107
NONL0108
NONL0109
NONL0110
NONL0111
NONL0112
NONL0113
NONL0114
NONL0115
NONL0116
NONL0117
NONL0118
NONL0119
NONL0120
NONL0121
NONL0122
NONL0123
NONL0124
NONL0125
NONL0126
NONL0127
NONL0128
NONL0129
NONL0130
NONL0131
NONL0132
NONL0133
NONL0134
NONL0135
NONL0136
NONL0137
NONL0138
NONL0139
NONL0140
NONL0141
NONL0142
NONL0143
NONL0144
NONL0145
NONL0146
NONL0147
NONL0148
NONL0149
NONL0150
NONL0151
NONL0152

3200	00 37 K=1,N	NONL0153
	KK=K	NONL0154
	IF(INDEX(K)-KA) 37,38,37	NONL0155
37	CONTINUE	NONL0156
39	ITEMP=INDEX(J)	NONL0157
	INDEX(J)=INDEX(KK)	NONL0158
	INDEX(KK)=ITEMP	NONL0159
700	CONTINUE	NONL0160
	IF(M) 2000,1000,2000	NONL0161
2000	L=N-1	NONL0162
	00 39 J=JA,NN	NONL0163
	LL=1	NONL0164
	00 42 K=1,N	NONL0165
	IF(DABS(A(K,J))-0.000)43,42,43	NONL0166
42	CONTINUE	NONL0167
	IZ=INDEX(N)	NONL0168
	IF(DABS(A(IZ,N))-1.00-02)46,46,44	NONL0169
44	IJL=1	NONL0170
	RETURN	NONL0171
	GO TO 10	NONL0172
46	A(IZ,J)=5.00000	NONL0173
	IZ=INDEX(N-1)	NONL0174
	IF(DABS(A(IZ,N))-1.00-04)47,47,43	NONL0175
47	A(IZ,J)=2.500	NONL0176
	LL=2	NONL0177
43	00 40 IJ=LL,L	NONL0178
	SUM1=0.000	NONL0179
	II=N-IJ	NONL0180
	I=INDEX(II)	NONL0181
	LL=II+1	NONL0182
	00 9300 K=LL,N	NONL0183
	IP=INDEX(K)	NONL0184
9300	SUM1=SUM1+A(I,K)*A(IP,J)	NONL0185
	A(I,J)=A(I,J)-SUM1	NONL0186
40	CONTINUE	NONL0187
39	CONTINUE	NONL0188
1000	DETERM=1.000	NONL0189
	00 900 I=1,N	NONL0190
	K=INDEX(I)	NONL0191
900	DETERM=DETERM*A(K,I)	NONL0192
	DETERM=DETERM*DET	NONL0193
	00 400 I=1,N	NONL0194
	00 400 J=JA,NN	NONL0195
	K=INDEX(I)	NONL0196
	L=J-N	NONL0197
400	A(I,L)=A(K,J)	NONL0198
10	RETURN	NONL0199
	END	NONL0200

C	SUBROUTINE PUNT(L,BEST,IC,ICB,N,ITRPT,ISW)	NONL0202
	DIMENSION X(40),BEST(40)	NONL0203
	COMMON X	NONL0204
	DOUBLE PRECISION X , BEST	NONL0205
	IF (ISW.EQ.3) GO TO 200	NONL0206
	GO TO (1,2,7),L	NONL0207
200	IF (L.EQ.2 .OR. L.EQ.3) GO TO 20	NONL0208
	RETURN	NONL0209
1	ICT=IC+1	NONL0210
	WRITE (6,3) ICT	NONL0211
3	FORMAT(1H 31H SYSTEM IS IN A SINGULAR REGION/1H 35H SINGULARITY OCCURRED ON ITERATION 14/1H 27H THE SINGULAR POINT FOLLOWS)	NONL0212
1	WRITE (6,4)(X(I),I=1,N)	NONL0213
4	FORMAT(1H E20.8)	NONL0214
	RETURN	NONL0215
2	WRITE (6,5) ICB	NONL0216
5	FORMAT(1H 33H NUMBER OF ITERATIONS EXCEEDS 100/ 1H 11H ITERATION 114,44H IS BEST ESTIMATE SO FAR AND IS GIVEN BELOW)	NONL0217
	WRITE (6,6)(BEST(I),I=1,N)	NONL0218
6	FORMAT(1H E20.8)	NONL0219
	DO 22 I=1,N	NONL0220
22	X(I)=BEST(I)	NONL0221
	RETURN	NONL0222
7	WRITE (6,10) ITRPT,IC	NONL0223
10	FORMAT(13H1 ITERATIONS 13,4H AND 13,45H ARE IDENTICAL INDICATING A CYCLIC CONDITION./43H THE BEST RESULTS SO FAR ARE GIVEN BELOW.)	NONL0224
1	WRITE (6,6)(BEST(I),I=1,N)	NONL0225
20	DO 21 I=1,N	NONL0226
21	X(I)=BEST(I)	NONL0227
	RETURN	NONL0228
	END	NONL0229
C	SUBROUTINE ITER(N,IC,REX,S)	NONL0230
	DIMENSION X(40),REX(40),S(40)	NONL0231
	COMMON X	NONL0232
	DOUBLE PRECISION X , REX , S	NONL0233
	WRITE (6,1) IC	NONL0234
1	FORMAT(1H0 20H ITERATION COUNT IS 13)	NONL0235
	WRITE (6,2)	NONL0236
2	FORMAT(1H 5X,55H ESTIMATED ROOT RELATIVE ERROR ABSOLUTE	NONL0237
1	ERROR)	NONL0238
	WRITE (6,3)(X(I),REX(I),S(I),I=1,N)	NONL0239
3	FORMAT(1H 3E20.8)	NONL0240
	RETURN	NONL0241
	END	NONL0242
C	SUBROUTINE FINAL(N,SSREX,SSAEX)	NONL0243
	DIMENSION X(40)	NONL0244
	COMMON X	NONL0245
	DOUBLE PRECISION X,SSREX,SSAEX	NONL0246
	WRITE (6,1)	NONL0247
1	FORMAT(1H0 25X,12H FINAL ROOT)	NONL0248
	WRITE (6,2)(X(I),I=1,N)	NONL0249
2	FORMAT(1H 20X,030.16)	NONL0250
	WRITE (6,3) SSREX	NONL0251
3	FORMAT(1H0 10X,38H SUM OF SQUARES OF RELATIVE ERRORS IS E20.9)	NONL0252
	WRITE (6,4) SSAEX	NONL0253
4	FORMAT(1H 10X,38H SUM OF SQUARES OF ABSOLUTE ERRORS IS E20.9)	NONL0254
	RETURN	NONL0255
	END	NONL0256

TABLE A-II. Listing of subroutine EVAL.

```

IBFTC LEF3      FULIST,REF,DECK,M94,XR7,DD
SUBROUTINE EVAL(P,G)
DOUBLE PRECISION X(40),P(40,41),G(40),LAMSNO
DOUBLE PRECISION LAM,NO,C(34),AU,S(3),K(5),KM,TAUX,TEM(6)
LOGICAL ISW,MSW
COMMON X,MURE,MSW
NAMELIST/INPUT/NO,AU,C,K,KM,LAM,S,TAUX,MURE
DATA ISW/.FALSE./
IF(ISW)GO TO 100
ISW=.TRUE.
50 READ(5,INPUT)
WRITE(6,INPUT)
MSW=.FALSE.
100 IF(MSW)GO TO 50
EVALUATE FUNCTIONS AND PARTIALS
VALUES NEEDED THROUGHOUT
LAMSNO=LAM*LAM*NO
FIRST EQN
G(1)=X(1)-X(2)-X(3)-X(6)-X(7)-X(8)
P(1,1) = 1.0
P(1,2) = -1.0
P(1,3) = -1.0
P(1,4) = 0.0
P(1,5) = 0.0
P(1,6) = -1.0
P(1,7) = -1.0
P(1,8) = -1.0
SECOND EQN
TEM(1)=K(1)/LAMSNO
TEM(2) = C(4)*NO*1.0D-10*NO
TEM(3) = C(5)*NO*1.0D-10*AU
TEM(4) = C(23)*NO*1.0D-10*AU
TEM(5) = C(24)*AU*1.0D-10*AU
G(2)=S(1)*NO-TEM(1)*X(2)-X(1)*X(2)*(C(1)
1+C(2)*NO*1.0D-10 + C(3)*X(1)*1.0D-10)
2-TEM(2)*X(2)-TEM(3)*X(2)-C(6)*AU*X(2)+C(7)*X(5)*X(5)
3-TEM(4)-TEM(5)
P(2,1)=-C(1)*X(2)-C(2)*NO*1.0D-10*X(2)-2.0*C(3)*X(1)*1.0D-10*X(2)
P(2,2)=-TEM(1)-C(1)*X(1)-C(2)*NO*1.0D-10*X(1)-C(3)*X(1)*1.0D-10*X(
1)-TEM(2)-TEM(3)-C(6)*AU
2-TEM(4)-TEM(5)
P(2,3) = 0.0
P(2,4) = 0.0
P(2,5)=2.0*C(7)*X(5)
P(2,6) = 0.0
P(2,7) = 0.0
P(2,8) = 0.0
THIRD EQN
TEM(1) =(C(1)+C(2)*NO*1.0D-10)*C(8)
TEM(2) = C(3)*C(8)*X(1)*1.0D-10
TEM(3) = TEM(1)+TEM(2)
G(3)=S(2)*NO+TEM(3)*X(1)*X(2)-X(4)/TAUX-
1C(9)*NO*X(4)
P(3,1)=X(2)*TEM(1)
1+2.0*TEM(2)*X(2)
P(3,2)=X(1)*TEM(3)
P(3,3) = 0.0

```

```

P(3,4)=-1.0/TAUX-C(9)*NU
P(3,5) = 0.0
P(3,6) = 0.0
P(3,7) = 0.0
P(3,8) = 0.0
C
FOURTH EQN
TEM(1)=KM/LAMSNU
TEM(2) =C(10)*(C(1)+C(2)*NO*1.0D-10)
TEM(3) =C(14)*NO*1.0D-10*NU
TEM(4) = C(10)*C(3)*X(1)*1.0D-10
TEM(5) = TEM(2)+TEM(4)
G(4)=S(3)*NO-TEM(1)*X(5)+TEM(5)*X(1)*X(2)+C(11)*C(16)*X(3)*X(1)
1-C(12)*X(5)*X(5)-C(13)*NU*X(5)-C(15)*AU*X(5)-TEM(3)*X(5)
2-C(25)*AU*X(5)
P(4,1)=TEM(2)*X(2)+C(11)*C(16)*X(3)
1+2.0*TEM(4)*X(2)
P(4,2)=TEM(5)*X(1)
P(4,3)=C(11)*C(16)*X(1)
P(4,4) = 0.0
P(4,5)=-TEM(1)-2.0*C(12)*X(5)-C(13)*NO-C(15)*AU-TEM(3)-C(25)*AU
P(4,6) = 0.0
P(4,7) = 0.0
P(4,8) = 0.0
C
FIFTH EQN
TEM(1)=K(2)/LAMSNU
TEM(2) =C(4)*NU*1.0D-10*NU
G(5)=-TEM(1)*X(3)-C(16)*X(1)*X(3)+TEM(2)*X(2)-C(17)*AU*X(3)
1+C(9)*NU*X(4)-C(26)*AU*X(3)
P(5,1)=-C(16)*X(3)
P(5,2)=TEM(2)
P(5,3)=-TEM(1)-C(16)*X(1)-C(17)*AU-C(26)*AU
P(5,4)=C(9)*NU
P(5,5) = 0.0
P(5,6) = 0.0
P(5,7) = 0.0
P(5,8) = 0.0
C
SIXTH EQN
TEM(1)=K(3)/LAMSNU
TEM(2) =C(18)+C(19)*NO*1.0D-10+C(22)*X(1)*1.0D-10
TEM(3) =C(20)*AU*1.0D-10*NU
TEM(4) = C(27)*NU*1.0D-10*NU
TEM(5) = C(28)*AU*1.0D-10*NU
TEM(6) = C(32)*NO*1.0D-10*NU
G(6)=-TEM(1)*X(6)-X(1)*X(6)*TEM(2)-TEM(3)*X(6)+C(6)*AU*X(2)+C(17)*
1AU*X(3)+C(15)*AU*X(5)
2-TEM(4)*X(6)-TEM(5)*X(6)+C(31)*NU*X(8)+TEM(6)*X(8)
P(6,1)=-X(6)*(C(18)+C(19)*NO*1.0D-10+2.0*C(22)*X(1)*1.0D-10)
P(6,2)=C(6)*AU
P(6,3)=C(17)*AU
P(6,4) = 0.0
P(6,5)=C(15)*AU
P(6,6)=-TEM(1)-TEM(2)*X(1)-TEM(3)-TEM(4)-TEM(5)
P(6,7) = 0.0
P(6,8) = C(31)+TEM(6)
SEVENTH EQN
TEM(1)=K(4)/LAMSNU
TEM(2) =C(20)*AU*1.0D-10*NU

```

```

TEM(3) = C(34)*AU*NU*1.0D-10
G(7)=-TEM(1)*X(7)-C(21)*X(1)*X(7)+TEM(2)*X(6)
1-C(29)*NU*X(7)+C(33)*AU*X(8)+TEM(3)*X(8)
P(7,1)=-C(21)*X(7)
P(7,2) = 0.0
P(7,3) = 0.0
P(7,4) = 0.0
P(7,5) = 0.0
P(7,6) =TEM(2)
P(7,7)=-TEM(1)-C(21)*X(1)-C(29)*NU
P(7,8) = C(33)*AU+TEM(3)
EIGHTH EQN
TEM(1) = K(5)/LAMSNO
TEM(2) = C(23)*AU*NU*1.0D-10
TEM(3) = C(27)*NU*NU*1.0D-10+C(28)*AU*NU*1.0D-10
TEM(4) = C(31)*NU+C(33)*AU
TEM(5) = C(32)*NU*NU*1.0D-10+C(34)*AU*NU*1.0D-10
G(8)=-TEM(1)*X(8)-C(30)*X(1)*X(8)+TEM(2)*X(2)+TEM(3)*X(6)
1+C(26)*AU*X(3)+C(29)*NU*X(7)-TEM(4)*X(8)-TEM(5)*X(8)
2+C(25)*AU*X(5)
P(8,1) = -C(30)*X(8)
P(8,2) = TEM(2)
P(8,3) = C(26)*AU
P(8,4) = 0.0
P(8,5) = C(25)*AU
P(8,6) = TEM(3)
P(8,7) = C(29)*NU
P(8,8) =-TEM(1)-C(30)*X(1)-TEM(4)-TEM(5)
RETURN
END

```

TABLE A-III. Example of input cards to computer cards.

```

RUN 519.1 TO 519.8 NE VS T(GAS) FOR A/N=1.00D-6 F=7.25D12
TEMP OK = 300,400,500,600,700,800,1000,1300
$GUESS X(1)=3.1D12,8.4D9,1.5D10,1.0,2.48D11,3.09D12,5.8D8,33*0.0,
EPS=1.0D-6, PRINT =2$
$INPUT LAM=2.016D-01, TAUX=1.00D-06, KM=1.70D18,
K=2.20D18,2.70D18,2.90D18,2.80D18,2.80D18,
S=1.740D-03,0.00D-03,0.870D-03,
C=2.70D-12,2.50D-20,1.08D-10,6.80D-22,5.00D-21,3.00D-12,5.60D-10,
1.00D-01,5.60D-12,1.00D-01,5.00D-01,5.60D-10,1.20D-15,1.30D-22,
4.60D-10,6.70D-07,3.00D-12,3.50D-12,2.50D-20,1.60D-21,2.00D-06,
1.08D-10,0.0,0.0,0.0,
4.60D-10,0.0,1.00D-24,1.00D-18,
0.0,2.00D-6,1.00D-17,0.0,1.00D-17,0.0,
AO=2.90D12,NO=2.90D18 $
$INPUT K=2.94D18,3.60D18,3.86D18,3.74D18,3.74D18, KM=2.27D18,
C(3)=2.90D-11, C(22)=2.90D-11,C(14)=6.00D-23,
C(31)=1.20D-14,C(33)=1.20D-14 $
C
C DELETED RUNS 519.3 THRU .7
C
$INPUT C(3)=1.00D-13, C(22)=1.00D-13,C(14)=3.40D-24,
C(31)=3.00D-08,C(33)=3.00D-08,
K=9.55D18,1.17D19,1.26D19,1.21D19,1.21D19,
KM=7.35D18, MORE=2 $

```


K	=	0.2200000000000000 19,	0.2700000000000000 19,	0.2300000000000000 19,
		0.2799999999999999 19,	0.2799999999999999 19,	
KM	=	0.1700000000000000 19,		
LAM	=	0.2016000000000000 00,		
S	=	0.1740000000000000 02,	0.0000000000000000 -38,	0.8599999999999980 -03,
TAUX	=	0.9999999999999970 -05,		
MORE	=	1,		
\$	END			

AC OVERFLOW AT 21224,AC SIG PART

AC OVERFLOW AT 21224,AC SIG PART

ITERATION COUNT IS 1

ESTIMATED ROOT	RELATIVE ERROR	ABSOLUTE ERROR
0.31000000E 13	0.33588179E 00	0.13980000E 11
0.84000000E 10	0.11787327E -01	0.59569325E 15
0.15000000E 11	0.51091838E 00	-0.87207813E 14
0.10000000E 01	0.16012485E 07	0.10488855E 17
0.24800000E 12	0.82684277E 00	0.26351682E 17
0.30900000E 13	0.33903862E 00	0.32575442E 18
0.58000000E 09	0.66333552E 00	0.35918558E 16
0.00000000E -38	0.55331027E 09	-0.55282120E 16

AC OVERFLOW AT 21224,AC SIG PART

AC OVERFLOW AT 21224,AC SIG PART

ITERATION COUNT IS 2

ESTIMATED ROOT	RELATIVE ERROR	ABSOLUTE ERROR
0.20587664E 13	0.34058881E 00	0.31900406E -03
0.83000000E 10	0.34784052E -01	0.80553557E 14
0.73362243E 10	0.17274464E 00	-0.10410066E 14
0.16012495E 07	0.51283857E 00	-0.26600894E 16
0.42542992E 11	0.77011835E -02	0.53464529E 16
0.20423707E 13	0.34287446E 00	0.96967605E 17
0.19525395E 09	0.65716690E 00	0.80122099E 15
0.56331027E 09	0.33870937E 00	-0.11730751E 16

ITERATION COUNT IS	14		RELATIVE ERROR	ABSOLUTE ERROR
ESTIMATED ROOT				
0.10988378E 12			0.33614555E-16	0.54240227E-05
0.88228813E 10			0.37789361E-16	-0.19079590E 00
0.68506209E 11			0.20627972E-16	0.76293945E-05
0.67296146E 04			0.38978857E-16	0.15625000E-01
0.43672428E 11			0.33960846E-17	0.12522125E 00
0.32044272E 11			0.19095586E-16	0.10318706E-02
0.19618057E 06			0.41044427E-16	-0.40424275E-05
0.51022346E 09			0.75847272E-16	0.39062500E-02

ITERATION COUNT IS	15		RELATIVE ERROR	ABSOLUTE ERROR
ESTIMATED ROOT				
0.10988378E 12			0.33642927E-16	0.53942204E-05
0.88228813E 10			0.37789348E-16	-0.19079590E 00
0.68506209E 11			0.20556344E-16	0.76293945E-05
0.67296146E 04			0.39035353E-16	0.15525000E-01
0.43672428E 11			0.33960861E-17	0.12522125E 00
0.32044272E 11			0.19116091E-16	0.10328293E-02
0.19618057E 06			0.40995556E-16	-0.40424266E-05
0.51022346E 09			0.62289724E-17	-0.39062500E-02

(Final Results for Run 519.1)

ITERATIONS 14 AND 15 ARE IDENTICAL INDICATING A CYCLIC CONDITION.
THE BEST RESULTS SO FAR ARE GIVEN BELOW.

0.10988378E 12	=	n _g ⁺
0.88228813E 10	=	Ar ⁺
0.68506209E 11	=	Ar ²
0.67296146E 04	=	Ar ^x
0.43672428E 11	=	Ar ^m
0.32044272E 11	=	Cs ⁺
0.19618057E 06	=	Cs ² ⁺
0.51022346E 09	=	ArCs ⁺

SECTION B

SECTION B

CALCULATION OF ELECTRON TEMPERATURES IN PLASMAS PRODUCED BY FISSION FRAGMENTS

ABSTRACT

A method of calculating electron temperatures in noble gas plasmas generated by fission fragments is presented. Knowledge of the production rate, initial energy and energy-degradation rate of fast electrons created directly by the fragments is used to determine the energy input rate by electron-electron collisions to the Maxwellian electron swarm which, in turn, loses energy via elastic collisions to the ambient ions and atoms. For a Penning-type noble gas mixture an additional though less important source of electron energy arises from the metastable-ionization process, and this also is taken into account. Results of the calculation presented for neon seeded with 0.01% argon at a total gas pressure of 90 torr show that at low values of neutron flux ($\sim 10^{10} \text{ cm}^{-2} \text{ sec}^{-1}$) and electron densities ($\sim 10^{10} \text{ cm}^{-3}$), the electron temperature is at or near the gas temperature, but at high neutron flux ($\sim 10^{13} \text{ cm}^{-2} \text{ sec}^{-1}$) and electron densities ($\sim 10^{12} \text{ cm}^{-3}$), the electron temperature is higher than the gas temperature by an important amount ($\sim 500^\circ \text{K}$). The significance of this result and its influence on previous computations is discussed.

CONTENTS

ABSTRACT	i
OBJECT	1
CONCLUSIONS	1
I. INTRODUCTION	1
II. PRODUCTION OF ENERGETIC ELECTRONS BY FISSION FRAGMENTS	2
(a) General Features of the Fission-Fragment Ionization Process	2
(b) Energy Balance Relationship for Fission-Fragments	3
III. ENERGY INPUT RATE TO ELECTRON SWARM	7
IV. ENERGY LOSS RATE OF ELECTRON SWARM	10
V. EXAMPLES OF CALCULATIONS AND RESULTS	13
(a) Values for Collision Frequencies	13
(b) Example of Electron Swarm Energy Gain and Loss Rates. .	15
(c) Electron Temperature Results	21
VI. SIGNIFICANCE OF RESULTS AND FURTHER STUDIES	24
REFERENCES	27

OBJECT

The purpose of the present study was to develop a theory for calculating electron temperatures in fission-fragment-generated plasmas. This information is important for evaluating the electrical conductivity of such plasmas considered for energy conversion application.

CONCLUSIONS

For plasmas generated by fission fragments penetrating noble gases at pressures of about 90 torr, the energy input rate to the electrons is sufficiently high at a neutron flux of $10^{13} \text{ cm}^{-2} \text{ sec}^{-1}$ to maintain electron temperatures at values significantly higher than the gas temperature. This nonequilibrium situation accounts for much of our observed temperature behavior particularly in the Ne-Ar system where theoretical predictions are now in excellent agreement with experiment.

I. INTRODUCTION

In our previous studies on plasmas generated by fission-fragment ionization of Ne-Ar and Ar-Cs gas mixtures¹⁻⁶ we considered the electrons to be in thermal equilibrium with the ambient ions and atoms. Such a notion arose principally from our estimates that the high energy electrons produced by the fission fragments were rapidly thermalized upon the cooler swarm electrons which in turn were quite closely coupled to the ion/atom temperature $T_{i,a}$. Further, our reaction kinetics analyses of Ne-Ar and Ar-Cs plasmas using electron swarm temperatures $T_e \approx T_{i,a}$ generally predicted well the magnitude and trends of the electron density measured in our microwave cavity experiments. Nevertheless, certain observed temperature effects are not consistent with theory; in particular, the variation of electron density n_e with cavity temperature in Ne-Ar, and especially in Ar-Cs, cannot be reconciled with our computations. This has motivated a reexamination of many temperature-dependent aspects of the reaction kinetics system, such as more careful estimates of certain important reaction rates, the possible formation of very temperature-sensitive heteronuclear ions^{7,8} and the validity of the approximation $T_e \approx T_{i,a}$. The present report deals with this last topic.

We show how the electron temperature can be calculated from energy balance relationships which start from fission fragment losses, and we present results for both Ne-Ar and Ar-Cs plasmas. It is found that $T_e > T_{i,a}$, generally by an important amount. Typically, the electron temperature in Ne-Ar is several hundred degrees above the ambient gas temperature of 300-500°K. For Ar-Cs, the calculation is less complete because we have not yet included the electron energy lost to excited cesium states; however, when this loss is neglected, we find $T_e \sim 2000^\circ\text{K}$ for $T_{i,a} \sim 500^\circ\text{K}$. The significance of these findings is discussed, and particularly noteworthy is that for the Ne-Ar plasma all our reliable experimental values of electron density obtained as functions of neutron flux and microwave cavity temperature can now be accurately computed by a detailed reaction kinetics model which takes into account the elevated electron temperature.⁹ This complete theory contains no adjustable parameters.

In Section II we discuss the manner in which fission fragments deposit their energy in the mixed gas to yield energetic electrons. Section III deals with the partition of the energetic-electron energy among the swarm electrons, ions and atoms so that the energy input rate to the swarm electrons may be calculated. As shown in Section IV, this energy input rate can then be equated with the swarm loss rate to determine the electron temperature. Computed values of electron temperature for experimental values of electron density are reported in Section V. Finally we make some concluding remarks in Section VI.

II. PRODUCTION OF ENERGETIC ELECTRONS BY FISSION FRAGMENTS

We discuss briefly the general characteristics of the fission-fragment ionization process; then we turn to some quantitative energy balance equations which are appropriate for our purpose.

(a). General Features of the Fission-Fragment Ionization Process

When a heavy energetic charged particle (such as an α -particle or fission fragment) penetrates a noble gas, it loses energy almost entirely by excitation and ionization of the gas.¹⁰ Of the primary ionizing collisions, the most probable are those in which a relatively slow secondary electron is

ejected with kinetic energy smaller than the ionization potential of the gas.¹¹ A fraction of the primary ionizing collisions, however, produce secondary electrons of relatively high energy, the so-called δ -rays, which produce further secondary ionization. Experimentally, the total ionization for single noble gases is roughly 3 times the primary ionization;¹¹ and although we do not directly require this knowledge for our subsequent analysis, it is instructive to use this fact to estimate the fraction of the primary ionizing collisions which produce δ -rays, for example, in argon at a pressure of 100 torr.

Fissioning atoms of ^{235}U yield fission fragments that at birth are conventionally divided into two median energy groups, viz., light fragments with kinetic energy of 98 MeV and mass 95 amu, and heavy fragments with kinetic energy of 67 MeV and mass 139 amu.¹² On the average, these fragments leave the uranium surface and enter the gas with about one-half their initial kinetic energy,¹³ so let us consider for convenience a fragment with energy E_{ff} of 40 MeV and a mean mass M_{ff} of 117 amu. The maximum energy ϵ_{max} that this fragment can transfer to a valence electron of mass m_e is $4\left[\frac{m_e}{M_{\text{ff}}}\right]E_{\text{ff}}$ which corresponds to a maximum electron velocity V_e of twice the fission-fragment velocity. With $E_{\text{ff}}=40$ MeV, we find $\epsilon_{\text{max}}=740$ eV, (or $V_e=1.6\times 10^9$ cm sec⁻¹). For the purpose of this simple physical picture, we do not inquire about the energy distribution of these δ -rays; rather we take a mean δ -ray energy of around 300 eV and calculate the number of ion pairs produced by this δ -ray for argon at 100 torr. We find that about 9 ion pairs will be produced by the 300 eV δ -ray over its range of approximately 0.007 cm. Thus, since the total ionization is roughly 3 times the primary ionization, we conclude that for every 4 primary ionizing collisions of fission fragments with the gas atoms, 1 δ -ray is produced which gives rise to about 9 ions pairs or about 2/3 of the total ionization. This is illustrated schematically in Fig. 1.

(b). Energy Balance Relationship for Fission Fragments

The total ionization produced by high energy charged particles in gases is generally measured by W , the mean energy expended per ion pair produced (eV/ip). W is related to the ionization and excitation losses in the following manner. For an energy E_0 absorbed by the gas, there are produced (ultimately) N_i singly charged atomic ions at an average energy expenditure of \bar{E}_i , N_x excited atoms at an average energy expenditure of \bar{E}_x and N_i

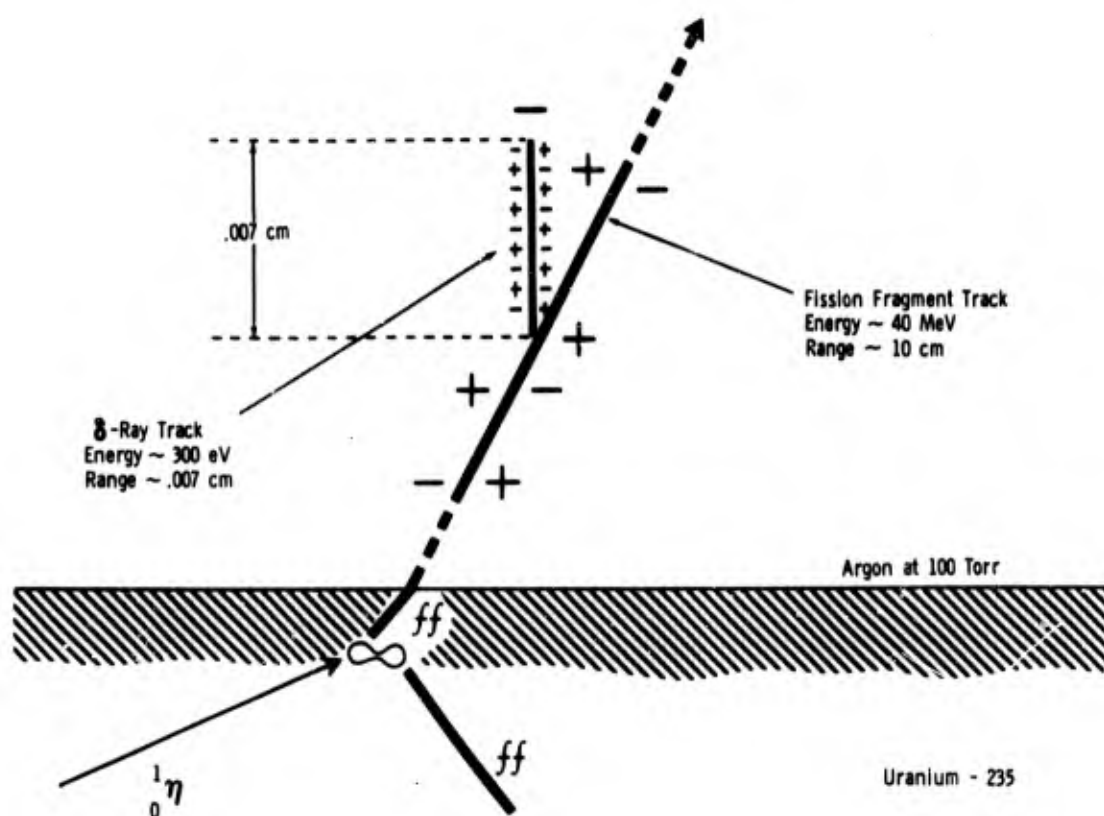


Fig. 1. Schematic of high-energy ionization processes induced by fission fragments in argon at 100 torr. About 2/3 of the total ionization is caused by the δ -ray.

subexcitation electrons having average kinetic energy $\bar{\epsilon}$. That is,

$$E_o = N_i \bar{E}_i + N_x \bar{E}_x + N_1 \bar{\epsilon}.$$

We are particularly interested in the value of $\bar{\epsilon}$ possessed by these subexcitation electrons which, in a single gas, lose their energy only via elastic collisions. Now by definition,

$$W = \frac{E_o}{N_i} = \bar{E}_i + \left(\frac{N_x}{N_i} \right) \bar{E}_x + \bar{\epsilon},$$

and it is further convenient to normalize the equation throughout with respect to V_i , the ionization energy of the gas:

$$\frac{W}{V_i} = \frac{\bar{E}_i}{V_i} + \left(\frac{N_x}{N_i} \right) \frac{\bar{E}_x}{V_i} + \frac{\bar{\epsilon}}{V_i}. \quad (1)$$

This equation has been studied in detail by Platzman.¹⁴ He showed that for the noble gases, the terms on the right hand side of the equation

could be evaluated from information that was independent of the absolute measurement of W . Thus Eq.(1) was properly verified. Platzman also found that the similar electronic configurations of the noble gases lead to terms in Eq.(1) which are constant, to within a few percent, for all the noble gases. However, Platzman's results are derived for α -particles and a slight correction should be made for fission fragments since the average value of W for fission fragments is 9% larger than that for α -particles.¹ Utterback and Miller¹⁵ have indicated that this larger value of W for fission fragments in argon arises mainly from an increase in the ratio N_x/N_i . Thus when W and N_x/N_i are adjusted to fission fragments, Platzman's noble-gas constants for Eq.(1) become, respectively,

$$1.82 \approx 1.06 + (0.53) 0.85 + 0.31. \quad (2)$$

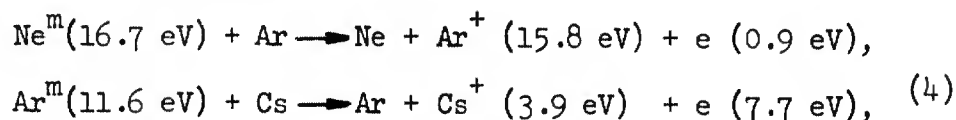
Note however that the value given by Platzman for the subexcitation electron energy $\bar{\epsilon} = 0.31 V_i$ remains unchanged. The quantity $\frac{E_i}{V_i} = 1.06$ exceeds unity because of the energy wasted in producing excited ions and multiple charged ions. The single average excitation energy $\bar{E}_x = 0.85 V_i$ is successful here for the noble gases because all excited levels lie fairly close to the ionization limit.

We see, then, that about 17% of the total energy absorbed to create an ion pair is carried away by the electron of average kinetic energy $0.31 V_i$ (i.e., 4.9 eV for Ar, 6.5 eV for Ne). This is the average steady-state result of the primary and secondary ionization processes discussed in our previous section (Fig. 1). Now these subexcitation electrons are produced at a constant rate S^+ - the ion generation rate - which has been discussed in detail in earlier reports.⁶ S^+ is a function of the density and nature of the gas N_0 , the uranium fuel load U , the neutron flux ϕ , and the tube geometry \vec{r} . It follows that the total production rate of subexcitation energy $\dot{\Sigma}_{sx}$ in $\text{eV cm}^{-3}\text{sec}^{-1}$ is

$$\dot{\Sigma}_{sx} = 0.31 V_i(N_0) S^+(N_0, U, \phi, \vec{r}). \quad (3)$$

So far, our discussion has been concerned with single noble gases. Consider now two binary-gas systems, viz., neon mixed with traces of argon where $[\text{Ar}]/[\text{Ne}] < 10^{-3}$, and argon mixed with traces of cesium where also $[\text{Cs}]/[\text{Ar}] < 10^{-3}$. The trace gas in each case is so dilute that its direct interaction with

fission fragments and δ -rays can be ignored. Thus Eq.(3) can be used explicitly to determine ξ_{sx} for the parent gas of each mixture. However, since the two binary-gas systems are Penning-type mixtures^{16,17} an additional ion production source exists as follows:



where the superscript m indicates metastable states. Both these reactions evidently produce electrons with energy corresponding to the difference between the metastable energy of the parent gas $V_m(N_o)$ and the ionization energy of the trace gas $V_i(A_o)$. This difference is very much larger for Ar-Cs than for Ne-Ar. Our reaction kinetics code for computing electron density in Ne-Ar and in Ar-Cs plasmas already includes the rate at which these metastable-ionization reactions proceed,³ and is given as $C_{15}[N_m][A_o]$ where C_{15} is the appropriate reaction rate coefficient in $\text{cm}^3\text{sec}^{-1}$. Thus we can write down the production rate $\xi_m (\text{eV cm}^{-3}\text{sec}^{-1})$ of electron energy from metastable states as

$$\xi_m = \{V_m(N_o) - V_i(A_o)\} C_{15}[N_m][A_o]. \quad (5)$$

We have, therefore, a total electron energy production rate of $\xi_{sx} + \xi_m^*$. In the Ne-Ar system for which we have completed our calculations,⁷ this energy will be dissipated directly as heat in elastic collisions with the swarm electrons, ions and atoms. There will be no appreciable excitation loss since the first excitation level of Ar(11.6 eV) is significantly higher than the initial energies of the fast electrons (6.5 eV, 0.9 eV). For Ar-Cs, much of $\xi_{sx} + \xi_m$ will still be dissipated in elastic collisions but it is also possible to have excitation of the low-lying cesium states. Since we have not yet included this excitation loss, the present temperature results for Ar-Cs must be regarded as preliminary. With this in mind, we next discuss the total elastic energy loss rate of the fast electrons in order to estimate the fraction F_1 of ξ_{sx} and F_2 of ξ_m lost to the swarm electrons to yield a swarm energy input rate of $F_1 \xi_{sx} + F_2 \xi_m$.

*Other possible sources of appreciable electron energy are ionizing collisions between pairs of metastable or excited states, and non-ionizing collisions of the second kind between metastable or excited states and slow electrons. However, we see from our previous reaction kinetics work that for our conditions, collisions between electrons, metastable and excited states are so infrequent that their contribution to the total electron energy rate $\xi_{sx} + \xi_m$ can be neglected.

III. ENERGY INPUT RATE TO ELECTRON SWARM

The energy loss rate by Coulomb collisions of a fast test particle injected into a plasma has been discussed in terms of relaxation times by various authors^{18,19,20} who have used both the Boltzmann²¹ and Fokker-Planck²² collision equations. In the present study involving relatively low degrees of ionization ($\frac{n_e}{N_0} < 10^{-6}$) we use electron-electron relaxation times in a simple manner to determine approximately the transfer of energy from the fast electrons to the electron swarm.

We note first that we have an ion generation rate $S^+ \sim 10^{16}$ ions $\text{cm}^{-3}\text{sec}^{-1}$ and an electron density $n_e \sim 10^{12} \text{cm}^{-3}$ when our Ne-Ar and Ar-Cs microwave cavities are filled to a pressure of about 100 torr and operated in a neutron flux of 1×10^{13} neutrons $\text{cm}^{-2}\text{sec}^{-1}$. Thus the average lifetime τ_{av} of an electron, defined by $\tau_{av} = \frac{n_e}{S^+}$, is $\sim 10^{-4}$ secs. Now each swarm electron was initially an energetic electron generated via the processes represented by expressions (3) and (5). We show in the succeeding sections that under our conditions an energetic electron rapidly loses its excess energy and becomes a member of the swarm in times τ_{fast} ranging from 10^{-6} to 10^{-8} secs. Furthermore, the Maxwellian relaxation of swarm electrons by Coulomb self-interaction²³ also occurs rapidly in times $\tau_{ee} \sim 10^{-7}$ secs for the electron temperatures $T_e \sim 1000^\circ\text{K}$ and values of $n_e \sim 10^{12} \text{cm}^{-3}$ of interest to us. Thus $\tau_{av} \gg \tau_{fast} + \tau_{ee}$. This means firstly that we can disregard the density of the fast electrons in comparison with the density of the swarm electrons since each electron spends essentially all its lifetime as a member of the swarm. Secondly, there is no high-energy tail to the swarm distribution function since interchange of electron energy is sufficiently rapid to preserve a Maxwell-Boltzmann distribution. Evidently we can then define the mean electron swarm energy in terms of a swarm temperature, viz., $\bar{\epsilon}_e = \frac{3}{2} kT_e$.

Now if ϵ is the energy of a fast electron from process (3) or (5), then its rate of energy loss under the present circumstances may be approximated by

$$\frac{d\epsilon}{dt} \approx - \frac{2m_e}{M_{N_0}} \nu_{ea}(\epsilon) \{\epsilon - \bar{\epsilon}_a\} - \nu_{ee}(\epsilon) \{\epsilon - \bar{\epsilon}_e\} \quad (6)$$

for $\epsilon \geq \bar{\epsilon}_e$, where the two terms represent, respectively, energy loss rates to the parent gas and to the electron swarm. $\frac{2m_e}{M_{N_0}}$ is the mean fractional energy

lost by the electron of mass m_e in collision with a neutral atom of mass M_{N_0} , $\nu_{ea}(\epsilon)$ is the electron-neutral atom collision frequency for momentum transfer, and $\epsilon - \bar{\epsilon}_a$ is the excess electron energy above the ambient kinetic energy $\bar{\epsilon}_a = \frac{3}{2} kT_a$ of the gas at temperature T_a . The quantity $\nu_{ee}(\epsilon)$ is the collision frequency for appreciable energy transfer between the hot electron and the swarm electrons and must be carefully defined as outlined below. For electron-neutral atom loss, we have included only the parent gas because the concentration of trace gas is always so dilute ($< 0.1\%$) that its effect in this regard may be ignored. Also note that Eq.(6) omits any electron-ion loss since in a quasi-neutral plasma ($n_e \approx n_i$) the hot electron will lose its energy much more efficiently in collisions with electrons than with ions. The reason for this stems not only from the fact that on a hard-sphere collision basis, equal particle masses yield maximum energy transfer. More importantly, the fast electron loses energy in Coulomb collisions mainly by a large number of distant collisions (in contrast to close ones) where light target particles such as electrons can react more rapidly and take away more energy in a fixed interaction time than can the heavy ions.

The characteristic or relaxation time for a test particle to be slowed down through Coulomb collisions with target particles has been defined by Chandrasekar^{19,20} who examined in detail the statistics of distant collisions. The reciprocal of this characteristic time for reduction of forward velocity ω may be regarded as a collision frequency defined by

$$\frac{d(\omega)}{dt} = -\omega \nu_{et}(\omega). \quad (7)$$

Here ν_{et} is given as

$$\nu_{et}(\omega) = 4 \pi n_t \omega p_0^2 \left(1 + \frac{m_e}{m_t}\right) \ln \Lambda \quad (8)$$

when the singly-charged target particles (sub t) have velocities much less than the velocity ω possessed by the test particle. The quantity $p_0 (= \frac{e^2}{m_e \omega^2})$ is a critical impact parameter which physically can be associated with a 90° deflection; Λ is the ratio of the Debye screening length of the field assembly to p_0 . If we write $\frac{1}{2} m_e \omega^2 = \epsilon$ where ϵ is in electron-volts, and consider a test electron scattered upon an electron swarm at temperature T_e , then with $m_t = m_e = m$ we obtain numerically

$$\nu_{ee}(\omega) = 7.7 \times 10^{-6} n_e \epsilon^{-3/2} \ln \Lambda(T_e),$$

where $\Lambda = 1.25 \times 10^4 T_e^{3/2} / n_e^{1/2}$. However $\nu_{ee}(\epsilon) = 2\nu_{ee}(\omega)$ since by definition

$$\frac{d(\epsilon)}{dt} = \epsilon \nu_{ee}(\epsilon),$$

but also from Eq.(7)

$$\frac{d(\epsilon)}{dt} = \frac{d(\frac{1}{2} m \omega^2)}{dt} = m \omega \frac{d\omega}{dt} = m \omega^2 \nu_{ee}(\omega) = \epsilon 2 \nu_{ee}(\omega).$$

Thus we arrive at the appropriate value for $\nu_{ee}(\epsilon)$ for insertion into Eq.(6), viz.,

$$\nu_{ee}(\epsilon) = 1.54 \times 10^{-5} n_e \epsilon^{-3/2} \ln \left\{ \frac{1.25 \times 10^4 T_e^{3/2}}{n_e^{1/2}} \right\} \text{sec}^{-1}, \quad (9)$$

where n_e is the swarm electron density cm^{-3} and ϵ is the fast electron energy in eV. Note that since the swarm temperature T_e appears only in the slowly varying logarithmic term, $\nu_{ee}(\epsilon)$ is only a weak function of T_e .

With all the terms of Eq.(6) defined, we next integrate the equation numerically to determine ϵ for various times t , i.e.,

$$- \int_{\epsilon_{\max}}^{\epsilon} \frac{d\epsilon}{L_{ea}(\epsilon) + L_{ee}(\epsilon)} = \int_0^t dt \quad (10)$$

where L_{ea} and L_{ee} are abbreviations for the electron-atom and electron-electron losses. ϵ_{\max} is the larger of $\{V_m(N_o) - V_i(A_o)\}$ or $0.31 V_i(N_o)$. Since $\bar{\epsilon}_e$ is to be determined and is unknown at this time, a first trial value of $\bar{\epsilon}_e$ must be selected. Furthermore it is necessary that $\bar{\epsilon}_e$ be always chosen greater than $\bar{\epsilon}_a$, at least by a small amount; e.g., $\bar{\epsilon}_e \geq \bar{\epsilon}_a + 0.001$ eV which corresponds to about 10°K difference and is well within the accuracy of the calculation. In this manner, infinitely long times are avoided since L_{ea} remains finite when the energy integrand is taken to its lowest value $\epsilon = \bar{\epsilon}_e$ whence $L_{ee} = 0$. However, with fast electron energies of several eV and electron swarm temperatures of tenths of an eV, the energy lost to the swarm is often only slightly influenced by the trial value selected for $\bar{\epsilon}_e$.

Now with $\epsilon = \epsilon(t)$, the energy-dependent collision frequencies ν_{ee} and ν_{ea}

are also known as functions of time. It follows that the energy lost by a fast electron to the electron swarm is

$$\int_0^{\tau_{\text{fast}}} v_{ee}(t) [\epsilon(t) - \bar{\epsilon}_e] dt$$

where τ_{fast} is the lifetime of the fast electron before it becomes a member of the swarm. Thus from Section II, the total energy input rate to the electron swarm in $\text{eV cm}^{-3}\text{sec}^{-1}$ becomes

$$F_1 \xi_{sx} + F_2 \xi_m = S^+(N_0, U, \phi, \vec{r}) \int_0^{\tau_1} v_{ee}(t) [\epsilon(t) - \bar{\epsilon}_e] dt + C_{15} [N_m] [A_0] \int_0^{\tau_2} v_{ee}(t) [\epsilon(t) - \bar{\epsilon}_e] dt$$

$$\left[\epsilon(0) = 0.31 V_i(N_0) \right] \quad \left[\epsilon(0) = V_m(N_0) - V_i(A_0) \right] \quad (11)$$

IV. ENERGY LOSS RATE OF ELECTRON SWARM

The electron swarm loses energy primarily by collisions of the electrons with the ambient ions and atoms. For our conditions of tube geometry, gas pressure, and electron density and temperature, the energy transported to the walls of the tube directly by electron diffusion is very much smaller than the energy transferred by the electrons to the atoms and ions.* Thus if $-\frac{dE}{dt}$ is the total energy loss rate of the electron swarm in $\text{eV cm}^{-3}\text{sec}^{-1}$, then

$$-\frac{dE}{dt} \approx \frac{2m_e}{M_{N_0}} \int_0^{\infty} (\epsilon - \bar{\epsilon}_a) v_{ea}(\epsilon) f(\epsilon) d\epsilon + \frac{2m_e}{M_{A+}} \int_0^{\infty} (\epsilon - \bar{\epsilon}_a) v_{ei}(\epsilon) f(\epsilon) d\epsilon \quad (12)$$

*The electron energy loss rate from ambipolar diffusion $\left(\frac{dE}{dt}\right)_{\text{diff}}$ is approximately $D_1 \left(1 + \frac{T_e}{T_i}\right) n_e \bar{\epsilon}_e$ where D_1 is the ion diffusion coefficient ($\approx 2\text{cm}^2\text{sec}^{-1}$ at room temperatures for neon at 90 torr) and $\Lambda^2 (= 0.04\text{ cm}^2)$ is the square of the characteristic diffusion length of our microwave cavity. The temperature results shown later in Table I for a neutron flux $1 \times 10^{13}\text{cm}^{-2}\text{sec}^{-1}$ indicate $T_e \approx 1000^\circ\text{K}$ (i.e., $\bar{\epsilon}_e \approx 0.13\text{ eV}$) for $T_{i,a} = 500^\circ\text{K}$ when $n_e = 1 \times 10^{12}\text{cm}^{-3}$. These data yield

$\left(\frac{dE}{dt}\right)_{\text{diff}} \approx 2 \times 10^{13}\text{eV cm}^{-3}\text{sec}^{-1}$. However, we also see from Table I that under these conditions, the input energy to the swarm from expression (3) only (neglecting metastable-ionization contributions) is $(5.39 \times 10^{15})(5.11) = 2.75 \times 10^{16}\text{ eV cm}^{-3}\text{sec}^{-1}$ which is over a 1000 times greater than that lost by diffusion. Thus we conclude that the sum of volume electron-atom and electron-ion energy losses are a factor of more than 1000 greater than the electron energy lost to the walls directly by ambipolar diffusion.

The first term is the elastic electron-atom loss rate where again the only elastic-atom losses that need be taken into account are those to the parent atoms of the gas mixture. The second term represents electron-ion losses to the dominant ions which, at the higher values of electron or ion density $n_i \approx 10^{12} \text{ cm}^{-3}$, are atomic ions of the trace gas A_+ . When the ion density falls to low values ($n_i \approx 10^{10} \text{ cm}^{-3}$) and the trace gas atomic ion no longer dominates so completely over molecular ions N_{2+} of the parent gas, then ion losses are no longer important in comparison with the neutral atom losses of the first term. Thus over our regime, the two terms of Eq.(12) suffice. $f(\epsilon)d\epsilon$ is the Maxwell-Boltzmann distribution for the number of electrons in the swarm cm^{-3} with energy in the range $\epsilon \rightarrow \epsilon+d\epsilon$. Occasionally, it is convenient to work with the fixed normalized distribution function $\left[\frac{F(y)}{n_e}\right] = 2.073 y^{1/2} e^{-3/2 y}$ where $y = \frac{\epsilon}{\epsilon_i}$ because $\frac{f(\epsilon)}{n_e} = \left[\frac{F(y)}{n_e}\right] \frac{1}{\epsilon_e}$ can then be readily determined from the normalized distribution for the selected value of $\bar{\epsilon}_e$. Note that Eq.(12) contains only one kinetic temperature $\frac{3}{2}kT_{i,a} = \bar{\epsilon}_a$ for both the ions and atoms since the energy exchange between them is so efficient. The electron-atom collision frequency for momentum transfer ν_{ea} is that which appeared in Eq.(6) but is now required over a wider range of electron energies. The electron-ion collision frequency ν_{ei} is obtained from Eq.(8), and with $m_e \ll m_i$ becomes

$$\nu_{ei}(\epsilon) = 3.86 \times 10^{-6} n_i \epsilon^{-3/2} \ln \left\{ \frac{1.25 \times 10^4 T_e^{3/2}}{n_i^{1/2}} \right\}. \quad (13)$$

The integrals of Eq.(12) cause problems, however, for values of ϵ much less than $\bar{\epsilon}_a$. The integrals diverge as $\epsilon \rightarrow 0$ which stems from the fact that the energy exchange between the electrons and the ions and atoms is approximated by using a distribution function for the electrons but an average energy for the ions and atoms. Accordingly, Eq.(12) states that electrons in the distribution function with values $\epsilon < \bar{\epsilon}_a$ will gain energy from the ions and atoms but at a rate which cannot be determined by the integrands. Now although a more rigorous energy exchange formalism is properly required to account for the very cold electrons, we can preserve the present simple scheme as follows.

We consider that when thermal equilibrium exists and the electrons are at the gas temperature, then

$$\int_0^{\bar{\epsilon}_a} (\epsilon - \bar{\epsilon}_a) v(\epsilon) F\left(\frac{\epsilon}{\bar{\epsilon}_a}\right) d\epsilon = - \int_{\bar{\epsilon}_a}^{\infty} (\epsilon - \bar{\epsilon}_a) v(\epsilon) F\left(\frac{\epsilon}{\bar{\epsilon}_a}\right) d\epsilon, \quad (14)$$

where v is either v_{ea} or v_{ei} . That is, the energy gained by the colder electrons of the swarm is balanced by the energy lost by the hotter electrons of the swarm in the well-behaved integrand $\bar{\epsilon}_a$ to ∞ . For $T_e > T_{i,a}$ we shall still write the electron energy gain as the right hand side of Eq.(14), although, in fact, the error involved by the procedure increases as $T_e - T_{i,a}$ increases. This, however, is acceptable since when $T_e - T_{i,a}$ is large and the electron swarm loses energy rapidly to the ions and atoms, we can neglect any electron-gain correction in excess of the gain at equilibrium when $T_e = T_{i,a}$. As $T_e - T_{i,a}$ is progressively reduced, thereby decreasing the electron swarm loss, the electron-gain approximation becomes progressively more accurate as it becomes relatively more important. Thus we rewrite the two terms of Eq.(12) as

$$\begin{aligned} -\frac{dE}{dt} \approx & \frac{2m_e}{M_{N_0}} \cdot n_e \left\{ \int_{\bar{\epsilon}_a}^{\infty} (\epsilon - \bar{\epsilon}_a) v_{ea}(\epsilon) \left[\frac{F(\frac{\epsilon}{\bar{\epsilon}_e})}{n_e} \frac{1}{\bar{\epsilon}_e} \right] d\epsilon - \int_{\bar{\epsilon}_a}^{\infty} (\epsilon - \bar{\epsilon}_a) v_{ea}(\epsilon) \left[\frac{F(\frac{\epsilon}{\bar{\epsilon}_a})}{n_e} \frac{1}{\bar{\epsilon}_a} \right] d\epsilon \right\} \\ & + \frac{2m_e}{M_{A+}} \cdot n_e \left\{ \int_{\bar{\epsilon}_a}^{\infty} (\epsilon - \bar{\epsilon}_a) v_{ei}(\epsilon) \left[\frac{F(\frac{\epsilon}{\bar{\epsilon}_e})}{n_e} \frac{1}{\bar{\epsilon}_e} \right] d\epsilon - \int_{\bar{\epsilon}_a}^{\infty} (\epsilon - \bar{\epsilon}_a) v_{ei}(\epsilon) \left[\frac{F(\frac{\epsilon}{\bar{\epsilon}_a})}{n_e} \frac{1}{\bar{\epsilon}_a} \right] d\epsilon \right\}. \end{aligned} \quad \dots (15)$$

Generally we find that a satisfactory upper bound for $\epsilon = \infty$ is $\epsilon \approx 12\bar{\epsilon}_e$, after which further contributions to the integrands become vanishingly small.

The above energy loss rate of the electron swarm has to equal the energy input to the swarm given previously by Eq.(11). The unknown is the electron temperature of the swarm $\bar{\epsilon}_e = \frac{3}{2} kT_e$. The procedure, then, is that for a given experimental value of electron density measured with the microwave cavity we select a trial value of T_e , and evaluate expressions (11) and (15) noting that (15) is much more sensitive than (11) to variations in T_e . Thus after selecting a second value of T_e which brings expression (15) into agreement with expression (11), a second value is computed for expression (11). Only

a few such iterations are required to bring the values of expressions (11) and (15) into agreement with a single value of T_e . An electron temperature is thus calculated for an experimental value of electron density.

This essentially completes the scope of the present paper. Further studies on predicting electron densities with our reactor kinetics theory^{3,5} now modified to include the present temperature calculation are mentioned in Section VI.

V. EXAMPLES OF CALCULATIONS AND RESULTS

(a) Values for Collision Frequencies: We require the electron-neutral collision frequency ν_{ea} for momentum transfer in both neon and argon for electron energies $0.026 \leq \epsilon \leq 8$ eV. This range has been covered for argon by Engelhardt and Phelps.²⁴ However, for neon the results of several investigators have to be combined and we have used the following data.

Chen²⁵ has measured the energy-dependence of the momentum transfer cross section $Q_{ea}(\epsilon)$ of electrons with neon atoms for very low-energy electrons, viz., over the temperature range 200 to 600°K. The experiment involved a microwave interferometer to study a decaying neon plasma. The measurements yielded a value for $Q_{ea}(\epsilon)$ consistent with the following two-term approximation:

$$Q_{ea} = 1.07 \times 10^{-17} + 2.17 \times 10^{-16} \epsilon^{\frac{1}{2}} \text{ cm}^2.$$

We have used this $Q_{ea}(\epsilon)$ expression for electron energies $0.026 \leq \epsilon \leq 0.125$ eV as shown in Fig. 2. Experimental determinations of $Q_{ea}(\epsilon)$ for higher electron energies $0.25 \leq \epsilon \leq 1.0$ eV have been reported by Gilardini and Brown²⁶ from microwave conductivity measurements in the afterglow of a pulsed discharge; their data are also shown in Fig. 2. The uppermost energy range $2 \leq \epsilon \leq 7$ eV in the figure represents the measurements of Ramsauer and Kollath²⁷ who used an electron-beam technique suitable for energies above 1 eV.²⁸ The solid curve of Fig. 2 drawn through the 3 sets of data points indicates the values of $Q_{ea}(\epsilon)$ used in the present work. The resultant collision frequency

$$\nu_{ea} = N_o Q_{ea} (5.93 \times 10^7 \epsilon^{\frac{1}{2}}) \text{ sec}^{-1}$$

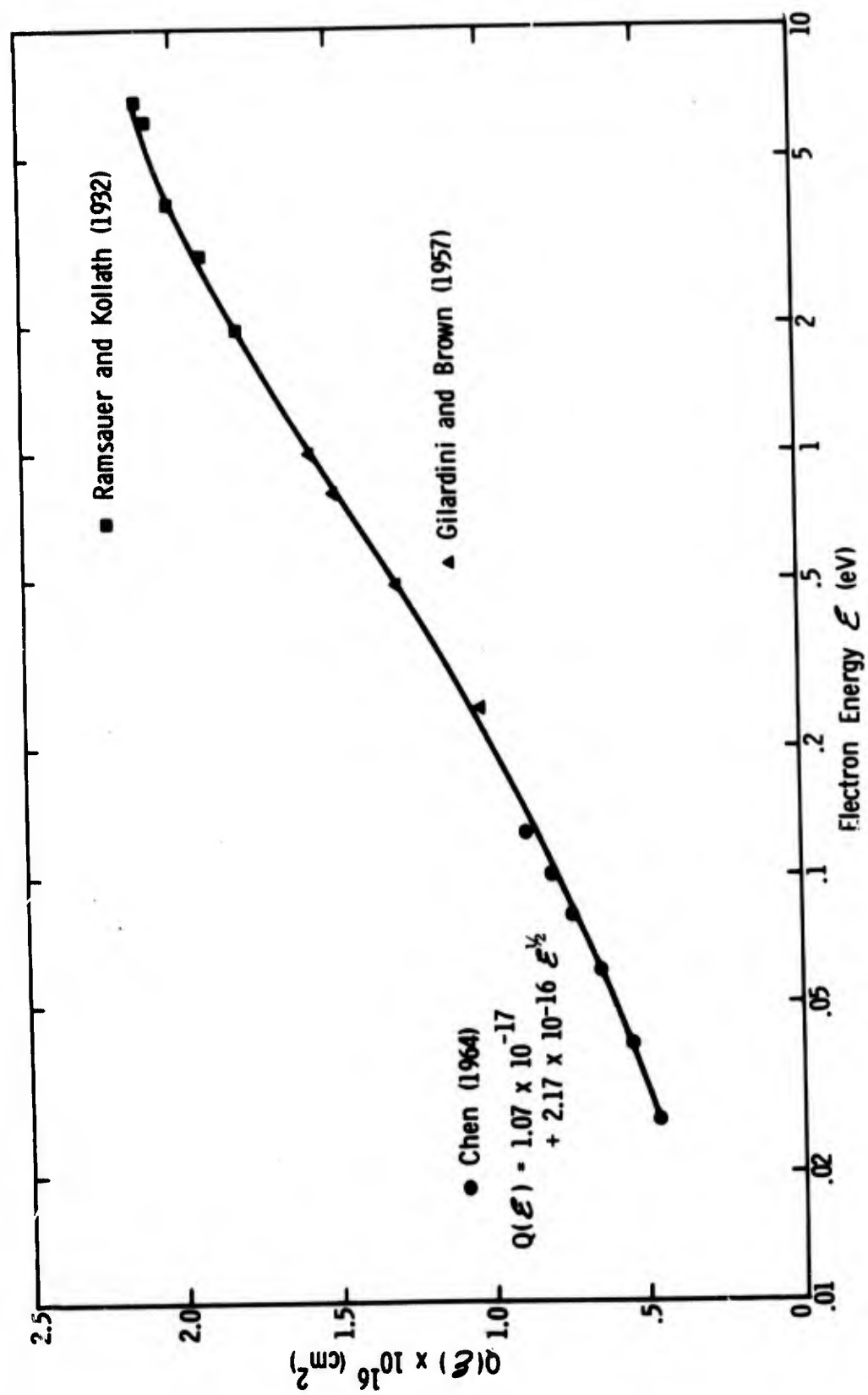


Fig. 2. Momentum transfer cross section of electrons with neon atoms.

is shown in Fig. 3 for a neon density $N_0 = 2.90 \times 10^{18} \text{ cm}^{-3}$ (or 90 torr at 300°K), which is the density of the gas in our Ne-Ar cavity ($\text{Ar/Ne} = 10^{-4}$).

The momentum transfer cross section reported by Engelhardt and Phelps for electrons in argon was determined from a numerical solution of the Boltzmann equation which incorporated trial momentum transfer and inelastic cross sections. These cross sections were then progressively refined by comparing various experimental transport coefficients with corresponding theoretical coefficients obtained by taking appropriate averages over the distribution function. The momentum transfer cross section so determined clearly exhibits the Ramsauer minimum as does the derived collision frequency shown in Fig. 3. The argon density of $3.22 \times 10^{18} \text{ cm}^{-3}$ (100 torr at 300°K) is the gas density in our Ar-Cs microwave cavity.

For comparison, Fig. 3 also shows values of $\nu_{ee}(\epsilon)$ and $\nu_{ei}(\epsilon)$ from Eqs. (9) and (13) for charge densities $n_e = n_i = 10^{12} \text{ cm}^{-3}$ and electron swarm temperatures T_e of around 1000°K. These collision frequencies are directly proportional to n_e but depend only weakly upon T_e via the argument of the logarithmic term. The dashed region of the ν_{ee} vs ϵ plot indicates the decreasing validity of the ν_{ee} expression as the energy of the fast electron decreases towards the average electron swarm energy. However, much accuracy is not required in this very low energy region since energy transfer rates here are no more than very small corrections to the overall input energy rate to the electron swarm.

(b) Example of Electron Swarm Energy Gain and Loss Rates: As an example of the temperature calculation, we consider some data obtained previously for the 7 mm-spacing Ne-Ar microwave cavity with $[\text{Ar}]/[\text{Ne}] = 10^{-4}$ and $[\text{Ne}] = 2.90 \times 10^{18} \text{ cm}^{-3}$. At a neutron flux of $5 \times 10^{11} \text{ cm}^{-2} \text{ sec}^{-1}$ we computed from our ion generation rate theory¹ a value of $S^+ = 9.35 \times 10^{-5} [\text{Ne}] = 2.71 \times 10^{14} \text{ ions cm}^{-3} \text{ sec}^{-1}$ at the center of the cavity and a neon metastable density from our reaction kinetics theory⁵ of $[\text{Ne}^m] \approx 1.7 \times 10^{10} \text{ cm}^{-3}$. The electron density determined from the change in resonant frequency of the cavity* was $2 \times 10^{11} \text{ cm}^{-3}$.

*For the purpose of the present example we visualize an electron density which is spatially uniform throughout the cavity so that the measured value of n_e can be identified with the values of S^+ and $[\text{Ne}^m]$ computed for the center of the cavity. To correlate properly our calculations with the average value of n_e determined experimentally, we integrate our computed spatial dependence of n_e over the electric field configuration of the cavity operating in the TM_{020} mode. For full details, the reader is referred to the succeeding report⁹ by C. B. Leffert.

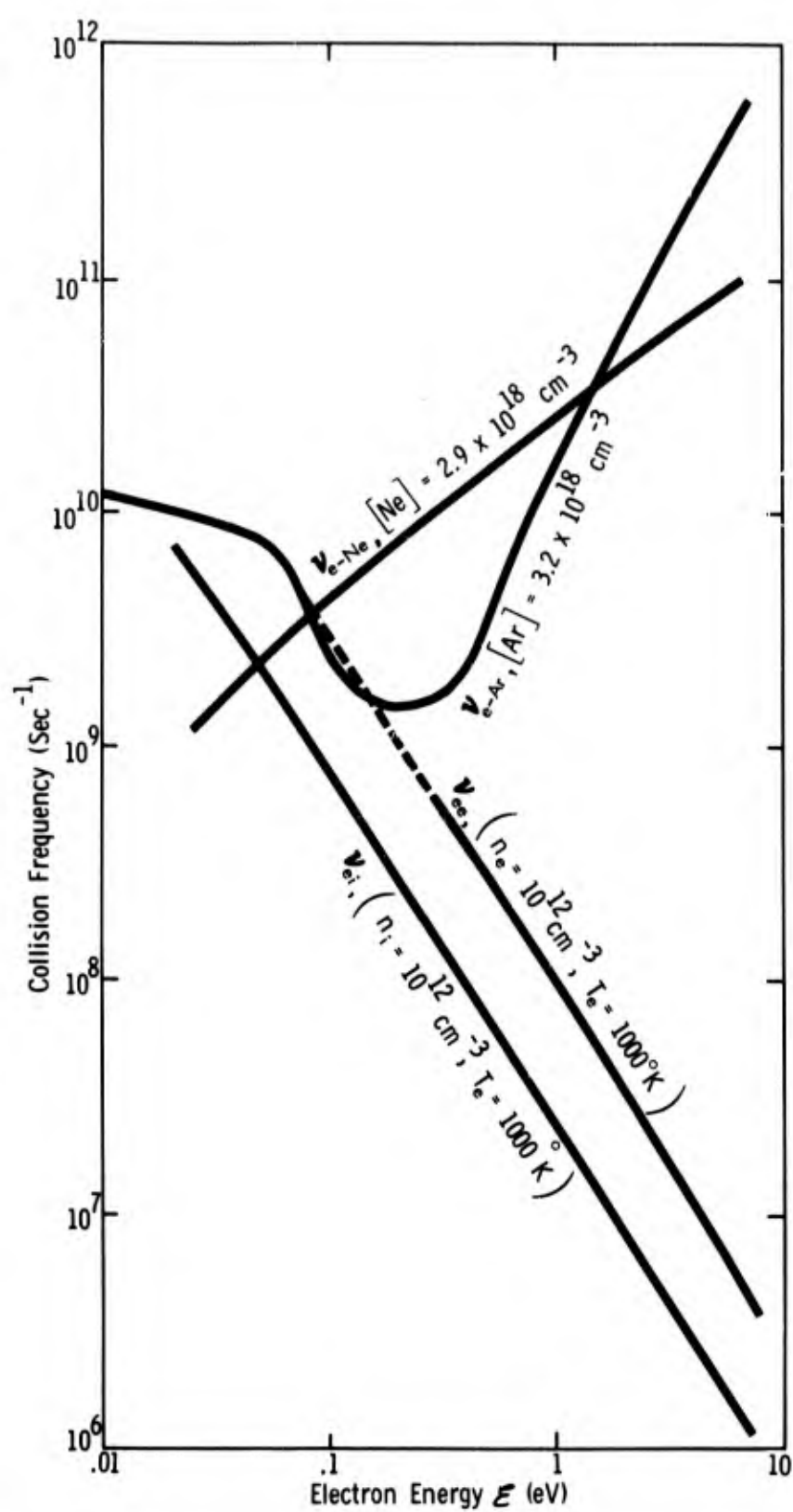


Fig. 3. Collision frequencies for e-Ar, e-Ne, e-e, and e-i as functions of electron energy.

Also, the average operating temperature of the cavity in this neutron flux was about 400°K. These are approximately mid-range values for our experiments which span neutron flux values of about 10^{10} - 10^{13} cm⁻²sec⁻¹ and electron densities of about 10^{10} - 3×10^{12} cm⁻³.

A trial value of T_e has to be selected in order to evaluate the energy input to the electron swarm given by expression (11). Our initial guess was $T_e = 600^\circ\text{K}$ ($\bar{\epsilon}_e = 0.078$ eV); that is, the electron swarm was taken to be 200°K hotter than the ambient ions and atoms ($T_{i,a} = 400^\circ\text{K}$) at the average cavity temperature. The final value of T_e , after only 1 iteration, was close to our initial guess, viz., $T_e = 525^\circ\text{K}$ ($\bar{\epsilon}_e = 0.068$ eV), and the final energy loss rate curves for the fast electron (discussed below) were essentially unchanged from those initially computed.

Figure 4 shows $(L_{ee} + L_{ea})^{-1}$ in sec/eV versus ϵ where the electron-atom loss rate $L_{ea} = \frac{2m_e}{M_{No}} \nu_{ea}(\epsilon) \{ \epsilon - \bar{\epsilon}_a \}$, and the electron-electron loss rate $L_{ee} = \nu_{ee}(\epsilon) \{ \epsilon - \bar{\epsilon}_e \}$. The area under the curve taken from the maximum fast electron energy of 6.47 eV ($0.31 V_i$ for the Ne-Ar system) to any other energy value, say ϵ_x , represents the time for the fast electron to lose energy from 6.47 to ϵ_x eV. Thus we see in Fig. 5 the energy degradation of the fast electron as a function of time (right side ordinate). Also shown are the energy loss rates to the atoms and swarm electrons as a function of time (left side ordinate). Note that the electron-atom loss dominates initially but that electron-electron coupling to the swarm takes over after 0.12 μsec . When ϵ becomes very close to $\bar{\epsilon}_e$, L_{ee} falls precipitously towards zero. However, since L_{ea} is still finite at $\epsilon = \bar{\epsilon}_e$, the height of the peak in Fig. 4 near $\epsilon = \bar{\epsilon}_e$ is also finite.

We can now evaluate expression (11) by integrating the energy loss rates over the lifetime of both the fast electron from fission fragments and the fast electron from metastable ionization. The resulting partition of energy is shown schematically in Fig. 6. The two terms for the total energy input rate to the electron swarm then become respectively:

$$\begin{aligned} F_1 \dot{\Sigma}_{sx} + F_2 \dot{\Sigma}_m &= S^+(3.49) + C_{15} [N_m][A_o] \quad (0.82) \\ &= 9.41 \times 10^{14} + 7.28 \times 10^{13} \quad (\text{with } C_{15} = 1.8 \times 10^{-11} \text{ from ref. 16}) \\ &= 1.01 \times 10^{15} \text{ eV cm}^{-3} \text{ sec}^{-1}. \end{aligned}$$

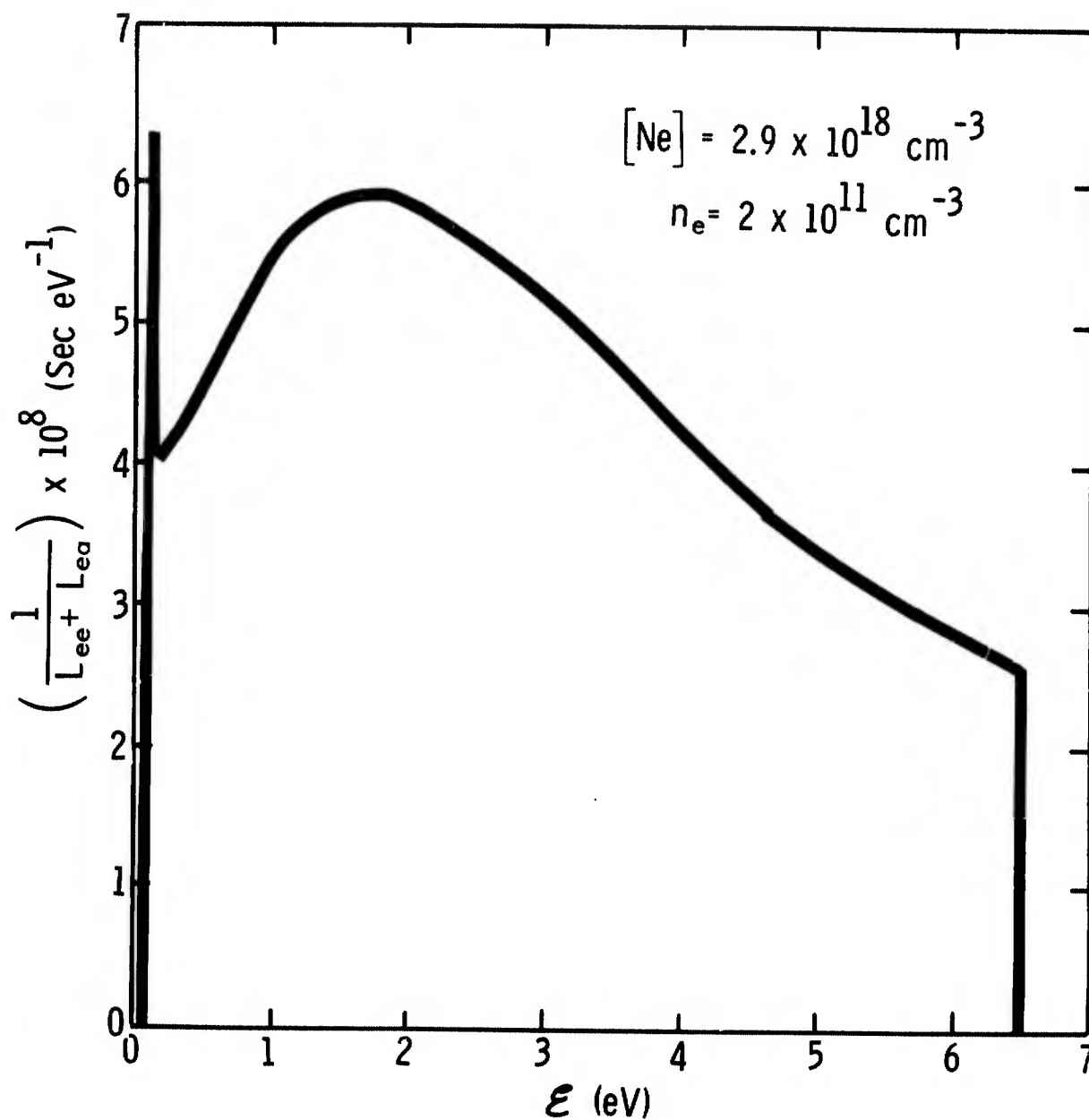


Fig. 4. Reciprocal of the sum of electron-electron and electron-atom loss rates in neon versus fast electron energy. Area under the curve represents the time for fast electron to lose energy.

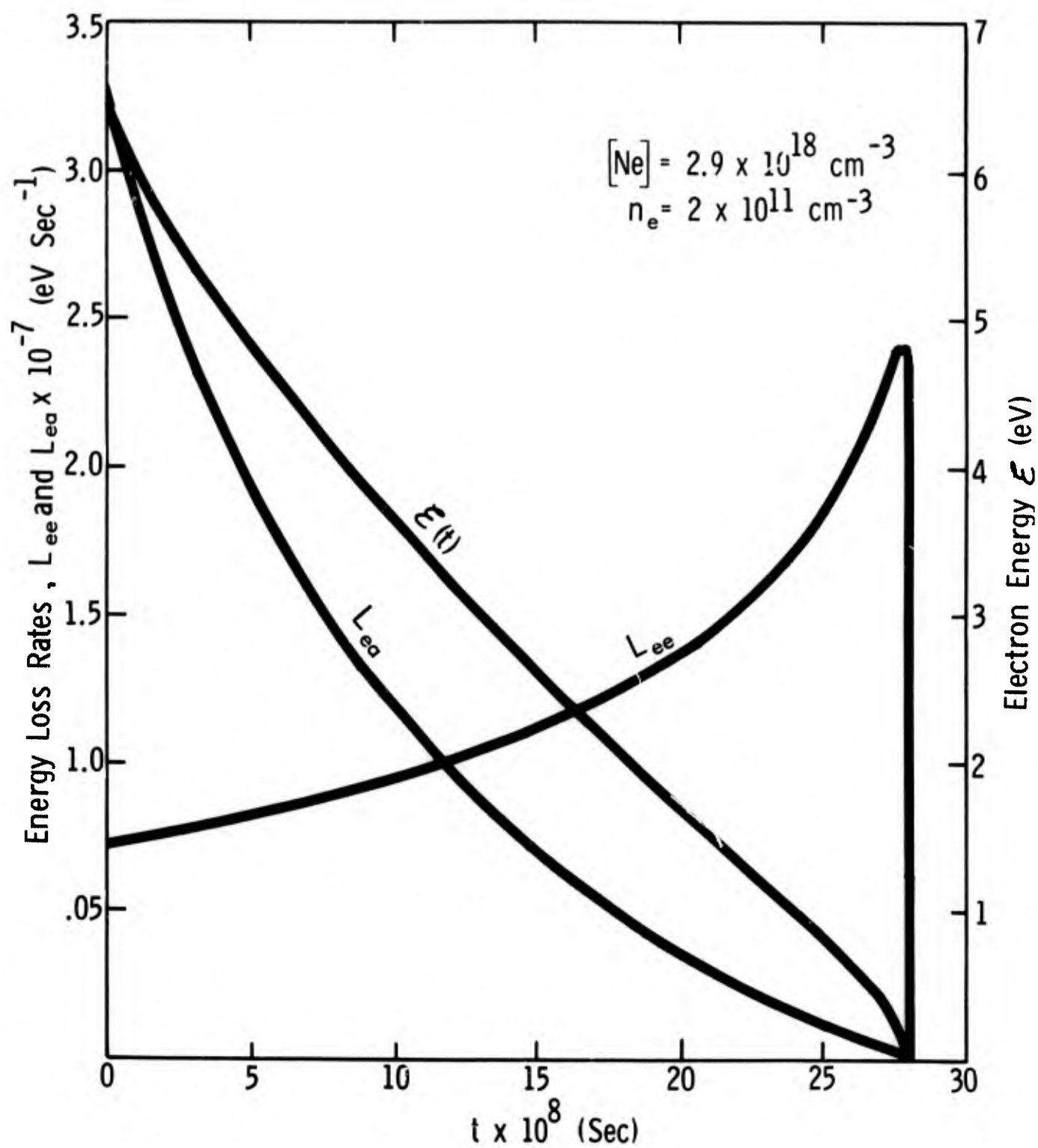


Fig. 5. Electron-atom loss rate, electron-electron loss rate, and fast electron energy versus time for neon.

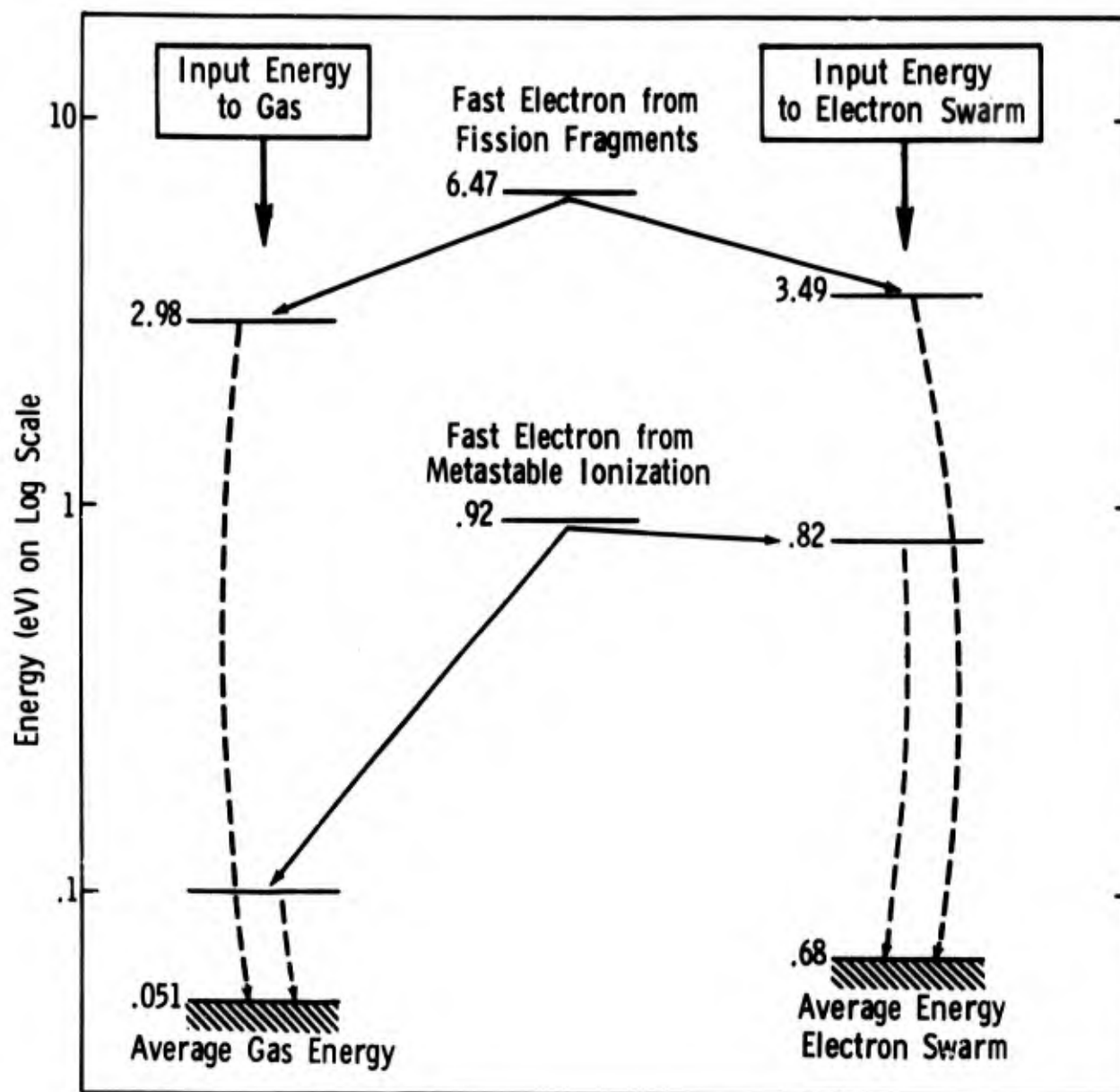


Fig. 6. Schematic energy diagram showing the energy lost by the fast electrons to the neon gas and to the electron swarm for $[\text{Ne}] = 2.90 \times 10^{18} \text{ cm}^{-3}$ and $n_e = 2 \times 10^{11} \text{ cm}^{-3}$.

Note that the contribution to the total energy input rate from the metastable-ionization process is only about 7%. While this term is generally small for Ne-Ar, it becomes more important for Ar-Cs since the initial electron energy is then increased from 0.9 to 7.7 eV (Eq. (4)).

The energy loss rate ($\text{eV cm}^{-3}\text{sec}^{-1}$) of the electron swarm for any set of values n_e , T_e , T_a can be immediately determined from expression (15). For the purpose of the present analytic discussion we note the following simplified procedure applicable to Ne-Ar. We find that for electron densities $\leq 3 \times 10^{12} \text{ cm}^{-3}$ the most important integrands are those containing v_{ea} , and this means that $-\frac{dE}{dt}/n_e$ is nearly independent of n_e . Thus, the electron swarm loss rate per electron can be conveniently plotted versus swarm temperature for a particular value of T_a , and we show typical curves in Fig. 7. Such curves once computed can be used in a general sense to read off the values of T_e which yield swarm loss rates equal to the previously determined swarm input rates. It should be emphasized that such a procedure cannot be used as conveniently for Ar-Cs since the value of v_{ea} is so low around the Ramsauer minimum that v_{ei} contributions (which depend on n_e) are still important even when n_e is less than 10^{12} cm^{-3} . However, there is still no problem in evaluating expression (15) for each chosen n_e , T_e , T_a .

We complete the present example by noting that the swarm energy input rate per electron is $\frac{1.01 \times 10^{15}}{2 \times 10^{11}} = 5.1 \times 10^3 \text{ eV sec}^{-1}$, which is also the swarm energy loss rate per electron and therefore from Fig. 7 corresponds to an electron temperature of about 525°K for the gas temperature of 400°K.

(c) Electron Temperature Results: Figure 8 shows the results of three temperature calculations for Ne-Ar which span the range of our experimental data.⁴ As input, we have used values of electron density of 10^{10} , 2×10^{11} and 10^{12} cm^{-3} corresponding respectively to neutron flux values of 10^{10} , 5×10^{11} and $10^{13} \text{ cm}^{-2}\text{sec}^{-1}$. The average cavity temperature rose with increasing flux and was in the neighborhood of 300, 400 and 500°K respectively. We see that at low flux values, the electrons are essentially in equilibrium with the atoms, but as the flux increases, the electron temperature increases faster than the ambient temperature reaching a distinctly non-equilibrium value of about 1000°K at $\phi \approx 1 \times 10^{13} \text{ neutrons cm}^{-2}\text{sec}^{-1}$.

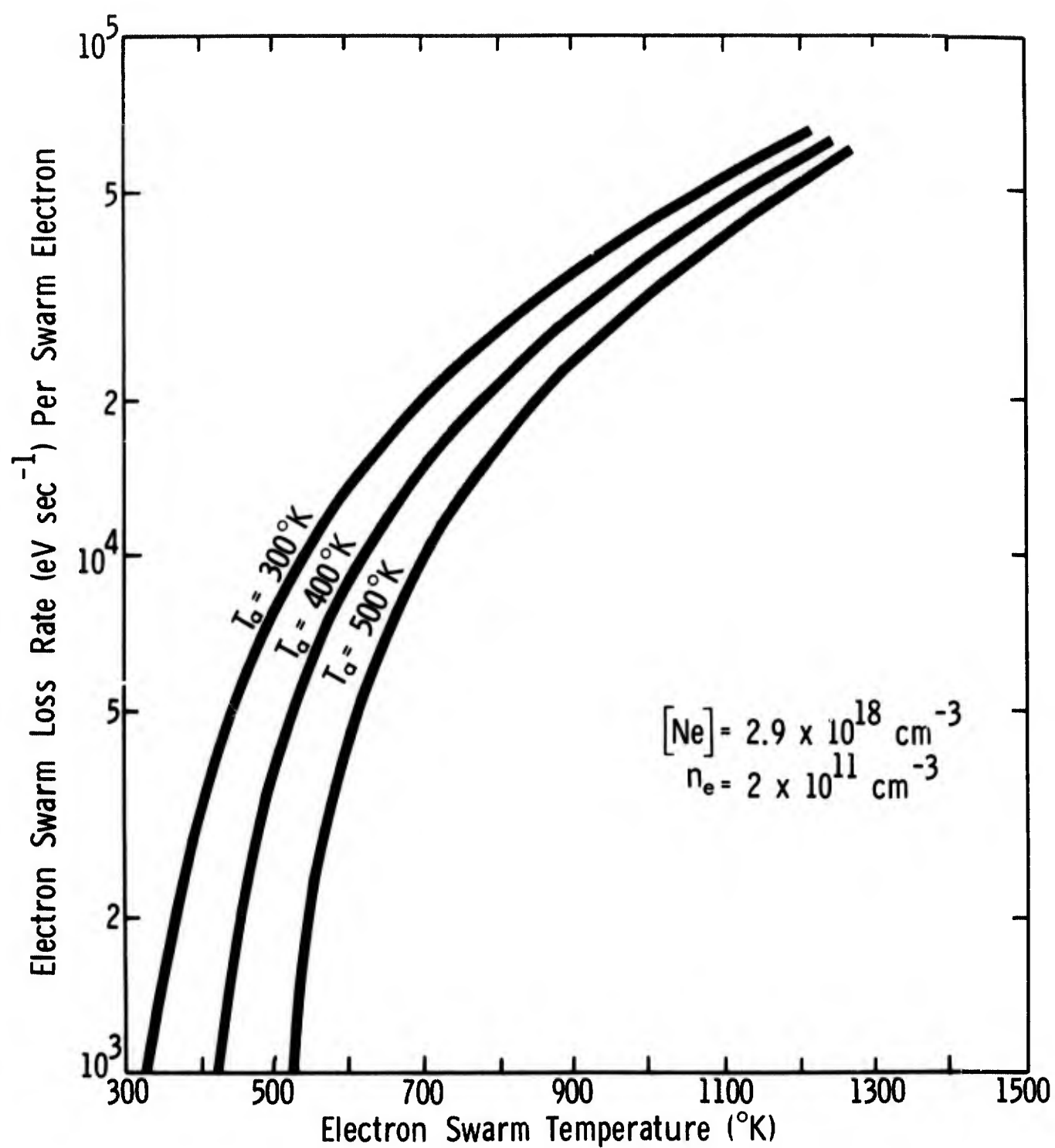


Fig. 7. Electron swarm loss rate per electron versus swarm temperature for three ambient neon gas temperatures.

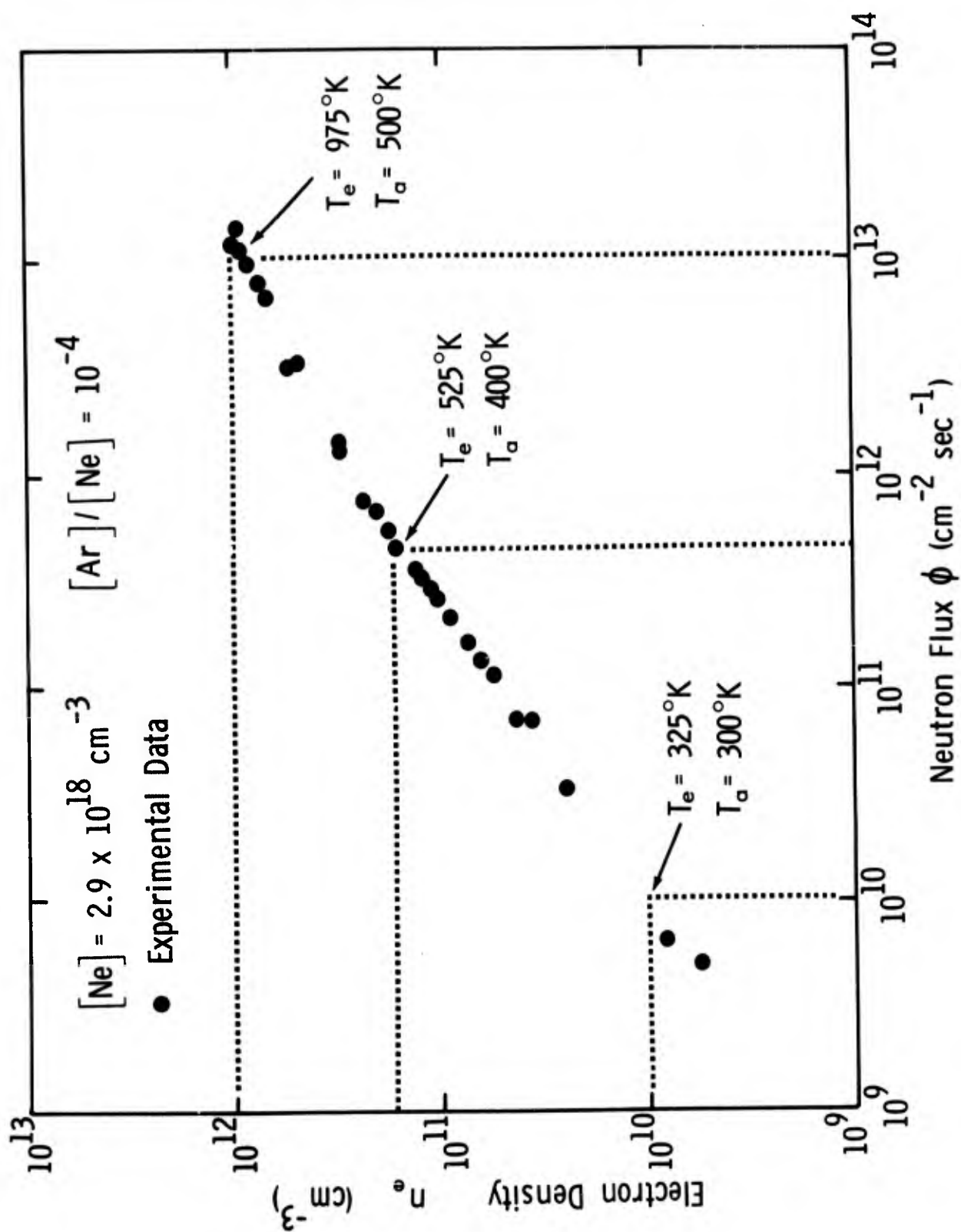


Fig. 8. Computed values of electron temperature T_e for 3 selected points along the experimental n_e - ϕ curve obtained with the Ne-Ar microwave cavity. Approximate values of the average cavity temperature which increased with ϕ are also shown.

The main reason for this can be extracted from the data shown in Table I. As n_e increases by a factor of 100, the dominant electron-electron energy coupling into the electron swarm (Column 5) increases by a factor of around four, and more importantly, the ion generation rate (or flux) increases by a factor of 1000. Thus the energy input to the swarm has increased by a factor ~ 4000 which is significantly larger than the increase in the number of electrons which share this energy. It is expected, therefore that the electron temperature will rise with ϕ over the range of parameters.

We have performed a similar calculation for the Ar-Cs system with $[Cs]/[Ar] = 10^{-4}$, $S^+ = 1.5 \times 10^{16} \text{ cm}^{-3} \text{ sec}^{-1}$ (at $\phi = 1 \times 10^{13} \text{ neutrons cm}^{-2} \text{ sec}^{-1}$ and $[Ar] = 3.22 \times 10^{18} \text{ cm}^{-3}$), $T_g \approx 600^\circ \text{K}$, and a selected value for n_e of 10^{12} cm^{-3} . As referred to earlier, no attempt was made here to modify the procedure to include the important low-lying excitation and ionization cross sections of cesium which are expected to be important energy loss sinks for the fast electrons. Thus with elastic losses only, we find that $T_e \approx 2200^\circ \text{K}$ or $\bar{\epsilon}_e \approx 0.29 \text{ eV}$ which places the average swarm energy right in the region of the Ramsauer minimum (Fig. 3) where the swarm cannot lose its energy very rapidly. However, we expect that the inclusion of inelastic cross sections will appreciably depress the swarm temperature (at the same time possibly increasing n_e) from the value given above.

VI. SIGNIFICANCE OF RESULTS AND FURTHER STUDIES

The values of T_e presented here for gas pressures ~ 90 torr show that although a thermal equilibrium approximation $T_e \approx T_{i,a}$ is adequate for the lower regions of neutron flux ϕ , such an approximation breaks down for values of $\phi \approx 10^{13} \text{ cm}^{-2} \text{ sec}^{-1}$ where $T_e \cdot T_{i,a} \sim 500^\circ \text{K}$ for the Ne-Ar system. It is of interest to compare this finding with the recent inpile radiometric electron-temperature measurements of Bhattacharya, Verdeyen, Adler and Goldstein.²⁹ For a radiation-induced plasma in pure neon, these authors report that at $p=60$ torr, $T_e=800^\circ \text{K}$, but for $p=90$ torr, $T_e \sim 437^\circ \text{K}$. Values of T_e at higher pressures could not be determined because of background microwave noise problems but T_e was considered to be $< 525^\circ \text{K}$ and essentially at the gas temperature, i.e., independent of reactor power. However, it is difficult to draw a close comparison between these results and our own because these workers did

TABLE I. Summary of temperature calculations for the Neon-Argon microwave cavity with $[Ne]=2.90 \times 10^{18} \text{ cm}^{-3}$ and $[Ar]=2.90 \times 10^{14} \text{ cm}^{-3}$. The cavity is a right-circular metal cylinder of 7 mm height which contains a uranium-235 foil brazed to an inside surface.

Neutron Flux ϕ $\text{cm}^{-2} \text{ sec}^{-1}$	(a) Ion Generation Rate S^+ $\text{cm}^{-3} \text{ sec}^{-1}$	(b) Electron Density n_e cm^{-3}	(c) Metastable Density N_m cm^{-3}	Swarm Input Energy from		Gas Temp T_a $^{\circ}\text{K}$	Electron Temp T_e $^{\circ}\text{K}$	Temperature Excess $(T_e - T_a)$ $^{\circ}\text{K}$
				Direct Fragments eV	Metastables eV			
1×10^{10}	5.39×10^{12}	1×10^{10}	3.36×10^8	1.15	0.69	300	320	20
5×10^{11}	2.71×10^{14}	2×10^{11}	1.70×10^{10}	3.49	0.82	400	525	125
1×10^{13}	5.39×10^{15}	1×10^{12}	3.44×10^{11}	5.11	0.79	500	975	475

(a) Computed from ion generation rate theory¹

(b) Experimental values from inpile microwave cavity⁴

(c) Computed from reaction kinetics theory⁵

not measure directly or calculate their value of ionization rate S^+ . Furthermore, the experimental conditions were importantly different. In the University of Illinois study, the gas ionization resulted from high-energy electrons produced mainly by γ -photons from a reactor pulsed to peak powers ~ 250 MW and so S^+ depended not only on the gas but also on the nature of the container walls. Even so, we note that a reactor power pulse which is ~ 100 times that used in our steady-state study (2 MW) would tend to bring the γ -ionization source up to the level of our fission fragment source (our $S^+(\text{fission fragments})/S^+(\gamma)$ is ~ 100) which may account for the similarity between the Illinois temperature data at 60 torr and the present results at 90 torr. However, much more information regarding the detailed nature and energy balance of the primary ionization processes is required for the experiments of Bhattacharya *et al.*, before meaningful electron temperature calculations from first principles can be undertaken for their experimental conditions.

The increase in the non-equilibrium value of T_e with ϕ is important to us from the standpoint of our reaction kinetics equations³ for predicting electron densities. In the previous report by C. B. Leffert,⁷ which was primarily a study of matching the reaction kinetics equations to the experimental Ar-Cs data by postulating the existence of ArCs^+ , it was found not only that ArCs^+ was an unlikely cause of discrepancy between theory and experiment, but also that an elevated electron temperature appeared to be a necessary condition for good agreement since the role of collisional-radiative recombination needed to be reduced by a factor of about 10. Thus with the present results of elevated electron temperature we expect better agreement between theory and experiment in Ar-Cs.

With respect to the results on Ne-Ar reported here, we emphasize that experimental values of electron density were used as input to the equations that yielded values for T_e . In this manner, the elevation of T_e above ambient was first clearly established. However, we can now remove this mix of experiment and theory and, from first principles, calculate an average electron density for comparison with experiment. A program for the simultaneous solution of n_e and T_e at a point in the plasma (written in FORTRAN VI for the IBM 7094 computer) is used to compute the radial dependence of electron density in the cavity. With an additional computer program and using well-known microwave theory, the electron density is then averaged over the square of the electric field in the cavity to yield computed values (with no adjustable parameters) that can be compared directly with the values of n_e determined from inpile experiments. The results of these studies are reported by C. B. Leffert⁹ in the following report.

REFERENCES

1. C. B. Leffert, D. B. Rees and F. E. Jamerson, J. Appl. Phys., 37, 133, (1966).
2. C. B. Leffert, D. B. Rees and F. E. Jamerson, Phys. Letters, 22, 423, (1966).
3. D. B. Rees, C. B. Leffert and F. E. Jamerson, Proc. IEEE Thermionic Specialist Conference (San Diego), p. 166, (1965).
4. C. B. Leffert and D. B. Rees, ONR Annual Report No. 7, Contract Nonr-3109(00), (Oct. 1966).
5. C. B. Leffert, D. B. Rees and F. E. Gifford, ONR Annual Report No. 6, Contract Nonr-3109(00), (Oct. 1965).
6. C. B. Leffert, D. B. Rees and F. E. Jamerson, ONR Annual Report No. 5, Contract Nonr-3109(00), (Oct. 1964).
7. C. B. Leffert, "Reaction Kinetic Studies of Ar-Cs Plasmas", Section A, Final ONR Annual Report No. 8, Contract Nonr-3109(00), (Oct. 1967).
8. D. B. Rees, "Heteronuclear Ions", Section A (h), Ref. 4.
9. C. B. Leffert, "Electron Densities in Fission Fragment Plasmas Generated in Microwave Cavities", Section C, Final ONR Annual Report No. 8, Contract Nonr-3109(00), (Oct. 1967).
10. A. Dalgarno, Atomic and Molecular Processes, (Ed. D. R. Bates), Academic Press, p. 622, (1962).
11. H. A. Bethe and J. Ashkin, Experimental Nuclear Physics, (Ed. E. Segre) Wiley, Vol. I, p. 232 (1952).
12. R. D. Evans, The Atomic Nucleus, McGraw-Hill, pp. 642-653, (1955); see also J. N. Anno, J. Appl. Phys., 5, 1678 (1962).
13. F. E. Jamerson, C. B. Leffert and D. B. Rees, J. Appl. Phys., 36, 355 (1965).
14. R. L. Platzman, Inter. J. Appl. Radiation and Isotopes, 10, 116 (1961).
15. N. G. Utterback and G. H. Miller, Phys. Rev., 116, 976 (1959).
16. D. B. Rees, "Production, Diffusion and Conversion Rates of Ions, Metastable and Excited States in Penning-Type Neon-Argon Plasma", Section D, Ref. 6, and GMRL, PH-384 (1964).
17. D. B. Rees, "Reaction Rates of Ions, Metastable and Excited States in Argon-Cesium Plasmas", Section A, Ref. 5; and GMRL, PH-412 (1965).
18. R. M. May, Phys. Rev., 135, A1009 (1964).
19. L. Spitzer, Physics of Ionized Gases, Interscience Publishers, (1950).
20. S. Chandrasekar, Astrophys. J., 93, 285 (1941).

21. S. Chapman and T. G. Cowling, Mathematical Theory of Non-Uniform Gases, Cambridge Univ. Press, (1960).
22. M. N. Rosenbluth, W. M. MacDonald and D. L. Judd, Phys. Rev., 107, 1 (1957).
23. D. J. Rose and M. Clark, Jr., Plasmas and Controlled Fusion, M. I. T./Wiley, p. 166, (1961).
24. A. G. Engelhardt and A. V. Phelps, Phys. Rev., 133, A375 (1964).
25. C. L. Chen, Phys. Rev., 135, A627 (1964).
26. A. L. Gilardini and S. C. Brown, Phys. Rev., 105, 31 (1957).
27. R. B. Brode, Revs. Modern Physics, 5, 257 (1933).
28. R. W. Crompton and R. L. Jory, IVth International Conference on Physics of Electronic and Atomic Collisions, (Quebec), Abstracts of Papers, p. 118, (1965).
29. A. K. Bhattacharya, J. T. Verdeyen, F. T. Adler and L. Goldstein, J. Appl. Phys., 38, 527 (1967).

SECTION C

SECTION C

ELECTRON DENSITIES IN FISSION-FRAGMENT-INDUCED PLASMAS IN MICROWAVE CAVITIES

ABSTRACT

The ion generation rate theory, the reaction kinetics theory and the non-equilibrium temperature theory for a noble gas plasma ionized by fission fragments are combined here in a single theory for predicting from first principles the electron density at a point in the plasma using digital computer techniques. The ion generation rate in the plasma is computed from known constants of the fission fragments and gases. The reaction kinetics theory for a binary Penning-type gas plasma and the non-equilibrium electron temperature theory are incorporated into a digital computer scheme which computes a self-consistent electron density-electron temperature pair (n_e, T_e) for a point in the plasma. The radial dependence of the electron density in a microwave cavity is obtained using input values of the ion generation rate as computed from the fission fragment flux penetrating the gas at various points within the cavity. Finally, with this radial dependence of n_e , and the known spatial dependence of the microwave field probing the plasma, an integrating computer code is used to obtain a value of the electron density averaged over the square of the electric field $\langle n_e \rangle_{av}$ for direct comparison with the inpile measured values from the Ne-Ar and Ar-Cs microwave cavities. The values of $\langle n_e \rangle_{av}$ for the Ne-Ar cavity ($[Ar]/[Ne] = 10^{-4}$), computed with no adjustable parameters, agreed well (within $\pm 20\%$) with the inpile microwave measurements over the complete range of neutron flux studied ($10^{10} \leq \phi \leq 10^{13} \text{ cm}^{-2} \text{ sec}^{-1}$). Also the electron swarm temperature in Ne-Ar was found to be as much as a factor of two higher than the gas temperature at the higher values of the neutron flux ($\phi \sim 1.5 \times 10^{13} \text{ cm}^{-2} \text{ sec}^{-1}$). This non-equilibrium condition explains in large part the experimental insensitivity of the electron density in Ne-Ar to variations in the average gas temperature. The computed values for argon-cesium agreed well with the inpile microwave data for low values of $[Cs]/[Ar]$ ($\approx 10^{-6}$) but the computed values were much too high for higher cesium atom concentrations ($[Cs]/[Ar] \gtrsim 5 \times 10^{-6}$). This behavior was expected since the theory does not, as yet, include terms necessary to account for inelastic collisions of hot electrons with the easily excited cesium atoms. Modifications to the codes are outlined to take into account the inelastic collisions.

CONTENTS

ABSTRACT	i
OBJECT	1
CONCLUSIONS	1
LIST OF SYMBOLS	3
I. INTRODUCTION	8
II. ELECTRON DENSITY-TEMPERATURE CODE (CW8)	11
A. <u>Electron Temperature Theory</u>	11
1. Input	13
2. Production Rate of Excess Energy	13
3. Energy Loss Rate of Energetic Electrons to Gas and Electron Swarm	13
4. Energy Gain of the Electron Swarm	14
5. Energy Loss of the Electron Swarm	15
6. Applicability of Model to Microwave Experiments. .	17
B. <u>Electron Temperature Subroutine (TELECT)</u>	19
1. Analytic Expression to Guide Convergence	19
2. Average Collision Frequency.	22
3. Integration Subroutines	23
4. Calling Statement and Argument List	24
5. Other Coding Considerations	25
6. Check of Output	25
C. <u>Electron Density Subroutine (NONLIN)</u>	25
1. Subroutines for the Electron-Density Subroutine (NONLIN)	26
2. Calling Statement and Argument List	27
D. <u>Main Control Program for Electron Density-Temperature Code (CW8)</u>	27
1. Input	29
2. Computation of Recombination Coefficient C_{22} (n_e, T_e)	29
3. Adjustment of Diffusion Coefficients for T_g and T_e . .	31
4. Convergence on (n_e, T_e) Solution	32
5. Core Size of Program and Running Time	32
6. Output for an Example Problem	32
III. RESONANT FREQUENCY SHIFT CODE (CW9)	34
A. <u>Microwave Theory</u>	35
1. Frequency Shift of the Cavity	35
2. Normal-Mode Fields for a Right Circular Cylinder .	37
B. <u>Computer Code (CW9)</u>	41

CONTENTS

IV. ANALYSIS OF INPILE MICROWAVE DATA	42
A. <u>Microwave Experiment</u>	42
B. <u>Analysis of Neon-Argon Microwave Data</u>	44
1. Average Gas Temperature $\langle T_{\text{gas}} \rangle_{\text{av}}$	44
2. Reaction Rates	44
3. Ion Generation Rate	47
4. Electron Density Versus Neutron Flux	49
5. Electron Density Versus Average Gas Temperature	50
C. <u>Analysis of Argon-Cesium Microwave Data</u>	54
1. Reaction Rate Coefficients	54
2. Comparison of Theory and Experiment	54
D. <u>Modifications to CW8 Code to Include Inelastic Collisions</u>	56
V. REFERENCES	58
APPENDIX A - ELECTRON DENSITY-TEMPERATURE CODE	A-i
APPENDIX B - RESONANT FREQUENCY-SHIFT CODE	B-i

OBJECT

The first objective for these studies was to use digital computer techniques to incorporate into one overall computational scheme our theories for (a) ion generation rate, (b) reaction kinetics, (c) non-equilibrium electron temperature, and (d) the existing theory for resonant microwave cavity response so that the electron density in our fission-fragment-generated noble-gas plasmas could be predicted from first principles. The second objective was to compare the predicted electron densities to the experimental values measured in the reactor with our Ne-Ar and Ar-Cs filled microwave cavities.

CONCLUSIONS

COMPARISON OF THEORY AND EXPERIMENT

1. Theoretical values of the average electron density $\langle n_e \rangle_{av}$ for the Ne-Ar cavity ($[Ar]/[Ne]=10^{-4}$), computed with no adjustable parameters, were in excellent agreement (within $\pm 20\%$) with the inpile microwave measurements over the complete range of neutron flux studied ($10^{10} \leq \phi \leq 10^{13} \text{ cm}^{-2} \text{ sec}^{-1}$).
2. The electron swarm temperature in Ne-Ar was found to be as much as a factor of two higher than the gas temperature at the higher values of the neutron flux, and this non-equilibrium condition explains in large part the experimental insensitivity of the electron density in Ne-Ar to variations in the average gas temperature.
3. The computed values of average electron density $\langle n_e \rangle_{av}$ for the Ar-Cs cavity agreed well with the inpile microwave measurements at the lowest value of $[Cs]/[Ar] (\approx 10^{-6})$ but the computed values were much too high for higher cesium atom concentrations ($[Cs]/[Ar] \gtrsim 5 \times 10^{-6}$) because the theory does not, as yet, include terms necessary to account for inelastic collisions of hot electrons with the easily excited cesium atoms.

COMPUTER TECHNIQUES

4. The simultaneous solution of the reaction kinetics theory ($n_e = n_e(T_e)$) and the electron temperature theory ($T_e = T_e(n_e)$) was successfully accomplished with an iteration procedure operating on computer codes for each to converge on a self-consistent value for the (n_e, T_e) pair. The FORTRAN-IV program for this code required about 23,000 cells of core storage (IBM 7094)

but the running time was quite short, viz., about 1 minute for a problem needing 11 solutions for (n_e, T_e) .

5. The radial dependence of the electron density in the microwave cavity was computed and coupled with the known spatial dependence of the microwave field to obtain the electron density averaged over the square of the electric $\langle n_e \rangle_{av}$ for direct comparison with measured values from the inpile microwave cavities.

LIST OF SYMBOLS

SYMBOL	FORTRAN NAME	DESCRIPTION	
<u>Physical Constants</u>			
c	KC	Speed of light, 2.99793×10^8 m sec ⁻¹	
e	Q	Charge of electron, 1.60210×10^{-19} Coulomb	
ϵ_0	KP	Permittivity of free space, 8.8540×10^{-12} farad m ⁻¹	
k	KB	Boltzmann constant, 1.3804×10^{-23} joule °K ⁻¹	
m _e	ME	Mass of electron, 9.1084×10^{-31} kg	
<u>Number Densities in Units of cm⁻³</u>			
<u>Generalized (with subscripts):</u>		<u>Specific (with superscripts):</u>	
N _o	NO	Neutral atom of major species	Ne or [Ne], Ar
A _o	AO	Neutral atoms of minor species	Ar, Cs
n _e	X(1)	Electrons	
N ₊	X(2)	Atomic ion of major species	Ne ⁺ , Ar ⁺
N ₂₊	X(3)	Molecular ion of major species	Ne ₂ ⁺ , Ar ₂ ⁺
N _*	X(4)	Excited state of major species	Ne [*] , Ar [*]
N _m	X(5)	Metastable state of major species	Ne ^m , Ar ^m
A ₊	X(6)	Atomic ion of minor species	Ar ⁺ , Cs ⁺
A ₂₊	X(7)	Molecular ion of minor species	Ar ₂ ⁺ , Cs ₂ ⁺
A _*		Excited state of minor species	Ar [*] , Cs [*]
Cs _o		[Cs] in equilibrium in bath	
<u>Dimensions</u>			
d	D	Height of right circular cylindrical cavity, cm	
ρ ₁	RH01	Radius of uranium foil, cm	
ρ ₂	RH02	Radius of right circular cylindrical cavity, cm	
Δ	LAM	Characteristic diffusion length of cavity, cm	
V		Volume of cavity, $\pi \rho_2^2 d$, cm ³	
t	TEL	Time, sec	
τ	TAUX	Decay time, sec	
<u>Nuclear Constants</u>			
A	A	Atomic mass, kg	
M	M	Molecular weight, kg	
R _{1j}	RR1(J)	Range of fission fragments in fissile fuel, cm(Q00 Code)	
Σ _f	SIGMA	Macroscopic fission cross section, cm ⁻¹	

SYMBOL	FORTTRAN NAME	DESCRIPTION
<u>Gas Constants</u>		
$M(N_O)$	MASNO	Molecular weight of N_O , kg
$M(A_O)$	MASAO	Molecular weight of A_O , kg
Q_{ea}	QE(I)	Electron-neutral atom momentum - transfer cross section, cm^2
V_i		Ionization potential, eV
$V_i(N_O)$	VINO	Ionization potential of N_O , eV
$V_i(A_O)$	VIAO	Ionization potential of A_O , eV
V_m		Energy level of metastable states, eV
$V_m(N_O)$	VMNO	Energy level of N_m , eV
μ_e	MUEL	Mobility of electrons, $cm^2 \text{ volt}^{-1} \text{ sec}^{-1}$
μ_+	MUION	Mobility of ions, $cm^2 \text{ volt}^{-1} \text{ sec}^{-1}$
D_e		Diffusion coefficient of electrons, $cm^2 \text{ sec}^{-1}$
D_+	DP	Diffusion coefficient of ions, $cm^2 \text{ sec}^{-1}$
D_m		Diffusion coefficient of metastable states $cm^2 \text{ sec}^{-1}$
D_a	DA	Ambipolar diffusion coefficient $cm^2 \text{ sec}^{-1}$
$D_{a,j}$		Ambipolar diffusion coefficient of ion J, $cm^2 \text{ sec}^{-1}$
$K_{a,j}$	K(J)	Diffusion coefficient at unit density of ion J $= (n_O = 2.69 \times 10^{19} \text{ cm}^{-3}) \times D_{a,j}, \text{ cm}^{-1} \text{ sec}^{-1}$
K_m	KM	Diffusion coefficient at unit density of N_m $= n_O \times D_m, \text{ cm}^{-1} \text{ sec}^{-1}$
C_1 to C_{22}	$C(1)$ to $C(22)$	Reaction rate coefficients defined in Refs.(2) and (5); 2-body, $cm^3 \text{ sec}^{-1}$; 3-body, $cm^6 \text{ sec}^{-1}$, and input values are $\times 10^{10}$ with scaling factor of 10^{-10} in code.

Variables

Independent:

P		Reactor power, MW
ϕ	XF	Neutron flux, $cm^{-2} \text{ sec}^{-1}$
p	XP	Pressure of gas, torr
T_U		Temperature of uranium side of cavity, °K
T_B		Temperature of cesium bath, °K (Cav.16)
ω		Microwave frequency (angular) of probing signal, rad sec^{-1}

Semi-independent:

T_K		Temperature of Kovar side of cavity, °K
$\langle T_{gas} \rangle_{av}$		Average temperature of gas in cavity, °K $= (T_U + T_K)/2$
f_O	FO	Resonant frequency (vacuum) of cavity cps

SYMBOL	FORTRAN NAME	DESCRIPTION
<u>Variables</u>		
<u>Semi-independent (continued):</u>		
$\vec{E}(\vec{r})$		Electric field distribution within cavity, volt/cm
S_+		Source rate of N_+ ions from fission fragments, $\text{cm}^{-3}\text{sec}^{-1}$
S_*		Source rate of N_* excited states directly from fission fragments, $\text{cm}^{-3}\text{sec}^{-1}$
S_m		Source rate of N_m metastable states directly from fission fragments, $\text{cm}^{-3}\text{sec}^{-1}$
S_1	S(1)	S_+/N_0 , cm^{-1}
S_2	S(2)	S_*/N_0 , cm^{-1}
S_3	S(3)	S_m/N_0 , cm^{-1}
S_1'		S_1/P , $\text{cm}^{-1}\text{MW}^{-1}$
T_g	TGAS	Gas temperature input to code, °K
<u>Dependent: (CW8 Code)</u>		
T_e	TESWRM	Temperature of electron swarm, °K
	TSWMIG	Temperature code input first guess
	TELI	Temperature code argument to TELECT subroutine
T_+, T_i		Temperature of ions, °K
v_{ea}		Electron collision frequency with neutral atoms, sec^{-1}
v_{ee}		Electron collision frequency with swarm electrons, sec^{-1}
v_{ei}		Electron collision frequency with ions, sec^{-1}
\bar{v}_e		Averaged electron collision frequency, sec^{-1} , see Eq.(27)
ϵ	EEL	Electron energy, eV
$\bar{\epsilon}_g$	EGS	Average energy of neutral atoms, eV
$\bar{\epsilon}_{es}$	ESM	Average energy of electron swarm
$\epsilon_{\max}(\text{FF})$	EMAX	Initial energy of energetic electron from a fission fragment, eV
$\epsilon_{\max}(\text{Pen})$	IMID	Initial energy of energetic electron from Penning ionization, eV
$(\epsilon \rightarrow \infty)/\bar{\epsilon}_{es}$	YINF	Minimum "infinite energy" (input) (≥ 12)
$\delta\epsilon$	DELTE	Lower cut-off energy differential (input) for decaying energetic electron viz., $= (\bar{\epsilon}_{es} + \delta\epsilon)$
ϵ_{\min}	EMIN	
$\Delta\epsilon$	DELE	Electron energy increment, eV (input)
$N(\Delta\epsilon)_1$	NSTEP1	Number of electron energy increments (first integrals)
$N(\Delta\epsilon)_2$	NSTEP2	Number of electron energy increments (second integrals)

SYMBOL	FORTTRAN NAME	DESCRIPTION
f		Maxwell-Boltzmann distribution function Eq.(13)
$F(y)$	FUNY (YEL)	" See Eq.(14)
y	YEL	$\tau / \bar{\epsilon}_{es}$ or $t / \bar{\epsilon}_g$
\dot{E}_{max}	SOURCE	See Eq.(3), = CE1 x LEFLOS + CE2 x LEMLOS
\dot{E}_{LS}	LSTLOS	See Eq.(17) = LSNLOS + LSILOS
<u>Dependent: (CW9 Code)</u>		
Δf	DELFREQ	Shift in resonant frequency, cps
f	FRQ	$= f_0 + \Delta f$ = shifted resonant frequency, cps
ω_0		$= 2\pi f_0$, sec^{-1}
$\Delta \omega$		$= 2\pi \Delta f$, sec^{-1}
J_λ		Bessel functions of integer order
J'_λ		derivative of J_λ (see Eq.(71))
$X_{\lambda m}$		roots of Bessel functions, see Eqs.(51) and (52)
k_1	K1	See Eq.(59)
k_3	K3	See Eq.(60)
k	K	See Eq.(61)
<u>Other CW8 Input Variables</u>		
	KIT	Iteration limit on TELECT inner iteration
	NITS	Iteration limit on CW8 outer iteration
δT	DIFCON	Convergence criterion on T_e , °K
	PRCNTC	Convergence criterion $\delta T / T_e$
	CONVL	Convergence criterion on $(\dot{E}_{max} - \dot{E}_{LS}) / \text{SOURCE}$
	EKM	See Eq.(85)
	E16	See Eq.(83)
	E21	See Eq.(84)
	L	Control vector for TABX interpolation subroutine
	MRPT	See section A-III Appendix A
	MORE	See section A-II Appendix A
<u>Other CW9 Input Variables</u>		
	NTJ	= 1, TE-mode; = 2, TM-mode.
ℓ	LB	mode designation (see section III A.2)
m	MB	
n	NB	

SYMBOL	FORTTRAN NAME	DESCRIPTION
	NSTPZ	Number of Δz increments
	NCTPR	Number of Δr increments
	NSR	} See sections B-IV and B-V, Appendix B
	NFR	
	EPSB	
	PRNTL	
	NSMORE	
	DIFFRN	
	MORE	

I. INTRODUCTION

In previous computations of the electron density (n_e) in fission-fragment-generated plasmas in microwave cavities we have assumed: (1) that the electron temperature (T_e) was equal to the gas temperature (T_g) in the plasma; and, (2) that the electron density was uniform throughout the volume of the microwave cavity.^{1,2} To date the agreement of our theory (which contains no adjustable parameters)³ with the inpile microwave measurements of electron density has been rather good but we wished to extend our theory to take into account the possible elevation of the electron temperature and spatial variation of the electron density within the cavity.

Recent computations from energy balance considerations by Rees⁴ have shown that the electron temperature can be appreciably higher than the gas temperature depending upon the ion generation rate and the electron density. However our reaction kinetics studies had already shown that the electron density was not only strongly dependent on the ion generation rate, but was also a sensitive function of the electron temperature particularly via collisional-radiative recombination (which varies as T_e^{-5}),^{1,2} so that now we have an implicit dependence of n_e on T_e and neither can be computed directly. An iterative procedure is needed to solve simultaneously the electron temperature and reaction kinetics equations to find a consistent (n_e, T_e) pair and this can usually be done conveniently with a computer. Section II of this report will describe such a computer code (hereafter called the "Electron Density-Temperature Code (CW8)") for calculating the (n_e, T_e) pair at a point in the plasma.

This first code consists of two main subroutines: (1) the "Electron Density Subroutine", a modification of the previous "Reaction Kinetics I Code",⁵ which computes n_e given T_e ; and (2) the new "Electron Temperature Subroutine" which computes T_e given n_e . The physics and method of computation for this second subroutine have been described earlier.⁴ The Electron Temperature Subroutine, itself, requires an iterative procedure to balance the energy input and output to the electron swarm, and the Electron Density Subroutine also uses iterative procedures to solve the N simultaneous equations for the reaction kinetics continuity equations.

This scheme is represented by the center block of Fig. 1. The first block of Fig. 1 represents the computations which make use of our "Ion Generation

Rate Code (Q00)" to prepare the input data to the Electron Density-Temperature Code (CW8).

The second major computer code discussed here is represented by the last block in Fig. 1, the "Resonant Frequency Shift Code (CW9)". This program relates the output from the Electron Density-Temperature Code to the change in resonant frequency of the microwave cavity. We note that the Electron Density - Temperature Code computes the (n_e, T_e) pair at a point in the plasma. However, our inpile measurements of the resonant frequency shift of the cavity respond to an integral average of the electron density over the square of the electric field throughout the volume of the cavity. This effect is well known⁶ and the computations necessary for its evaluation are straightforward - that is, providing the variation of $n_e(r)$ is available. Thus with our theory for the generation rate of ions in gases by fission fragments (Code Q00 in Fig. 1)^{7,8} we first calculate the source rate of ions at each point in the cavity. Then with the Electron Density-Temperature Code we compute the electron density at each point in the cavity. Finally we compute the resonant frequency shift of the cavity (last block in Fig. 1) for direct comparison with the experimental measurements. This final "Resonance Frequency Shift Code (CW9)" is discussed in Section III of the report.

The assembly of computer codes shown in Fig. 1 embrace much of our theory developed to date for our nuclear generated plasmas and thus most of the physics contained in these codes has been described in other reports. The emphasis here will be on the computer techniques used to solve the equations for the two new programs, and those techniques needed to tie together all of the codes to predict the resonant frequency characteristics of our inpile microwave cavity. Symbols and FORTRAN names for the equation variables are listed in a table at the beginning of the report. Listings and other program details are presented in Appendix A for the Electron Density-Temperature Code and in Appendix B for the Resonant Frequency Shift Code.

Finally this complex of computer codes was used to analyze all of our inpile microwave data on the neon-argon system and part of the data on the argon-cesium system and the results are presented in Section IV of this report.

THEORETICAL ELECTRON DENSITIES FOR MICROWAVE EXPERIMENTS

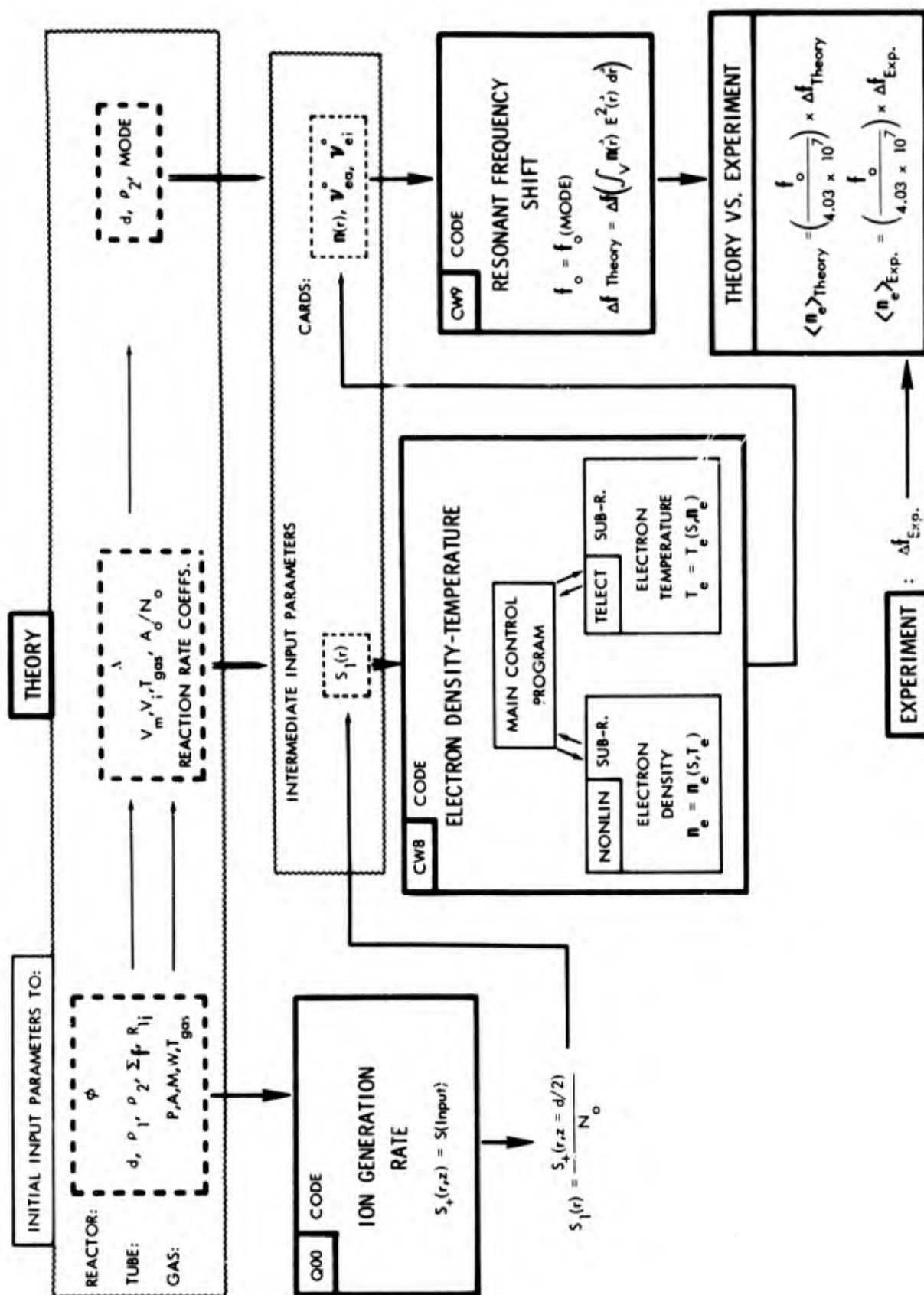


Fig. 1. The hierarchy of computer codes which embodies our noble-gas plasma theory. No adjustable parameters are used in this computation which starts from fundamental measurements, computes the ion generation rate, electron density and temperature distribution and ends with the predicted response of a microwave cavity.

II. ELECTRON DENSITY-TEMPERATURE CODE (CW8)

As pointed out in the introduction, the Electron Density-Temperature Code (CW8) consists of two main subroutines: 1) the Electron Density Subroutine (NONLIN) and 2) the Electron Temperature Subroutine (TELECT). This code also involves an important main control program and a number of subroutines of lesser importance. A block diagram of the Electron Density-Temperature Code is shown in Fig. 2. The Electron Density Subroutine is made up of a number of other subroutines which had been written for the previous Reaction Kinetics Code.³ Only minor modifications were needed to make this set of subroutines into one unit with the subroutine calling name of NONLIN. The new elements of the Electron Density-Temperature Code are the Electron Temperature Subroutine and the Main Control Program which will be described in detail in this section.

The Electron Temperature Subroutine will be described first, then the modifications to the Reaction Kinetics Code to make it into an Electron Density Subroutine, and finally the Main Control Program which uses these two subroutines to find the (n_e, T_e) pair.

A. Electron Temperature Theory

In the fission fragment ionization of noble gases most of the electrons are produced with energy less than the excitation energy of the noble gases but appreciably higher than the average energy of the swarm electrons that make up the plasma. As the energetic electrons are "thermalized" by elastic collisions, much of the excess energy is lost to neutral atoms but an appreciable fraction is transferred via Coulomb collisions directly to the electron swarm. This latter process produces a non-equilibrium state in which the electron swarm is heated to a "temperature" higher than the "temperature" of the ambient neutral atoms and ions. The physics of the various possible energy transfer collisions has been investigated by Rees⁴ who developed a theory to predict this non-equilibrium electron temperature from the steady-state ion generation rate, the electron density and other parameters of the gas. A summary of the method of calculation is presented below and the reader is referred to Reference (4) for a more detailed discussion. The symbols are defined in the List of Symbols at the beginning of this report.

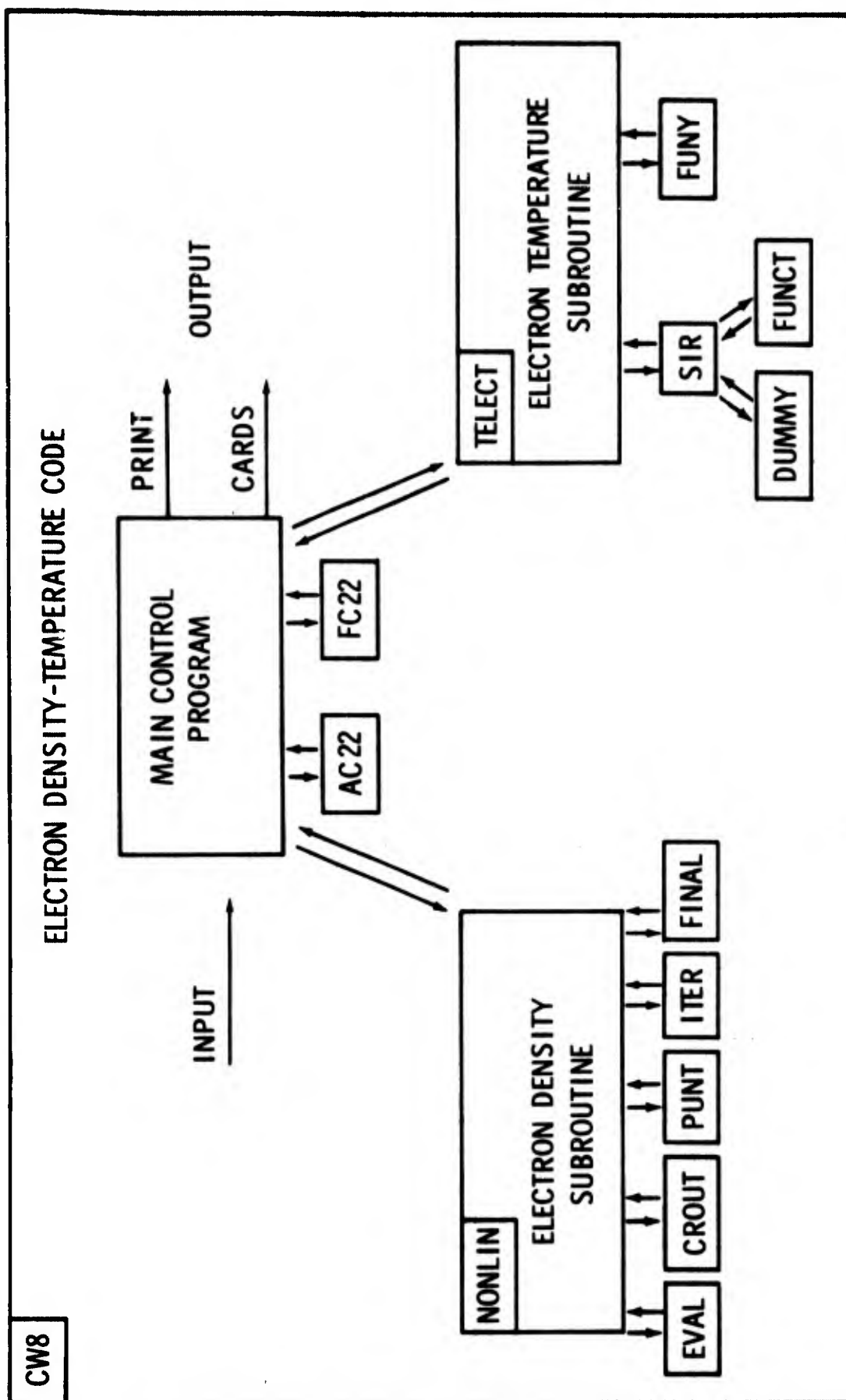


Fig. 2. Electron Density-Temperature Code (CW8)

1. Input. Consider a gas mixture comprising N_0 major and A_0 minor atom densities at total pressure p and temperature T_g and subjected to a fission fragment flux which produces an ion generation rate S_1 . Suppose that we have already determined the density of electrons n_e and metastable states N_m . Characteristics of the gas are the mass of the atoms of the major species $M(N_0)$ and the minor species $M(A_0)$ and their first ionization potentials $V_i(N_+)$ and $V_i(A_+)$. The metastable level of the major species (V_m) and the Penning ionization reaction rate (C_{15}) with the neutral atom of minor species are also needed. Assuming separate Maxwell-Boltzmann distributions we can express the average energy of the gas atoms and swarm electrons in terms of their temperatures or

$$\bar{\epsilon}_g = 3/2 kT_g/e \quad (1)$$

$$\bar{\epsilon}_{es} = 3/2 kT_e/e. \quad (2)$$

It is this last value, $\bar{\epsilon}_{es}$, that we wish to calculate. We shall calculate $\bar{\epsilon}_{es}$ in an energy balance that sets the gain in energy of the electron swarm from the energetic electrons equal to the loss of energy of the electron swarm to the neutral gas atoms and ions.

2. Production Rate of Excess Energy. The total production rate of excess electron energy (\dot{E}_{max}) which would be available to heat the electron swarm is given by the sum of the electron energy production rate from the fission fragments and the electron energy production rate via the Penning ionization from the metastable states.

$$\dot{E}_{max} = 0.30 V_i(N_+) S_1 N_0 + C_{15} N_m A_0 [V_m(N_m) - V_i(A_+)]. \quad (3)$$

As the energetic electrons "thermalize" and lose this excess energy, part is lost to the neutral atoms and part (which we wish to find) is lost to the electron swarm. The distribution of these two losses, however, varies with the electron energy (ϵ).

3. Energy Loss Rate of Energetic Electrons to Gas and Electron Swarm.

The energy loss rate of an energetic electron $(d\epsilon/dt)^*$ is given in terms of its energy (ϵ , eV) and collision rates with the neutral atoms (ν_{ea}) and

* In this model any energy loss in inelastic collisions is neglected. This is a valid approximation for neon-argon but not for argon-cesium where $\epsilon_{max}^{(FF)} = 0.30 V_i(N_+) > V_i(A_+)$.

and electrons of the swarm (v_{ee}) as

$$\frac{d\epsilon}{dt} = -L_{ea}(\epsilon, \bar{\epsilon}_g) - L(\epsilon, \bar{\epsilon}_{es}) \quad (4)$$

where

$$L_{ea}(\epsilon, \bar{\epsilon}_g) = \left(\frac{2 m_e}{M(N_o)}\right) v_{ea}(\epsilon)(\epsilon - \bar{\epsilon}_g) \quad (5)$$

and

$$L_{ee}(\epsilon, \bar{\epsilon}_{es}) = v_{ee}(\epsilon)(\epsilon - \bar{\epsilon}_{es}). \quad (6)$$

The collision rate with the neutrals is expressed in terms of the electron velocity $v(\epsilon)$, $\text{cm/sec} = 5.93 \times 10^7 \sqrt{\epsilon}$ and the cross section for momentum transfer $Q_{ea}(\epsilon)$, cm^2 as

$$v_{ea} = 5.93 \times 10^7 \sqrt{\epsilon} Q_{ea}(\epsilon) N_o. \quad (7)$$

The collision frequency for Coulomb scattering of the energetic electrons on the swarm electrons is expressed in terms of the electron density and swarm temperature (T_{es}) as

$$v_{ee} = 1.54 \times 10^{-5} n_e \epsilon^{-3/2} \ln \left\{ \frac{1.25 \times 10^4 T_e^{-3/2}}{n_e^{1/2}} \right\} \quad (8)$$

4. Energy Gain of the Electron Swarm. Using Eq.(4) we can compute the energy versus time profile of a decaying electron.

$$t(\epsilon) = \int_{\epsilon_{\max}}^{\epsilon} \frac{d\epsilon'}{L_{ea}(\epsilon') + L_{ee}(\epsilon')} \quad (9)$$

Now that we have $\epsilon = \epsilon(t)$ in Eq.(9), we can compute individually the total energy gain of the electron swarm from the energetic fission fragment electrons ($\epsilon_{\max}^{(FF)} = 0.30 V_1(N_+)$) and from the energetic Penning electrons ($\epsilon_{\max}^{(Pen)} = V_m(N_m) - V_1(A_+)$).

$$\dot{E}_{GS}(\bar{\epsilon}_{es}) = S_1 N_0 \int_{t(\epsilon_{\max}(FF))}^{t(\bar{\epsilon}_{es})} v_{ee}(t') (\epsilon(t') - \bar{\epsilon}_{es}) dt' + C_{15} N_0 A_0 \int_{t(\epsilon_{\max}(Pen))}^{t(\bar{\epsilon}_{es})} v_{ee}(t') (\epsilon(t') - \bar{\epsilon}_{es}) dt' \quad (10)$$

5. Energy Loss of the Electron Swarm. The electrons of the swarm exchange energy predominantly with the neutral atoms and ions* — according to the expression

$$-\dot{E}_s(\bar{\epsilon}_{es}) = \left(\frac{2m_e}{M(N_0)} \right) \int_{\epsilon=0}^{\infty} (\epsilon - \bar{\epsilon}_g) v_{ea}(\epsilon) f(\epsilon) d\epsilon + \left(\frac{2m_e}{M(A_+)} \right) \int_{\epsilon=0}^{\infty} (\epsilon - \bar{\epsilon}_g) v_{ei}(\epsilon) f(\epsilon) d\epsilon \quad (11)$$

where we have set the average energy of the ions ($\bar{\epsilon}_i$) equal to that of the gas ($\bar{\epsilon}_g$) and have taken the ion mass equal to that of the minor species (A_+) which is in accord with the results from our previous Reaction Kinetics studies² where we found the atomic ion of the minor gas species to be the predominant ion in the plasma for the conditions of interest to us. The electron ion collision frequency v_{ei} is given by

$$v_{ei} = 3.86 \times 10^{-6} n_e \epsilon^{-3/2} \ln(1.25 \times 10^4 T_e^{3/2} / n_e^{1/2}). \quad (12)$$

Now the average energy of the electron swarm is contained in the distribution function of $f(\epsilon)$ where $f(\epsilon)d\epsilon$ is the total number of electrons in the swarm per cm^3 with energy between ϵ and $\epsilon+d\epsilon$, that is

$$f(\epsilon) = \frac{n_e}{\bar{\epsilon}_{es}} \left(\frac{F'(y)}{n_e} \right) = \frac{n_e}{\bar{\epsilon}_{es}} F(y) \quad (13)$$

where $F(y) = 2.073 y^{1/2} e^{-3/2y}$ and $y = \epsilon / \bar{\epsilon}_{es}$. (14)

If the average swarm temperature is greater than the average gas temperature in Eq.(11), that is ($\bar{\epsilon}_{es} > \bar{\epsilon}_g$), then $\dot{E}_s < 0$ and the swarm loses energy to the neutral atoms and ions. If $\bar{\epsilon}_{es} = \bar{\epsilon}_g$, $\dot{E}_s = 0$ which means the sum of the integrals from $\epsilon=0$ to $\bar{\epsilon}_g$ equals the sum of the integrals from $\bar{\epsilon}_g$ to ∞ .

* Again, inelastic collisions are neglected and, of course, we are deliberately excluding the gain term from the energetic electrons.

Now to solve Eq.(11) we must make an approximation which takes advantage of this last fact. Because of our limited knowledge of interaction rates and distribution functions at very low electron energies, our expressions for these cause the integrals in Eq.(11) to diverge as $\epsilon \rightarrow 0$. We can always break up the integrals in Eq.(11) as

$$\int_{\epsilon=0}^{\infty} Z(\epsilon) d\epsilon = \int_{\epsilon=\bar{\epsilon}_g}^{\infty} Z(\epsilon) d\epsilon + \int_{\epsilon=0}^{\bar{\epsilon}_g} Z(\epsilon) d\epsilon \quad (15)$$

where $Z(\epsilon)$ represents one of the integrands in Eq.(11).

When $\bar{\epsilon}_{es} > \bar{\epsilon}_g$ we have no trouble integrating the first integral on the right hand side of (15). Now we claim that, when for the swarm $\bar{\epsilon}_{es} = \bar{\epsilon}_g + \Delta\epsilon$ because of the gain of energy from the energetic electrons, the gain of energy of the swarm from the neutrals and ions (last term on right hand side of Eq.(15) with $F(y)$ centered on $y = \epsilon/\bar{\epsilon}_{es}$) can be approximated by the gain of energy of the swarm from the neutrals and ions where $\Delta\epsilon = 0$. However when $\Delta\epsilon = 0$, the last term on right hand side of Eq.(15) equals the negative of the first term with $F(y)$ centered on $y = \epsilon/\bar{\epsilon}_g$. Our approximation is then

$$\int_{\epsilon=0}^{\infty} Z(y = \epsilon/\bar{\epsilon}_{es}) d\epsilon = \int_{\epsilon=\bar{\epsilon}_g}^{\infty} Z(y = \epsilon/\bar{\epsilon}_{es}) d\epsilon - \int_{\epsilon=\bar{\epsilon}_g}^{\infty} Z(y = \epsilon/\bar{\epsilon}_g) d\epsilon \quad (16)$$

Using this approximation in Eq.(11) we have finally for the loss rate of the electron swarm (using expressions (5), (12) and (14))

$$\begin{aligned} -\dot{E}_{LS}(\bar{\epsilon}_{es}) = & \int_{\epsilon=\bar{\epsilon}_g}^{\infty} n_e L_{ea}(\epsilon) \left[\frac{F(y = \epsilon/\bar{\epsilon}_{es})}{\bar{\epsilon}_{es}} - \frac{F(y = \epsilon/\bar{\epsilon}_g)}{\bar{\epsilon}_g} \right] d\epsilon \\ & + \int_{\epsilon=\bar{\epsilon}_g}^{\infty} n_e \left(\frac{2m_e}{M(A_+)} \right) v_{ei}(\epsilon) (\epsilon - \bar{\epsilon}_g) \left[\frac{F(y = \epsilon/\bar{\epsilon}_{es})}{\bar{\epsilon}_{es}} - \frac{F(y = \epsilon/\bar{\epsilon}_g)}{\bar{\epsilon}_g} \right] d\epsilon \end{aligned} \quad (17)$$

Now the problem is to find a value of the average electron swarm energy $\bar{\epsilon}_{es}$ such that the gain in energy by the electron swarm from the energetic electrons in Eq.(10) is balanced by the loss in energy of the electron swarm to the neutral atoms and ions in Eq.(17) or

$$\dot{E}_{GS}(\bar{\epsilon}_{es}) + \dot{E}_{LS}(\bar{\epsilon}_{es}) = 0. \quad (18)$$

Having solved this set of equations the temperature of the electron swarm is then

$$T_e = 2/3 \bar{\epsilon}_{es} e/k. \quad (19)$$

In general, neither Eq.(10) nor (17) can be solved analytically because the electron-neutral atom cross sections (Q_{ea}) cannot be expressed readily in analytic form. Numerical (or graphical)⁴ techniques must be used for those integrals involving tabular functions and for rapid solution of such problems digital computer techniques are particularly well suited.

6. Applicability of Model to Microwave Experiments. In the theory just described we compute the electron temperature for a point in the gas from an energy balance on volume processes taking place in the close neighborhood of the point. That is, we assume the mean free paths of the energy sharing particles are much smaller than the dimensions of the cavity and we also assume that there is no transport of energy via grad T_e . We intend to use this theory to help us predict the distribution of electron density within our microwave cavity so we now examine the limits of validity of these assumptions for the actual cavity tested.

The microwave cavity was a right circular cylinder of radius $\rho_2=1.136$ cm and height $d=0.70$ cm. First we consider electron diffusion to the walls of the cavity. The axial diffusion length $\Lambda_d=d/\pi=0.223$ cm and the radial diffusion length $\Lambda_\rho=\rho_2/2.4=0.473$. The total diffusion length $\Lambda(1/\Lambda^2=1/\Lambda_\rho^2+1/\Lambda_d^2)$ is 0.202 cm. We see that of those electrons lost by diffusion, most are lost in the axial direction since $\Lambda \simeq \Lambda_d$. Electrons in neighborhoods separated by distances of order $\Lambda=0.202$ cm along the radius are therefore effectively decoupled from diffusion mixing. When volume recombination losses become large, as they are expected to be in many cases, the lifetime of the electrons

becomes much shorter and this further localizes the effects of diffusion. The relative rates of electron loss by diffusion and volume recombination will depend upon many other factors, including the electron temperature, and these effects are accounted for in the reaction kinetics equations.

We know from previous computations⁷ that the ion generation rate (S) is fairly uniform in the direction of the axis of such a tube but does decrease radially because at a point in the gas the solid angle of the uranium foil, of finite diameter ($\rho_1 < \rho_2$), decreases with increasing radius. Diffusion is negligible in the radial direction so that the electron density can be computed at points along the radius of the tube using the reaction kinetics theory and the computed ion generation rate at that point on the radius. We must now decide whether a specific electron swarm temperature can be assigned to each of these points along the radius.

Besides the energy losses directly to the atoms and ions in the neighborhood of a point, the excess energy of an electron swarm can be transported away via Coulomb collisions ($\text{grad } T_e$) as well as by mass transport ($\text{grad } n_e$). We have already decided that ($\text{grad } n_e$) is small in the radial direction so the question of whether a specific electron swarm temperature can be assigned to each point along the radius depends upon whether a significant fraction of the excess of the electron swarm energy (over the gas temperature) is lost by Coulomb collision to the electrons of adjacent neighborhoods rather than to the nearest neutral atoms and ions. We can answer this question immediately from the boundary conditions on the plasma.

We have seen that the energetic electrons lose their energy to the swarm and to the ambient neutral atoms in times ($\tau \sim 10^{-8}$ sec) very short compared to the lifetime of an average swarm electron ($\tau \sim 10^{-4}$ sec).⁴ Therefore an electron swarm of unit volume must lose energy at a rate equal to the input rate from the energetic electrons which is of the order of the ion generation rate (S) times the energy of the energetic electrons (ϵ_{max}), i.e., the total loss rate of excess energy of the swarm is roughly ($S\epsilon_{\text{max}}V$) where V is the volume of the cavity.

Now consider the electrons at the wall of the cavity. We assume these electrons strike the wall with energy equal to the average electron swarm energy $\epsilon_{\text{es}} = \epsilon_g + \Delta\epsilon$. The maximum energy that could be transported to the wall by these electrons would be for the case where none are reflected from the wall. The total arrival rate at the wall cannot exceed SV so the total energy

transported via the electrons cannot exceed $SV\Delta\epsilon$. Since we expect $\Delta\epsilon \ll \epsilon_{\max}$ we conclude that the excess energy of the swarm is quickly transferred to the neutral atoms and ions at the point of origin of the energy and then in turn these atoms and ions transfer that energy to the walls via $(\text{grad } T_g)$.

On the basis of these arguments we will proceed to use both the reaction kinetics theory and the electron temperature theory to compute the (n_e, T_e) solutions as a function of the varying ion generation rate along the radius (at mid-height) of the cavity.

Because of the axial diffusion of the electrons, the electron density decreases in magnitude from the mid-height position in the axial direction towards the walls. This axial variation $(n_e(z))$ would be negligible if the ions are lost predominantly by volume recombination (as expected); on the other hand, the electron density would vary as $\cos(z/\Lambda_d)$ if the ions are lost predominantly by diffusion. Later in the Resonant Frequency Shift Code we shall program the integrals over the volume of the cavity to account for any known variation in the axial direction. However, in the analysis of the data we shall neglect this axial variation.

B. Electron Temperature Subroutine (TELECT)

The equations for the electron temperature above were programmed for solution on the IBM 7094 computer in the FORTRAN IV language. The flow diagram for this program is shown in Fig. A-2 in Appendix A. As mentioned before this code was written as a subprogram of the more general Electron-Density-Temperature Code. This subroutine is concerned with the inner-iteration to obtain $T_e = T_e(n_e)$ while the Electron-Density-Temperature Code is concerned with the outer-iteration on both T_e and n_e . The following paragraphs will describe the major considerations to guide the inner iteration to a successful solution for T_e , given n_e .

1. Analytic Expression to Guide Convergence: The efficiency or speed of convergence of iteration techniques depends in large part on the ability to estimate a good value of the trial variable ("good next guess") from information generated in the previous trials. Now we seek a value of $\bar{\epsilon}_{es}$ to solve Eq.(18) but we do not require the sum of the gain and loss terms to be identically zero. We ask that the absolute value of the difference $(|\Delta \dot{E}|)$ be less than some number $(\Delta \dot{E}_C)$ that we have prejudged to be a satisfactory

convergence criterion, that is

$$|\Delta \dot{E}|_1 = |\dot{E}_{GS}(\bar{\epsilon}_{es})_1 - \dot{E}_{LS}(\bar{\epsilon}_{es})_1| \quad (20)$$

and
$$|\Delta \dot{E}|_{\text{final}} \leq \Delta \dot{E}_C. \quad (21)$$

The gain term \dot{E}_{GS} of the electron swarm from the energetic electrons can be expected to be relatively insensitive to the average electron swarm energy $\bar{\epsilon}_{es}$ since for our condition we expect $\bar{\epsilon}_{es} \ll \epsilon_{\text{max}}(\text{FF})$ or $\epsilon_{\text{max}}(\text{Pen.})$. However the loss term, \dot{E}_{LS} , for the energy transfer from the swarm electron to the ambient gas can be expected to be very sensitive to the average electron swarm energy, or more appropriately to $(\bar{\epsilon}_{es} - \bar{\epsilon}_g)$, depending upon the nature of the gas. The electrons of the electron swarm are expected to lose their energy predominantly to the neutral atoms rather than to the ions for the plasma condition of interest to us. The cross section for momentum transfer of electrons to neon⁹ and argon¹⁰ are shown in Fig. 2 and it is clear that the loss of energy to the neutral atoms $\dot{E}_{LS}(\bar{\epsilon}_{es})$ for these two gases will behave quite differently particularly when $\bar{\epsilon}_{es}$ increases above ~ 0.05 eV. Neon cross sections increase monotonically with increasing electron energy but argon exhibits the characteristic Ramsauer minimum at electron energies near ~ 0.3 eV. The expression to predict the next "good guess" must reflect this difference in behavior of Q_{ea} .

To obtain a "good next guess" for the trial variable, $(\bar{\epsilon}_{es})_{i+1}$ for the neon-argon system where $[\text{Ar}] \ll [\text{Ne}]$, we assume that the energy gain of the swarm from the energetic electrons \dot{E}_{GS} changes linearly with increasing $\bar{\epsilon}_{es}$ and that the energy loss rate of the swarm to the ambient gas \dot{E}_{LS} changes linearly with increasing $\bar{\epsilon}_{es}$. From Eq.(17) $\dot{E}_{LS}(\bar{\epsilon}_{es} = \bar{\epsilon}_g) = 0$ and we can compute $\dot{E}_{GS}(\bar{\epsilon}_g)$ so that

$$\bar{\epsilon}_{es,i+1} = \frac{\dot{E}_{GS}(\bar{\epsilon}_g) [(\bar{\epsilon}_{es})_i - \bar{\epsilon}_g]}{\dot{E}_{LS}(\bar{\epsilon}_{es})_i - [\dot{E}_{GS}(\bar{\epsilon}_{es})_i - \dot{E}_{GS}(\bar{\epsilon}_g)]} + \bar{\epsilon}_g \quad (22a)$$

This approximation worked well for neon-argon and gave a convergence within 5% on \dot{E} (i.e., $(\Delta \dot{E} / \dot{E}_{GS}) \leq 0.05$) generally after only a few (< 6) iterations.

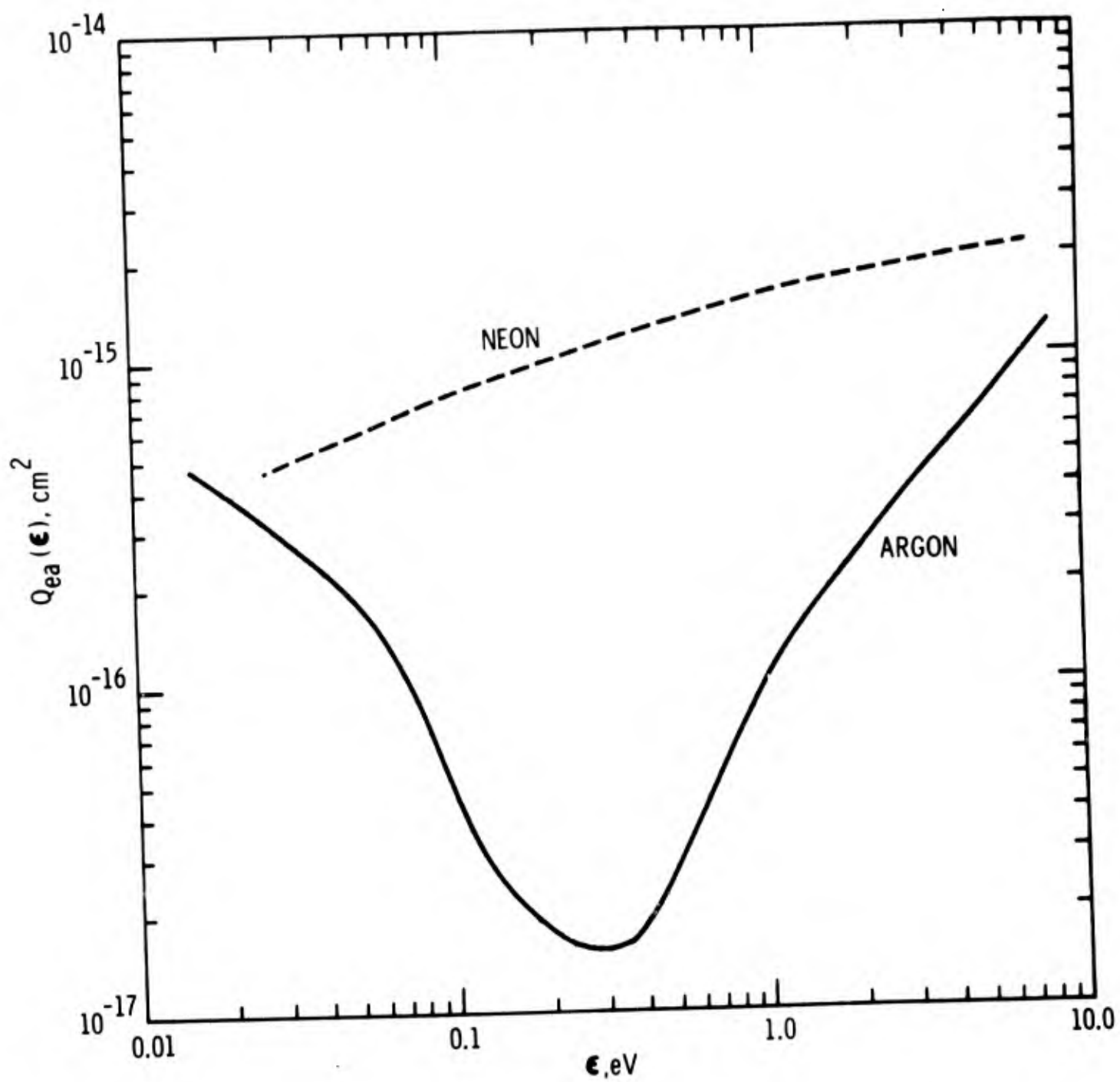


Fig. 3. Momentum transfer cross sections for electrons in neon⁹ and argon¹⁰.

For the argon-cesium system with $[Cs] \ll [Ar]$, the linear approximation, Eq.(22a), caused the trial values to diverge from the correct solution. For 0.1 eV $\approx (\bar{\epsilon}_{es} - \bar{\epsilon}_g) \lesssim 1.0$ in argon-cesium it was found from the first code run using Eq.(22a) that $\dot{E}_{LS} \propto (\bar{\epsilon}_{es} - \bar{\epsilon}_g)^2$. Using this relationship and the insensitivity of \dot{E}_{GS} to $\bar{\epsilon}_{es}$ (i.e., $\dot{E}_{GS}(\bar{\epsilon}_g) \approx \dot{E}_{GS}(\bar{\epsilon}_{es})$) we obtain instead of Eq.(22a)

$$(\bar{\epsilon}_{es})_{i+1} = \left(\frac{\dot{E}_{GS}(\bar{\epsilon}_{es})_i}{\dot{E}_{LS}(\bar{\epsilon}_{es})_i} \right)^{1/2} ((\bar{\epsilon}_{es})_i - \bar{\epsilon}_g) + \bar{\epsilon}_g \quad (22b)$$

For the argon-cesium system Eq.(22a) was used for $(\bar{\epsilon}_{es} - \bar{\epsilon}_g) \leq 0.05$ eV and Eq.(22b) for $(\bar{\epsilon}_{es} - \bar{\epsilon}_g) > 0.05$ eV and convergence within 5% was generally obtained in less than 6 iterations.*

2. Average Collision Frequency: Later in this report we will need for the Resonant Frequency Shift Code an average collision frequency $\bar{\nu}_e$ to account for the damping of the electron motion in the E-M microwave field. This information can be obtained from the data already computed by the equations above. The corresponding differential equation for each integral term (j) in Eq.(11) is

$$d(\dot{E}_S)_j = \left(\frac{2m_e}{M_j} \right) \nu_{ej}(\epsilon) f(\epsilon) (\epsilon - \bar{\epsilon}_g) d\epsilon \quad (23)$$

and we can define an average collision frequency for energy transfer $\bar{\nu}_{ej}$ such that

$$\bar{\nu}_{ej} = \frac{\left(\frac{2m_e}{M_j} \right) \int_{\epsilon=0}^{\infty} (\epsilon - \bar{\epsilon}_g) \nu_{ej}(\epsilon) f(\epsilon) d\epsilon}{\left(\frac{2m_e}{M_j} \right) \int_{\epsilon=0}^{\infty} (\epsilon - \bar{\epsilon}_g) f(\epsilon) d\epsilon} = \frac{- (\dot{E}_S)_j}{\left(\frac{2m_e}{M_j} \right) n_e (\dot{\epsilon}_{es} - \bar{\epsilon}_g)} \quad (24)$$

Following the same logic that led from Eq.(11) to Eq.(17) we can compute an average neutral atom collision frequency $\bar{\nu}_{ea}$ and an average ion collision frequency $\bar{\nu}_{ei}$ as

$$\bar{\nu}_{ea} = \frac{- (\dot{E}_{LS})_a}{\left(\frac{2m_e}{M(N_O)} \right) n_e (\bar{\epsilon}_{es} - \bar{\epsilon}_g)} \quad (25)$$

*This last "alternate version" was used on the computations reported here for both the Ne-Ar and Ar-Cs systems.

and

$$\bar{v}_{ei} = \frac{-(\dot{E}_{LS})_i}{\left(\frac{2m_e}{M(A^+)}\right) n_e (\bar{\epsilon}_{es} - \bar{\epsilon}_g)} \quad (26)$$

where $-(E_{LS})_a$ and $-(E_{LS})_i$ are the first and second terms of Eq.(17). For the Resonant Frequency Shift Code we combine the above values (after convergence on $\bar{\epsilon}_{es}$) to obtain \bar{v}_e as follows

$$\bar{v}_e = \bar{v}_{ea} + \frac{M(A^+)}{M(N_o)} \bar{v}_{ei} \quad (27)$$

3. Integration Subroutines: There are many integrations to be performed in this calculation (see Fig. A-2, Appendix A) and nearly all with tabular functions as integrands. These integrations (on a function, $F(X)$) are performed numerically with Simpson's rule using a fixed number of steps (N , input) for each variable.

$$\int_{X_{LL}=X_1}^{X_{UL}=X_{LL}+N \Delta X} F(X) dX = \frac{\Delta X}{3} \sum_{n=1}^{n=N/2} (F_{2n-1} + 4F_{2n} + F_{2n+1}) \quad (28)$$

Thus, since the limits of integration (X_{LL} and X_{UL}) are also variable, the increment size ($\Delta X = (X_{UL} - X_{LL})/N$) will change from integration to integration. The same subroutine, SIR, performs integrations for both analytic and tabular functions, $F(X)$, having been given the name of a one-argument FORTRAN function as the first entry of its argument list - SIR (F,XLL, XUL, N). The listing for this numerical integration FORTRAN function, SIR, is given in Table A-II in Appendix A.

Tabular functions must be handled differently depending upon whether the increment range is known in advance, that is, depending upon whether the value of the independent variable is an entry of the tabular array or intermediate to other entries of the array. When the function "F" is tabular, two different FORTRAN functions may be used viz., DUMMY(X) or FUNCT(X). DUMMY(X) expects to find in a labeled-common block a FORTRAN variable array XAR containing both a monotonic table of values for the independent variable X and a FORTRAN

variable array GAR containing the corresponding values for the dependent (tabular) function, $F(X)$. This FORTRAN function, i.e. DUMMY, is used when the range (and thus, the increment) for the integration are known in advance and when the program can be arranged so that the values of the independent variable X_n specified by the FORTRAN function SIR and the corresponding values of the function $F(X_n)$ can be found and preset in the XAR and GAR arrays. A call to DUMMY(A) causes a search of the XAR array until

$$(X(I)-A) \leq \epsilon \quad (29)$$

where

$$\epsilon = \frac{|X_2 - X_1|}{5} \quad (30)$$

The value of GAR(I) is returned as $F(A)$. Again the "calling" program must preset XAR and GAR before calling SIR with an argument of DUMMY (for F). The listing for this FORTRAN function, DUMMY, is given in Table A-III in Appendix A.

The FORTRAN function FUNCT(X) uses the interpolation routine TABX and expects to find in a labeled-common block not only the XAR and GAR arrays for X and $F(X)$ but also a control array L(7) for TABX. A call to FUNCT(A) causes TABX to interpolate the argument A into the sequence of X-values in XAR and return an interpolated value $F(A)$ from the $F(X)$ values in GAR. The order of interpolation is preset in the control array. FUNCT(X) is used for the function name entry F in the integration subroutine SIR when the range for the integration is not known in advance or when the values of the independent variable X_n specified by SIR are intermediate to those listed in the XAR array. A value of $F(X)$ obtained by extrapolation out of the range of XAR is noted by FUNCT. The listing for this FORTRAN function, FUNCT, is given in Table A-IV in Appendix A.

The XAR and GAR arrays were dimensioned with 101 cells and since both arrays are used over again in each of the integrations in Fig. A-2 it was necessary to provide other temporary storage arrays. A minimum of three additional arrays were needed: XE2(101), GE2(101) and EE1(101).

4. Calling Statement and Argument List: The FORTRAN-IV calling statement and argument list for the Electron Temperature Subroutine is

CALL TELECT (X, TELI, TESWRM)

where

X	= Array for the number densities of the N particle species in the plasma. This is a double precision array with dimension 40 and the values will have been provided by a previous call to the Electron Density Subroutine, NONLIN.
TELI	= Is the first trial value for the electron swarm temperature to be used in the inner-iteration.
TESWRM	= The returned converged value of the electron swarm temperature (i.e. for $n_e = X(1)$).

The arguments are dummy names to the calling program and could be renamed there.

5. Other Coding Considerations: Within the scope of this report it is not possible to cover all the coding details. Those readers who have some FORTRAN coding experience will be able to decipher much from the flow diagram in Fig. A-2. For those who intend to make some use of these codes a few additional remarks are made. The input to this subroutine is read in the Main Control program for the code and will be described later in Section II, D.4. The output from within this subroutine is considered intermediate but it can be printed out depending upon the Main Program input to the switch PRNT⁴ (1=No, 2=Yes). An example of this output is given in Table A-XIII in Appendix A.

The FORTRAN-IV NAMELIST mode for writing data was used. The function statement for the generalized Maxwell-Boltzmann electron distribution for energy for Eq.(14) is shown in Table A-V in Appendix A.

6. Check of Output: When the subroutine was first programmed, it was run separately on a check problem which had been solved by graphical integration techniques.⁴ Each of the internal integration steps and the final answer agreed satisfactorily with the hand calculation.

The complete print-output from this subroutine for an example problem is displayed in Table A-XIII in Appendix A and is discussed in some detail there. Normally this output is considered intermediate and is suppressed and only the final result is printed by the Main Control program (Section II-D.) as in Table A-XII in Appendix A.

C. Electron Density Subroutine (NONLIN)

The Electron Temperature Subroutine described above is the second subprogram of the Electron-Density-Temperature Code. The first subprogram, the

Electron Density Subroutine, consists of our previous Reaction Kinetics Code³ modified slightly to make it available as a subroutine in the outer iteration loop on electron density and temperature. The Reaction Kinetics Code starts with input on the ion (and metastable) generation rate from fission fragments, the gas and electron temperatures and various other geometrical and gas parameters; then solves N simultaneous, algebraic, non-linear, reaction kinetics rate equations to find the steady-state density of the N particle species of the plasma. This computer code was written in double precision in the FORTRAN-IV language and since this has already been described in some detail³ only the modifications will be discussed here.

1. Subroutines for the Electron Density Subroutine (NONLIN): The main subroutine NONLIN and the various other subroutines used by NONLIN are shown in block diagram forms in Fig. 2 and the primary function of these subroutines are listed below:

- NONLIN - Main control subroutine for solution of the N simultaneous non-linear algebraic equations.
- EVAL - Subprogram which contains the N equations to be solved and the equations for the various partial derivatives.
- CROUT - Subprogram for determinant evaluation.
- PUNT - Write output subprogram for best values of the roots when singularities are encountered or when the iteration count is exceeded.
- ITER - Write output subprogram for the intermediate values of the roots and errors.
- FINAL - Write output subprogram for the final converged values of the roots and errors.

Listings of these subroutines were presented in Reference (3) as part of the older Reaction Kinetics Code (F36). In this older F36 code, the title cards were read by a short Main Control program and most of the input data was read in by the subroutine EVAL. To make these programs compatible as an Electron Density subroutine, the Reaction Kinetics Main Control program was deleted and "read-input" and control was transferred to the Main Control program for the Electron Density-Temperature Code to be described later (Sect. II D). The EVAL subroutine was rewritten so that it now obtains the necessary input data via a labeled-common block from the new Main Control program. A listing of the revised EVAL subroutine is presented in Table A-VI in Appendix A. The only other change made was to use a labeled-common block, COM1, for the X-array in the ITER and FINAL subroutines.

2. Calling Statement and Argument List: The FORTRAN-IV calling statement and argument list for the Electron Density subroutine is

CALL NONLIN (N, X, EPS, ISW, L)

where

- N = Number of simultaneous kinetics equations to be solved.
- X = Array for the number densities of the N particle species in the plasma. This is a double precision array with dimension 40 and initial estimates must be provided in the calling program.
- EPS = Allowed absolute error (used 1×10^{-6}).
- ISW = Output switch for printing results
 - = 1 = Final results only
 - = 2 = Intermediate and final results
 - = 3 = No printed output
- L = Error indicator
 - = 1 = If singularity occurred
 - = 2 = If number of iterations exceeded 100
 - = 3 = If cyclic condition occurred
 - = 4 = If good solution was found.

The argument list above consists of dummy names which are important, of course, to the subroutine program but not to the calling program. In the Main Control program (Sec. II D) we call this subroutine with different names for some of these arguments. We continue with the names X and EPS but call NX for X and RTN for L. During the outer iteration we call NONLIN with the name PRNT1 (for ISW) for the input switch value for intermediate print output and after convergence we call NONLIN with the name PRNT2 (for ISW) for the intermediate print output. The first trial values for the X-array are read in a NAMELIST-input statement with name GUESS in the Main Control program together with the input values for EPS, PRNT1, PRNT2 and NX as shown in Table A-XII (page A-21).

D. Main Control Program for the Electron Density-Temperature Code (CW8)

The Electron Density-Temperature Code is made up of the Electron Density subroutine (Sec. II D above) for $n_e = n_e(T_e)$, the Electron Temperature subroutine (Sec. II C above) for $T_e = T_e(n_e)$, and an overall control program (see Fig. 2) to guide the outer-iteration to a solution for compatible values for both (n_e, T_e) . It is this last control program which we will now describe.

As well as guiding the outer-iteration, this Main Control program must perform a number of additional tasks. The diagram in Fig. A-1 shows the

details of the flow of the program but the sequence of operations is given roughly by the following list:

1. Read in the input data;
2. Write out the input data;
3. Manipulate the fixed constants;
4. Preparations for first call to NONLIN (performed only once):
 - a. Adjust reaction rate coefficients for gas temperature ($T_{GAS}=T_g$),
 - b. Adjust reaction rate coefficients for first guess (input) for electron swarm temperature ($TELI=TSWMLG$) and use analytic expression for $C(22)$,
 - c. Call NONLIN for $n_e=n_e(T_e=TSWMLG)$ and go to (5);
5. Preparations for repeated calls to NONLIN:
 - a. Adjust reaction rate coefficients for trial value of electron swarm temperature ($TELI$) and in particular, adjust the values for the collisional radiative recombination coefficient $C(22)$ by double interpolation on $\alpha(n_e, T_e)$,
 - b. Call NONLIN for $n_e=n_e(T_e=TELI)$;
6. Call TSELECT for $T_e=T_e(n_e)=TESWRM$;
7. Check convergence and go either to (5) or (8);
8. Write output requested for above computation;
9. Repeat entire procedure for each point requested along the mid-height radius of the microwave cavity;
10. Write out a summary of the output from each radial point; and
11. Punch out on cards a summary of the output from each radial point so that this information may be fed as input directly to the final Resonance Frequency Shift Code (CW9).

This code was again written in FORTRAN-IV language. In addition to Fig.A-1, Appendix A contains the listing of the program (Tables A-VII to A-X) and printed examples of the input cards (Table A-XI) and output sheets (Tables A-XII and A-XIII). Further discussion of the Main Control program of this CW8 code given below is confined to a few brief notes on input, convergence and running time, and also some additional details on steps (4) and (5) above to obtain the important collisional-radiative recombination coefficient C_{22} and the adjustment of the diffusion coefficients for T_g and T_e .

1. Input: An example of a set of input cards to this code is given in Table A-XI in Appendix A. All of the input data are promptly printed out for the record. The two title cards are read in via "A-conversion" and then some of the data are read in via NAMELIST statements and some via FORMAT statements. The NAMELIST statements for input are useful particularly for repeating a problem with only one, or a few, parameters changed. Also the NAMELIST statements for computed output (e.g., MAM1 to MAM4 in Table A-VII) save much programming time.

2. Computation of Recombination Coefficient $C_{22}(n_e, T_e)$: We have added to our theory a method for computing the temperature of the electron swarm because we were convinced that any elevation of the temperature of the electron swarm over the ambient gas temperature would greatly influence the value of the electron density predicted for our theory. The influence of an elevated electron swarm temperature will be carried into the reaction kinetics equations via a number of the reaction rate coefficients, but particularly, through the reaction rate coefficient $C(22) = C_{22}$ for collisional radiative recombination for the atomic ion of the minor gas species (A_+). Some additional discussion is needed to explain how the value of this important coefficient is obtained — particularly so, since the method now differs from that employed in the older Reaction Kinetics Code (F36).

In the reaction kinetics equations we have already expressed the loss of the minor gas atomic ion by a 3-body process as⁵

$$C22LOS = C_{22} A_+ n_e^2. \quad (31)$$

However the 2-body collisional radiative recombination rate coefficients computed by Bates, Kingston and McWhirter,¹¹ $\alpha(n_e, T_e)$, for this process are a function of the electron density as well as the electron temperature and in terms of their coefficients

$$C22LOS = \alpha(n_e, T_e) A_+ n_e \quad (32)$$

so we have

$$C_{22}(n_e, T_e) = \frac{\alpha(n_e, T_e)}{n_e}. \quad (33)$$

In the limit of high collision frequency ($n_e \rightarrow \infty$) the recombination rates $\alpha(n_e, T_e)$ approach asymptotic values $\alpha_0(T_e)$ ¹¹ and in this limit the recombination rates can be expressed analytically by

$$C_{22}(T_e) \simeq 2.6 \times 10^{-19} (250/(T_e, ^\circ K))^5 \text{ cm}^{-6} \text{ sec}^{-1}. \quad (34)$$

In this code we use the 2-body rate coefficients of Bates, Kingston and McWhirter except that on the first pass on a new problem (Step (4b) in list) we improve the guess on n_e (for $\alpha(n_e, T_e)$) by using Eq.(34) (via the function FC22(TELI), Table A-X) on our first call to the Electron Density Subroutine (NONLIN). After this call to NONLIN all subsequent computations (step 5a in list) use a value of $C_{22}(n_e, T_e)$ computed according to Eq.(33).

The values of $\alpha(n_e, T_e)$ are read in as a double-subscripted array, ALFA(I,J) at compile time via BLOCK DATA input (see Table A-VIII) along with the corresponding electron density array ZNEA(I) and electron temperature array TELIA(J). The $\alpha(n_e, T_e)$ array is then normalized using Eq.(34)

$$\alpha'(n_e, T_e) = \frac{\alpha(n_e, T_e)}{C_{22}(T_e)} \quad (35)$$

After having obtained from NONLIN in step 4 the improved guess on the electron density X(1) using TSWM1G in Eq.(34) and the input first guess on the plasma densities, GUESS: X(I), entry is made to the normalized ALFA(I,J) array via the function AC22(TE,ZNE) in Table A-IX to perform a double interpolation (using the TABXZ Library subroutine) on both n_e and T_e to obtain the normalized value

$$CAC22 = AC22(X(1), TSWM1G). \quad (36)$$

The value of $C_{22}(n_e, T_e)$ corresponding to Eq.(33) is given by

$$C(22) = FC22(TELI=TSWM1G)*CAC22 \quad (37)$$

Finally, with this value for the collisional radiative recombination rate, entry is again made to the Electron Density subroutine NONLIN in step 5 to obtain the first value of the electron density $n_e = n_e(TSWM1G)$ (and metastable density, $N_m = X(6)$) to be used as input to the Electron Temperature subroutine TELECT to obtain $T_e = T_e(n_e)$.

3. Adjustment of Diffusion Coefficients for T_g and T_e : The ambipolar diffusion coefficient for ions N_+ diffusing together with electrons n_e is given by

$$D_a = \frac{\mu_e D_+ + \mu_+ D_e}{\mu_e + \mu_+} \quad (38)$$

The mobility of the ions (μ_+) is much less than the mobility of the electrons (μ_e), $\mu_+ \ll \mu_e$, so if we substitute this and the relations $D_+/\mu_{o+} = kT_+/e$ and $D_e/\mu_{oe} = kT_e/e$ in Eq.(38) we get

$$D_a = \mu_{o+} \left(\frac{kT_+}{e} \right) \left(1 + \frac{T_e}{T_+} \right) \quad (39)$$

where μ_{o+} is the ion mobility at standard conditions of 273°K and 760 torr. When the ions and electrons are in thermal equilibrium Eq.(39) reduces to the familiar expression $D_a = 2\mu_{o+} (kT_+/e) = 2D_+$.

In our previous studies we have used the ambipolar diffusion coefficient at unit atom density, K_a , defined by $K_a = n_0 D_a^5$ where $n_0 (2.69 \times 10^{19} \text{ cm}^{-3})$ is the number density of atoms at 760 torr and 273°K and we assumed that the electrons were in equilibrium with the ions and neutral gas atoms ($T_e = T_+ = T_g$) so that

$$K_a(300^\circ\text{K}) = 2 n_0 \left(\frac{k \cdot 300}{e} \right) \mu_{o+} = 1.4 \times 10^{18} \mu_{o+} \text{ cm}^{-1} \text{ sec}^{-1} \quad (40)$$

where μ_{o+} in $\text{cm}^2 \text{ V}^{-1} \text{ sec}^{-1}$.

We wish to preserve the input values for $K_a(300^\circ\text{K})$ and we will adjust for T_g and T_e in terms of $K_a(300^\circ\text{K})$ as follows. We assume that the ions are at the same temperature as the gas atoms $T_+ = T_g$ and we substitute $K_a = n_0 D_a$ into Eq.(39)

$$K_a(T_g, T_e) = \left(\frac{\mu_{o+}}{n_0} \right) \left(\frac{kT_g}{e} \right) \left(1 + \frac{T_e}{T_g} \right) \quad (41)$$

Now our previous quantity $K_a(300^\circ\text{K})$ is given by Eq.(41) as

$$K_a(300^\circ\text{K}) = K(300, 300) = \left(\frac{\mu_{o+}}{n_0} \right) \left(\frac{k \cdot 300}{e} \right) \times 2 \quad (42)$$

We now write Eq.(41) in terms of (42) for each ion species j as

$$K_{a,j}(T_g, T_e) = K_{a,j}(300) \left(\frac{T_g}{300} \right) \left(\frac{1 + T_e/T_g}{2} \right) \quad (43)$$

In the Main Control program we first adjust for T_g and then for T_e according to Eq.(43).

4. Convergence on (n_e, T_e) Solution: The Electron Temperature subroutine (TELECT), as described in the previous Sec. II B, accepts as input the electron density and trial value of the electron swarm temperature (TELI) and returns a converged value of the electron swarm temperature (TESWRM) that is compatible with the input value of the electron density. Immediately upon return from the TELECT subroutine, the input value of the electron density (TELI) is compared to the output value (TESWRM) and if the difference does not meet the input convergence criteria, all the electron temperature dependent reaction rate coefficients (including C(22)) are readjusted for the new electron swarm temperature (TESWRM). The Electron Density subroutine (NONLIN) is again called for a new value of the electron density $n_e = n_e(\text{TESWRM})$ and the process is repeated until the convergence criterion is met (~ 2 -5 iterations for a convergence of 5% on T_e).

Other parts of the Main Control Program of the Electron Density-Temperature Code involve various input-output statements and the manipulation necessary to repeat the entire computation of the (n_e, T_e) pair for each ion source rate (XSR(N)) at each of the $N = \text{NSR}$ points along the radius of the microwave cavity. Also, by using the NAMELIST input format, this entire procedure can be repeated for a change in any (or all) of the input variables by having set the switch MORE to 1 and adding an appropriate NAMELIST card stating only the name of the changed variable with its new value.

5. Core Size of Program and Running Time: The entire Electron Density-Temperature Code, including the (Reaction Kinetics) Electron Density subroutine and the Electron Temperature subroutine, occupies about 23,000 cells of core storage and to obtain 11 (n_e, T_e) solutions for 10 increments along the radius of a microwave cavity requires about one minute execution time on the IBM 7094 computer.

6. Output for an Example Problem: The printed output for an example problem is displayed in Tables A-XII and A-XIII in Appendix A. The output in Table A-XII represents the normal minimum print-output with only the PRNT3 switch on (=2). These data are discussed in Section A-II of Appendix A. The output in Table A-XIII represents the output from the CW3 Code with all of the print switches on and in particular, the intermediate output from the TELECT subroutine is displayed. The sequence of computations in

the **TELECT** subroutine is discussed in section A-III and each step is related to the computed values of this example problem. Also additional details on the physics of our plasmas are brought out in the discussion.

III. RESONANT FREQUENCY SHIFT CODE

The theory and resonant cavity techniques for measuring the electron density in a plasma with microwaves are well known.^{13,14} We have described in some detail in earlier reports^{1,2} our inpile microwave measurements of electron density for both neon-argon and argon-cesium systems. There also, we reviewed the pertinent microwave theory and explained the simplifying assumptions we had used to analyze the experimental results. In particular we assumed that the electron density was uniform over the volume of the cavity. The predicted values of electron density from our earliest Reaction Kinetics Code have agreed fairly well with the values of the average electron density we obtained from the measured shift in resonant frequency of the cavity. However now with the new Electron Density-Temperature Code for predicting the electron density distribution in the cavity, we can relate the frequency shift of a resonant microwave cavity to the electron density distribution within that cavity. This improvement involves integration of the computed electron density distribution over the electric field within the cavity and permits us to make use of the following additional information obtained in the experiments.

We had designed our microwave cavity to operate in the fundamental TM_{020} mode. However we found in our inpile measurements that as we swept over a large range of input microwave frequency that other fundamental modes of the cavity had been excited. The information that we desire, that is the electron density distribution, is contained in the frequency shift for each of these modes although it does involve a different distribution of the electric field within the cavity. Even with our simplifying assumption of a uniform electron density we were able to take advantage of these additional signals. At the higher values of neutron flux and electron density in the argon-cesium system the resonant frequency of our fundamental TM_{020} mode would shift to such an extent that the signal would disappear in the noise either because of decreased coupling through the microwave window or because the signal moved out of the effective range of the microwave generator. However, before this signal had disappeared off-scale, signals from other modes had appeared and particularly the strong TM_{210} mode. This signal had a vacuum resonance frequency below the effective range of the microwave generator and therefore could be followed, once it had appeared, up to the maximum electron density generated.

In this section we first set down the basic equations from microwave theory that we need to solve for the shift in resonance frequency as a function of the electron density and electric field distribution within the cavity. Then we list the equations for the electric fields of the normal-modes of the cylindrical cavity in terms of the Bessel functions and their derivatives and finally we describe the computer code which performs the many numerical integrations necessary to obtain the predicted shift in resonant frequency for the particular fundamental mode desired.

A. Microwave Theory

1. Frequency Shift of the Cavity: The equations which express the change in the resonance properties of a microwave cavity with the introduction of a plasma were first derived by Slater¹² and developed by others.¹³ We have reviewed this theory, as it applies to our experiments, in a previous report¹ and described how these relations led to the well known formula which relates the shift in the resonant angular frequency ($\Delta\omega$) of a microwave cavity to the electron density distribution $n_e(\vec{r})$ and electric field distribution $\vec{E}(\vec{r})$ within the cavity:^{13,14}

$$\frac{\Delta\omega}{\omega_0} = \frac{1}{2} \frac{e^2}{\epsilon_0 m_e \omega_0^2} \left(\frac{1}{1 + \bar{\nu}_e^2 / \omega_0^2} \right) \frac{\int_V n_e(\vec{r}) E^2(\vec{r}) d\vec{r}}{\int_V E^2(\vec{r}) d\vec{r}} \quad (44)$$

The validity of this expression depends upon $\Delta\omega \ll \omega_0$, where ω_0 is the resonant frequency of the empty cavity.* In this expression e and m_e are the electronic charge and mass of the electron, ϵ_0 is the permittivity of free space, $\bar{\nu}_e$ is the average collision frequency of the electrons and V is the volume of the cavity.

Now we do not have available the full distribution of electron density $n_e(\vec{r})$ from our theory, but from the Electron Density-Temperature Code (CW8) described in Section II we can compute $n_e(r, z=d/2)$ along the mid-height radius of the cavity. Later in the analysis of the data in Section IV we will assume the electron density uniform in the axial direction z ; nevertheless, in this computer program for solution of Eq.(44) we shall maintain more generality and provide the means for an axial variation of n_e if, and when,

*The presence of un-ionized gas does not significantly perturb ω_0 .

that variation becomes available.* We do this by assuming that the electron density distribution can be expressed in a functional form with complete separation of the variables r and z , viz.

$$n_e(\vec{r}) = n_0 F_r(r) F_z(z) \quad (45)$$

$$\text{where} \quad n_0 = n(r=0, z=d/2) \quad (46)$$

$$\text{and} \quad 0 \leq F_z(z) \leq 1 \quad \text{and} \quad 0 \leq F_r(r) \leq 1.$$

If we write $\omega_0 = 2\pi f_0$, where f_0 is the microwave frequency in cps, and use Eq.(45) in (44) we obtain

$$\Delta f, \text{ cps} = \left(\frac{e^2}{8\epsilon_0 m_e \pi^2} \right) \left(\frac{1}{1 + \bar{v}_e^2/\omega_0^2} \right) \frac{n_0}{f_0} G(\vec{r}) \quad (47)$$

$$\text{where} \quad G(\vec{r}) = \frac{\int_V F_r(r) F_z(z) E^2(\vec{r}) d\vec{r}}{\int_V E^2(\vec{r}) d\vec{r}} \quad (48)$$

and $0 \leq G(\vec{r}) \leq 1$. In cps units, Eq. (47) becomes

$$\Delta f, \text{ cps} = 4.03 \times 10^7 \left(\frac{1}{1 + \bar{v}_e^2/\omega_0^2} \right) \left(\frac{n_0}{f_0} \right) G(\vec{r}) \quad (49)$$

n_0 is computed in the CW8 code and we have also shown in Eq.(27) in Section IIB.2 how to obtain \bar{v}_e from the output of the CW8 code.

We wish to evaluate f_0 and $G(\vec{r})$ in general terms in order that the code be applicable to any normal-mode of the cavity.

* If the plasma were completely controlled by axial diffusion (i.e. $n_e = n_0 \cos(\pi(z/d - 1/2))$) then $\langle n_e \rangle = 0.64 n_0$. With appreciable recombination loss, as we expect, the correction would be somewhat less. However, the actual axial correction in Eq.(48) depends also upon the axial variation of the electric field for the particular mode. This is of some convenience since as we shall see later, $E^2(\vec{r})$ in Eq.(44) for our cavity can also be expressed as a sum of terms each of which has complete separation of the variables r and z viz. $E^2(\vec{r}) = \sum_i F_{Ei}(r) F_{Ei}(z)$. A distribution function $n_e(r, z)$ could also be handled by numerical techniques with a modest increase in programming complexity.

2. Normal-Mode Fields for a Right Circular Cylinder¹⁵: The normal-mode fields in a completely lossless cavity are obtained by solving Maxwell's equations subject to the boundary conditions that \vec{E} be normal to all boundary surfaces and \vec{H} be tangential. The solutions are essentially a set of characteristic resonant frequencies and vector functions, \vec{E} and \vec{H} , describing the spatial configurations of the normal-mode fields. The normal-mode fields of a cavity are conveniently divided into two sets, transverse-electric and transverse-magnetic modes where the axis of reference for a right circular cylinder is along the cylinder axis z . The transverse electric TE-modes have no \vec{E} components along z and the transverse magnetic TM-modes have no \vec{H} components along z . The normal modes are further defined in terms of three integers ℓ, m, n . For the TE-modes

ℓ = number of full-period variations of E_r with respect to θ

m = number of half-period variations of E_θ with respect to r , and

n = number of half-period variations of E_z with respect to z .

For TM-modes, the integers are correspondingly defined in terms of the components of \vec{H} . The normal-mode fields are expressed in terms of trigonometric and Bessel functions.

The resonant frequencies of the (empty) microwave cavity, f_0 , are given in terms of the roots of the Bessel functions and the dimensions of the cavity as

$$f_0, \text{ cps} = \frac{c}{2\pi} \sqrt{\left(\frac{X_{\ell m}}{\rho_2}\right)^2 + \left(\frac{\pi n}{d}\right)^2} \quad (50)$$

where c = velocity of light (cm sec^{-1}) and ρ_2 and d are the radius and height of the cavity in cm. The quantities $X_{\ell m}$ are given in terms of the roots, and derivatives of the roots, of the Bessel functions as follows

$$X_{\ell m} = m^{\text{th}} \text{ root of } J'_\ell(x) = 0 \text{ for the TE-modes;} \quad (51)$$

$$X_{\ell m} = m^{\text{th}} \text{ root of } J_\ell(x) = 0 \text{ for the TM-modes;} \quad (52)$$

These roots are listed later in the input to the code in Table B-IV, Appendix B.

The normal-mode electric fields are given by the following equations:

For the TE-modes,

$$E_r = -\ell \frac{J_\ell(k_1 r)}{k_1 r} \sin \ell \theta \sin k_3 z \quad (53)$$

$$E_\theta = -J'_\ell(k_1 r) \cos \ell \theta \sin k_3 z \quad (54)$$

$$E_z = 0 \quad (55)$$

For the TM-modes,

$$E_r = -\frac{k_3}{k} J'_\ell(k_1 r) \cos \ell\theta \sin k_3 z \quad (56)$$

$$E_\theta = \ell \frac{k_3}{k} \frac{J_\ell(k_1 r)}{k_1 r} \sin \ell\theta \sin k_3 z \quad m > 0 \quad (57)$$

$$E_z = \frac{k_1}{k} J_\ell(k_1 r) \cos \ell\theta \cos k_3 z \quad (58)$$

where

$$k_1 = \frac{X_{\ell m}}{\rho_2} \quad (m > 0) \quad (59)$$

$$k_3 = \frac{\pi n}{d} \quad (n > 0) \quad (60)$$

$$k = \sqrt{k_1^2 + k_3^2} \quad (61)$$

We have now to use these equations to evaluate $G(\vec{r})$ in Eq. (48). First, we note that the square of the electric field appears in Eq. (48). Second, we observe that although we plan for a variation of $n_e(\vec{r})$ through the functions $F_r(r)$ and $F_z(z)$ in Eq. (48), we expect no variation of the electron density in the azimuthal direction θ and we can immediately integrate out the θ dependence in the electric field components. We do not include here the intermediate steps in the derivations but instead, we set down the final equations used to evaluate $G(\vec{r})$ in Eq. (48). Also we mix nomenclature and define some of the functional terms by their FORTRAN variable names that we shall use later. First, we rewrite Eq. (48) in terms of the FORTRAN variable names for the integrals in the numerator (XNUM) and denominator (XDEN) as

$$G(\vec{r}) = \frac{XNUM}{XDEN} \quad (62)$$

For the TE-modes we have:

$$\begin{aligned} XNUM &= \int_V F_r(r) F_z(z) E^2(\vec{r}) d\vec{r} \\ &= \pi \left[XZS \left(\frac{\ell^2}{k_1^2} XR1 + XR2 \right) \right] \end{aligned} \quad (63)$$

where

$$XZS = \int_0^d F_z(z) \sin^2(k_3 z) dz \quad (64)$$

$$XR1 = \int_0^{\rho_2} F_r(r) \left(\frac{J_l^2(k_1 r)}{r} \right) dr \quad (65)$$

$$XR2 = \int_0^{\rho_2} F_r(r) (J_l'^2(k_1 r) r) dr \quad (66)$$

and

$$XDEN = \int_V E^2(\vec{r}) d\vec{r} = \pi \left[VZS \left(\frac{l^2}{k_1^2} VR1 + VR2 \right) \right] \quad (67)$$

where

$$VZS = \int_0^d \sin^2(k_3 z) dz = \frac{d}{2} \quad (68)$$

$$VR1 = \int_0^{\rho_2} \frac{J_l^2(k_1 r)}{r} dr \quad (69)$$

$$VR2 = \int_0^{\rho_2} J_l'^2(k_1 r) r dr \quad (70)$$

For the TM-modes we have:

$$XNUM = \pi \left[XZS (XR2 + \left(\frac{l^2}{k_1^2} \right) \left(\frac{k_3^2}{k^2} \right) XR1) + XZC \left(\frac{k_1^2}{k^2} \right) XR3 \right] \quad (71)$$

where

$$XZC = \int_0^d F_z(z) \cos^2(k_3 z) dz \quad (72)$$

$$XR3 = \int_0^{\rho_2} F_r(r) J_l^2(k_1 r) r dr \quad (73)$$

and

$$XDEN = \pi \left[VZS (VR2 + \left(\frac{l^2}{k_1^2} \right) \left(\frac{k_3^2}{k^2} \right) VR1) + VZC \left(\frac{k_1^2}{k^2} \right) VR3 \right] \quad (74)$$

where

$$VZC = \int_0^d \cos^2(k_3 z) dz = \frac{d}{2} \quad (75)$$

$$VR3 = \int_0^{\rho_2} J_l^2(k_1 r) r dr \quad (76)$$

We note that the expressions for XNUM and XDEN above are composed of terms which are products of integrals over one variable (r or z) and we can perform the overall integrations in separate steps.*

*For the more general distribution function $n_e(r, z)$ we would have performed the integrations over r and z in nested FORTRAN DO-loops.

Before we take up the computer program for the solution of these equations we set down an important recursion formula which expresses the derivative of a Bessel function of integer order ℓ in terms of the Bessel function of order ℓ and $\ell+1$ ¹⁶

$$J'_\ell(y) = \left(\frac{\ell}{y}\right) J_\ell(y) - J_{\ell+1}(y). \quad (77)$$

We will make use of this expression to obtain the derivative of a Bessel function in conjunction with a FORTRAN-subroutine for evaluating the Bessel function itself.

Later in the analysis of the experimental microwave data we will find it convenient to compare experiment and theory in terms of an "electron density" rather than the frequency shift. We do this in terms of an electron density averaged over the square of the electric field in the cavity. From Eq.(49) we have

$$\frac{\Delta f f_o}{4.03 \times 10^7} = \left(\frac{1}{1 + \bar{v}_e^2 / \omega_o^2} \right) n_o G(\vec{r}) \quad (78)$$

where now both sides have the dimensions of electron density, cm^{-3} . We compute the right-hand side from theory and call it the theoretical average electron density (see also Fig. 1).

$$\langle n_e \rangle_{\text{Theo.}} = \left(\frac{1}{1 + \bar{v}_e^2 / \omega_o^2} \right) n_o G(\vec{r}) \quad (79)$$

$$\text{or} \quad = \left(\frac{f_o}{4.03 \times 10^7} \right) \Delta f_{\text{Theo.}} \quad (80)$$

as in Fig. 1.

We compute the left-hand side of Eq.(78) using the measured resonant frequency shift and call it the experimental average electron density

$$\langle n_e \rangle_{\text{Exp}} = \left(\frac{f_o}{4.03 \times 10^7} \right) \Delta f_{\text{Exp.}} \quad (81)$$

This value is a constant times a measured quantity. Both $\Delta f_{\text{Exp.}}$ and f_o depend upon the mode of the cavity.

B. Computer Code (CW9)

The computations described above are somewhat tedious in that they require a number of numerical integrations with the proper switching to permit computation for a number of cavity modes; nevertheless, no iteration techniques are involved and the problem is a straight-through computation. This Resonance Frequency Shift Code (CW9) was written in FORTRAN-IV language for the IBM-7094 computer and the flow diagram, source program listings and input-output examples are presented in Appendix B. For the numerical integrations we use the subroutine SIR together with the tabular-function subroutines, DUMMY and FUNCT. These subroutines have already been described in Section IIB.3. We had available a FORTRAN-IV library-subroutine "BESSEL" to compute the various Bessel functions and this was used in conjunction with the recursion Eq.(77) to evaluate the Bessel function derivatives.

IV. ANALYSIS OF INPILE MICROWAVE DATA

In the previous two sections of this report we have described how we calculate, with the aid of a digital computer, an average electron density for our inpile microwave cavities. We recall that the reaction kinetics equations for electron density discussed in earlier ONR reports now form part of a more comprehensive theory which both determines and takes into account non-equilibrium electron temperatures and non-uniform electron density distributions within the cavity. In the following section we present electron-density results from this theory and compare them with our previously reported inpile microwave measurements of average electron density.

In order that we might exhibit the influence of the non-equilibrium electron temperature apart from the effects due to the non-uniform density distribution and other changes of lesser importance, we have written a modified version (CW8-B) of the CW8 code in which all computations were the same except that we set $T_e = T_{\text{gas}}$. Computations from this CW8-B code without electron heating will be compared with the predictions from our new theory.

Most of the analysis presented in this section is for the neon-argon microwave data. However, we do report on a few computer runs for the argon-cesium system but these last results confirmed our previous conclusions in section IIA.3 that the electron temperature theory must be modified for the argon-cesium system to include inelastic collisions. Finally, we outline our plans to modify the Electron Density-Temperature Code to account for the major inelastic losses in the energy decay of the energetic electrons and for the fractional increase in ion generation rate that accrues.

A. Microwave Experiment

The microwave measuring circuit and resonant cavity have been described in detail previously.² We shall review here only those details needed to explain the limitations on our variation of the operating conditions. We used K-band microwaves from a sweep generator (H.P.696A) with an effective range of 22.0 to 26.5 GHz. The microwave cavity was supported at the end of a long length (~ 20 ft) of waveguide inside an aluminum containment tube. This 3 inch o.d. aluminum tube was placed in a reflector position at the edge of the reactor core. For the inpile runs on the neon-argon cavity the neutron flux was

varied by changes in reactor power. For the inpile runs on the argon-cesium cavity the reactor power was held constant at 2.0 MW and the entire microwave assembly (including the generator) was lifted vertically by a screw-jack so that the microwave cavity could be moved from the maximum neutron flux position at the mid-plane of the core ($\phi_{\text{max}} \approx 1.4 \times 10^{13} \text{ cm}^{-2} \text{ sec}^{-1}$ at $P=2\text{MW}$) to a minimum flux about 1 ft above the core ($\phi_{\text{max}} \approx 0.004 \phi_{\text{max}}$).

The neon-argon and argon-cesium cavities had the same overall dimensions: o.d.=2.272 cm, height=0.7 cm with a U-235 foil 0.001 inch thick and 1.9 cm in diameter bonded to the inside surface of one end cap. For the neon-argon cavity we directed the end of a small ($\sim 1/4$ inch o.d.) tubing at the outside surface of this end cap so that the fission heat could be dissipated by a cooling stream of nitrogen gas. For the argon-cesium cavity an enlarged pump-out tubulation became the cesium reservoir and we directed another nitrogen gas cooling tube at this reservoir to give some control of bath temperature. The important point to these design details is that we were very limited in our ability to vary the gas temperature inside the cavity since the modest fission heat (~ 80 watts max) depended upon the neutron flux and we could vary the average temperature of the cavity walls from the condition for maximum N_2 cooling ($\sim 320^\circ\text{K}$) to the condition for no N_2 cooling ($\sim 750^\circ\text{K}$ for maximum neutron flux). For the argon-cesium cavity we were further limited in maximum average cavity temperature by the heat dissipation needed to control the temperature of the cesium bath. Had we anticipated the anomalous dependence of electron density on the wall temperature of the argon-cesium cavity we could have added to the design an oven similar to that employed on our argon-cesium ionization tube.⁵

We constructed and operated inpile only one neon-argon cavity (No.14) and one argon-cesium cavity (No. 16) of this design.* The neon-argon cavity was filled to a gas pressure of 90 torr ($\text{Ne}=\text{N}_0=2.9 \times 10^{18} \text{ cm}^{-3}$) with a mixture of $\text{Ar}/\text{Ne}=1.0 \times 10^{-4}$. The argon-cesium cavity was filled to a gas pressure of 90 torr ($\text{Ar}=\text{N}_0=2.9 \times 10^{18} \text{ cm}^{-3}$) of argon and by adjusting the cesium bath temperature we were able to vary the mixture of Cs/Ar from $\sim 1 \times 10^{-6}$ to $\sim 1 \times 10^{-3}$.

*One previous inpile run had been made on a neon-argon ($\text{Ar}/\text{Ne}=10^{-3}$) cavity (No.9) with different dimensions ($d=0.5$ cm). This cavity was operated without a sweep generator and only one data point was obtained before the cavity failed.¹

B. Analysis of Neon-Argon Microwave Data

Most of the inpile data on this cavity were taken for the condition of maximum N_2 -gas cooling, viz., minimum average cavity (or gas) temperature, and the neutron flux was varied by varying the reactor power. We will present this data as a function of neutron flux but before we can compute a predicted curve from our theory we must select from the experimental data values which are representative of the average gas temperature at each value for the neutron flux. Also, two inpile runs were made at two different but fixed values of neutron flux in which the temperature of the cavity was varied from the minimum to the maximum temperature obtainable within the limits of the N_2 gas flow. These data will be presented separately together with the values of electron density predicted from theory. In all cases we will present the data as points on a graph with the predictions from our theory as a solid curve. We also include the computed values from the CW8-B code as a dashed curve to show by comparison the effect of the elevated electron swarm temperature.

1. Average Gas Temperature $\langle T_{\text{gas}} \rangle_{\text{av}}$: Chromel-alumel thermocouples were spot-welded to the center of the outside surface of each end of the cylindrical cavity. We recorded temperature measurements for both the thermocouple on the end containing the uranium ($T_U, ^\circ\text{K}$) and the thermocouple on the bare Kovar-end ($T_K, ^\circ\text{K}$). We define the average gas temperature as

$$\langle T_{\text{gas}} \rangle_{\text{av}} = 1/2 (T_U + T_K). \quad (82)$$

A plot of this average temperature of the cavity walls versus the neutron flux is presented in Fig. 4 for the last two runs on the cavity. The circular data points are for the condition of maximum cooling and most of our microwave measurements were taken at higher values of neutron flux ($\gtrsim 10^{12} \text{ cm}^{-2} \text{ sec}^{-1}$).

The solid curve drawn through the data points was used to obtain values for $T_g = \langle T_{\text{gas}} \rangle_{\text{av}}$ for the computer runs. Values for the computed electron swarm temperature are shown by the dashed line but these will be discussed later.

2. Reaction Rates: Input values for the reaction rate coefficients for the reaction kinetics equations in the Electron Density subroutine have been presented for the example problem in Table A-XII (page A-22). Most of these values were discussed in a previous report⁵ and those coefficients whose values have been changed will be discussed now. The new method of computing the

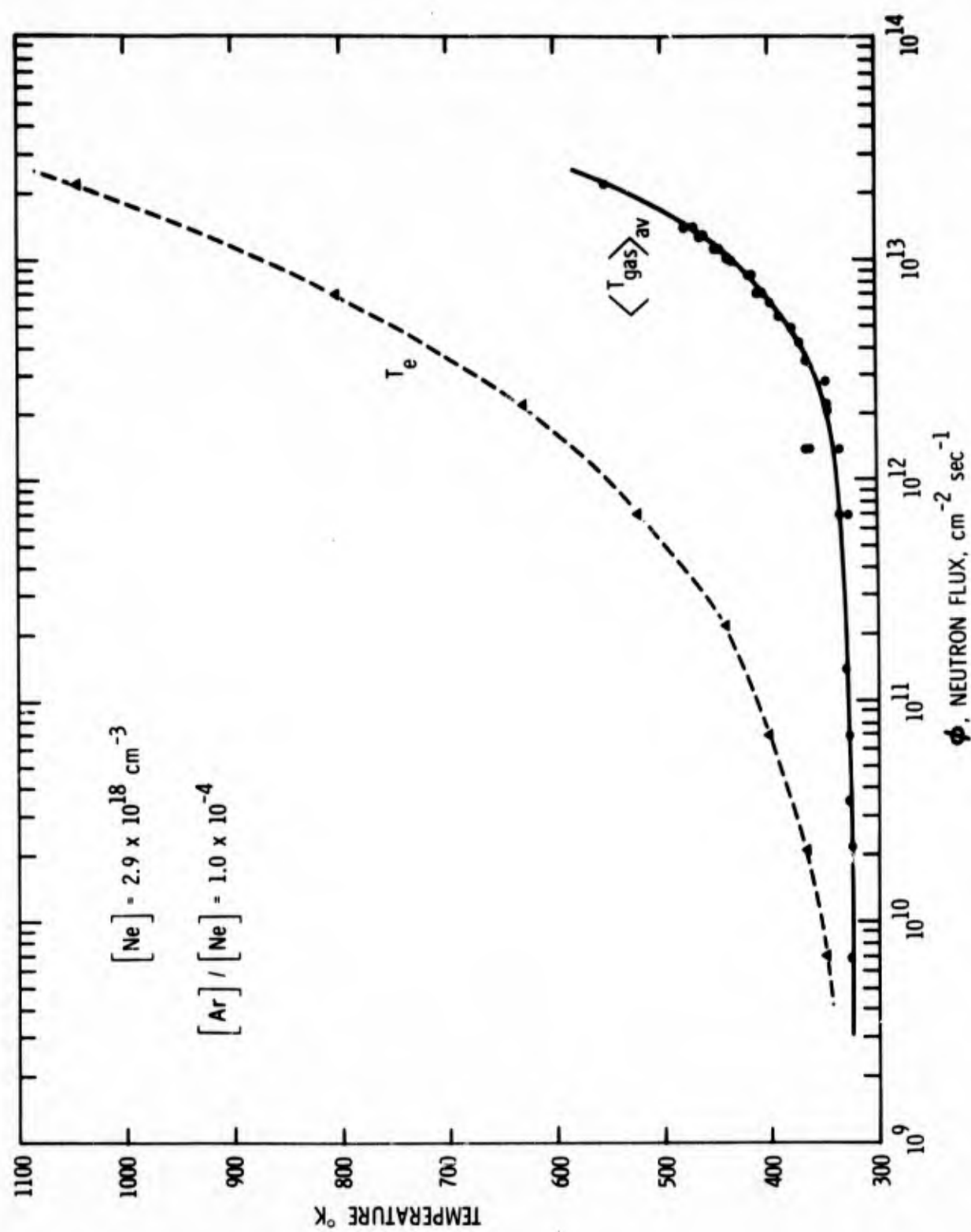


Fig. 4. Computed electron swarm temperature T_e , and average temperature of microwave cavity $\langle T_{\text{gas}} \rangle_{\text{av}}$ as functions of neutron flux. These data are for the condition of maximum cooling rate of the cavity.

important collisional radiative recombination coefficient $C_{22}(n_e, T_e)$ has been discussed in section IID.2. A dependence on electron temperature has also been built into the dissociative recombination coefficient C_{16} for the generalized reaction $N_{2+} + e^- \rightarrow 2N_0$ and for the dissociative recombination coefficient C_{21} for the generalized reaction $A_{2+} + e^- \rightarrow 2A_0$ as:

$$C_{16}(T_e) = C_{16}(300^\circ K) (300/T_e, ^\circ K)^{E16} \quad (83)$$

$$\text{and} \quad C_{21}(T_e) = C_{21}(300^\circ K) (300/T_e, ^\circ K)^{E21} \quad (84)$$

where E16 and E21 are the input FORTRAN names of the exponents in the simple power law.

Frommhold and Biondi¹⁷ have studied the temperature dependence of the dissociation recombination of Ne_2^+ and N_2^+ ions and found that $\alpha(Ne_2^+)$ decreases slowly with T_e for $300 \leq T_e \leq 3000^\circ K$ and $T_+ = T_g = 300^\circ K$. They indicate that the closest simple power law to fit the data is a $T_e^{-1/3}$ variation. Therefore we set E16=0.333 in Eq.(83) and use the previous discussed value of $C_{16}(300^\circ K) = 2.2 \times 10^{-7} \text{ cm}^3 \text{ sec}^{-1}$ from the studies of Oskam and Mittelstadt.¹⁸ Hess¹⁹ has also reported for neon that $\alpha(Ne_2^+)$ varies as $T_e^{-0.25}$ for $300 \leq T_e \leq 600^\circ K$ and varies as $T_e^{-0.4}$ for $900 \leq T_e \leq 2400^\circ K$. These numbers are in good agreement with the simple power law we have selected.

Fox and Hobson²⁰ have reported for shock tube experiments that $\alpha(Ar_2^+)$ varies as $T^{-3/2}$ for $1000 \leq T_m \leq 3000^\circ K$. Even though the gas atoms and ions probably also reach elevated temperatures in these experiments, the relative velocity of approach of the ion and electron is given essentially by the electron velocity, so we select E21=1.5 in Eq.(84) and use the previous value of $C_{21}(300^\circ K) = 6.7 \times 10^{-7} \text{ cm}^3 \text{ sec}^{-1}$ also from the studies of Oskam and Mittelstadt.¹⁸

We have explained how the diffusion coefficients for the ions are adjusted for T_g and T_e in section IID.3. Phelps²¹ has found that the neon metastable states have a temperature dependence for their diffusion coefficient of $T^{0.73}$ for $77 \leq T \leq 500^\circ K$. We have therefore provided for a simple power law variation of K_m in the code for adjustment for the gas temperature in terms of the input value $K_m(300^\circ K)$

$$K_m(T_g) = K_m(300^\circ K) \left(\frac{T_g}{300} \right)^{EKM} \quad (85)$$

where EKM is the input FORTRAN name of the exponent. For the neon metastables Ne^m , $\text{EKM}=0.73$ and $K_m(300^\circ\text{K})=5.5 \times 10^{18} \text{ cm}^{-1} \text{ sec}^{-1}$ as derived in Reference (5) from the work of Phelps.²¹

3. Ion Generation Rate: We have described in an earlier ONR report⁵ our ion generation rate theory and the QOO code by which we compute the ion source rate at each point in the tube ($S_+(\vec{r})$) from the properties of the fission fragments, the properties of the gas and the geometry of the tube. Also in Reference (5) we gave values for the important properties of the fission fragments and the gas constants (for both Ne and Ar). To obtain the values of ion source rate $S_1 (=S_+/N_0)$ used in these neon-argon studies we made a run with the QOO Code for the geometry of the microwave cavity and a gas filling of pure neon at 90 torr pressure ($N_0=2.9 \times 10^{18} \text{ cm}^{-3}$). Previous to our inpile microwave runs we had calibrated the reactor neutron flux inside a mockup of our microwave cavity with gold-activation techniques. For the QOO Code computation, then, we obtain the total fission cross section (Σ_f) of the fission fragment source directly from the composition of the uranium-nickel film without adjusting for neutron attenuation in the support structure: 0.12 vol. fract. of nickel with 0.88 vol. fract. of uranium of 93% enrichment and density of 18.7 gm cm^{-3} yields $\Sigma_f=21.7 \text{ cm}^{-1}$ for $\sigma_f(\text{U-235})=582\text{b}$ and 0.95 self-shielding. The light fission fragment range is $6.62 \times 10^{-4} \text{ cm}$ and the heavy fragment range is $5.05 \times 10^{-4} \text{ cm}$ for this U-Ni alloy.

For an input neutron flux of $\phi=1.0 \times 10^{13} \text{ cm}^{-2} \text{ sec}^{-1}$ the QOO Code gave a value of $S_1=S_+/N_0=1.86 \times 10^{-3} \text{ sec}^{-1}$. We made the inpile microwave runs at specified values of reactor power (P) and since the flux calibration gave $\phi = 1.45 \times 10^{13} \text{ cm}^{-2} \text{ sec}^{-1}$ for $P=2.1 \text{ MW}$ we have $S_1'=S_+/N_0 P \approx 1.30 \times 10^{-3} \text{ sec}^{-1} \text{ MW}^{-1}$.

For the fission fragment generation rate of neon metastable states we have used $S_3=0.465 S_1$. This value was computed from our reaction kinetics theory and was verified by two inpile runs with our ion generation rate tube for pure neon and a neon-argon mixture.⁵

The distribution of the ion source rate along the mid-height radius of the tube as determined from the QOO Code run was used to obtain the source rates printed out for the example problem in Table A-XII (page A-31) in Appendix A. The source rates for that problem ($P=1\text{MW}$, $\phi=6.9 \times 10^{12} \text{ cm}^{-2} \text{ sec}^{-1}$) is plotted in Fig. 5 versus the radial distance from the center of the tube. The CW8 code output for the electron swarm temperature and the electron density are also plotted versus r in Fig. 5.

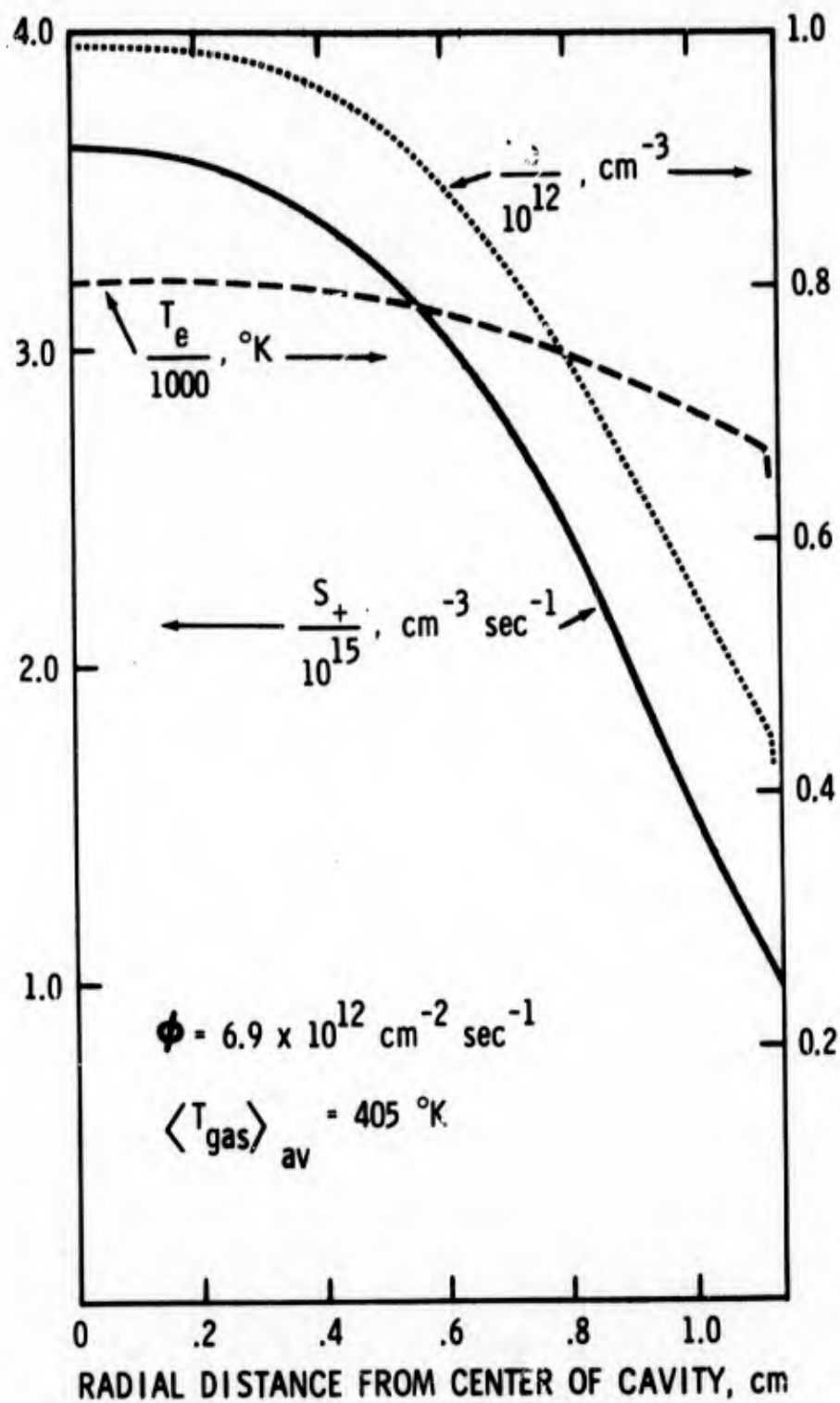


Fig. 5. Computed variation of ion generation rate (S_+), electron temperature (T_e) and electron density (n_e) along the radius of the cavity.

4. Electron Density Versus Neutron Flux: With the input data as described above and the gas temperatures as obtained from Fig. 4, the following computer runs were made, first on the CW8 code, and then on the CW9 code.

TABLE I. CW8 Computer Runs

Run No.	Reactor Power, kW	Neutron Flux $\text{cm}^{-2} \text{sec}^{-1}$	T_g °K	S_1, sec^{-1}
109.1	1	6.9×10^9	322	1.300×10^{-6}
109.2	3.16	2.18×10^{10}	323	4.108×10^{-6}
109.3	10	6.9×10^{10}	326	1.300×10^{-5}
109.4	31.6	2.18×10^{11}	329	4.108×10^{-5}
109.5	100	6.9×10^{11}	333	1.300×10^{-4}
109.6	316	2.18×10^{12}	345	4.108×10^{-4}
109.7	1000	6.9×10^{12}	405	1.300×10^{-3}
109.8	3160	2.18×10^{13}	555	4.108×10^{-3}

For each of these runs electron densities and temperatures were obtained at 11 points along the mid-height radius of the cavity as in Run 109.7 in Table A-XII (page A-31). The electron temperatures computed for the center of the cavity are plotted versus the neutron flux in Fig. 4. At the lower values of neutron flux the electrons are heated only slightly above the gas temperature. However as the ion generation rate (S_1) increases with neutron flux, the energy input to the electron swarm (\dot{E}_{max} in Eq.(3)) increases and the electron swarm temperature increases much more rapidly than the gas temperature and at a high neutron flux of $1.0 \times 10^{13} \text{cm}^{-2} \text{sec}^{-1}$, $T_g \approx 440^\circ\text{K}$ while $T_e(r=0) \approx 900^\circ\text{K}$.

The CW8 code output distribution of electron density along the mid-height radius of the cavity was fed as input to the CW9 code for the TM_{020} mode and the computed average electron density output is plotted as the solid curve in Fig. 6. The experimental values are plotted (see Eq.(81)) as points and the fit is seen to be very good (error $\leq \pm 20\%$).

The experimental points which are represented as squares in Fig. 6 were actually taken with no cooling of the cavity. For the data points at $\phi < 10^{11} \text{cm}^{-2} \text{sec}^{-1}$ there was little heating of the cavity, however, for the points where $10^{11} \leq \phi \leq 10^{12} \text{cm}^{-2} \text{sec}^{-1}$ the average gas temperature was higher than the values taken from the curve in Fig. 4 and therefore the fit between experiment

and theory below $\phi \sim 10^{12} \text{ cm}^{-2} \text{ sec}^{-1}$ is even better than shown. Above $\phi \sim 2 \times 10^{12} \text{ cm}^{-2} \text{ sec}^{-1}$, the experimental data dip slightly ($\lesssim 20\%$) below our theoretical curve. We offer no explanation of this slight deviation. The fractional loss of ions by diffusion is very small even at the higher electron temperature (DIFFRN=0.13, Table A-XII (page A-27)) and so our assumption of no axial variation of n_e yields only slightly higher computer values for $\langle n_e \rangle$.

The dashed curve from the CW8-B code for $T_e = T_g$ produces values considerably lower than the experimental data and the difference in $\langle n_e \rangle_{\text{Theo}}$ is proportional to $T_e - T_g$ in Fig. 4. We consider this difference in the fit of the two computed curves as further confirmation of the non-equilibrium condition that we predict for our plasmas.

Some of the more important reaction rates are listed in Table II as a function of the neutron flux. Also listed are the solutions for the six important species of the plasma and both the reaction rates and density of species were computed for a point at the center of the tube. In all of these cases, Ar^+ is the major ion species and the primary ion Ne^+ is lost by 3-body molecular ion formation to Ne_2^+ followed by rapid dissociative recombination. At low values of n_e (at low neutron flux) Ar^+ is lost by molecular ion formation and diffusion while at higher values of n_e , the collisional radiative recombination rate becomes predominant.

5. Electron Density Versus Average Gas Temperature: Two inpile runs were made at two different but fixed values of neutron flux (ϕ) and the electron density was varied as a function of $\langle T_{\text{gas}} \rangle$. In both cases (see Figs. 7 and 8) very little variation of $\langle n_e \rangle$ with $\langle T_{\text{gas}} \rangle$ was obtained.

In Fig. 7 for the lower value of $\phi = 3.5 \times 10^{12} \text{ cm}^{-2} \text{ sec}^{-1}$ the fit of the new theory with electron heating ($T_e \approx 800^\circ \text{K}$) is good, particularly, the slope matches that of the data. The dashed curve shows the prediction with no electron heating ($T_e = T_g$) and besides predicting values too low the derivation $\partial \langle n_e \rangle / \partial T_g$ is too high.

In Fig. 8 for the higher neutron flux ($\phi = 1.4 \times 10^{13} \text{ cm}^{-2} \text{ sec}^{-1}$) the magnitude of the predicted values from the new theory with electron heating ($T_e \approx 1000^\circ \text{K}$) are higher than the data as in Fig. 5, however the slope agrees somewhat better with the data than that from the CW8-B code with $T_e = T_g$.

TABLE II. Reaction rates and number density of species in a Ne-Ar plasma (center of tube values).

REACTOR POWER, kW		3.16	31.6	316	3160
Neutron Flux, cm ⁻² sec ⁻¹		2.2 x 10 ¹⁰	2.2 x 10 ¹¹	2.2 x 10 ¹²	2.2 x 10 ¹³
$\langle T_{gas} \rangle_{av}$, °K		323	329	345	555
T_e , °K		365	445	630	1045
Reaction Rates, cm ⁻³ sec ⁻¹					
$S_1[Ne]$ (Fission Fragment Ionization)		1.2 x 10 ¹³	1.2 x 10 ¹⁴	1.2 x 10 ¹⁵	1.2 x 10 ¹⁶
$C_{15}[Ne^m][Ar]$ (Penning Ionization)		3.9 x 10 ¹²	4.0 x 10 ¹³	4.0 x 10 ¹⁴	4.0 x 10 ¹⁵
$C_4[Ne^+][Ne]^2$ (3-b Molecular Ion Formation)		1.2 x 10 ¹³	1.2 x 10 ¹⁴	1.2 x 10 ¹⁵	1.2 x 10 ¹⁶
$C_{22}[Ar^+][Ar]^2$ (3-b Collisional Radiative Rec.)		1.9 x 10 ¹¹	1.3 x 10 ¹³	2.6 x 10 ¹⁴	3.0 x 10 ¹⁵
$C_{20}[Ar^+][Ar][Ne]$ (3-b Molecular Ion Formation)		2.8 x 10 ¹²	1.8 x 10 ¹³	8.7 x 10 ¹³	4.5 x 10 ¹⁴
$(K_u/\Lambda^2[Ne][Ar^+])$ (Ar ⁺ - Diffusion Loss)		1.3 x 10 ¹²	9.5 x 10 ¹²	5.7 x 10 ¹³	4.8 x 10 ¹⁴
Densities, cm ⁻³ (where $[Ne]=2.9 \times 10^{18}$, $[Ar]=2.9 \times 10^{14}$ and $[Ar]/[Ne]=10^{-4}$)					
n_e		1.7 x 10 ¹⁰	9.4 x 10 ¹⁰	4.3 x 10 ¹¹	2.2 x 10 ¹²
$[Ne^+]$		2.4 x 10 ⁷	2.4 x 10 ⁸	2.5 x 10 ⁹	2.5 x 10 ¹⁰
$[Ne_2^+]$		3.2 x 10 ⁹	6.5 x 10 ⁹	1.6 x 10 ¹⁰	3.9 x 10 ¹⁰
$[Ne^*]$		-	-	-	-
$[Ne^m]$		7.5 x 10 ⁸	7.7 x 10 ⁹	7.7 x 10 ¹⁰	7.6 x 10 ¹¹
$[Ar^+]$		1.3 x 10 ¹⁰	8.7 x 10 ¹⁰	4.1 x 10 ¹¹	2.1 x 10 ¹²
$[Ar_2^+]$		3.3 x 10 ⁸	5.2 x 10 ⁸	9.1 x 10 ⁸	2.0 x 10 ⁹

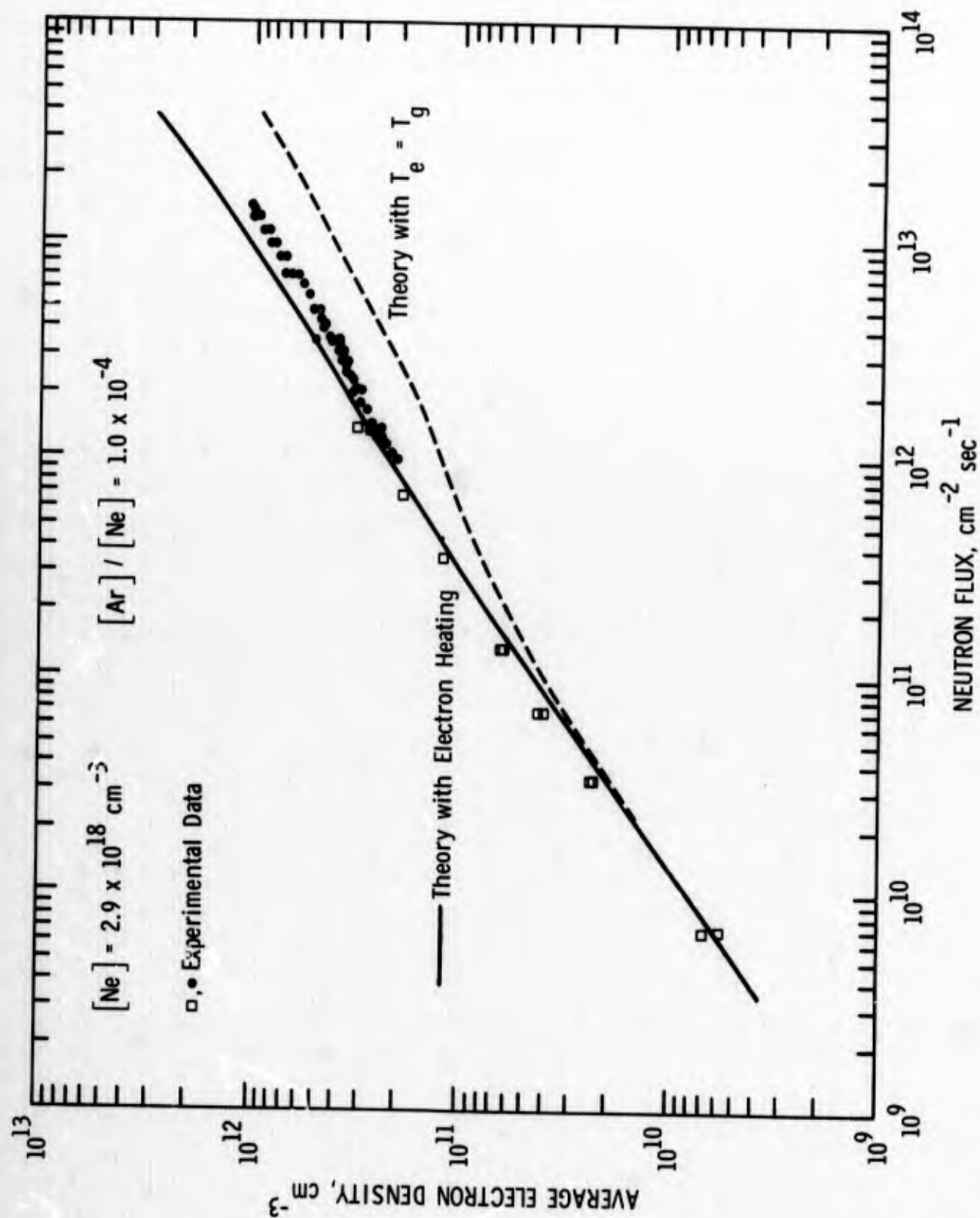


Fig. 6. Comparison of experimental values of electron density with theoretical predictions (solid curve) for the neon-argon microwave cavity. When the elevation of electron temperature above ambient is not taken into consideration and we assume $T_e = T_g$, the theoretical values of n_e (shown by the dotted curve) depart markedly from the experimental data.

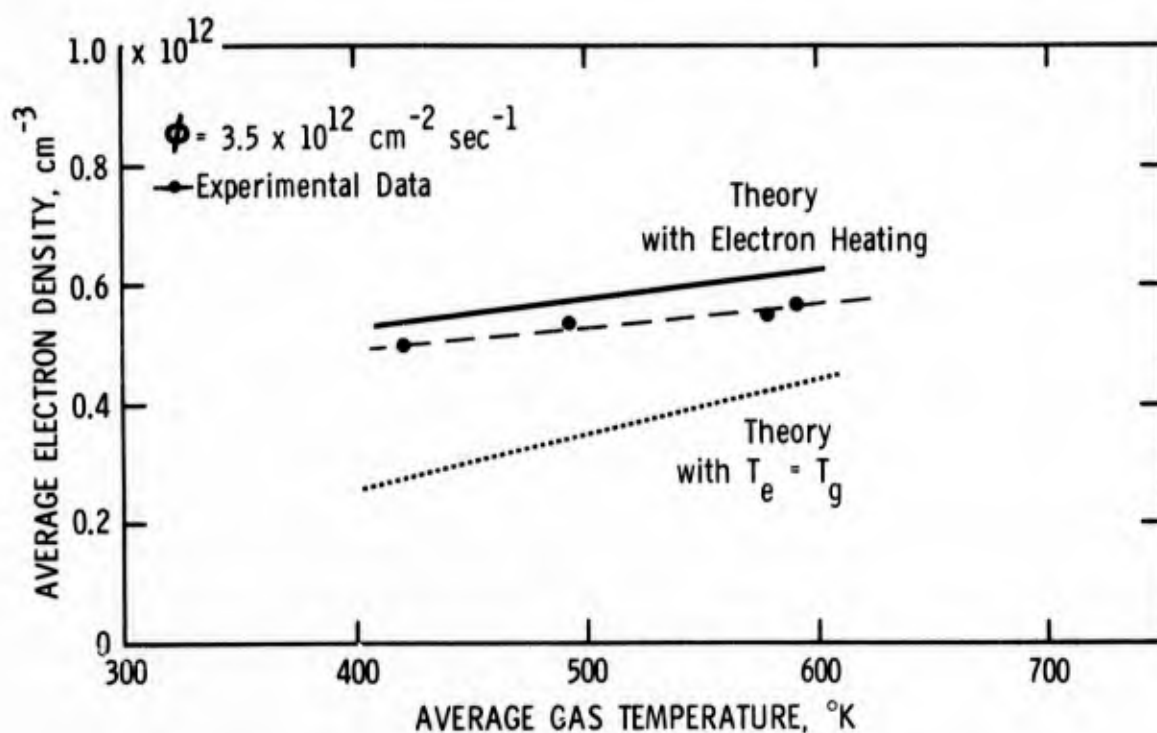


Fig. 7. Comparison of computed and experimental variations of the average electron density n_e versus the average gas temperature $\langle T_{gas} \rangle$ at a moderate neutron flux of $\phi = 3.5 \times 10^{12} \text{ cm}^{-2} \text{ sec}^{-1}$.

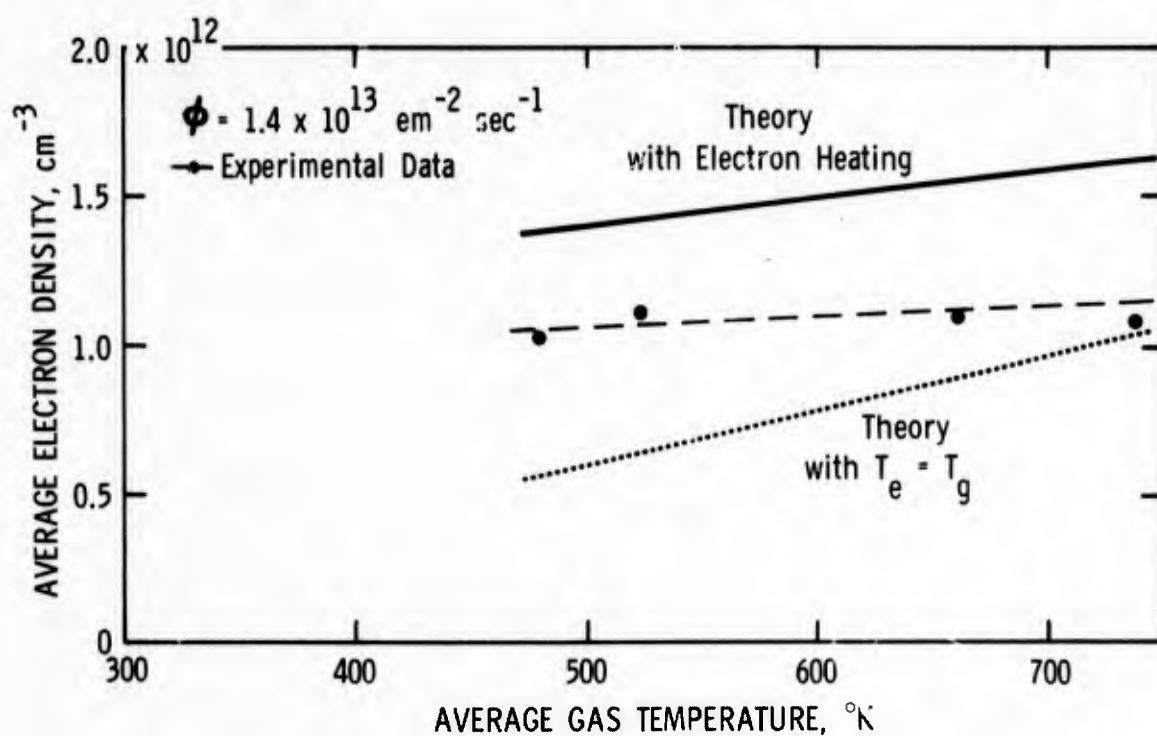


Fig. 8. Comparison of computed and experimental variations of the average electron density n_e versus the average gas temperature $\langle T_{gas} \rangle$ at a high neutron flux of $\phi = 1.4 \times 10^{13} \text{ cm}^{-2} \text{ sec}^{-1}$.

C. Analysis of Argon-Cesium Microwave Data

We do not expect to fit the argon-cesium microwave data with our new theory because as yet we have not included the terms for electron cooling by inelastic collisions. These terms will be important as the energetic electrons decay in energy in the presence of neutral cesium atoms. However, we had made some inpile microwave measurements on argon-cesium at a very low cesium to argon ratio ($Cs/Ar \sim 3.0 \times 10^{-6}$) where the error due to neglecting these inelastic collisions should be minimal. We report here on three CW8 code runs on the argon-cesium system, $Cs/Ar = 1.0 \times 10^{-6}$, $Cs/Ar = 3.0 \times 10^{-6}$ and $Cs/Ar = 1.0 \times 10^{-5}$ and compare the predicted values with experimental results.

1. Reaction Rate Coefficients: Almost all of the reaction rate coefficients for the argon-cesium system have been discussed before^{1,3,5} and, of course, many of the important parameters for argon have been discussed in Section III. For the temperature dependence of the dissociative recombination rate C_{16} for Ar_2^+ we have used the simple power law in Eq.(83) with $E_{16} = 0.7$ from the data of Mehr and Biondi.²² For the temperature dependence of the similar rate C_{20} for Cs_2^+ we set $E_{20} = 0.50$ in Eq.(84) after Bates and Dalgarno.²³ For the volume destruction of argon metastable states in three-body collisions with argon atoms (C_{14}) we use the value derived in Reference (1)(Section A). We have already presented the momentum transfer cross section for electrons in argon $Q_{ea}(r)$ in Fig. 2.

For the ion generation rate, a QOO code run on pure argon gave $S_1(r=0) = S_1(r=0, z=d/2)/N_0 = 1.05 \times 10^{16} / 2.9 \times 10^{18} = 3.62 \times 10^{-3} \text{ sec}^{-1}$ for a neutron flux of $1.0 \times 10^{13} \text{ cm}^{-2} \text{ sec}^{-1}$. Since the neutron flux calibration gave a value of $\phi = 1.44 \times 10^{13} \text{ cm}^{-2} \text{ sec}^{-1}$ at a reactor power of $P = 2 \text{ MW}$ we have $S_1' = S_1/N_0 P = 2.61 \times 10^{-3} \text{ sec}^{-1} \text{ MW}^{-1}$. * For the fission fragment production rate of argon metastable states we assumed a value of S_3/S_1 similar to that computed for neon, that is we set $S_3 = 0.5 S_1$ for argon.

2. Comparison of Theory and Experiment: The inpile microwave run on argon-cesium reported here was made at a neutron flux of $\phi = 1.44 \times 10^{13} \text{ cm}^{-2} \text{ sec}^{-1}$. The cesium to argon ratio was varied from $Cs/Ar = 3 \times 10^{-6}$ to 1.2×10^{-3} with careful attention to maintain the $\langle T_{gas} \rangle_{av} = 644^\circ \text{K}$. We show only the first of four experimental points of this data in Fig. 9 up to $Cs/Ar = 1.5 \times 10^{-5}$. The * In our previous studies of the Ar-Cs microwave data⁵ we have used the average value, $\langle S_+(r) \rangle_{av}$, from the QOO Code run which gave $S_1 = 2.40 \times 10^{-3} \text{ sec}^{-1}$ and $S_1 = 1.73 \times 10^{-3} \text{ sec}^{-1} \text{ MW}^{-1}$.

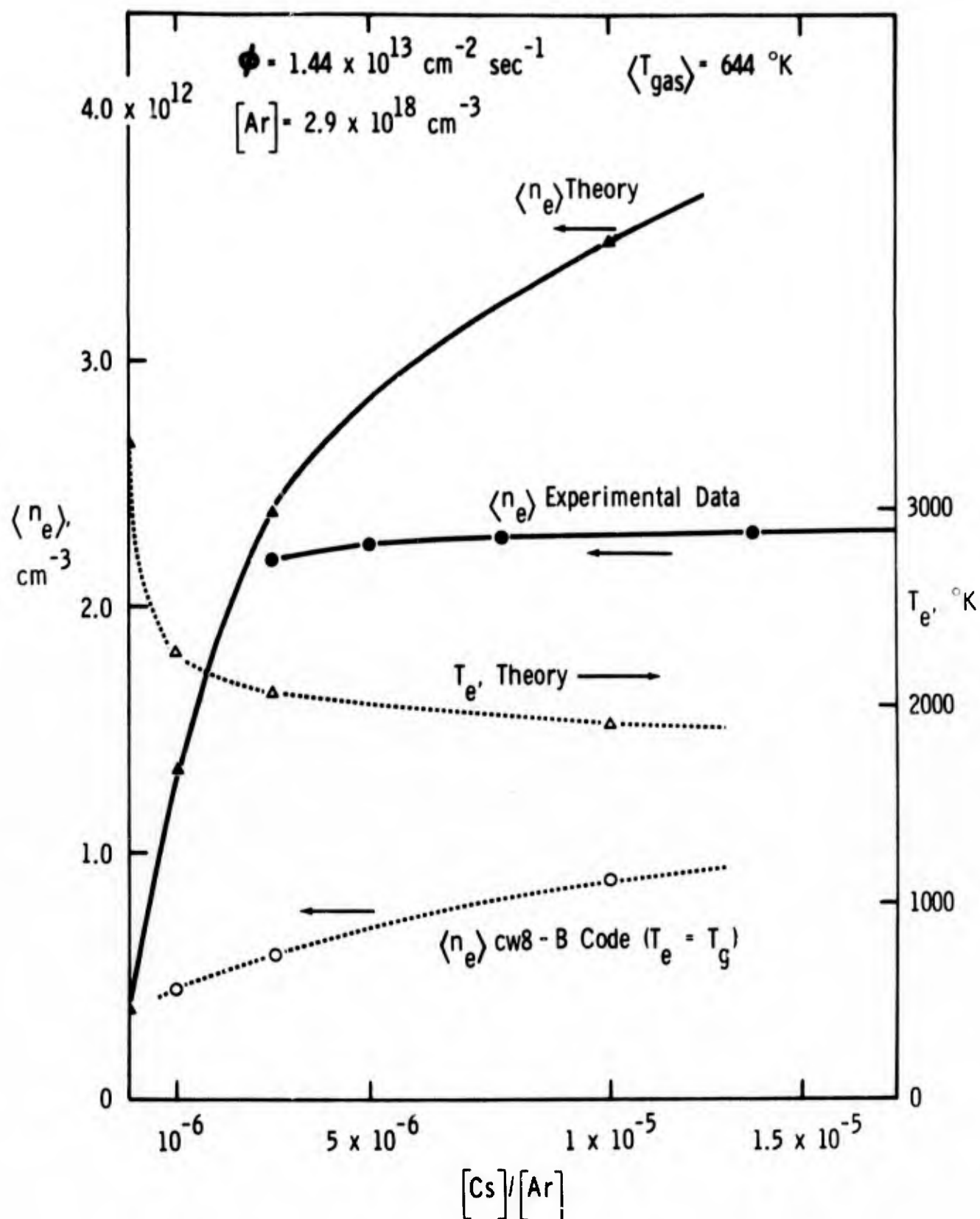


Fig. 9. Comparison of experimental values of $\langle n_e \rangle$ versus $[Cs]/[Ar]$ with theoretical values computed without taking into account inelastic electron losses with cesium atoms; the corresponding electron temperature T_e is indicated. Also shown for interest are the low values of $\langle n_e \rangle$ obtained by neglecting the elevation of T_e .

three code predictions for the average electron density at $Cs/Ar=10^{-6}$, 3×10^{-6} and 10^{-5} are joined by the solid curve to the code predictions for pure argon ($Cs/Ar=0$). Also shown are the predicted electron swarm temperatures from the CW8 code for the center of the cavity and, for comparison, the predicted values of $\langle n_e \rangle$ for $T_e = T_g$.

At low Cs/Ar the predictions for $\langle n_e \rangle$ from our theory agree well with the experimental data but with increasing Cs/Ar the theoretical curve increases much too rapidly. We think this is because the electron temperature is not quenched sufficiently in the absence of inelastic collisions with the neutral cesium atoms. The values for the CW8-B code for $T_e = T_{gas}$ are much too low with no electron heating. These data certainly demonstrate the critical importance of the electron swarm temperature.

D. Modifications to CW8 Code to Include Inelastic Collisions

We have reexamined the kinetics of the argon-cesium system in light of changes needed to account for A) additional cooling of the energetic electrons by inelastic collisions, B) additional cooling of the electron swarm by inelastic collisions and C) increase in the generation rate of Cs^+ ions from A) and B).

We shall not go into the complexity of many interactions involved but give only our (tentative) conclusions. One of the important considerations was whether we had to introduce one or more additional reaction kinetics equations to account for the presence of the cesium excited states inasmuch as these could be further stimulated to the cesium ion. We concluded that even with some trapping of the resonant radiation, the lifetime of the excited states was too short to contribute significantly to the generation rate of cesium ions in our plasmas. We plan to add terms to \dot{E}_{GS} in Eq.(10) for transfer of energy to both excite and ionize cesium atoms. On the other hand, we expect the electron swarm temperature to be sufficiently low that we do not need to add corresponding terms to $(-\dot{E}_{LS})$ in Eq.(17) to account for similar reactions with the electrons in the high energy tail of the distribution.

To account for the increased source of cesium ions we intend to add the cesium ions produced in the decay of the energetic electron, as an additional source term back into the Electron Density subroutine (TELECT). This term may be significant at low values of Cs/Ar where the source rate of Cs ions is

considerably less than the source rate of argon ions ($S_1 N_0$). Also we may need to add a cesium conservation equation to the set of kinetics equations to take into account the depletion of available neutral cesium atoms at low values of Cs/Ar and at high fractional ionization of the cesium, viz., $Cs^+ + Cs = Cs_0$ where Cs_0/Ar is fixed by the cesium bath temperature.

V. REFERENCES

1. C. B. Leffert, D. B. Rees and F. E. Gifford, ONR Annual Report No. 6, Contract Nonr-3109(00), (Oct. 1965). For the theory and results of the first inpile microwave experiment on neon-argon see also: D. B. Rees, C. B. Leffert and F. E. Jamerson, Proc. IEEE Thermionic Specialist Conference (San Diego)(Oct. 1965).
2. C. B. Leffert and D. B. Rees, ONR Annual Report No. 7, Contract Nonr-3109(00), (Oct. 1966).
3. C. B. Leffert, "Reaction Kinetic Studies of Ar-Cs Plasmas", Section A, Final ONR Annual Report No. 8 (Unclassified Vol. I), Contract Nonr-3109(00), (Oct. 1967). Note: Adjustable parameters were used in this study to obtain a very good final fit to the Ar-Cs microwave data but the fit even without these parameters had been fair.
4. D. B. Rees, "Calculation of Electron Temperatures in Plasmas Produced by Fission Fragments", Section B, Final ONR Annual Report No. 8 (Unclassified Vol. I), Contract Nonr-3109(00), (Oct. 1967).
5. C. B. Leffert, D. B. Rees and F. E. Jamerson, ONR Annual Report No. 5, Contract Nonr-3109(00), (Oct. 1964). For more detail and a listing of the F36 Reaction Kinetics Code see Ref. 3. For more detail and a listing of the Q00 Ion Generation Rate Code see Ref. 7.
6. D. J. Rose and S. C. Brown, J. Appl. Phys. 23, 1027 (1952); see also Ref. 14.
7. C. B. Leffert, "Ion Generation Rate Theory and Analysis of Experimental Current-Voltage Data", PH-391 (Feb. 1965). This Q00 code and results are also described in Ref. 5 (without the listing). Results were also published in Ref. 8.
8. C. B. Leffert, D. B. Rees and F. E. Jamerson, J. Appl. Phys. 37, 133, (1966).
9. C. L. Chen, Phys. Rev., 135, A627 (1964); A. L. Gilardini and S. C. Brown, Phys. Rev., 105, 31 (1957); R. B. Brode, Revs. Modern Physics, 5, 257, (1933).
10. A. G. Engelhardt and A. V. Phelps, Phys. Rev., 133, A375 (1964).
11. D. R. Bates, A. E. Kingston and R. W. P. McWhirter, Proc. Roy. Soc., A267, 297, 1962 and A270, 155 (1962); also D. R. Bates and A. E. Kingston, Proc. Phys. Soc., 83, 43 (1964).
12. J. C. Slater, Revs. Modern Phys. 18, 441 (1946).

13. D. J. Rose and S. C. Brown, "Methods of Measuring the Properties of Ionized Gases at High Frequencies I. Measurement of Q; II. Measurement of Electric Field; III. Measurement of Discharge Admittance and Electron Density", J.A.P. 23, 711, (1952); J.A.P. 23 719 (1952); J.A.P. 23 1028 (1952).
14. M. A. Heald and C. B. Wharton, Plasma Diagnostics with Microwaves, Wiley (1965).
15. C. G. Montgomery, Technique of Microwave Measurements Part II, p.297, McGraw-Hill (1947).
16. M. Abramowitz and I. A. Stegun, Handbook of Mathematical Functions, p.361, Dover (1965).
17. L. Frommhold and M. A. Biondi, 19th Gaseous Electronics Conference, Atlanta (Oct.1966).
18. H. J. Oskam and V. R. Mittelstadt, Phys. Rev., 132, 1445 (1963).
19. W. Hess, Z. Naturforsch, 20, 451 (1965).
20. J. N. Fox and R. M. Hobson, Phys. Rev. Letters, 17, 161 (July,1966).
21. A. V. Phelps, Phys. Rev., 114, 1011, (1959).
22. F. J. Mehr and M. A. Biondi, 20th Gaseous Electronics Conference, San Francisco, (Oct. 1967).
23. D. R. Bates, Atomic and Molecular Processes, p. 264, Academic Press (1962).

APPENDIX A - ELECTRON DENSITY-TEMPERATURE CODE

CONTENTS

A-I.	INTRODUCTION	A-1
	<u>Flow Diagrams</u>	
	Fig. A-1 Electron Density-Temperature Main Program .	A-2
	Fig. A-2 Electron Temperature Subroutine (TELECT) .	A-3
	<u>Listings for Electron Temperature Subroutine (TELECT)</u> .	
	Table A-I Electron Temperature Subroutine (TELECT)	A-4
	Table A-II Numerical Integration Routine (SIR) . .	A-7
	Table A-III Tabular Function Search (DUMMY)	A-8
	Table A-IV Tabular Function Interpolation (FUNCT) .	A-8
	Table A-V Function Statement for the Generalized Maxwell-Boltzmann Distribution (FUNY) .	A-8
	<u>Listings for Electron Density Subroutine (NONLIN)</u>	
	Table A-VI EVAL Subroutine for Electron Density Subroutine	A-9
	<u>Listings for Electron Density-Temperature Code (CW8)</u>	
	Table A-VII Main Control Program	A-12
	Table A-VIII Block Data Input Statement (at Compile Time) for Collisional Radiative Recom- bination Coefficients $\alpha(n_e, T_e)$	A-17
	Table A-IX Function Sub-Program for Double-Interpo- lation on the Double-Subscripted Array AC22(TE, ZNE)	A-17
	Table A-X Function Statement for Analytic Approximation to C(22)	A-17
	Table A-XI Example of Input (Cards) to Electron Density-Temperature Code	A-18
A-II.	CW8 CODE MINIMUM PRINT-OUTPUT	A-19
	Table A-XII Representative Output from the Electron Density-Temperature Code (CW8)	A-21
A-III.	CW8 CODE MAXIMUM PRINT-OUTPUT; TELECT PRINT-OUTPUT . .	A-32
	Table A-XIII Intermediate Output from CW8 Code; Output from the Electron Temperature Subroutine (TELECT)	A-36

APPENDIX A

ELECTRON DENSITY-TEMPERATURE CODE

A-I. INTRODUCTION

This appendix contains the detail for the Electron Density-Temperature Code (CW8). The flow diagrams for the Electron Density-Temperature Main Program, Fig. A-1, and the Electron Temperature Subroutine (TELECT), Fig. A-2, have been referenced often in the body of the report and are particularly useful for following the logic of the programs. Listings for all of the source-programs for the Electron Temperature subroutine are presented in Tables A-I to A-V. For the Electron Density subroutine only the listing for the source sub-program EVAL is presented in Table A-VI. The balance of this program remains essentially unchanged as reported elsewhere.³ The listings of the source programs for the Main Program of the Electron Density-Temperature Code are presented in Tables A-VII to A-X. A listing of the input cards to this code for an example problem are presented in Table A-XI.

The minimum print-output for the example problem is discussed in section A-II and the output sheets are reproduced in Table A-XII. The intermediate print-output, mainly from the Electron Temperature subroutine for the same example problem, is discussed in section A-III and the output sheets are reproduced in Table A-XIII.

The discussions in sections A-II and A-III contain considerable physics for here we see the magnitude of the quantities which previously could be discussed only in general terms. Also this discussion further points out how the numerical solution was tailored to the physics of our particular plasma problems.

[illegible]

Fig. A-1. Flow diagram for the Electron Density-Temperature Main Program.

FOR ELECTRON TEMPERATURE

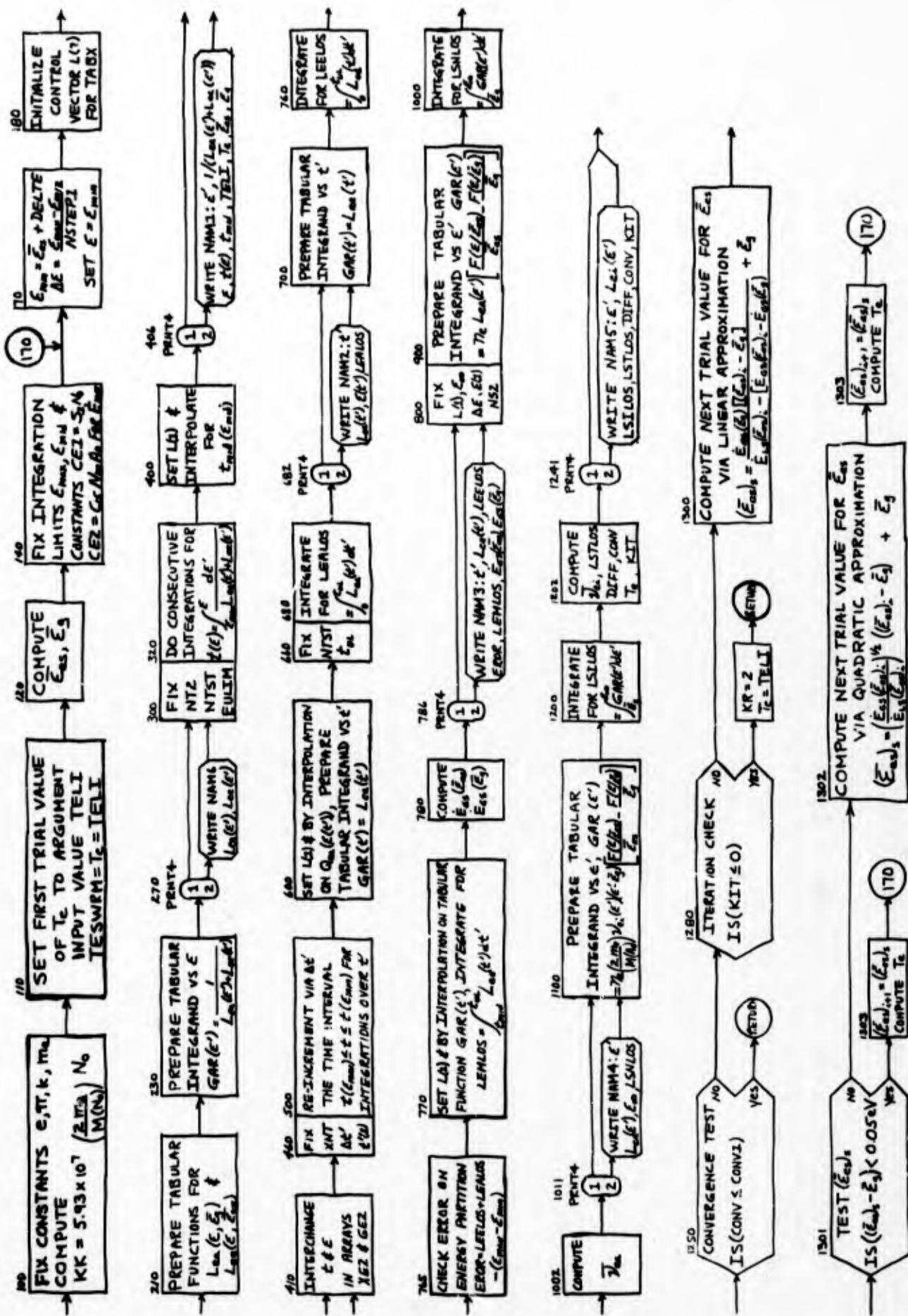


Fig. A-2. Flow diagram for the Electron Temperature Subroutine (TELECT)

TABLE A-I. Electron Temperature Subroutine (TELECT)

```

$IBFTC TEL6CW8 FULIST,REF,LECK,M94,XR7,CC
C****
C
CXXXX THIS IS THE SUBROUTINE TELECT
C****      GIVEN THE ELECTRON DENSITY X(1) AND METASTABLE DENSITY X(5)
C****      AND FIRST GUESS ON ELECTRON SWARM TEMPERATURE (TELI), THE
C****      COMPUTED VALUE OF THE SWARM TEMPERATURE (TESWRM) IS RETURNED
C****      TOGETHER WITH THE AVERAGE ELECTRON COLLISION FREQUENCIES FOR
C****      MOMENTUM TRANSFER WITH THE NEUTRALS(CFRNO) AND THE IONS(CFRAI)
C****      (THESE FREQ. ARE 2*FREQ. FOR LOSS OF FORWARD VELOCITY)
C****
      SUBROUTINE TELECT(X,TELI,TESWRM,CFRNO,CFRAI)
C****
C****
      DIMENSION X(40)
      DIMENSION C(34),K(5),S(3)
      DIMENSION XE(100),QE(100)
      DIMENSION L(7),XAR(101),GAR(101)
      DIMENSION XE2(101),GE2(101),EE1(101)
      DIMENSION XLEA(101),XLEE(101)
      EXTERNAL DUMMY,FUNCT
      COMMON/COM1/X
      COMMON/COM2/NG,AD,C,K,KM,LAM,S,TAUX
      COMMON/COM3/VINC,VIAQ,VMNO,MASNC,MASAG,TGAS,TSWMIG,DELTE,
INSTEP1,NSTEP2,YINF,NQE,XE,QE,KIT,CCNV1,EKM,E16,E21,PRNT4,KR
      COMMON/COM4/L,XAR,GAR
      DOUBLE PRECISION X
      DOUBLE PRECISION NG,AD,C,K,KM,LAM,S,TAUX
      REAL MASNO,MASAG
      REAL KB,ME,KK,LEA,LEE,LEALCS,LEELCS,LEMLOS,LSNLCS,LEI,LSILO,
      ILSTLCS
      INTEGER PRNT4
      NAMELIST/NAM1/XAR,GAR,XE2,GE2,TMID,TELI,TESWRM,ESM,EGS
      NAMELIST/NAM2/XAR,GAR,EE1,LEALCS
      NAMELIST/NAM3/XAR,GAR,LEELCS,EROR,LEMLOS,SOURCE,SREF
      NAMELIST/NAM4/XAR,GAR,EINF,LSNLCS
      NAMELIST/NAM5/XAR,GAR,LSILO,LSLCS,DIFF,CONV,KIT
      NAMELIST/NAM6/XLEA,XLEE
100  C=1.6021E-19
101  PI=3.1415926
102  KB=1.3804E-23
103  ME=9.1084E-31
104  KK=(2.*ME/MASNC)*NG*5.93E7
110  TESWRM=TELI
120  ESM=3.*KB*TELI/(2.*Q)
130  EGS=3.*KB*TGAS/(2.*C)
140  AA=0.3*VINC
141  BB=VMNO-VIAQ
150  IF(AA-BB)151,160,160
151  EMAX=BB
152  EMIC=AA
153  CE1=C(15)*X(5)*AC
154  CE2=S(1)*NO
155  GO TO 170
160  EMAX=AA
161  EMIC=BB

```

```

162 CE1=S(1)*NO
163 CE2=C(15)* X(5)*AO
170 EMIN=ESM+DELTE
171 DELE=(EMAX-EMIN)/FLCAT(NSTEP1)
172 EEL=EMIN
C*** CCNTRCL ARRAY FOR TABX
180 L(1)=NCE
181 L(2)=1
182 L(3)=1
183 L(4)=1
184 L(5)=1
185 L(7)=L(7)
190 NS1=NSTEP1+1
200 DO 250 NE=1,NS1
210 LEA=KK*TABX(XE,CE,EEL,L)*(EEL-EGS)*SQRT(EEL)
220 LEE=(1.54E-5*X(1)/EEL**1.5)*(ALOG(1.25E4*TESWRM**1.5/(X(1))**0.5))
221 *(EEL-ESM)
222 XLEA(NE)=LEA
223 XLEE(NE)=LEE
230 XAR(NE)=EEL
231 GAR(NE)=1./(LEA+LEE)
232 EEL=EEL+DELE
250 CONTINUE
270 GO TO (300,278),PRNT4
278 WRITE (6,279)
279 FORMAT(1H ,62HELETRCN KE LOSS TO NEUTRALS(LEA) AND ELECTRON SWARM(
1LEE) VS KE)
280 WRITE (6,NAM6)
300 NT2=NSTEP1/2+1
302 NIST=-2
303 EUPLIM=EMAX
320 DO 390 NT=1,NT2
330 NTST=NTST+2
340 XE2(NT)=EUPLIM
350 GE2(NT)=-SIR(DUMMY,EMAX,EUPLIM,NTST)
360 EUPLIM= EUPLIM-2.*DELE
390 CONTINUE
400 L(1)=NT2
405 TMID=TABX(XE2,GE2,EMID,L)
406 GO TO (410,407),PRNT4
407 WRITE (6,408)
408 FORMAT(1H ,41HXAR=KE, GAR=1/(LEA+LEE), XE2=KE, GE2=TIME)
409 WRITE (6,NAM1)
410 DO 450 NT=1,NT2
420 SAVEX=XE2(NT)
430 XE2(NT)=GE2(NT)
440 GE2(NT)=SAVEX
450 CONTINUE
460 XNT=NT2-1
470 DELT=XE2(NT2)/XNT
480 TEL=XE2(1)
500 DO 550 NT=1,NT2
510 XAR(NT)=TEL
520 EE1(NT)=TABX(XE2,GE2,TEL,L)
530 TEL=TEL+DELT
550 CONTINUE
560 L(1)=NCE

```

```

600 DO 650 NT=1,NT2
610 EEL=EE1(NT)
620 GAR(NT)=KK*TABX(XE,GE,EEL,L)*(EEL-EGS)*SQRT(EEL)
650 CONTINUE
660 NTST=NSTEP1/2
670 TUPLIM=XAR(NT2)
680 LEALCS=SIR(DUMMY,0,TUPLIM,NTST)
682 GO TO (700,683),PRNT4
683 WRITE (6,684)
684 FORMAT(1H ,81HXAR=TIME, GAR=LEA(T), EEL=KE(T), LEALOS=NEUTRAL LOSS
1FROM MOST ENERGETIC ELECTRONS)
685 WRITE(6,NAM2)
700 DO 750 NT=1,NT2
710 EEL=EE1(NT)
720 GAR(NT)=(1.54E-05*X(1)/EEL**1.5)*(ALOG(1.25E4*TESWRM**1.5/(X(1))**
10.5))*(EEL-ESM)
750 CONTINUE
760 LEELCS=SIR(DUMMY,0,TUPLIM,NTST)
765 EROR=LEELCS+LEALOS-(EMAX-EMIN)
770 L(1)=NT2
775 LEMLCS=SIR(FUNCT,TMID,TUPLIM,NTST)
780 SOURCE=CE1*LEELCS+CE2*LEMLCS
785 SREF=(CE1+CE2)*(ESM-EGS)+SOURCE
786 GO TO (800,787),PRNT4
787 WRITE (6,788)
788 FORMAT(1H ,93HXAR=TIME, GAR=LEE(T), LEELCS=LOSS TO ELECTRON SWARM
1FROM HIGH-E ELECTRONS, LEMLCS=FROM MID-E )
790 WRITE(6,NAM3)
800 L(1)=NCE
820 EINF=YINF*ESM
840 DELE=(EINF-EGS)/FLCAT(NSTEP2)
850 EEL=EGS
860 NS2=NSTEP2+1
900 DO 990 NE=1,NS2
910 LEA=KK*TABX(XE,GE,EEL,L)*(EEL-EGS)*SQRT(EEL)
920 YEL=EEL/ESM
930 FY1=FLNY(YEL)
940 YEL=EEL/EGS
950 FY2=FLNY(YEL)
960 XAR(NE)=EEL
970 GAR(NE)=LEA*(FY1/ESM-FY2/EGS)*X(1)
980 EEL=EEL+DELE
990 CONTINUE
1000 LSNLOS=SIR(DUMMY,EGS,EINF,NSTEP2)
1002 CFRNC=LSNLOS/(X(1)*2.*ME*(ESM-EGS)/MASNO)
1010 EEL=EGS
1011 GO TO (1100,1012),PRNT4
1012 WRITE (6,1013)
1013 FORMAT(1H ,73HXAR=E, GAR=LEA(E)(SWARM TO NEUTRALS), LSNLOS= TOTAL
1SWARM TO NEUTRAL LOSS)
1015 WRITE(6,NAM4)
1100 DO 1190 NE=1,NS2
1110 LE1=(3.86E-6*X(1)/EEL**1.5)*(ALOG(1.25E4*TESWRM**1.5/(X(1))**0.5))
1120 YEL=EEL/ESM
1130 FY1=FLNY(YEL)
1140 YEL=EEL/EGS
1145 FY2=FLNY(YEL)
1150 XAR(NE)=EEL
1155 GAR(NE)=2.*ME/MASAC*(EEL-EGS)*LE1*(FY1/ESM-FY2/EGS)*X(1)
1160 EEL=EEL+DELE
1190 CONTINUE

```



```

1200 LSILCS=SIR(DUMMY,EGS,EINF,NSTEP2)
1202 CFRAI=LSILCS/(X(1)*2.*ME*(ESM-EGS)/MASAO)
1210 LSTLCS=LSNLCS+LSILCS
1220 DIFF=SCURCE-LSTLCS
1230 CCNV= (ABS(DIFF))/SCURCE
1235 TESWRM=2.*ESM*C/(3.*KB)
1240 KIT=KIT-1
1241 GO TO (1250,1242),PRNT4
1242 WRITE (6,1243)
1243 FORMAT(1H ,85HXAR=E, GAR=LEI(E)(SWARM TO IONS), LSILCS=TOTAL SWARM
      LTC ICN LOSS, LSTLCS=LSNLCS+LSILCS)
1245 WRITE(6,NAM5)
1250 IF(CCNV-CCNV1)1400,1400,1280
1280 IF(KIT)1290,1290,1300
1290 KR=2
1291 TESWRM=TELI
1295 GO TO 1400
1300 ESS=(SREF*(ESM-EGS)/(LSTLCS-(SOURCE-SREF)))+EGS
1301 IF(ESS-EGS-0.05)1303,1302,1302
1302 ESS=SQRT(SOURCE/LSTLCS)*(ESM-EGS)+EGS
1303 ESM=ESS
1310 TESWRM=2.*ESM*C/(3.*KB)
1340 GO TO 170
1400 RETURN
      END

```

TABLE A-II. Numerical Integration Routine (SIR)

```

$IBFIC SIRICW8 FULIST,REF,DECK,M94,XR7,DD
C      SIMPSON RULE INTEGRATION
C      XLCLIM,UPLIM ARE LOWER AND UPPER LIMITS,RESP.
C      NSTEP IS NUMBER OF STEPS AND MUST BE EVEN
C      F IS FUNCTION OF ONE INDEPENDENT VARIABLE TO BE
C      INTEGRATED.F MUST BE A FORTRAN DEFINED FUNCTION
C      OR A TABULAR FUNCTION STORED IN ARRAYS XAR,GAR.
C
C      FUNCTION SIR(F,XLCLIM,UPLIM,NSTEF)
C
C
C      SIR=C.0
C      IF(UPLIM-XLCLIM)3,100,3
C      3 XN=NSTEF
C      DEL=(UPLIM-XLCLIM)/XN
C      Y1=F(XLCLIM)
C      5 DO 18 I=1,NSTEF,2
C      X1=I
C      Y2=F(XLCLIM+X1*DEL)
C      10 Y3=F(XLCLIM+(X1+1.00 )*DEL)
C      15 SIR=SIR+Y1+4.0 *Y2+Y3
C      18 Y1=Y3
C      SIR=DEL*SIR/3.0
C      100 RETURN
C      END

```

TABLE A-III. Tabular Function Search (DUMMY)

```

$IBFTC DUMICW8 FULIST,REF,DECK,M94,XR7,DD
FUNCTION DUMMY(ARG)
C****
  DIMENSION XAR(101),GAR(101)
  COMMON/COM1/XAR,GAR
C****
  10 CC 200 I=1,101
    B1=1
    IF(XAR(I+1)-XAR(I))30,200,12
  12 TEST=ABS(XAR(I+1)-XAR(I))/(5.0E(*B1))
    TEST1=XAR(I+1)-XAR(I)
    GO TO 15
  200 CONTINUE
    CC TO 30
  15 CC 5 I=1,101
    IF(ABS(ARG-XAR(I))-TEST) 20,20,25
  25 IF(TEST)26,30,27
  26 IF(ARG-XAR(I))5,20,30
  27 IF(ARG-XAR(I))30,20,5
    5 CONTINUE
  30 DUMMY=ARG
    WRITE(6,101) ARG,XAR(I-1),XAR(I),XAR(I+1)
  101 FORMAT(1H ,4E15.8)
    CALL RLE(C,45HX NOT IN TABLE, VALUE DUMMY(X) NOT RETURNABLE)
    RETURN
  20 DUMMY=GAR(I)
    RETURN
  END

```

TABLE A-IV. Tabular Function Interpolation (FUNCT)

```

$IBFTC FCTICW8 FULIST,REF,DECK,M94,XR7,DD
FUNCTION FUNCT(ARG)
  DIMENSION LA(7),XR2FR(51),XNRFR(51)
  COMMON/COM2/LA,XR2FR,XNRFR
  FUNCT=TABX(XR2FR,XNRFR,ARG,LA)
  I=LA(6)
  GO TO (10,20),I
  10 RETURN
  20 WRITE(6,21) ARG
  21 FORMAT(34F00EXTRAPOLATION OCCURRED WITH ARG= ,E20.8)
    RETURN
  END

```

TABLE A-V. Function Statement for the Generalized Maxwell-Boltzmann Distribution (FUNY)

```

$IBFTC FNYICW8 FULIST,REF,DECK,M94,XR7,DD
FUNCTION FUNY(ARG)
  FUNY=2.073*ARG**0.5*EXP(-1.5*ARG)
  RETURN
  END

```

TABLE A-VI. EVAL Subroutine for Electron Density Subroutine

```

C      EVLICH
      SUBROUTINE EVAL(P,G)
      DOUBLE PRECISION X(40),P(40,41),C(40),LAMSNO
      DOUBLE PRECISION LAM,NO,C(34),AO,S(3),K(5),KM,TAUX,TEM(6)
      COMMON/CCM1/X
      COMMON/COM2/NO,AO,C,K,KM,LAM,S,TAUX
C      EVALUATE FUNCTIONS AND PARTIALS
C      VALUES NEEDED THROUGHOUT
      LAMSNO=LAM*LAM*NO
C      FIRST EQN
      G(1)=X(1)-X(2)-X(3)-X(6)-X(7)-X(8)
      P(1,1) = 1.0
      P(1,2) =-1.0
      P(1,3) =-1.0
      P(1,4) = 0.0
      P(1,5) = 0.0
      P(1,6) =-1.0
      P(1,7) =-1.0
      P(1,8)=-1.0
C      SECOND EQN
      TEM(1)=K(1)/LAMSNO
      TEM(2) = C(4)*NO*1.0D-10*NO
      TEM(3) = C(5)*NO*1.0D-10*AO
      TEM(4) = C(23)*NO*1.0D-10*AC
      TEM(5) = C(24)*AC*1.0D-10*AO
      G(2)=S(1)*NO-TEM(1)*X(2)-X(1)*X(2)*(C(1)
1+C(2)*NO*1.0D-10 + C(3)*X(1)*1.0D-10)
      2-TEM(2)*X(2)-TEM(3)*X(2)-C(6)*AO*X(2)+C(7)*X(5)*X(5)
      3-TEM(4)-TEM(5)
      P(2,1)=-C(1)*X(2)-C(2)*NO*1.0D-10*X(2)-2.0*C(3)*X(1)*1.0D-10*X(2)
      P(2,2)=-TEM(1)-C(1)*X(1)-C(2)*NO*1.0D-10*X(1)-C(3)*X(1)*1.0D-10*X(
11)-TEM(2)-TEM(3)-C(6)*AO
      2-TEM(4)-TEM(5)
      P(2,3) = 0.0
      P(2,4) = 0.0
      P(2,5)=2.0*C(7)*X(5)
      P(2,6) = 0.0
      P(2,7) = 0.0
      P(2,8) = 0.0
C      THIRD EQN
      TEM(1) =(C(1)+C(2)*NO*1.0D-10)*C(8)
      TEM(2) = C(3)*C(8)*X(1)*1.0D-10
      TEM(3) = TEM(1)+TEM(2)
      G(3)=S(2)*NO+TEM(3)*X(1)*X(2)-X(4)/TAUX-
1C(9)*NO*X(4)
      P(3,1)=X(2)*TEM(1)
      1+2.0*TEM(2)*X(2)
      P(3,2)=X(1)*TEM(3)
      P(3,3) = 0.0
      P(3,4)=-1.0/TAUX-C(9)*NO
      P(3,5) = 0.0
      P(3,6) = 0.0
      P(3,7) = 0.0
      P(3,8) = 0.0
C      FOURTH EQN
      TEM(1)=K(1)/LAMSNO
      TEM(2) =C(10)*(C(1)+C(2)*NO*1.0D-10)

```


TEM(3) = C(14)*NC*1.0D-10*NO
 TEM(4) = C(10)*C(3)*X(1)*1.0D-10
 TEM(5) = TEM(2)+TEM(4)
 G(4) = S(3)*NC-TEM(1)*X(5)+TEM(5)*X(1)*X(2)+C(11)*C(16)*X(3)*X(1)
 1-C(12)*X(5)*X(5)-C(13)*NC*X(5)-C(15)*AC*X(5)-TEM(3)*X(5)
 2-C(25)*AC*X(5)
 P(4,1) = TEM(2)*X(2)+C(11)*C(16)*X(3)
 1+2.0*TEM(4)*X(2)
 P(4,2) = TEM(5)*X(1)
 P(4,3) = C(11)*C(16)*X(1)
 P(4,4) = 0.0
 P(4,5) = -TEM(1)-2.0*C(12)*X(5)-C(13)*NC-C(15)*AC-TEM(3)-C(25)*AC
 P(4,6) = 0.0
 P(4,7) = 0.0
 P(4,8) = 0.0

C

FIFTH EQN
 TEM(1) = K(2)/LAMSNO
 TEM(2) = C(4)*NO*1.0D-10*NC
 G(5) = -TEM(1)*X(3)-C(16)*X(1)*X(3)+TEM(2)*X(2)-C(17)*AC*X(3)
 1+C(9)*NO*X(4)-C(26)*AC*X(3)
 P(5,1) = -C(16)*X(3)
 P(5,2) = TEM(2)
 P(5,3) = -TEM(1)-C(16)*X(1)-C(17)*AC-C(26)*AC
 P(5,4) = C(9)*NO
 P(5,5) = 0.0
 P(5,6) = 0.0
 P(5,7) = 0.0
 P(5,8) = 0.0

C

SIXTH EQN
 TEM(1) = K(3)/LAMSNO
 TEM(2) = C(18)+C(19)*NC*1.0D-10+C(22)*X(1)*1.0D-10
 TEM(3) = C(20)*AC*1.0D-10*NC
 TEM(4) = C(27)*NC*1.0D-10*NO
 TEM(5) = C(28)*AC*1.0D-10*NO
 TEM(6) = C(32)*NC*1.0D-10*NC
 G(6) = -TEM(1)*X(6)-X(1)*X(6)*TEM(2)-TEM(3)*X(5)+C(6)*AC*X(2)+C(17)*
 1AC*X(3)+C(15)*AC*X(5)
 2-TEM(4)*X(6)-TEM(5)*X(6)+C(31)*NC*X(8)+TEM(6)*X(8)
 P(6,1) = -X(6)*(C(18)+C(19)*NC*1.0D-10+2.0*C(22)*X(1)*1.0D-10)
 P(6,2) = C(6)*AC
 P(6,3) = C(17)*AC
 P(6,4) = 0.0
 P(6,5) = C(15)*AC
 P(6,6) = -TEM(1)-TEM(2)*X(1)-TEM(3)-TEM(4)-TEM(5)
 P(6,7) = 0.0
 P(6,8) = C(31)+TEM(6)

C

SEVENTH EQN
 TEM(1) = K(4)/LAMSNO
 TEM(2) = C(20)*AC*1.0D-10*NC
 TEM(3) = C(34)*AC*NC*1.0D-10
 G(7) = -TEM(1)*X(7)-C(21)*X(1)*X(7)+TEM(2)*X(6)
 1-C(29)*NC*X(7)+C(33)*AC*X(8)+TEM(3)*X(8)
 P(7,1) = -C(21)*X(7)
 P(7,2) = 0.0
 P(7,3) = 0.0
 P(7,4) = 0.0
 P(7,5) = 0.0

```

P(7,6) = TEM(2)
P(7,7) = -TEM(1) - C(21)*X(1) - C(29)*NC
P(7,8) = C(33)*AC + TEM(3)
C
EIGHTH FCN
TEM(1) = K(5)/LAMSNC
TEM(2) = C(23)*AC*NC*1.0D-10
TEM(3) = C(27)*ND*NC*1.0D-10 + C(28)*AC*NC*1.0D-10
TEM(4) = C(31)*AC + C(33)*AC
TEM(5) = C(32)*ND*NC*1.0D-10 + C(34)*AC*ND*1.0D-10
G(8) = -TEM(1)*X(8) - C(30)*X(1)*X(8) + TEM(2)*X(2) + TEM(3)*X(6)
1 + C(26)*AC*X(3) + C(29)*NC*X(7) - TEM(4)*X(8) - TEM(5)*X(8)
2 + C(25)*AC*X(5)
P(8,1) = -C(30)*X(8)
P(8,2) = TEM(2)
P(8,3) = C(26)*AC
P(8,4) = 0.0
P(8,5) = C(25)*AC
P(8,6) = TEM(3)
P(8,7) = C(29)*NC
P(8,8) = -TEM(1) - C(30)*X(1) - TEM(4) - TEM(5)
RETURN
END

```

TABLE A-VII. Electron Density-Temperature Code (CW8)
Main Control Program

```

SIBFTC MNL9CW8 FULIST,REF,DECK,M94,XR7,DD
C****
C****
C      THIS IS THE MAIN PROGRAM FOR THE ELECTRON DENSITY-TEMPERATURE CODE
C****
C****      REACTION KINETICS SUBROUTINE          = NONLIN
C****      ELECTRON SWARM TEMPERATURE SUBROUTINE = TELECT
C****

DIMENSION X(40),TITLE(12),SUBTIT(12)
DIMENSION C(34),K(5),S(3)
DIMENSION XE(100),QE(100)
DIMENSION KS(5),K1(5)
DIMENSION L(7),XAK(101),GAR(101)
DIMENSION R2(50),FRR2(50),XSR(50),XNR(50),XTR(50),XCFND(50),XCFAI(
150)
DIMENSION TELIA(6),ZNEA(7),ALFA(7,6)
COMMON/CCM1/X
COMMON/CCM2/NU,AG,C,K,KM,LAM,S,TAUX
COMMON/CCM3/VIND,VIAL,VMNC,MASNC,MASAC,TGAS,TSWMIG,DELTE,
1NSTEP1,NSTEP2,YINF,NQE,XE,QE,KIT,CONV1,EKM,E16,E21,PRNT4,KR
COMMON/CCM4/L,XAK,GAR
COMMON/CCM5/TELIA,ZNEA,ALFA
DOUBLE PRECISION X,EPS
DOUBLE PRECISION NU,AG,C,K,KM,LAM,S,TAUX
DOUBLE PRECISION KS,KMS,K1,KM1,C3S,C16S,C21S,C22S
REAL MASNU,MASAC
INTEGER PRNT1,PRNT2,PRNT3,PRNT4,RTN
NAMELIST/GLESS/X,EPS,PRNT1,PRNT2,PRNT3,PRNT4,NX,NQE,NSR
NAMELIST/INPLT/NU,AG,C,K,KM,LAM,S,TAUX,
1VIND,VIAL,VMNC,MASNC,MASAC,
2TGAS,TSWMIG,DELTE,NSTEP1,NSTEP2,
3YINF,KIT,NITS,DIFCLN,PRNTIC,CENV1,
4EKM,E16,E21,L,
5MRPT,MCRE
NAMELIST/MAP1/K,KM,C,AL,NL,CAC22,NR2,S
NAMELIST/MAM2/KIT,TESWRP,TELI,DIFI,PRNTIE,NIT
NAMELIST/MAM3/NR2,TESWRM,TELI,DIFT,PRNTE,KIT,CFRAL,CFRAI
NAMELIST/MAM4/C22LUS,C2CLUS,DIFLUS,DIFFKN
C****
C****      PRNT1 AND PRNT2 (=1) = NO   FOR INTERMEDIATE KINETICS OUTPUT
C****              (=2) = YES   FOR INTERMEDIATE KINETICS OUTPUT
C****      PRNT3(1=NO,2=YES) FOR INTERMEDIATE MAIN OUTPUT
C****      PRNT4(1=NO,2=YES) FOR INTERMEDIATE TELECT OUTPUT
C****      NX = NO OF KINETICS EQUATIONS
C****      NQE = NO OF X-SECTION INPLT POINTS IN XE-QE ARRAY
C****
C****      MCRE=2 SIGNIFIES END OF PROBLEM
C****      MCRE=1 SIGNIFIES REPEAT - CHANGING ONLY NEW INPUT DATA
C****              ONE A-RECORD CARD (SUBTIT) MUST PRECEED EACH SUB-INPUT
C****              LAST SUB-INPLT SHOULD SET MCRE=2
C****
C**** READ AND WRITE TITLE OF PROBLEM
10 READ(5,11)TITLE
11 FORMAT(12A6)
12 READ(5,13)SUBTIT
13 FORMAT(12A6)
15 WRITE(6,16)TITLE,SUBTIT

```

```

16 FORMAT(1F1,20X,12A6/21X,12A6)
C**** READ AND WRITE GUESS (OF DENSITY OF PLASMA SPECIES)
20 READ(5,GUESS)
25 WRITE(6,GUESS)
C****
C**** WRITE COLLISIONAL RADIATIVE RECOMBINATION RATES (BATES, ET AL)
WRITE(6,26)
26 FORMAT(1FC,78F INPUT FOR COLLISIONAL RADIATIVE RATES ALFA(I,J) FOR
11E=TELIA(J) AND NE=ZNEA(I))
WRITE(6,27)(TELIA(J),J=1,6)
27 FORMAT(1FC,5X,6E10.2)
WRITE(6,28)(ZNEA(I),(ALFA(I,J),J=1,6),I=1,7)
28 FORMAT(7E10.2)
C**** CONVERT ALFA(I,J) TO CORRECTION FACTOR TO ANALYTIC C(22)
DO 29 I=1,7
ZNE=ZNEA(I)
DO 29 J=1,6
TEA=TELIA(J)
ALFA(I,J)=(ALFA(I,J)*1.0E10/ZNE)/FC22(TEA)
29 CONTINUE
WRITE(6,27)(TELIA(J),J=1,6)
WRITE(6,28)(ZNEA(I),(ALFA(I,J),J=1,6),I=1,7)
C**** READ AND WRITE CROSS SECTIONS
30 READ(5,31)(XE(N),QE(N),N=1,NCE)
31 FORMAT(6E12.6)
40 WRITE(6,41)(XE(N),QE(N),N=1,NCE)
41 FORMAT(1FC,54H INPUT FOR NEUTRAL SCATTERING CROSS SECTION XE(I),QE(
11)/(2E20.8))
C**** READ AND WRITE SOURCE DISTRIBUTION FOR COMPUTATIONS ALONG RADIUS
C**** WHEN NSF .GR. C
42 IF (NSR) 50,50,43
43 READ(5,44)(R2(N),FRR2(N),N=1,NSR)
44 FORMAT(6E12.6)
45 WRITE(6,46)(R2(N),FRR2(N),N=1,NSR)
46 FORMAT(1FC,56H INPUT FOR SOURCE DISTRIBUTION ALONG RADIUS R2(I),FRR
4712(I)/(2E20.8))
50 NCFE=1
C****
C**** READ AND WRITE INPUT FOR KINETICS SUBROUTINE (NONLIN)
C**** READ AND WRITE INPUT FOR TEMPERATURE SUBROUTINE (TELECT)
C****
60 READ(5,INPUT)
70 WRITE(6,INPUT)
71 NCREA=2
72 N11=N11S
73 NR2=1
74 LR=NSR
76 IF(1SWMIG) 77,77,80
77 NCREA=1
78 1SWMIG=1ESWRFM
80 IF(1SWMIG-1GAS) 90,90,120
90 1SWMIG=1GAS+100.0
92 GO TO 120
C**** SAVE KINETICS INPUT
120 KMS = KM
121 CBS = C(3)
122 C16S = C(16)

```

```

123 C21S=C(21)
124 C22S=C(22)
125 GO TO (130,126),MCREA
126 S1S=S(1)
127 S3S=S(3)
130 DO 139 N1=1,5
131 KS(NT)=K(NT)
139 CONTINUE
C**** ADJUST DIFFUSION COEFFICIENTS FOR TGAS
140 KM1=KMS*(TGAS/300.)**EKM
150 DO 159 N1=1,5
151 K1(NT)=KS(NT)*(TGAS/300.)
159 CONTINUE
C**** SET TRIAL VALUE OF ELECTRON SWARM TEMPERATURE (TELI) TO
C**** INPUT FIRST GUESS VALUE (TSWM1G)
160 TELI=TSWM1G
161 KITS=K11
C****
C LUTER ITERATION ON ELECTRON SWARM TEMPERATURE
C**** CALLS SUBROUTINE NONLIN FOR ELECTRON AND METASTABLE DENSITY
C**** WITH INPUT ADJUSTED FOR TRIAL VALUE OF TELI
C**** CALLS SUBROUTINE TELECT FOR ELECTRON SWARM TEMPERATURE
C**** FOR INPUT OF ELECTRON DENSITY AND SOURCE RATE
C**** ITERATION COUNT LIMIT IS NIT
C****
C**** ADJUST INPUT TO NONLIN FOR TELI
169 GO TO (200,170),MCREA
170 KM=KM1
171 DO 177 N1=1,5
175 K(NT)=K1(NT)*(1.+TELI/TGAS)/2.
177 CONTINUE
179 CAC22=1.0
180 C(22)=FC22(TELI)*CAC22
181 C(3)=C(22)
182 C(16)=C16S*(300./TELI)**E16
183 C(21)=C21S*(300./TELI)**E21
185 GO TO (195,186),PRNT3
186 WRITE (6,187)TELI
187 FORMAT(1F0,56HREACTION RATE COEFFICIENTS ADJUSTED FOR TESWRM = TEL
11 = ,E15.7,26H (C22 FROM ANALYTIC EXP.))
190 WRITE(6,MAM1)
195 CALL NCALIN(INX,X,EPS,PRNT1,RTN)
200 KM=KM1
201 KR=1
202 DO 207 N1=1,5
205 K(NT)=K1(NT)*(1.+TELI/TGAS)/2.
207 CONTINUE
208 XEL=X(1)
209 CAC22=AC22(TELI,XEL)
210 C(22)=FC22(TELI)*CAC22
211 C(3)=C(22)
212 C(16)=C16S*(300./TELI)**E16
213 C(21)=C21S*(300./TELI)**E21
215 GO TO (230,216),PRNT3
216 WRITE (6,217)TELI
217 FORMAT(1F0,56HREACTION RATE COEFFICIENTS ADJUSTED FOR TESWRM = TEL
11 = ,E15.7,23H (C22 FROM ALFA TABLE))

```

```

220 WRITE(6,MAM1)
230 CALL NCNLIN(X,X,EPS,PRNT1,RTN)
240 CALL TELECT(X,TELI,TESWRM,CFRNO,CFRA1)
245 GO TO (250,475),KR
250 DIFT=TESWRM-TELI
251 ADIFT=AES(DIFT)
252 PRNTE=ALIFT/TESWRM
254 NNIT=NIIS-NIT+1
255 GO TO (270,256),PRNT3
256 WRITE (6,257) NNIT
257 FORMAT(1FC,36F+VALUES FOR TRIAL NUMBER ON TESWRM = ,I4)
260 WRITE(6,MAM2)
270 NIT=NIT-1
280 IF(ADIFT-DIFCON) 400,400,250
290 IF(PRNTE-PRNTC) 400,400,300
300 IF(NIT) 450,450,310
310 TELI=TESWRM
320 GO TO 200
C****
400 WRITE(6,401)NNIT
401 FORMAT(1FC,44F+ITERATION ON TESWRM COMPLETE ON TRIAL NO. = ,I4)
402 WRITE(6,MAM3)
404 TELI=TESWRM
405 KM=KM1
406 DO 408 NT=1,5
407 K(NT)=K1(NT)*(1.+TELI/TGAS)/2.
408 CONTINUE
409 XEL=X(1)
410 CAC22=AC22(TELI,XEL)
411 C(22)=FC22(TELI)*CAC22
412 C(3)=C(22)
413 C(16)=C16S*(300./TELI)**E16
414 C(21)=C21S*(300./TELI)**E21
418 WRITE(6,MAM1)
420 CALL NCNLIN(X,X,EPS,PRNT2,RTN)
421 C22LOS=X(1)*X(6)*C(22)*X(1)*1.0D-10
422 C2CLOS=C(20)*AC*1.0D-10*NL*X(6)
423 DIFLOS=(F(3)/(LAM*LAM*NL))*X(6)
424 DIFFRN=DIFLOS/(DIFLOS+C22LOS+C2CLOS)
425 WRITE(6,MAM4)
430 GO TO 500
450 WRITE(6,460)
460 FORMAT(1FC,31F+ITERATION COUNT EXCEEDED ON NIT)
470 GO TO 500
475 WRITE(6,476)
476 FORMAT(1FC,50F+ITERATION COUNT EXCEEDED ON KIT, GO TO NEW PROBLEM)
477 GO TO 500
C**** REINSTATE INPLT
500 KM=KMS
510 C(3)=C3S
520 C(16)=C16S
530 C(21)=C21S
540 C(22)=C22S
542 KIT=KIT1
550 DO 559 NT=1,5
552 K(NT)=KS(NT)
559 CONTINUE

```

```

560 IF(LR-1)600,562,562
562 XSR(NR2)=S(1)
564 XNR(NR2)=X(1)
566 XTR(NR2)=TESWRM
568 XCFNO(NR2)=CFRNO
570 XCFAI(NR2)=CFRAI
571 NR2=NR2+1
572 LR=LR-1
573 IF(LR-1)565,574,574
574 S(1)=S1S*FRF2(NR2)
575 S(3)=S3S*FRF2(NR2)
576 TEL1=TESWRM
577 NIT=NITS
580 NR22=NR2-1
581 WRITE(6,16)TITLE,SUBTIT
582 WRITE(6,583)NR22
583 FORMAT(1F0,12HSCOLUTION FOR,13,31H INCREMENTS FROM CENTER OF TUBE)
584 GO TO 200
585 WRITE(6,16)TITLE,SUBTIT
586 WRITE(6,588)
588 FORMAT(1F0,45HSUMMARY OF DISTRIBUTIONS ALONG RADIUS OF TUBE)
590 WRITE(6,591)
591 FORMAT(1F0,2X, 5HRADIALS,CP,11X,9HSOURCE/NO,11X,10HEL-DENSITY,10X,
111HEL-TEMP.,0K,6X,17HAV.CCL.FR.-NEUTS.,3X,15HAV.CCL.FR.-1CNS)
592 WRITE(6,593) (R2(N),XSR(N),XNR(N),XTR(N),XCFNO(N),XCFAI(N),N=1,NSR
1)
593 FORMAT(6E20.8)
594 WRITE(7,595)NSR,XSR(1),XCFNO(1),XCFAI(1),(R2(N),XNR(N),XTR(N),N=1,
1NSR)
595 FORMAT(13/(6E12.5))
596 GO TO (599,597),MRPT
597 S(1)=S1S
598 S(3)=S3S
599 GO TO 500
600 GO TO(610,10),MCRE
610 READ(5,611)SUBTIT
611 FORMAT(12A6)
615 WRITE(6,16)TITLE,SUBTIT
620 READ(5,621)GLESS
622 WRITE(6,623)GLESS
630 GO TO 60
END

```

TABLE A-VIII. Block Data Input Statement (at Compile Time) for Collisional Radiative Recombination Coefficients $\alpha(n_e T_e)$.

```

$IBFTC BDT2CW8 FULIST,REF,DECK,M94,XR7,DD
BLOCK DATA
DIMENSION TELIA(6),ZNEA(7),ALFA(7,6)
COMMON/COM5/TELIA,ZNEA,ALFA
DATA(TELIA(J),J=1,6)/250.,500.,1000.,2000.,4000.,8000./
DATA(ZNEA(I),(ALFA(I,J),J=1,6),I=1,7)/1.0E+8,7.8E-11,1.2E-11,3.2E-
112,1.3E-12,6.4E-13,3.3E-13,1.0E+9,3.8E-10,3.3E-11,6.0E-12,1.8E-12,
27.5E-13,3.6E-13,1.0E+10,2.8E-9,1.5E-10,1.6E-11,3.1E-12,9.8E-13,4.1
3E-13,1.0E+11,2.7E-8,1.0E-9,6.1E-11,7.1E-12,1.6E-12,5.1E-13,1.0E+12
4,2.6E-7,9.0E-9,3.6E-10,2.4E-11,3.2E-12,7.4E-13,1.0E+13,2.6E-6,8.8E
5-8,3.0E-9,1.2E-10,9.3E-12,1.3E-12,1.0E+14,2.6E-5,8.8E-7,2.9E-8,9.4
6E-10,4.0E-11,3.2E-12/
END

```

TABLE A-IX. Function Sub-program for Double-interpolation on the Double-subscripted Array AC 22 (TE,ZNE).

```

$IBFTC A221CW8 FULIST,REF,DECK,M94,XR7,DD
FUNCTION AC22(TE,ZNE)
DIMENSION LA(9),TELIA(6),ZNEA(7),ALFA(7,6)
COMMON/COM5/TELIA,ZNEA,ALFA
LA(1)=6
LA(2)=7
LA(3)=0
LA(4)=1
LA(5)=1
LA(7)=2
LA(8)=2
LA(9)=7
AC22=TABXZ(TELIA,ALFA,ZNEA,TE,ZNE,LA)
I=LA(6)
GO TO (10,20,20,20),I
10 RETURN
20 WRITE(6,21) AC22,I
21 FORMAT(1H1,35HEXTRAPOLATION WITH AC22 AND LA(6) =,E20.8,15)
RETURN
END

```

TABLE A-X. Function Statement for Analytic Approximation to C(22).

```

$IBFTC C222CW8 FULIST,REF,DECK,M94,XR7,DD
FUNCTION FC22(ARG)
FC22=2.6CE-09*(250./ARG)**5. (Note: Scaling factor of  $10^{-10}$  in code.)
RETURN
END

```


TABLE A-XI. Example of Input (Cards) to Electron Density-Temperature Code
 Gas: Neon-Argon, Ar/Ne = 1.0×10^{-4}
 Pressure: $p = 90$ torr, $N_0 = 2.9 \times 10^{18}$ sec $^{-1}$
 Reactor Power: 1.0 MW, $\phi = 0.72 \times 10^{13}$ cm $^{-2}$ sec $^{-1}$

```

SDATA
  RUN 109.7          ELECTRON DENS. + TEMP.  M-WAVE CAV-14  RUN 64
  RUN 109.7  S=1.300E-3*NO  TGAS=405 OK  TSWM1G=600 OK
  $GUESS X(1)=1.0D12,1.0D10,2.0D10,2.0D03,2.0D11,1.0D12,1.0D09,33*0.0,
  EPS=1.0D-6,PRNT1=1, PRNT2=1, PRNT3=2, PRNT4=1, NX=8, NQE=17, NSR=11 $
  0.260 E-01  0.456 E-16  0.400 E-01  0.541 E-16  0.600 E-01  0.639 E-16
  0.800 E-01  0.721 E-16  0.150 E-00  0.880 E-16  0.200 E-00  0.960 E-16
  0.300 E-00  1.100 E-16  0.400 E-00  1.200 E-16  0.490 E-00  1.270 E-16
  0.810 E-00  1.480 E-16  1.000 E-00  1.550 E-16  2.000 E-00  1.780 E-16
  3.000 E-00  1.890 E-16  4.000 E-00  1.960 E-16  5.000 E-00  2.02 E-16
  6.250 E-00  2.060 E-16  6.760 E-00  2.090 E-16
  1.00 E-03  1.0000E 0  0.1145E 0  0.9955E 0  0.2280E 0  0.9818E 0
  0.3415E 0  0.9574E 0  0.4550E 0  0.9194E 0  0.5685E 0  0.8634E 0
  0.6820E 0  0.7837E 0  0.7955E 0  0.6744E 0  0.9090E 0  0.5371E 0
  1.0225E 0  0.3990E 0  1.1360E 0  0.2809E 0
  $INPUT  LAM=2.016D-01, TAUX=5.00D-08, KM=5.50D18,
  K=5.70D18,9.10D18,1.00D19,9.50D18,C.00D00,
  S=1.300D-03,0.000D-03,0.605D-03,
  C=3.20D-12,2.70D-20,1.08D-09,5.80D-22,5.00D-22,4.00D-13,8.00D-10,
  1.00D-01,8.00D-11,1.00D-01,5.00D-01,8.00D-10,1.84D-15,5.00D-24,
  1.80D-11,2.20D-07,4.00D-13,4.00D-12,2.70D-20,2.50D-21,6.70D-07,
  1.08D-09,12*0.0,
  NO=2.90D18, AO=2.90D14,
  VINO=21.56, VMNO=16.68, VIAO=15.76, MASNO=3.371E-26, MASA0=6.671E-26,
  TGAS=405.0, TSWM1G=600.0, DELTE=0.01, NSTEP1= 40, NSTEP2= 40,
  YINF=12.0 , KIT=10 ,NITS=10 ,DIFCON= 5.0, PRCNTC=0.05, CONV1=0.05,
  EKM=0.73 , E16=0.333, E21=1.50 , L(1)=0.0,0.0,0.0,0.2, MRPT=1, MORE=1 $
  RUN 109.7-REPEAT LAST POINT ABOVE (NR2=11) WITH FULL PRINT OUTPUT
  $GUESS  PRNT1=2, PRNT2=2, PRNT3=2, PRNT4=2, NSR=0 $
  $INPUT  TSWM1G=0, MRPT=2, MORE=2 $

```

A-II. CW8 MINIMUM PRINT-OUTPUT

An example of the input data (cards) to the Electron Density-Temperature Code is given in Table A-XI, and an example of the printed output (from input in Table A-XI) is given in Table A-XII for minimum printed output (except PRNT 3=2) and in Table A-XIII for complete printed output. The first 3 pages of Table A-XII show the printed record of the input data to be used by the Electron Density subroutine, the Electron Temperature subroutine and the Main Control program.

Under the NAMELIST-input GUESS in Table A-XII, the entries X,EPS,PRNT1, PRNT2 and NX have been discussed in section IIC.2. PRNT3 is the switch (1=No,2=Yes) for intermediate print output from the Main Control program and PRNT4 serves the same function for the Electron Temperature subroutine (TELECT). Bypassing "NQE" and "NSR" for the moment, the first ALFA(I,J)-array in Table A-XII is the Bates, Kingston and McWhirter cross sections¹¹ discussed in section IID.2 and the second ALFA(I,J)-array is the normalized values according to Eq.(35). Now, NQE is the number of elastic scattering cross section values to be read from cards into the XE-,QE-arrays at the top of the second page of Table A-XII and NSR is the number of values of (fractional) ion source rate along the cavity radius to be read into the R2-, FRR2-arrays in Table A-XII. Notice from the last entry in the FRR2-array in Table A-XII, that the ion generation rate at the cavity cylindrical wall is 28.1% of the ion generation rate at the center of the cavity. From the NAMELIST INPUT for the Electron Density subroutine input in Table A-XII, the ion generation rate at the center of the cavity for this problem was $S^+(r=0)=S_1 N_0 = 3.77 \times 10^{15} \text{ cm}^{-3} \text{ sec}^{-1}$.

Table A-XII (page A-23) gives mainly the input to the Electron Temperature subroutine. These items are defined in the "LIST OF SYMBOLS" at the beginning of the report and many are mentioned in the discussion in section A-III for the intermediate output in Table A-XIII.

Table A-XII (page A-24) shows the input and (minimum) output from the Electron Density subroutine (NONLIN) for two calls; the first with C(22) from Eq.(34) and the second with C(22) from Eq.(35). The output array X(I) of the number densities (cm^{-3}) of the various plasma species have been shifted to the right of the page and these are identified in Table A-XII (page A-27) for the final values. The (minimum) output from the first call

to the Electron Temperature subroutine (TELECT) is shown at the top of Table A-XII (page A-25). This first pass required $(10-5=5)$ iterations to converge within 5% ($CONV1=0.05$) on an electron swarm temperature ($TEWSRM \approx 921^\circ\text{C}$) compatible with the input value of the electron density $n_e \approx 6.6 \times 10^{11} \text{ cm}^{-3}$). The returned value of the electron swarm temperature ($TESWRM$) did not meet the convergence criterion ($PRCNTC=0.05$) for agreement with the input value $TELI$, that is $PRCNTE = 0.348$ was not less than $PRCNTC$, so another call was made to NONLIN with $TELI = 921^\circ\text{C}$.

These alternate calls to NONLIN and TELECT subroutines continued until after the third call to TELECT, $PRCNTE \approx 0.02 < 0.05$. The output from iteration 2 has been deleted but the output from the last (3) iteration on TELECT is presented in Table A-XII (page A-26).

A final call was then made to NONLIN to obtain the plasma densities for the converged value of the electron swarm temperature (804.5°C). This output is given in Table A-XII (page A-27) and the final solution of (n_e, T_e) for the center of the microwave cavity was (804.5°C , $9.90 \times 10^{11} \text{ cm}^{-3}$).

This process was repeated for each of the $NSR=11$ points along the mid-height radius of the microwave cavity (along which only the source S was changing). The output from these intermediate points has been deleted except for the last radial point (at the outside wall) which is shown in Table A-XII (pages A-28 to A-30). This code was programmed to use the converged values from the last problem as the first-guess values to the next problem with the switch $MORE=1$. The succeeding problems along the radius, therefore, converged much faster than the first problem.

Finally, the print out of a summary of the pertinent output data from each problem (along the radius) is shown in Table A-XII (page A-31).^{*} Part of this data is also punched on cards for input to the next code for the Resonance Frequency Shift of the cavity. The data from these cards are printed out in Table B-3.

^{*}The values vary step-wise along r since the convergence criterion on T_e was modest ($PRCNTC=0.05$).

REACTION RATE COEFFICIENTS ADJUSTED FOR TEMPERATURE = TEL1 = 0.6000000E+03 (C22 FROM ANALYTIC EXP.)

K	=	0.95474555555555940 19,	0.15242500000000000 20,	0.16749999999999999 20,
		0.15912500000000000 20,	0.00000000000000000 -38,	

[illegible]

$\Delta G = -0.2965 \text{ kcal/mol} \approx -1.24 \text{ kJ/mol}$

CAC22 = 3.1000000E 01.

$$= 0.13300000$$

ENC

SMAN I

0-1679999999 2J.

= J. 315555555590-11.

0.270000000000000000-19.
0.4595959595959595980-21.
0.595959595959595970-01.
0.50000000000000000000
0.495999999999999999-23.
0.399599999999999999-12.
0.2499999999999999990-20.
0.000000000000000000-38.

0 = C.29CCCCCCCCCCCCC 15.

AC22 = 2.12100261E 01.

0.13000000000000002

C.6145999999999999-03.

A-24

VALUES FOR TRIAL NUMBER ON TESKMP = 1

SMAP2

KIT = 5.
TESKMP = 0.92084454E 03.
TELI = 0.00000000E 03.
DIFT = 0.32084454E 03.
PRCNLE = 0.34842450E 00.
NIT = 10.
\$ END

REACTION RATE COEFFICIENTS ADJUSTED FOR TESKMP = TELI = 0.9208449E 03 (C72 FROM ALFA TABLE)

SMAP1

K = 0.1259552693176269D 20.
0.2759254486627115D 20.
KM = 0.6847054751854473D 19.
C = 0.31555555555555999D 11.
0.57555555555555999D 21.
0.75555555555555999D 09.
0.95555555555555999D 01.
0.13555555555555999D 14.
0.15142626666666649D 06.
0.2700000000000000D 19.
0.6235332246080575D 11.
0.0000000000000000D 38.
0.0000000000000000D 38.
0.0000000000000000D 38.
0.0000000000000000D 38.
0.2209741566975910D 20.
0.2010864825948079D 20.
0.0000000000000000D 38.
0.2700000000000000D 19.
0.4599999999999999D 21.
0.9999999999999999D 01.
0.5000000000000000D 00.
0.4599999999999999D 23.
0.3999999999999999D 12.
0.2499999999999999D 20.
0.0000000000000000D 38.
0.0000000000000000D 38.
0.0000000000000000D 38.
0.0000000000000000D 38.
0.6235332246080575D 11.
0.3999999999999999D 10.
0.7999999999999999D 09.
0.1800000000000000D 10.
0.3999999999999999D 11.
0.1245882033742964D 06.
0.0000000000000000D 38.
0.0000000000000000D 38.
0.0000000000000000D 38.
0.0000000000000000D 38.
0.0000000000000000D 38.
0.0000000000000000D 38.
ITERATIONS 9 AND 10 ARE IDENTICAL INDICATING A CYCLIC CONDITION.
THE BEST RESULTS SO FAR ARE GIVEN BELOW.

AU = 0.2900000000000000D 15.
NU = 0.2900000000000000D 19.
CAC22 = 0.16255034E 01.
NR2 = 1.
S = 0.1300000000000000D 02.
\$ END

0.6049999999999999D 03.

NOTE: The output from iteration 2 was deleted to show the output from the last iteration (3) on this first radial point (NR2=1), where one convergence criteria was satisfied, that is $\Delta T_e = \text{DIFT} \approx 16^\circ\text{C} \neq \text{DIFCON} = 5.0^\circ\text{C}$ but $\left| \frac{\Delta T_e}{T_e} \right| \text{PRONTC} \approx 0.02 \leq \text{PRONTC} = 0.05$.

ITERATIONS 7 AND 8 ARE IDENTICAL INDICATING A CYCLIC CONDITION.
THE BEST RESULTS SO FAR ARE GIVEN BELOW.

C.98762609E 12
C.78063145E 10
J.24631765E 11
C.30527491E 04
C.24351555E 12
C.53390034E 12
C.12875765E 10
C.CCCCCC00E-38

VALUES FOR TRIAL NUMBER CN TESWPM = 3

SWAP2
KIT = 0.
TESWPM = C.80445201E C3.
TELI = C.78784334E C3.
DIFT = C.16611671E C2.
PRCATE = C.20645673E-C1.
NIT = 8.

\$ ENL

ITERATION CN TESWPM COMPLETE CN TRIAL NO. = 3

SWAP3
NR2 = 1.
TESWPM = C.80445201E C3.
TELI = C.78784334E C3.
DIFT = C.16611671E C2.
PRCATE = C.20645673E-C1.
KIT = 0.
CFRAC = C.72265743E 10.
CFRAT = C.20062741E C9.

\$ END

NOTE: Output from final call to NONLIN after convergence on electron swarm temperature.
(for first radial point (NR2=1))

```

$MAMP1
K      = 0.114897441052525760 20.
        0.19145656842545630 20.
        0.20157533518473300 20.

KM     = 0.6847054751e544730 19.

C      = 0.21555555555555559990-11.
        0.57555555555555559980-21.
        0.75555555555555559980-09.
        0.55555555555555559970-01.
        0.18255555555555559990-14.
        0.15840632349252760-06.
        0.2705000000000000-19.
        0.56052345555555559980-11.
        0.0000000000000000-38.
        0.0000000000000000-38.
        0.0000000000000000-38.
        0.0000000000000000-38.

AG      = 0.2900000000000000 15.

NO      = 0.2900000000000000 19.

CAC22  = 0.127444430 01.

NR2     = 1.

S       = 0.1300000000000000-02.

```

```

        0.96052845555555559990-11.
        0.35999999999999999990-12.
        0.75999999999999999980-10.
        0.75999999999999999980-09.
        0.1800000000000000-10.
        0.39999999999999999990-11.
        0.15258311249315740-06.
        0.0000000000000000-38.
        0.0000000000000000-38.
        0.0000000000000000-38.
        0.0000000000000000-38.
        0.60499999999999999990-03.

```

```

$ FAC
ITERATIONS 6 AND 7 ARE IDENTICAL INDICATING A CYCLIC CONDITION.
THE BEST RESULTS SO FAR ARE GIVEN BELOW.

```

```

0.58555555555555559990-12
0.78555555555555559990-10
0.24255555555555559990-11
0.29473555555555559990-04
0.24352755555555559990-12
0.55611235555555559990-12
0.1330000000000000-10
0.0000000000000000-38

```

```

$MAMP4
C22LOS = 0.35515755E 15. = C(22) x Ai x ne2 = loss of Ar+ via collisional radiative recombination
C20LOS = 0.201027e2E 15. = C(20) x Ai x Ao x No = loss of Ar+ via 3-body molecular ion (Ar2+) formation
DIFLOS = 0.163518e4E 15. = K(6) x Ai / (Ne2 x Te) = loss of Ar+ via diffusion
DIFFN = 0.12939254E CC. = DIFLOS / (DIFLOS + C22LOS) = fractional loss of Ar+ via diffusion.
$ ENC

```

```

RUN 104.7      ELECTRON DENS. + TEMP.  M-WAVE CAV-14  RUN 64
RUN 104.7      S=1.300E-3ANG  TGAS=405 UK  TSMIG=600 UK

```

REACTION RATE COEFFICIENTS ADJUSTED FOR $T_{SRM} = T_{EL} = 0.7073514E 03$ (C22 FROM ALPHA TABLE)

0.1356732803176880 20.
0.1761223652547990 20.
0.0000000000000000-38.
0.16870662471771240 20.
0.18539189529418940 20.

[illegible]

AD	=	C.29CCCCC0CCCC000 15,	C.46736748F 12	0.16994449518476820-03,
ND	=	C.29CCCCC0CCCC000 19,	C.21751536E 10	
CAL22	=	C.1264C439E 01,	C.13685257F 11	
NR2	=	11,	C.3723CC33E C3	
	=		C.68655545E 11	
	=		C.4524C940E 12	
	=		C.1093C2E2E 1C	
	=		C.CCCCCCCE-3E	
	=	0.365165589595C14190-03,	0.0030307000100000-3B,	

111 7.

TEL! = 0.7C735137E C3.

PRCNET = C.36563245E-01.

END

REACTION RATE COEFFICIENTS ADJUSTED FOR $T_{\text{SRM}} = T_{\text{ELI}} = 0.6509988 \text{ eV}$ (L22 FROM ALFA TABLE)

[illegible]

ITERATIONS 5 AND 6 ARE IDENTICAL INDICATING A CYCLIC CONDITION. THE BEST RESULTS SO FAR ARE GIVEN BELOW.

AI	=	0.290000000000000000 15,	0.42555494E 12
NU	=	0.290000000000000000 19,	0.21754251E 10
CAC22	=	0.13205464E 01,	0.14600135E 11
NH2	=	11,	0.4524364E 03
S	=	0.36516555E0612190-03,	0.68651125E 11
			0.40775570E 12
			0.5593352E 05
			0.0000000E-38
			0.200000000000000000-38,
			0.1694449916476420-03,

WALLES FOR TRIAL NUMBER ON TESTHP = 2

SNAPZ	SNAP3
KIT =	KIT =
TESM =	TESM =
TELI =	TELI =
DIPT =	DIPT =
PRCITE =	PRCITE =
NIT =	NIT =
\$ ENL	\$ ENL

NR2=11

147MS

K = 0.1018071271384660 20.
0.1656662523061110 20.

0.6847C94751e54473D 19.

C = .3155555555990-11.
C = .5755555555980-21.

0-755555555555555598D-C9.
0-5555555555555555970-01.
0-1835555555555555940-14.
0-166640224004268D-C6.
0-2700000000000000-19.
0-2612874581340240-10.
0-0000000000000000-38.
0-0000000000000000-38.
0-0000000000000000-38.
0-0000000000000000-38.

[illegible]

00 = C.290000;C00000000 19.

$$ACZZ = 220^\circ \quad 0.135427 \text{ deg CL}$$

11.

03-015535-2

END

ITERATIONS 6 AND 7 ARE IDENTICAL INDICATING A CYCLIC CONDITION. THE BEST RESULTS SO FAR ARE GIVEN BELOW.

RE-300000000
C.CCC000000
57 9552678
21 C.41755188E
11 C.6869361E
ED 9596959
11 399494F
01 399494F
12 C.43552259E

4444

STCS = 0.207141060 15.

COLCS = C.67874283E 14.

FLCS = SJ74 0.6:221641F 14.

FFN = C.176727435 CC.

END

0.1

Summary of output data at the NER-11 radial points.

RUN 105.7 ELECTRON UENS. + TEMP. M-MAVE CAV-14 RUN 64
RUN 105.7 S=1.300E-3*NU TGA5=405 UK TSMIG=500 UK

SUMMARY OF DISTRIBUTIONS ALONG RADIUS OF TUBE

RADIUS*CM	SOURCE/NU	EL-DENSITY	EL-TEMP.*UK	AV.CUL.FR.-NEUTS.	AV.CUL.FR.-IONS
0.1000000E-02	0.1300000E-02	0.9895000E 12	0.8044520E 03	0.7226574E 10	0.2006274E 09
0.1145000E 00	0.1290000E-02	0.9903000E 12	0.8044519E 03	0.7226574E 10	0.2043949E 09
0.2280000E 00	0.1270000E-02	0.9839000E 12	0.8044519E 03	0.7226573E 10	0.2038417E 09
0.3415000E 00	0.1240000E-02	0.9724000E 12	0.8044519E 03	0.7226573E 10	0.2017670E 09
0.4550000E 00	0.1190000E-02	0.9541000E 12	0.8044519E 03	0.7226573E 10	0.1984355E 09
0.5685000E 00	0.1120000E-02	0.8822000E 12	0.7733000E 03	0.7022899E 10	0.1962955E 09
0.6820000E 00	0.1010000E-02	0.8390000E 12	0.7733000E 03	0.7022899E 10	0.1794849E 09
0.7955000E 00	0.8767199E-03	0.7490000E 12	0.7449873E 03	0.6836444E 10	0.1711343E 09
0.9090000E 00	0.6584300E-03	0.6462747E 12	0.7200023E 03	0.6670359E 10	0.1508699E 09
0.1022500E 01	0.5186999E-03	0.5492756E 12	0.7073513E 03	0.6585734E 10	0.1212630E 09
0.1136000E 01	0.3651700E-03	0.4355225E 12	0.6665803E 03	0.6311104E 10	0.1013037E 09

A-III. CW8 MAXIMUM PRINT-OUTPUT; TELETYPE PRINT-OUT

An example of the intermediate print-out from this code is shown in Table A-XIII in Appendix A. Normally the intermediate output is not requested if only the final converged values of T_e and n_e are desired. With the intermediate print switches (PRNT1 to PRNT4 off (=1), the converged value of T_e would be printed out in the Main Program as TESWRM under \$MAM3 (see Table A-XII, page A-29) and the converged value for $n_e = X(1)$ in the final values of $X(1)$ (see Table A-XII, page A-30). The intermediate print options are generally used in the initial checkout of the program or for check out of a problem where convergence was not obtained or the results showed an obvious blow-up in the internal computations. Because of the many steps in the inner and outer iterations, very many printed pages are obtained when all of the intermediate print switches are turned on. In order to obtain an example of the full print-out, and particularly of the Electron Temperature subroutine print-out, with a minimum number of pages, the last point (NR2=11) of the code run described above (see Table A-XI) was repeated so that all of the converged values from the first solution would be passed internally to the first trial values for the second solution. This was accomplished by setting MRP=2 and TSWMLG=0 (normally TSWMLG=TGAS).

Comparison of Tables A-XIII and A-XII, page A-30, show that the converged values from the first solution were passed to the input for the repeat solution. The intermediate output from the Electron Density subroutines is shown in Table A-XIII, (page A-38). Values of the tabular functions during the various steps of the numerical integrations are shown in Tables A-XIII (pages A-39 to A-41). The Tables are identified in the code print-out and a better understanding of the physical content can be obtained by reference to the program listing (Table A-I) or the flow diagram (Fig. A-2).

For this example problem on Neon-Argon where $V_1(N_e^+) = 21.56$ eV, the energy of the most energetic electrons produced by the fission fragments ($0.30 V_1(N_+)$ in Eq.(3)) is 6.47 eV, the last entry in the XAR-array in Table A-XIII, (page A-39). In Eq.(9) we are going to obtain the time for the electron to decay from the maximum value ($\epsilon_{\max} = 6.47$ eV) to the energy ϵ and then we are going to vary from ϵ_{\max} to ϵ_{\min} . We cannot follow the electron all the way down to the swarm energy ($\epsilon_{\min} = \epsilon_{es}$) because according to Eq.(9) this would take

an infinite amount of time. However, we are not interested in the distribution of energy loss of the electron while the electron spends long periods of time at energies only infinitesimally greater than $\bar{\epsilon}_{es}$. We will be satisfied to account for $\approx 99\%$ of the energy loss of the energetic electron and so we need follow the electron down only to $\epsilon_{min} = \bar{\epsilon}_{es} + \Delta\epsilon$ where $\Delta\epsilon/\epsilon_{max} \leq 0.01$. In this problem $\Delta E = \text{DELTE (input)} = 0.01$ eV, so we do account for 99.8% of the energy loss of the electron. Now $\bar{\epsilon}_{es} = \text{ESM} = 0.0862$ eV so $\epsilon_{min} = \text{EMIN} = 0.0962$ eV* and this is the first entry in the XAR-array.

For the 41 energy values (for the NSTEP1=40 energy increments) in this array, the corresponding values of $L_{ea}(\epsilon)$ for Eq.(5) are given in the XLEA-array, $L_{ee}(\epsilon)$ for Eq.(6) in the XLEE-array and $1/(L_{ea}(\epsilon) + L_{ee}(\epsilon))$ for the integrand of Eq.(9) in the GAR-array. The energy decay time of the electrons corresponding to the integral in Eq.(9) is given in the GE2 array versus the energetic electron energy in the XE2-array. The last entry in the GE2-array shows that it takes $\tau_T = 1.81 \times 10^{-7}$ sec for the electron to decay in energy from $\epsilon_{max} = 6.47$ eV to $\epsilon_{min} = 0.0962$ eV. This "thermalization time", τ_T , is very much shorter than the average (\sim recombination) lifetime of a swarm electron, which is $\tau_R \approx n_e/S^+ \approx 2 \times 10^{-4}$ sec.

The energetic electrons produced in Penning ionization are produced with energy $V_m(N_m) - V_1(A_+) = 0.92$ eV ($=\epsilon_{mid} = \text{EMID}$) and the time for an energetic electron produced by a fission fragment (6.47 eV) to decay to this energy (0.92 eV) is given by interpolation on the XEZ- and GEZ-arrays to obtain $\text{TMID} = 1.60 \times 10^{-7}$ sec. Actually, we are not interested in following an electron from $t=0$ to $t=\text{TMID}$ but rather in following the Penning-electron from ϵ_{mid} to ϵ_{min} or from $t=\text{TMID}$ to $t(\epsilon_{min})$. TMID is the lower limit of integration for the second integral in Eq.(10).

In the program we now prepare for the first integral in Eq.(10). The decay time is made the independent variable and moved to the XE2-array and energy is made the dependent variable and transferred to the GE2-array. The decay time $t(\epsilon_{max}(\text{FF}))$ is then divided into NSTEP/2 equal increments and stored in the XAR-array in \$NAM2 in Table A-XIII (page A-40) and the corresponding energy values are obtained from interpolation on the XE2- and GE2-arrays and stored in the EEL-array in Table A-XIII (page A-40). Before we

*The fact that in our computations we have abandoned the energetic electrons with an excess energy ($\Delta\epsilon$) appreciable with respect to $\bar{\epsilon}_{es}$ is not important. As we shall see, their lifetime is very short compared to the electrons of the swarm and therefore their number few.

perform the first integral in Eq.(10) we first perform (for a check, later) a similar integral for the energy transferred from the energetic electron to the neutral atoms (LEALOS). Values of the integrand, $v_{ea}(t')(\epsilon(t') - \bar{\epsilon}_{es})$, corresponding to the XAR values of (ϵ) are stored in the GAR-array in \$NAM2 in Table A-XIII (page A-40). A numerical integration (via SIR) on the XAR-, GAR-arrays yields LEALOS=2.08 eV for the energy lost to the neutral atoms of the original 6.47 eV of the energetic electron.

Values of the first integrand are computed next and stored in the GAR-array in \$NAM3 in Table A-XIII (page A-40). The numerical integration on the XAR-, GAR-arrays now yields a value of LEELOS=4.34 eV as the energy transferred from the energetic electron directly to the electron swarm. The sum of the energy transferred (LEELDS+LEALOS) should equal the loss of the electron energy $(\epsilon_{max} - \epsilon_{min})$ and it does within the error, EROR=0.043 eV.

We see that of the $6.47 - 0.0962 = 6.3738$ eV of energy lost by the energetic electron, our numerical integrations for the energy transfer to the neutral atoms and electron swarm have agreed to within $0.046/6.3738 < 1\%$.

To obtain the second integral in Eq.(10) (LEMLOS), a second numerical integration is performed on the values still in the XAR-, GAR-array where only the lower limit in the argument list of SIR is charged to TMID= 1.60×10^{-7} sec. This yields a value of LEMLOS=0.857 eV. The value of the total energy source rate to the electron swarm is \dot{E}_{GS} in Eq.(10) and is given by SOURCE= 4.90×10^{15} eV cm⁻³sec⁻¹ in Table A-XIII (page A-40).

We now prepare to compute the integrals in Eq.(17) for the energy loss rate of the electron swarm ($-\dot{E}_{LS}$). We take for an effective value of the upper limit (∞) of the integrals in Eq.(17) the quantity EINF=YINFxESM where YINF=12 to give EINF=1.03 eV in Table A-XIII (page A-41). The energy range (EINF-EGS) is divided into NSTEP2=40 increments and the 41 energy values stored in the XAR-array in \$NAM4 in Table A-XIII (page A-41). Values of the first integrand of Eq.(17) corresponding to the energy values of the XAR-array are stored in the GAR-array in \$NAM4 in Table A-XIII (page A-41). A numerical integration via SIR on the XAR-, GAR-arrays yield the value of LSNLOS= 5.02×10^{15} eV cm⁻³sec⁻¹ for the energy loss rate of the electron swarm to neutral atoms.

Values of the second integrand in Eq.(17) corresponding to energy values of the XAR-array are stored in the GAR-array in \$NAM5 in Table A-XIII (page A-41)

and a numerical integration on these arrays yields a value of $LSILOS = 4.17 \times 10^{13} \text{ eV cm}^{-3} \text{ sec}^{-1}$ for the energy loss rate of the electron swarm to the ions. The total energy loss rate of the swarm corresponding to \dot{E}_{LS} in Eq.(17) is $LSTLOS = LSNLOS + LSILOS = 5.07 \times 10^{15} \text{ eV cm}^{-3} \text{ sec}^{-1}$. The difference between the energy gain and loss of the electron swarm ($DIFF = |SOURCE - LSTLOS|$) meets the input convergence criterion ($CONV1 = 0.05$) on the first internal trial (as expected for this repeat run) since $CONV = |DIFF|/SOURCE = 0.033 \leq CONV1$.

The output in Table A-XIII, pages A-42 and A-43, from the Main Control program are similar to the output described in the previous section D-5.

TABLE A-XIII. Intermediate output from CW8 code; output from the Electron-Temperature Subroutine (TELECT)

[illegible]

KH	=	C.545555555555555595D 19.							
LAP	=	0.2016000000000000 00.							
S	=	0.3651655555555555C1219D-03.	C.0000000000000000-38.	0.1699444991647682D-03.					
TALX	=	0.5000000000000000D-07.							
VINC	=	0.21560000E C2.							
VIAC	=	0.15160000E C2.							
VMNC	=	0.16680000E C2.							
MASAC	=	0.32710000E-25.							
MASAC	=	0.66710000E-25.							
TGAS	=	0.40500000E C3.							
TSMIG	=	0.00000000E-38.							
DELTE	=	0.15000000E-C1.							
NSTEP1	=	40.							
NSTEP2	=	40.							
VINF	=	0.12000000E C2.							
KTI	=	10.							
NITS	=	10.							
DIFLEN	=	0.00000000E C1.							
PRCNUC	=	0.00000000E-C1.							
CCNVT	=	0.00000000E-C1.							
ERP	=	0.73000000E CC.							
F16	=	0.33300000E CC.							
E21	=	0.15000000E C1.							
L	=	17.	1.	1.	1.	1.	1.	1.	2.
MRPT	=	2.							
MCRE	=	2.							
\$ FAC									
REACTION RATE COEFFICIENTS ADJUSTED FOR TSMNM = TELI = 0.6605804E 03 (C22 FROM ALFA TABLE)									
SMAP1									
K	=	0.101800127138366D 20.	0.162523025557743D 20.	0.1785967316216959D 20.					
		0.169668552306111D 20.	0.0000000000000000-38.						

KM = C.68470947518544730 19.
C = 0.315555555555555599990-11.
0.575555555555555599990-21.
0.755555555555555599990-09.
0.955555555555555599990-01.
0.183555555555555599990-14.
0.16864022240042680-06.
0.270000000000000000000-19.
0.26965087636805590-10.
0.000000000000000000000-38.
0.000000000000000000000-38.
0.000000000000000000000-38.
0.000000000000000000000-38.

AD = 0.290000000000000000000 15.
NC = C.290000000000000000000 19.
CAL22 = 0.12505766 C1.
NR2 = 1.
S = 0.365165555555555599990-03.
\$ END

ITERATION CLNT IS 1
ESTIMATED FOOT
C.43552255E 12
C.21754636E 10
C.14355463E 11
C.43155669E 03
C.68693061E 11
C.41795188E 12
C.55578257E 09
C.00000000E-38

RELATIVE ERROR
C.62755755E-03
C.12053553E-05
0.62473211E-03
0.11647564E-02
C.15564377E-05
C.6755244E-03
C.48826101E-04
C.00000000E-38

ABSOLUTE ERROR
0.12695789E-04
-0.26267391E 09
0.26267391E 09
0.26267391E 09
-0.19068587E-01
-0.50465131E 12
0.00000000E-38
C.00000000E-38

ITERATION CLNT IS 7
ESTIMATED FOOT
C.43575556E 12
0.21754662E 10
C.14350477E 11
C.43149342E 03
C.68653168E 11
C.41823418E 12
C.55583152E 09
C.00000000E-38

RELATIVE ERROR
C.49633563E-17
C.87841084E-16
C.18042567E-16
C.16788423E-15
C.18555233E-16
C.62555497E-16
C.31201076E-16
C.00000000E-38

ABSOLUTE ERROR
-0.24437574E-04
-0.93505859E-01
-0.76293945E-05
0.31250000E-01
0.68832397E-01
-0.31250000E-01
0.78125000E-02
0.00000000E-38

ITERATION CLNT IS 8
ESTIMATED FOOT
C.43575556E 12
C.21754662E 10
C.14350477E 11
C.43149342E 03
C.68653168E 11
C.41823418E 12
C.55583152E 09
C.00000000E-38

RELATIVE ERROR
C.49618570E-17
C.87841065E-16
C.18037993E-16
0.27552897E-16
C.1802365E-16
C.62555809E-16
C.31200984E-16
C.00000000E-38

ABSOLUTE ERROR
-0.24437904E-04
-0.93505859E-01
0.76293945E-05
0.31250000E-01
0.68832397E-01
-0.31250000E-01
0.78125000E-02
C.00000000E-38

0.26065087636805590-10.
0.359999999999999999990-12.
0.759999999999999999990-17.
0.799999999999999999990-09.
0.180000000000000000000-10.
0.399999999999999999990-11.
0.20229161683470010-06.
0.000000000000000000000-38.
0.000000000000000000000-38.
0.000000000000000000000-38.
0.000000000000000000000-38.

0.270000000000000000000-19.
0.499999999999999999990-21.
0.959999999999999999990-01.
0.500000000000000000000 00.
0.499999999999999999990-23.
0.359999999999999999990-12.
0.249999999999999999990-20.
0.000000000000000000000-38.
0.000000000000000000000-38.
0.000000000000000000000-38.
0.000000000000000000000-38.

0.16994449918476820-03.

0.000000000000000000000-38.

Iterations 2 - 6 deleted.

FINAL VALUES

ITERATIONS 7 AND 8 ARE IDENTICAL INDICATING A CYCLIC CONDITION.
THE BEST RESULTS SO FAR ARE GIVEN BELOW.

C.43575556E 12
C.21754662E 10
C.14350477E 11
C.43149342E 03
C.68653168E 11
C.41823418E 12
C.55583152E 09
C.00000000E-38

ELECTRON KE LOSS TO NEUTRALS(LEA) AND ELECTRON SWARM(LEE) VS KE

SWAP6

XLFA = 0.9945750E 05. 0.26282890E 06. 0.49047643E 06. 0.78752637E 06.
 0.11151460E 07. 0.19065550E 07. 0.23651548E 07. 0.28646408E 07.
 0.34029234E 07. 0.35777025E 07. 0.45857172E 07. 0.58670648E 07.
 0.65540636E 07. 0.72704566E 07. 0.80150916E 07. 0.95761741E 07.
 0.10389724E 08. 0.11230250E 08. 0.12096730E 08. 0.13976442E 08.
 0.14653002E 08. 0.15826886E 08. 0.17638033E 08. 0.18947387E 08.
 0.19928507E 08. 0.20588948E 08. 0.22028537E 08. 0.24130425E 08.
 0.25314765E 08. 0.26465504E 08. 0.28487481E 08. 0.30127739E 08.
 0.31416314E 08. -0.0000000E-19. -0.0000000E-19. -0.0000000E-19.

XLFB =

0.12025402E 08. 0.25243277E 08. 0.47775901E 08. 0.40021538E 08.
 0.37136517E 08. 0.34703073E 08. 0.32776624E 08. 0.29629740E 08.
 0.28356686E 08. 0.27232823E 08. 0.26231492E 08. 0.24518777E 08.
 0.23773553E 08. 0.23101216E 08. 0.22478383E 08. 0.21369777E 08.
 0.20673437E 08. 0.20410047E 08. 0.19976179E 08. 0.19185156E 08.
 0.18823268E 08. 0.18481062E 08. 0.18156864E 08. 0.17556498E 08.
 0.17277788E 08. 0.17011507E 08. 0.16757930E 08. 0.16232243E 08.
 0.15959166E 08. 0.15844926E 08. 0.15491032E 08. 0.15250310E 08.
 0.1507475E 08. -0.0000000E-19. -0.0000000E-19. -0.0000000E-19.

\$ ENC

XAR=KE, GAR=1/(LEA+LEE), XL2=KL, GF2=IIE

SWAP1

XAM =

0.5e150301E-01. 0.25544639E 00. 0.41474321E 00. 0.73333350E 00.
 0.89263150E 00. 0.10514281E 01. 0.12112544E 01. 0.15238168E 01.
 0.16851131E 01. 0.18484093E 01. 0.20077055E 01. 0.21670017E 01.
 0.24855942E 01. 0.26448904E 01. 0.28041866E 01. 0.29634828E 01.
 0.32823752E 01. 0.34413714E 01. 0.36006677E 01. 0.37599639E 01.
 0.40785536E 01. 0.42378525E 01. 0.43971487E 01. 0.45564449E 01.
 0.46750334E 01. 0.50343336E 01. 0.51936298E 01. 0.53529260E 01.
 0.56715184E 01. 0.58308147E 01. 0.59901109E 01. 0.61494071E 01.
 0.64675555E 01. -0.0000000E-19. -0.0000000E-19. -0.0000000E-19.

GAR =

0.76716364E-07. 0.19599106E-07. 0.20816537E-07. 0.24508529E-07.
 0.26142381E-07. 0.27583142E-07. 0.28832380E-07. 0.30774551E-07.
 0.31486533E-07. 0.32040473E-07. 0.32449401E-07. 0.32740944E-07.
 0.32567811E-07. 0.32925418E-07. 0.33279390E-07. 0.33740964E-07.
 0.33986324E-07. 0.34160526E-07. 0.34179011E-07. 0.340714760E-07.
 0.34544521E-07. 0.349147909E-07. 0.35285867E-07. 0.35621261E-07.
 0.35877185E-07. 0.36315157E-07. 0.365782174E-07. 0.368245919E-07.
 0.37416580E-07. 0.37632583E-07. 0.378097421E-07. 0.37937057E-07.
 0.37934751E-07. -0.0000000E-19. -0.0000000E-19. -0.0000000E-19.

KE2 =

0.64580000E 01. 0.61454075E 01. 0.58308150E 01. 0.55122255E 01.
 0.48750376E 01. 0.45564451E 01. 0.42378526E 01. 0.39192826E 01.
 0.32820752E 01. 0.25634827E 01. 0.26448904E 01. 0.23262978E 01.
 0.16851129E 01. 0.13705204E 01. 0.107519280E 01. 0.73333355E 00.
 0.6150607E-01. -0.0000000E-19. -0.0000000E-19. -0.0000000E-19.
 -0.0000000E-08. 0.73210879E-08. 0.14379913E-07. 0.22040284E-07.
 0.3450717E-07. 0.47253918E-07. 0.56361618E-07. 0.65820693E-07.
 0.85671513E-07. 0.5563532E-06. 0.11640725E-06. 0.1169523E-06.
 0.1757541E-06. 0.14732545E-06. 0.15550123E-06. 0.16481974E-06.
 0.18138971E-06. -0.0000000E-19. -0.0000000E-19. -0.0000000E-19.

GE2 =

0.31233355E-07. 0.30123355E-07. 0.28646408E-07. 0.27504715E-07.
 0.2632976E-06. 0.12732976E-06. 0.17234758E-06. 0.17234758E-06.
 -0.0000000E-19. -0.0000000E-19. -0.0000000E-19. -0.0000000E-19.

TMIC	=	C.16CC7E20E-C6.
TELI	=	0.66658C39E C3.
TESWRM	=	0.66658C39E C3.
ESP	=	C.8615C761E-C1.
EGS	=	0.52343261E-C1.

```

$ END
XAR=TIME, CAR=LEA(T), EEI=KE(T), LEALCS=NEUTRAL LOSS FROM MOST ENERGETIC ELECTRONS

```

SNAM2

χ^2_{min}	=	-0.0000000E+00	0.90694603E+06	0.18138721E+07	0.27203381E+07	0.36277841E+07
		0.45347301E+07	0.54416762E+07	0.63486222E+07	0.72555681E+07	0.81625141E+07
		0.90694601E+07	0.95764061E+07	0.10883352E+08	0.11799298E+08	0.12697244E+08
		0.13604150E+08	0.14511136E+08	0.15418082E+08	0.16325028E+08	0.17231974E+08
		0.18138520E+08				

[illegible][illegible]

REALCS = 0.20762831E C1.

```

      & ENC  

      LPAR=TIME. GAR=LEE(T). LEELCS=LOSS TO ELECTRON SWARM FROM HIGH-E ELECTRONS. LENLCS=FROM MID-E

```

33A

[illegible][illegible]

ELCLS =	0.4338575E 01.
WCR =	0.42271516E-01.
EMCLS =	0.8569100E 00.
OLCE =	0.4902136E 16.
REF =	0.49550000E 16.

END

XAR=E. GAR=LEAUE(SWARM TC NEUTRAL). LSNLCS= TOTAL SWARM TC NEUTRAL LOSS

\$NAM4

XAR = 0.523433361E-01. 0.768800005E-01. 0.10141665E 00. 0.12543329E 00. 0.15048994E 00.
0.17502658E 00. 0.19956322E 00. 0.224863651E 00. 0.24863651E 00. 0.27317315E 00.
0.29770575E 00. 0.32224644E 00. 0.34678308E 00. 0.37131572E 00. 0.39585637E 00.
0.42039301E 00. 0.44492965E 00. 0.46946630E 00. 0.49400294E 00. 0.51853958E 00.
0.54307622E 00. 0.56761286E 00. 0.59214950E 00. 0.61668614E 00. 0.64122277E 00.
0.66575541E 00. 0.69029605E 00. 0.71483269E 00. 0.73936933E 00. 0.76390597E 00.
0.78844261E 00. 0.81297525E 00. 0.83751589E 00. 0.86205253E 00. 0.88658917E 00.
0.91112581E 00. 0.93566245E 00. 0.96019909E 00. 0.98473573E 00. 0.10092724E 01.
0.10338090E 01. 0.10583300E-19. 0.10828500E-19. 0.11073700E-19. 0.11318900E-19.
0.11564100E-19. 0.11809300E-19. 0.12054500E-19. 0.12299700E-19. 0.12544900E-19.
0.12790100E-19. 0.13035300E-19. 0.13280500E-19. 0.13525700E-19. 0.13770900E-19.
0.14016100E-19. 0.14261300E-19. 0.14506500E-19. 0.14751700E-19. 0.15000000E-19.

GAR = -0.00000000E-38. 0.12877138E 16. 0.71239039E 16. 0.13932008E 17. 0.14218857E 17.
0.21976800E 17. 0.22495504E 17. 0.21377913E 17. 0.19218926E 17. 0.16555891E 17.
0.13815375E 17. 0.11208049E 17. 0.89036954E 16. 0.69520985E 16. 0.53497819E 16.
0.40616411E 16. 0.30524063E 16. 0.22742855E 16. 0.16822265E 16. 0.12374805E 16.
0.90463859E 15. 0.65760212E 15. 0.47558579E 15. 0.34234648E 15. 0.24538107E 15.
0.17518591E 15. 0.12461401E 15. 0.88339566E 14. 0.62427560E 14. 0.43982217E 14.
0.30501274E 14. 0.21649956E 14. 0.15115450E 14. 0.10542302E 14. 0.73250899E 13.
0.50455058E 13. 0.35247511E 13. 0.24391140E 13. 0.16633091E 13. 0.11624062E 13.
0.80023662E 12. 0.00000000E-19. 0.00000000E-19. 0.00000000E-19. 0.00000000E-19.
EINF = 0.10338090E 01.
LSNLCS = 0.52247407E 16.

\$ END
XAR=E. GAR=LEAUE(SWARM TC LCN). LSNLCS=TOTAL SWARMTC LCN LOSS. LSTLCS=LSNLCS+LSILCS

\$NAM5

XAR = 0.522433361E-01. 0.768800005E-01. 0.10141665E 00. 0.12543329E 00. 0.15048994E 00.
0.17502658E 00. 0.19956322E 00. 0.224863651E 00. 0.24863651E 00. 0.27317315E 00.
0.29770575E 00. 0.32224644E 00. 0.34678308E 00. 0.37131572E 00. 0.39585637E 00.
0.42039301E 00. 0.44492965E 00. 0.46946630E 00. 0.49400294E 00. 0.51853958E 00.
0.54307622E 00. 0.56761286E 00. 0.59214950E 00. 0.61668614E 00. 0.64122277E 00.
0.66575541E 00. 0.69029605E 00. 0.71483269E 00. 0.73936933E 00. 0.76390597E 00.
0.78844261E 00. 0.81297525E 00. 0.83751589E 00. 0.86205253E 00. 0.88658917E 00.
0.91112581E 00. 0.93566245E 00. 0.96019909E 00. 0.98473573E 00. 0.10092724E 01.
0.10338090E 01. 0.10583300E-19. 0.10828500E-19. 0.11073700E-19. 0.11318900E-19.
0.11564100E-19. 0.11809300E-19. 0.12054500E-19. 0.12299700E-19. 0.12544900E-19.
0.12790100E-19. 0.13035300E-19. 0.13280500E-19. 0.13525700E-19. 0.13770900E-19.
0.14016100E-19. 0.14261300E-19. 0.14506500E-19. 0.14751700E-19. 0.15000000E-19.
LSTLCS = 0.41652143E 14.
LSILCS = 0.00000000E 16.
DIFF = -0.10425421E 15.

CCAV = 0.33505664E-01.

KII = 5.

\$ ENL

A-41

VALUES FOR TRIAL NUMBER CN TESARM = 1

\$NAME

KIT = 5.
TESARM = 0.6656027E C3.
TELI = 0.6656039E C3.
CIFT = -0.2288184E-C4.
PRCATE = 0.34336720E-C7.

NIT = 10.

\$ EAC

ITERATION CN TESARM COMPLETE CN TRIAL NO. = 1

\$NAME

NR2 = 1.
TESARM = 0.6656027E C3.
TELI = 0.6656039E C3.
CIFT = -0.2288184E-C4.
PRCATE = 0.34336720E-C7.

KIT = 9.

CFRAC = 0.6311042E 10.
CFRAT = 0.10352854E C5.

\$ EAC

APPENDIX B - RESONANT FREQUENCY-SHIFT CODE

CONTENTS

B-I. INTRODUCTION	B-1
B-II. INPUT	B-1
B-III. CORE SIZE OF PROGRAM AND RUNNING TIME	B-1
B-IV. MINIMUM OUTPUT FOR AN EXAMPLE PROGRAM	B-1
B-V. INTERMEDIATE OUTPUT FOR AN EXAMPLE PROBLEM	B-2
Fig. B-1. Flow Diagram for the Resonant Frequency-Shift Code	B-4
Table B-I. Listing of Resonant Frequency-Shift Code.	B-5
Table B-II. Listing of Function Statement for Axial Distribution of n_e	B-9
Table B-III. Example of Input Cards to Resonant Frequency-Shift Code (CW9)	B-9
Table B-IV. Example of Minimum Print-Output for an Example Problem (TM_{020} -Mode)	B-10
Table B-V. Example of Maximum Print-Output for an Example Problem (TE_{211} -Mode)	B-13

APPENDIX B

RESONANT FREQUENCY-SHIFT CODE

B-I. INTRODUCTION

The flow diagram for this computer code is presented in Fig. B-1 and a listing of the source program in Table B-I. Some of the data are read in via NAMELIST statements and some via FORMAT statements. Also NAMELIST statements are used for printed-output and the intermediate printed-output can be obtained with the print-switch PRNT1 (1=No, 2=Yes). The roots of the Bessel functions are read in via DATA-input at compile time. The FORTRAN-function statement for the axial distribution of n_e is given in Table B-II.

B-II. INPUT

The listing of a set of input cards for this CW9 code is given in Table B-III for an example problem which is a continuation of the problem presented in section IID. In fact, the input cards 6 through 12 listed in Table B-III are the punched-output cards from the CW8 code. The first two "title" cards are read in via "A-conversion" and the \$INPUT-data via a NAMELIST statement.

B-III. CORE SIZE OF PROGRAM AND RUNNING TIME

This program occupies about 13,000 cells of core storage. The example problem (2 solutions) required about 1 minute's execution time on the IBM 7094 computer.

B-IV. MINIMUM OUTPUT FOR AN EXAMPLE PROBLEM

The printed output from the example problem is displayed in Tables B-IV and B-V. In order to demonstrate the generality of the code, the example problem called for two solutions for the input electron density distribution: the first for the TM_{020} mode with minimum print-output (Table B-IV) and the second for the TM_{211} mode with complete print-output (Table B-V).

The first printed-output in Table B-IV are the roots of the Bessel function, X_{lm} , as defined for the TE-modes in Eq.(51) and printed in the first column, and for the TM-modes in Eq.(52) and printed in the second column. The NAMELIST-\$INPUT data in Table B-IV (page B-10) include the cavity dimensions, the mode definition,* the atomic masses of gas atoms, the number of increments for the numerical integrations, the number of points along the radius (NSR) for which information on the input cards are to be read or the number of points along the radius (NFR) for which normalized values of the electron density are to be read. EPSB is an error input variable to the BESSEL subroutine and PRNT1 is the switch for the intermediate print-output (1=No, 2=Yes). NSMORE and MORE are switches for control of repetitive runs using NAMELIST-input (see Fig. B-1). The last record of input is the information on the input cards which were obtained from the CW8 code.

The first output of the code, with PRNT1=1 for minimum print-output, are the terms under NAMELIST-\$NAM1 defined in Eqs.(59)(60) and (61). The first term (f_0) under \$NAM2 is the vacuum resonant frequency for the cavity according to Eq.(50) and for this TM_{020} mode is $f_0 = 23.20 \times 10^9$ cps or 23.20 GHz. KF is the leading constant in Eq.(47), $COLFRQ = \bar{v}_e$ and CCOLF is the factor $(1/(1+\bar{v}_e^2/\omega_0^2))$ in Eq.(47) which is very nearly equal to unity. The warning statement of "extrapolation for argument=0" came from the subroutine FUNCT (Table A-IV) because a value was requested at $r=0$ whereas the first r -entry in Table B-IV (page B-13) is at $r = 1.0 \times 10^{-3}$ cm (due to Q00 code limitations for $S^+(r)$ near $r=0$). Values of the integrals in the numerator and denominator of Eq.(62) are printed out under \$NAM13 as well as $G(\vec{r})$ which for this problem lowers the "average density" about 16% below the center of cavity value, n_0 . The predicted shift in resonant frequency is 1.45 GHz or about 6% of f_0 . FRQ is the frequency after the shift due to the plasma, i.e. $f_0 + \Delta f$. NEMID is the input electron density at the center of the cavity, n_0 , and NEAVE = $\langle n_e \rangle_{Theo}$ from Eq.(80).

B-V. INTERMEDIATE OUTPUT FOR AN EXAMPLE PROBLEM

The output in Table B-II is a solution for another mode, TM_{211} , on the same electron density distribution. This was accomplished without reading in a complete set of new input cards (see Table B-III) by setting MORE=1 in

*See definition of symbols at beginning of source program listing in Table B-1.

the first problem and NSMORE=1 in this last problem and adding only one TITLE-card and one NAMELIST-INPUT card. On this last input card PRNT1=2 in order to display the intermediate output.

The printed-output through \$NAM2 on the second page of Table B-V is similar to that described for Table B-IV above. The intermediate output under \$NAM3 through \$NAM12 are the values of the XAR-array, the GAR-array and the final value for the numerical integration for each integration performed. The particular integration can be identified by the FORTRAN name for the integral and the equations in section IIIA.2. Because we selected a uniform distribution of electron density in the axial direction (see Table B-II) all of the numerical integrations over z resulted in a value $0.35 \pm 3 \times 10^{-7}$ which is very close to the correct value of $\frac{d}{2}=0.35$.

The output under \$NAM13 is Table B-V (page B-16) is similar to that described for Table B-IV above. The vacuum resonance frequency ($f_o=24.97$ GHz) for this TM_{211} mode is higher than that for the TM_{020} mode ($f_o=23.20$ GHz) and the predicted frequency for this mode $FRQ=26.14$ GHz would have been off-scale on our microwave sweep generator. Because of the different electric field distribution the predicted electron density averaged over the electric field ($NEAVE=0.729 \times 10^{12} \text{ cm}^{-3}$) is appreciably lower than that predicted for the TM_{020} mode ($0.837 \times 10^{12} \text{ cm}^{-3}$).

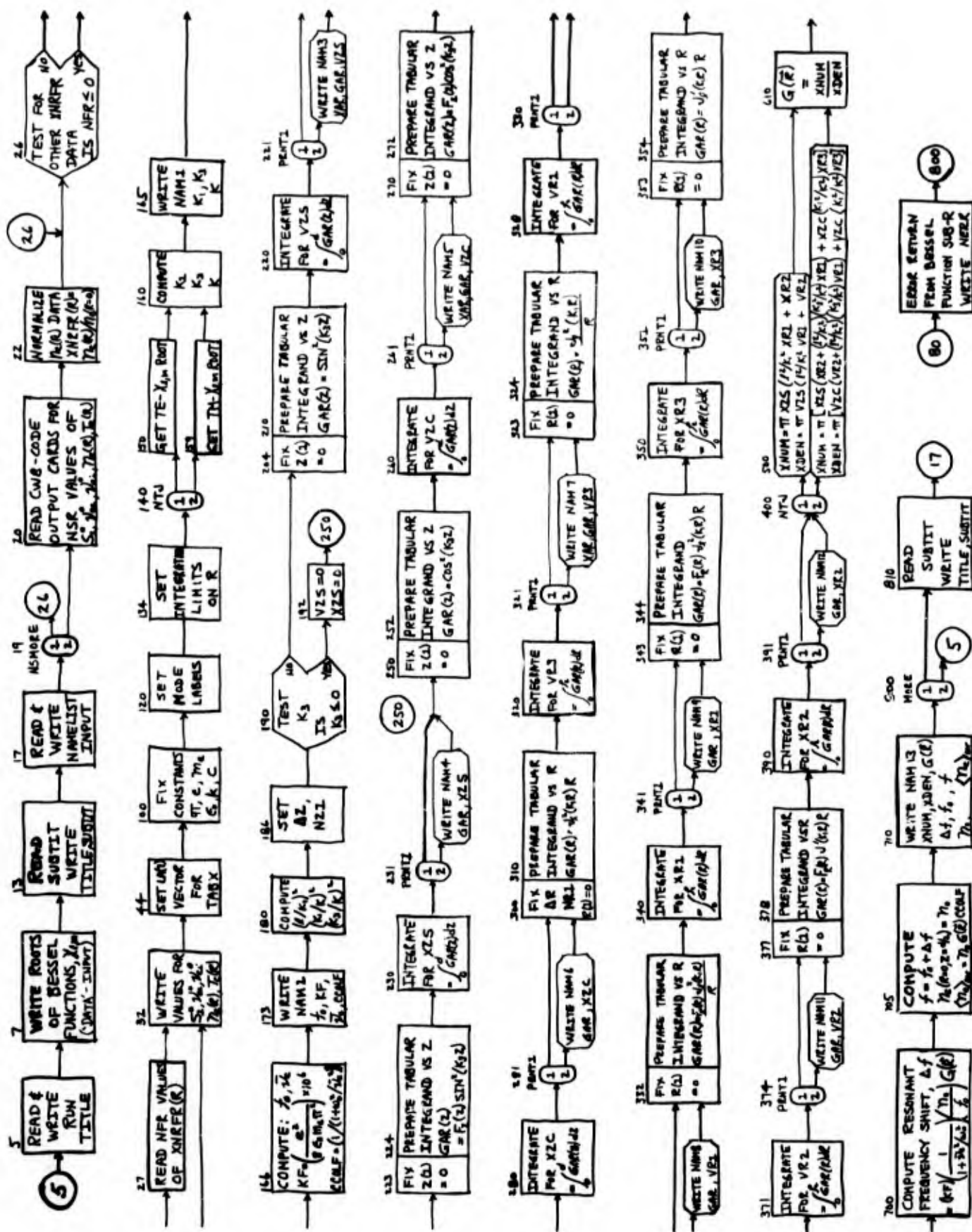
[illegible]

Fig. B-1. Flow diagram for the Resonant Frequency-Shift Code

TABLE B-I. Resonant Frequency-Shift Code (CW9)

Listing of Program

```

$IBFTC MNP3CW9 FULIST,REF,DECK,M94,XR7,DD
C
C
C**** THIS IS THE MAIN PROGRAM FOR THE MICROWAVE FREQUENCY SHIFT CODE
C****      JOB NO IS CW9
C
C****      ELECTRON DENSITY DISTRIBUTION ALONG RADIUS CAN BE OBTAINED
C****      FROM OUTPUT CARDS FROM ELECTRON TEMPERATURE CODE CW8
C
C****      D      = THICKNESS OF CAVITY,CM
C****      RHO2   = RADIUS OF CAVITY,CM
C
C****      SELECTION OF CAVITY MODE  TJ(LB,MB,NB)  *
C****      NTJ=1 FOR TJ=TE MODES      NTJ=2 FOR TJ=TM MODES
C****      LB = L  FOR L = 0 THRU 4
C****      MB = M  FOR M = 0 THRU 3
C****      NB = N  FOR N = 0 THRU 3
C
C****      *SEE TECHNIQUE OF MICROWAVE MEASUREMENTS-2,P-297,MCGRAW-HILL,1947
C****      L= NO. OF FULL-PERIOD VARIATIONS OF E-R WITH RESPECT TO O
C****      M= NO. OF HALF-PERIOD VARIATIONS OF E-O WITH RESPECT TO R
C****      N= NO. OF HALF-PERIOD VARIATIONS OF E-R WITH RESPECT TO Z
DIMENSION TITLE(12),SUBTIT(12),XSR( 1),XCFNO( 1),XCFAL( 1)
DIMENSION R2(51),XNR(51),XTR(51),TEROOT(5,4),TMROOT(5,4)
DIMENSION XAR(101),GAR(101)
DIMENSION LA(7),XR2FR(51),XNRFR(51)
COMMON/COM1/XAR,GAR
COMMON/COM2/LA,XR2FR,XNRFR
COMMON/COM3/D,RHO2,DIFFRN
INTEGER PRNT1
REAL K,K1,K3,KB,KC,KF,KP,ME,MASNO,MASAO,NEMID,NEAVE
NAMELIST/INPUT/D,RHO2,NTJ,LB,MB,NB,MASNO,MASAO,NSTPZ,NSTPR,NSR,
INFR,EPSB,PRNT1,NSMORE,DIFFRN,MORE
NAMELIST/NAM1/K1,K3,K
NAMELIST/NAM2/F0,KF,COLEFRQ,CCOLF
NAMELIST/NAM3/XAR,GAR,VZS
NAMELIST/NAM4/GAR,XZS
NAMELIST/NAM5/XAR,GAR,VZC
NAMELIST/NAM6/GAR,XZC
NAMELIST/NAM7/XAR,GAR,VR3
NAMELIST/NAM8/GAR,VR1
NAMELIST/NAM9/GAR,XR1
NAMELIST/NAM10/GAR,XR3
NAMELIST/NAM11/GAR,VR2
NAMELIST/NAM12/GAR,XR2
NAMELIST/NAM13/XNUM,XDEN,GFR,DFLEFRQ,F0,FRQ,NEMID,NEAVE
NAMELIST/NAM20/NERR
EXTERNAL DUMMY
ASSIGN 80 TO LABEL
IF (.FALSE.) GO TO 80
5 READ(5,11)TITLE
6 WRITE(6,12)TITLE
7 WRITE(6,8)
8 FORMAT(1H0,25HROOTS OF BESSEL FUNCTIONS/
1      4X,50H      X(L,M)=MTH ROOT OF D/DX(JL(X))=0 FOR TE MODES/
2      4X,50H      X(L,M)=MTH ROOT OF      JL(X) =0 FOR TM MODES/
3 5X,54HX(L,M),S STORED IN TEROOT(L+1,M+1) AND TMROOT(L+1,M+1))

```



```

DATA((TEROOT(I,J),J=1,4),I=1,5)/0.0,3.832,7.016,10.174,0.0,1.841,
15.333,8.536,0.0,3.054,6.706,9.970,0.0,4.201,8.015,11.346,0.0,5.318
2.9,282,12.682/
DATA((TMROOT(I,J),J=1,4),I=1,5)/0.0,2.405,5.520, 8.654,0.0,3.832,
17.016,10.174,0.0,5.136,8.417,11.620,0.0,6.380,9.761,13.015,0.0,
27.588,11.065,14.373/
9 WRITE(6,10) ((TEROOT(I,J),TMROOT(I,J),J=1,4),I=1,5)
10 FORMAT(1H0,2E20.8)
11 FORMAT(12A6)
12 FORMAT(1H1,20X,12A6)
13 READ(5,11)SUBTIT
15 WRITE(6,16)TITLE,SUBTIT
16 FORMAT(1H1,20X,12A6/21X,12A6)
17 READ (5,INPUT)
18 WRITE(6,INPUT)
19 GO TO(26,20),NSMORE
20 READ (5,21) NSR,XSR(1),XCFNO(1),XCFAI(1),(R2(N),XNR(N),XTR(N),N=1,
1NSR)
21 FORMAT(13/(6E12.5))
22 DO 25 N=1,NSR
23 XR2FR(N)=R2(N)/R2(NSR)
24 XNRFR(N)=XNR(N)/XNR(1)
25 CONTINUE
26 IF (NFR) 32,32,27
27 READ(6,28) (XR2FR(N),XNRFR(N),N=1,NFR)
28 FORMAT(6E12.5)
32 WRITE(6,33) XSX(1),XCFNO(1),XCFAI(1)
33 FORMAT(1H0,40HCENTER OF CAVITY VALUES-- (SOURCE/NO) = ,E20.8/
1 ,3X,38HELECTRON-NEUTRAL COLLISION FREQUENCY =,E20.8/
2 ,3X,38HELECTRON-ION COLLISION FREQUENCY =,E20.8)
34 WRITE(6,35) NSR
35 FORMAT(1H0,13,71H INPUT VALUES(NSR) FOR RADIUS(R2), EL-DENSITY(XNR
1), EL-TEMPERATURE(XTR))
36 WRITE(6,37) (R2(N),XNR(N),XTR(N),N=1,NSR)
37 FORMAT(1H0,3E20.8)
C**** CONTROL ARRAY FOR TABX
44 LA(1)=NSR
45 LA(2)=1
46 LA(3)=1
47 LA(4)=1
48 LA(5)=1
49 LA(7)=2
70 GO TO 100
80 WRITE(6,NAM20)
85 GO TO 800
100 PI=3.14159E0
101 Q=1.60210E-19
102 ME=9.1084E-31
103 KP=8.8540E-12
104 KB=1.3804E-23
105 KC=2.99793E8
120 XL=LB
121 XM=MB
122 XN=NB
130 L1=LB+1
131 M1=MB+1
132 N1=NB+1
134 R2MIN=R2(1)
136 R2MAX=R2(NSR)
140 GO TO (150,159),NTJ

```

```

150 XLM=TEROOT(L1,M1)
151 GO TO 160
159 XLM=TMRROOT(L1,M1)
160 K1=XLM/RH02
162 K3=XN*PI/D
164 K =SQRT(K1**2+K3**2)
165 WRITE(6,NAM1)
166 FO=KC*1.0E2*K/(2.0*PI)
168 KF=((((Q/ME)*Q)/KP)/(8.0*PI*PI))*1.0E6
170 COLFRQ=XCFNO(1)+XCFAI(1)*MASAO/MASNO
172 CCOLF=1.0/(1.0+COLFRQ*COLFRQ/(2.*PI*FO)**2)
173 WRITE(6,NAM2)
180 XLK1=(XL/K1)**2
182 XK1K=(K1/K)**2
184 XK3K=(K3/K)**2
186 DELZ=D/FLOAT(NSTPZ)
187 NZ1=NSTPZ+1
190 IF(K3) 192,192,204
192 VZS=0.0
194 XZS=0.0
196 GO TO 250
204 Z=0.0
210 DO 219 NZ=1,NZ1
212 GAR(NZ)=(SIN(K3*Z))**2
214 XAR(NZ)=Z
216 Z=Z+DELZ
219 CONTINUE
220 VZS=SIR(DUMMY,0.0,D,NSTPZ)
221 GO TO (223,222),PRNT1
222 WRITE(6,NAM3)
223 Z=0.0
224 DO 229 NZ=1,NZ1
226 GAR(NZ)=GAR(NZ)*FZ(Z)
228 Z=Z+DELZ
229 CONTINUE
230 XZS=SIR(DUMMY,0.0,D,NSTPZ)
231 GO TO (250,232),PRNT1
232 WRITE(6,NAM4)
250 Z=0.0
252 DO 259 NZ=1,NZ1
254 GAR(NZ)=(COS(K3*Z))**2
255 XAR(NZ)=Z
256 Z=Z+DELZ
259 CONTINUE
260 VZC=SIR(DUMMY,0.0,D,NSTPZ)
261 GO TO (270,262),PRNT1
262 WRITE(6,NAM5)
270 Z=0.0
272 DO 279 NZ=1,NZ1
274 GAR(NZ)=GAR(NZ)*FZ(Z)
275 Z=Z+DELZ
279 CONTINUE
280 XZC=SIR(DUMMY,0.0,D,NSTPZ)
281 GO TO (300,282),PRNT1
282 WRITE(6,NAM6)
300 DELR=RH02/FLOAT(NSTPR)
302 NR1=NSTPR+1
304 R=0.0

```

```

310 DO 319 NR=1,NR1
312 R1=R*K1
314 Y=BESSEL(R1, LB, 1, EPSB, LABEL, NERR)
315 GAR(NR)=(Y**2)*R
316 XAR(NR)=R
317 R=R+DELR
319 CONTINUE
320 VR3=SIR(DUMMY, 0.0, RHO2, NSTPR)
321 GO TO (323, 322), PRNT1
322 WRITE(6, NAM7)
323 R=0.0
324 DO 327 NR=1,NR1
325 GAR(NR)=GAR(NR)/(R*R)
326 R=R+DELR
327 CONTINUE
328 VR1=SIR(DUMMY, 0.0, RHO2, NSTPR)
330 GO TO (332, 331), PRNT1
331 WRITE(6, NAM8)
332 R=0.0
333 DO 337 NR=1,NR1
334 FR2=R/RHO2
335 GAR(NR)=GAR(NR)*FUNCT(FR2)
336 R=R+DELR
337 CONTINUE
340 XR1=SIR(DUMMY, 0.0, RHO2, NSTPR)
341 GO TO (343, 342), PRNT1
342 WRITE(6, NAM9)
343 R=0.0
344 DO 347 NR=1,NR1
345 GAR(NR)=GAR(NR)*R*R
346 R=R+DELR
347 CONTINUE
350 XR3=SIR(DUMMY, 0.0, RHO2, NSTPR)
351 GO TO (353, 352), PRNT1
352 WRITE(6, NAM10)
353 R=0.0
354 DO 369 NR=1,NR1
356 R1=R*K1
358 YB1=BESSEL(R1, LB, 1, EPSB, LABEL, NERR)
360 YB2=BESSEL(R1, LB+1, 1, EPSB, LABEL, NERR)
362 Y=(FLOAT(LB)/R1)*YB1-YB2
364 GAR(NR)=(Y**2)*R
368 R=R+DELR
369 CONTINUE
371 VR2=SIR(DUMMY, 0.0, RHO2, NSTPR)
374 GO TO (377, 376), PRNT1
376 WRITE(6, NAM11)
377 R=0.0
378 DO 385 NR=1,NR1
379 FR2=R/RHO2
380 GAR(NR)=GAR(NR)*FUNCT(FR2)
382 R=R+DELR
385 CONTINUE
390 XR2=SIR(DUMMY, 0.0, RHO2, NSTPR)
391 GO TO (400, 392), PRNT1
392 WRITE(6, NAM12)
400 GO TO (500, 600), NTJ
500 XNUM=PI*XZS*(XLK1*XR1+XR2)
505 XDEN=PI*VZS*(XLK1*VR1+VR2)

```

```

510 GFR=XNUM/XDEN
515 GO TO 700
600 XNUM=PI*(XZS*(XR2+XLK1*XK3K*XR1)+XZC*XK1K*XR3)
605 XDEN=PI*(VZS*(VR2+XLK1*XK3K*VR1)+VZC*XK1K*VR3)
610 GFR=XNUM/XDEN
700 DELFRQ=(KF*CCOLF*XNR(1)/FO)*GFR
705 FRQ=FO+DELFRQ
706 NEMID=XNR(1)
707 NEAVE=XNR(1)*GFR*CCOLF
710 WRITE(6,NAM13)
800 GO TO(810,5),MORE
810 READ(5,811)SUBTIT
811 FORMAT(12A6)
812 WRITE(6,16)TITLE,SUBTIT
813 GO TO 17
      END

```

TABLE B-II. Function statement for axial distribution of n_e .

```

$IBFTC FZZ4CW9 FULIST,REF,DECK,M94,XR7,DD
      FUNCTION FZ(ARG)
      COMMON/COM3/D,RHO2,DIFFRN
      PI=3.14159
      D2=D/2.
      FZ=(COS((PI/2.)*((ARG/D2)-1.)))*DIFFRN
      RETURN
      END

```

TABLE B-III. Example of input cards to Resonant Frequency Shift Code (CW9).
 (Cards 6 to 12 are punched output from CW8 code.
 See Table A-XII (page A-31).)

```

$DATA
  RUN 109.7.1,109.7.2 RES. FREQ. SHIFT M-WAVE CAV-14 (NE-AR) RUN 64
  RUN 109.7.1 P=1000.KW S=1.300E-3 TGAS=405 OK TM(0,2,0) MODE
$INPUT D=0.7, RHO2=1.13525, NTJ=2, LB=0, MB=2, NB=0,
  MASNO=3.371E-26, MASAO=6.671E-26, NSTPZ=10, NSTPR=10, NSR=11, NFR=0,
  EPSB=0.001, PRNT1=1, NSMORE=2, DIFFRN=0.000E-00, MORE=1 $
11
0.13000E-02 0.72266E 10 0.20063E 09 0.10000E-02 0.98951E 12 0.80445E 03
0.11450E 00 0.99031E 12 0.80445E 03 0.22800E 00 0.98398E 12 0.80445E 03
0.34150E 00 0.97247E 12 0.80445E 03 0.45500E 00 0.95419E 12 0.80445E 03
0.56850E 00 0.88222E 12 0.77331E 03 0.68200E 00 0.83960E 12 0.77331E 03
0.79550E 00 0.74909E 12 0.74499E 03 0.90900E 00 0.64627E 12 0.72000E 03
0.10225E 01 0.54928E 12 0.70735E 03 0.11360E 01 0.43552E 12 0.66658E 03
  RUN 109.7.2 P=1000.KW S=1.300E-3 TGAS=405 OK TE(2,1,1) MODE
$INPUT NSMORE=1,NTJ=1, LB=2, MB=1, NB=1, PRNT1=2, MORE=2 $

```

TABLE B-IV.

RUN 109.7.1.109.7.2 RES. FREQ. SHIFT M-WAVE CAV-14 (NE-AR) RUN 64

ROOTS OF BESSEL FUNCTIONS
 $X(L,M)=MTH\ ROOT\ OF\ C/DX(JL(X))=0$ FOR TE MODES
 $X(L,M)=MTH\ ROOT\ OF\ JL(X)=0$ FOR TM MODES
 $X(L,M), S$ STORED IN TEROOT(L+1,M+1) AND TMRGOT(L+1,M+1)

C.0000000E-38	C.0000000E-38
C.3832000E 01	C.2405000E 01
C.7016000E 01	C.5520000E 01
C.1317400E 02	C.8554000E 01
C.0000000E-38	C.0000000E-38
C.1841000E 01	C.3822000E 01
C.5333000E 01	C.7016000E 01
C.5536000E 01	C.1017400E 02
C.0000000E-38	C.0000000E-38
C.3054000E 01	C.5136000E 01
C.6706000E 01	C.8417000E 01
C.5570000E 01	C.1162000E 02
C.0000000E-38	C.0000000E-38
C.4201000E 01	C.6380000E 01
C.8015000E 01	C.5761000E 01
C.11346000E 02	C.13015000E 02
C.0000000E-38	C.0000000E-38
C.5318000E 01	C.7588000E 01
C.92815999E 01	C.11065000E 02
C.12682000E 02	C.14373000E 02

RUN 179.7.1,109.7.2 RES. FREQ. SHIFT M-WAVE CAV-14 (NE-AR) RUN 04
 PLW 109.7.1 P=1000.KW S=1.300E-3 TGAS=475 OK TM(0.2,0) MODE

```

$INPLT
D      = 0.70000000E 00.
RHC2   = 0.11352500E 01.
NTJ    = 2.
LB     = 0.
MB     = 2.
NS     = 3.
MASNC  = 0.33710000E-25.
MASAC  = 0.66710000E-25.
NSTPZ  = 17.
NSTPR  = 10.
NSK    = 11.
NFR    = 7.
EPSH   = 0.10000000E-02.
PRNT1  = 1.
NSMCRF = 2.
DIFFRN = 0.00000000E-39.
MORE   = 1.
$ ENC
  
```

CENTER OF CAVITY VALUES-- (SOURCE/NO) = 0.13300000E-02
 ELECTRON-NEUTRAL COLLISION FREQUENCY = 0.7226000E 10
 ELECTRON-ION COLLISION FREQUENCY = 0.20063000E 09

11 INPUT VALUES(NSR) FOR RADIIUS(R2), EL-DENSITY(XNR), EL-TEMPERATURE(XTR)

0.10000000E-02	0.98551000E 12	0.80445000E 03
0.11450000E 00	0.95031000E 12	0.80445000E 03
0.22800000E 00	0.96396000E 12	0.80445000E 03
0.34150000E 00	0.97247000E 12	0.80445000E 03
0.45500000E 00	0.98419000E 12	0.80445000E 03
0.56850000E 00	0.99222000E 12	0.77331000E 03
0.68200000E 00	0.83960000E 12	0.77331000E 03

0.7555000E 00 0.7490500E 12 0.7449900E 03
 0.9090000E 00 0.5462700E 12 0.7200000E 03
 0.1022500E 01 0.5492800E 12 0.7073500E 03
 0.1136500E 01 0.4355200E 12 0.5055800E 03

\$NAME1

K1 = 0.48623651E 01.
 K3 = 0.0000000E-38.
 K = 0.48623651E 01.

\$ FNC

\$NAME2

FD = 0.2220000E 11.
 KF = 0.40305612E 01.
 COLFRQ = 0.76236343E 10.
 CCCLF = 0.55727229E 00.

\$ ENC

EXTRAPOLATION OCCURRED WITH ARG=

0.7073500E-38

EXTRAPOLATION OCCURRED WITH ARG=

0.7073500E-38

\$NAME3

XNUM = 0.1353750E 00.
 XDEN = 0.16424072E 00.
 GFR = 0.84855502E 00.
 DELFRQ = 0.14549750E 10.
 FD = 0.2220000E 11.
 FRQ = 0.24655058E 11.
 NEMIC = 0.58951000E 12.
 NEAVE = 0.83740676E 12.

\$ ENC

TABLE B-V.

RUN 109.7.1.109.7.2 RES. FREQ. SHIFT M-WAVE CAV-14 (NE-AR) RUN 64
 RUN 109.7.2 P=1000.KW S=1.300E-3 TGAS=405 OK TE(2,1,1) MODE

\$INPUT
 D = 0.7000000E 00.
 RHC2 = 0.11352500E 01.
 NTJ = 1.
 LB = 2.
 MB = 1.
 NB = 1.
 MASNC = 0.3371000E-25.
 MASAC = 0.6671000E-25.
 NSTPZ = 10.
 NSTPR = 10.
 NSR = 11.
 NFR = 0.
 EPSB = 0.1000000E-02.
 PRNT1 = 2.
 NSMORE = 1.
 DIFFRA = 0.0000000E-38.
 MORE = 2.
 \$ END

CENTER OF CAVITY VALUES-- (SOURCE/NC) = 0.13000000E-02
 ELECTRON-NEUTRAL COLLISION FREQUENCY = 0.7226600E 10
 ELECTRON-ION COLLISION FREQUENCY = 0.2006300E 09

11 INPUT VALUES(NSR) FOR KALILS(R?), EL-DENSITY(XNR), EL-TEMPERATURE(XTR)

0.1000000E-02	0.56551000E 12	0.8044500E 03
0.1145000E 00	0.9903100E 12	0.8044500E 03
0.2280000E 00	0.5835800E 12	0.8044500E 03
0.2415000E 00	0.9724700E 12	0.8044500E 03
0.4550000E 00	0.9541900E 12	0.8044500E 03
0.5685000E 00	0.8822200E 12	0.7733100E 03
0.6820000E 00	0.8396000E 12	0.7733100E 03

0.7955000E 00 0.7490000E 12 0.7449000E 03
 0.5090000E 00 0.6462700E 12 0.7200000E 03
 0.1022500E 01 0.5442800E 12 0.7073500E 03
 0.1136000E 01 0.4355200E 12 0.6665800E 03

\$NAME1

K1 = 0.26901063E 01.
 K3 = 0.444875857E 01.
 K = 0.52324304E 01.

\$EAC

\$NAME2

FO = 0.2496000E 11.
 KF = 0.40305612E 08.
 COLFRQ = 0.76230343E 10.
 CCCLF = 0.95764365E 00.

\$END

\$NAME3

XAK = 0.0000000E-38.
 0.3500000E 00.
 0.7000000E 00.
 GAR = 0.0000000E-38.
 0.1000000E 01.
 0.72048556E-11.
 VZS = 0.3500000E 00.
 \$END

0.21000000E 00.
 0.56000000E 00.
 -0.0000000E-19.
 0.65450773E 00.
 0.34549356E 00.
 -0.0000000E-19.

0.14000000E 00.
 0.49000000E 00.
 -0.0000000E-19.
 0.34549098E 00.
 0.65451028E 00.
 -0.0000000E-19.

0.70000000E-01.
 0.42000000E 00.
 -0.0000000E-19.
 0.95491344E-01.
 0.90450945E 00.
 -0.0000000E-19.

0.0000000E-38.
 0.1000000E 01.
 0.72048556E-11.

0.3500000E 00.
 0.3500000E 00.

0.90450786E 00.
 0.95492928E-01.
 -0.0000000E-19.

\$NAME4

GAR = 0.0000000E-38.
 0.1000000E 01.
 0.72048556E-11.
 XZS = 0.3500000E 00.
 \$END

0.65450773E 00.
 0.34549356E 00.
 -0.0000000E-19.

0.34549098E 00.
 0.65451028E 00.
 -0.0000000E-19.

0.95491344E-01.
 0.90450945E 00.
 -0.0000000E-19.

0.0000000E-38.
 0.1000000E 01.
 0.72048556E-11.

0.3500000E 00.
 0.3500000E 00.

0.90450786E 00.
 0.95492928E-01.
 -0.0000000E-19.

\$NAP5				
XAR	=	0.00000000E-38. 0.35000000E 00. 0.70000000E 00.	0.70000000E-01. 0.42000000E 00. -0.00000000E-19.	0.14000000E 00. 0.50000000E 00. -0.00000000E-19.
GAR	=	0.10000000E 01. 0.18012164E-11. 0.10000000E 01.	0.90450865E 00. 0.95490552E-01. -0.00000000E-19.	0.34549226E 00. 0.65450706E 00. -0.00000000E-19.
VZC	=	0.34555568E 00.		
\$ ENC				
\$NAP6				
GAR	=	0.10000000E 01. 0.18012164E-11. 0.10000000E 01.	0.90450865E 00. 0.95490552E-01. -0.00000000E-19.	0.34549226E 00. 0.65450706E 00. -0.00000000E-19.
XZC	=	0.34555568E 00.		
\$ ENC				
\$NAP7				
XAR	=	0.00000000E-38. 0.56762459E 00. 0.11352500E 01.	0.11352500E 00. 0.68114999E 00. -0.00000000E-19.	0.45410000E 00. 0.10217250E 01. -0.00000000E-19.
GAR	=	0.00000000E-38. 0.32411875E-01. 0.26857191E 00.	0.15430770E-04. 0.67413598E-01. -0.00000000E-19.	0.12276473E-01. 0.22945789E 00. -0.00000000E-19.
VR3	=	0.87113526E-01.		
\$ ENC				
\$NAP8				
GAK	=	0.00000000E-38. 0.1359614E 00. 0.20670072E 00.	0.11973044E-02. 0.14529879E 00. -0.00000000E-19.	0.27962706E-01. 0.21059752E 00. -0.00000000E-19.
VR1	=	0.12078588E 00.		
\$ ENC				
EXTRAPOLATION OCCURRED WITH ARC=				
\$NAP9				
GAR	=	0.00000000E-38. 0.89714442E-01. 0.91856923E-01.	0.11982986E-02. 0.12332053E 00. -0.00000000E-19.	0.57424076E-01. 0.12203431E 00. -0.00000000E-19.
XRI	=	0.85732352E-01.		
\$ ENC				

\$NAME10					
GAR	=	0.0000000E-38, 0.28905826E-01, 0.11838451E 00, 0.55794640E-01,	0.15443583E-04, 0.57216448E-01, -0.0000000E-19,	0.46099739E-03, 0.88005796E-01, -0.0000000E-19,	0.31878781E-02, 0.11348235E 00, -0.0000000E-19,
XR3	=				0.11841221E-01, 0.12739429E 00, -0.0000000E-19,
\$ FAC					
\$NAME11					
GAR	=	0.0000000E-38, 0.35365990E-01, 0.12555310E-05,	0.66177377E-03, 0.39179095E-01, -0.0000000E-19,	0.46562793E-02, 0.33629010E-01, -0.0000000E-19,	0.13218052E-01, 0.20986000E-01, -0.0000000E-19,
VR2	=	0.20383179E-01,			0.25025413E-01, 0.68627170E-02, -0.0000000E-19,
\$ ENC					
EXTRAPCLATION OCCURRED WITH ARG=					
\$NAME12			0.0000000E-38		
GAR	=	0.0000000E-38, 0.31540110E-01, 0.55435309E-06,	0.66232330E-03, 0.33252767E-01, -0.0000000E-19,	0.46305522E-02, 0.25466893E-01, -0.0000000E-19,	0.12991653E-01, 0.13713136E-01, -0.0000000E-19,
XR2	=	0.17004089E-01,			0.24138158E-01, 0.38101588E-02, -0.0000000E-19,
\$ ENC					
\$NAME13					
XNUM	=	0.70800520E-01,			
XDEN	=	0.95819740E-01,			
GFR	=	0.73855284E 00,			
WELFRQ	=	0.11777016E 10,			
FO	=	0.24906004E 11,			
FRC	=	0.26144785E 11,			
NEMIC	=	0.98951000E 12,			
NFAVE	=	0.72541902E 12,			
\$ FAC					

DISTRIBUTION

	<u>No .Copies</u>
Office of Naval Research Power Branch, Code 429 Department of the Navy Washington, D. C. 20360	1
Cognizant ONR Area Branch Office	1
U. S. Naval Research Laboratory Technical Information Division Washington, D. C. 20390	6
Director, Office of Naval Research Branch Office 495 Summer Street Boston, Massachusetts 02210	1
Director of Special Projects (SP-001) Department of the Navy Washington, D. C. 20360	1
Naval Ship Systems Command Department of the Navy Washington, D. C. 20360 Attn: Code 03422 (Mr. B. B. Rosenbaum) Code 08 (Mr. L. Schlanger) Code 6437D (Mr. V. Gardner) Code 2012 Code 6660	1 1 1 2 1
Naval Ordnance Systems Command Department of the Navy Washington, D. C. 20360 Attn: Library	1
Defense Documentation Center (STI) Cameron Station Alexandria, Virginia 22314	20
Commandant U. S. Marine Corps, Code CSY-3 Headquarters, Marine Corps Washington, D. C. 20380	1
National Aeronautics and Space Administration 1520 H. Street, N. W. Washington, D. C. 20546 Attn: James Lynch Arvin Smith	1 1

UNCLASSIFIED

Security Classification

DOCUMENT CONTROL DATA - R&D		
(Security classification of title, body of abstract and indexing annotation must be entered when the overall report is classified)		
1. ORIGINATING ACTIVITY (Corporate author) Research Laboratories, General Motors Corporation 12 Mile and Mound Roads, Warren, Michigan 48090		2a. REPORT SECURITY CLASSIFICATION UNCLASSIFIED
		2b. GROUP N A
3. REPORT TITLE INVESTIGATIONS ON THE DIRECT CONVERSION OF NUCLEAR FISSION ENERGY TO ELECTRICAL ENERGY IN A PLASMA DIODE.		
4. DESCRIPTIVE NOTES (Type of report and inclusive dates) Final Report No. 8 - November 1, 1966 to October 31, 1967		
5. AUTHOR(S) (Last name, first name, initial) Leffert, Charles B. Rees, David B.		
6. REPORT DATE October 31, 1967 (Published 2/28/68)	7a. TOTAL NO. OF PAGES 208	7b. NO. OF REFS 60
8a. CONTRACT OR GRANT NO. Nonr-3109(00)	8b. ORIGINATOR'S REPORT NUMBER(S) GMR -	
b. PROJECT NO. 099-345		
c.	9b. OTHER REPORT NO(S) (Any other numbers that may be assigned this report)	
d.	None	
10. AVAILABILITY/LIMITATION NOTICES Qualified requesters may obtain copies of this report from DDC.		
11. SUPPLEMENTARY NOTES None	12. SPONSORING MILITARY ACTIVITY Office of Naval Research (Zip Code: Power Branch (Code 429) 20360) Department of the Navy, Washington, D.C.	
13. ABSTRACT This is the unclassified section (Vol. I) of the Final Report under Contract Nonr-3109(00), Office of Naval Research, dealing with fission-fragment-generated plasmas for thermionic energy conversion. Results of the past year's work are presented under three major headings, viz., "(A) - Reaction Kinetic Studies of Ar-Cs Plasmas", where the possible influence of a heteronuclear ArCs^+ ion is considered and rejected; "(B) - Calculation of Electron Temperatures in Plasmas Produced by Fission Fragments", where we discover that a non-equilibrium electron temperature exists at the higher values of neutron flux; and "(C) - Electron Densities in Fission-Fragment-Induced Plasmas in Microwave Cavities", where much of our previous theories are collected, enlarged and incorporated into a comprehensive set of computer codes which predict accurately electron densities in the Ne-Ar system. Preceding the detailed discussion of these 3 topics is a summary (in Section I) of the main results of studies (A), (B), and (C). Also in Section I we survey our past work and offer some general comments and conclusions on the present status and utility of the fission-fragment ionization scheme for use in thermionic diodes.		

DD FORM 1473
1 JAN 64UNCLASSIFIED
Security Classification

Security Classification

14. KEY WORDS	LINK A		LINK B		LINK C	
	ROLE	WT	ROLE	WT	ROLE	WT
1. Direct energy conversion 2. Thermionics 3. Gaseous electronics 4. Plasma physics						

INSTRUCTIONS

1. ORIGINATING ACTIVITY: Enter the name and address of the contractor, subcontractor, grantee, Department of Defense activity or other organization (*corporate author*) issuing the report.

2a. REPORT SECURITY CLASSIFICATION: Enter the overall security classification of the report. Indicate whether "Restricted Data" is included. Marking is to be in accordance with appropriate security regulations.

2b. GROUP: Automatic downgrading is specified in DoD Directive 5200.10 and Armed Forces Industrial Manual. Enter the group number. Also, when applicable, show that optional markings have been used for Group 3 and Group 4 as authorized.

3. REPORT TITLE: Enter the complete report title in all capital letters. Titles in all cases should be unclassified. If a meaningful title cannot be selected without classification, show title classification in all capitals in parenthesis immediately following the title.

4. DESCRIPTIVE NOTES: If appropriate, enter the type of report, e.g., interim, progress, summary, annual, or final. Give the inclusive dates when a specific reporting period is covered.

5. AUTHOR(S): Enter the name(s) of author(s) as shown on or in the report. Enter last name, first name, middle initial. If military, show rank and branch of service. The name of the principal author is an absolute minimum requirement.

6. REPORT DATE: Enter the date of the report as day, month, year; or month, year. If more than one date appears on the report, use date of publication.

7a. TOTAL NUMBER OF PAGES: The total page count should follow normal pagination procedures, i.e., enter the number of pages containing information.

7b. NUMBER OF REFERENCES: Enter the total number of references cited in the report.

8a. CONTRACT OR GRANT NUMBER: If appropriate, enter the applicable number of the contract or grant under which the report was written.

8b, 8c, & 8d. PROJECT NUMBER: Enter the appropriate military department identification, such as project number, subproject number, system numbers, task number, etc.

9a. ORIGINATOR'S REPORT NUMBER(S): Enter the official report number by which the document will be identified and controlled by the originating activity. This number must be unique to this report.

9b. OTHER REPORT NUMBER(S): If the report has been assigned any other report numbers (*either by the originator or by the sponsor*), also enter this number(s).

10. AVAILABILITY/LIMITATION NOTICES: Enter any limitations on further dissemination of the report, other than those imposed by security classification, using standard statements such as:

- (1) "Qualified requesters may obtain copies of this report from DDC."
- (2) "Foreign announcement and dissemination of this report by DDC is not authorized."
- (3) "U. S. Government agencies may obtain copies of this report directly from DDC. Other qualified DDC users shall request through _____."
- (4) "U. S. military agencies may obtain copies of this report directly from DDC. Other qualified users shall request through _____."
- (5) "All distribution of this report is controlled. Qualified DDC users shall request through _____."

If the report has been furnished to the Office of Technical Services, Department of Commerce, for sale to the public, indicate this fact and enter the price, if known.

11. SUPPLEMENTARY NOTES: Use for additional explanatory notes.

12. SPONSORING MILITARY ACTIVITY: Enter the name of the departmental project office or laboratory sponsoring (paying for) the research and development. Include address.

13. ABSTRACT: Enter an abstract giving a brief and factual summary of the document indicative of the report, even though it may also appear elsewhere in the body of the technical report. If additional space is required, a continuation sheet shall be attached.

It is highly desirable that the abstract of classified reports be unclassified. Each paragraph of the abstract shall end with an indication of the military security classification of the information in the paragraph, represented as (TS), (S), (C), or (U).

There is no limitation on the length of the abstract. However, the suggested length is from 150 to 225 words.

14. KEY WORDS: Key words are technically meaningful terms or short phrases that characterize a report and may be used as index entries for cataloging the report. Key words must be selected so that no security classification is required. Identifiers, such as equipment model designation, trade name, military project code name, geographic location, may be used as key words but will be followed by an indication of technical context. The assignment of links, rules, and weights is optional.

UNCLASSIFIED

Security Classification